Water Resources and Drought in International Iberian River Basins under Future Climates

Selma de Brito Guerreiro

Thesis submitted for the degree of Doctor of Philosophy

School of Civil Engineering and Geosciences

Faculty of Science Agriculture and Engineering

Newcastle University

November 2014

POPH QUALIFICAR É CRESCER.
QREN QUADRO DE REFERÊNCIA ESTRATÉGICO NACIONAL PORTUGAL 2007.2013
GOVERNO DA REPÚBLICA PORTUGUESA
UNIÃO EUROPEIA Fundo Social Europeu

Abstract

Increases in water consumption in agriculture, tourism and industry have exacerbated the problem of water resources management in Iberia, and the transboundary character of many of its rivers adds to the problem. Drought has caused water restrictions, destruction of crops, livestock deaths and widespread forest fires in Iberia in recent years.

The aim of this PhD is to undertake an impact assessment of climate change on the water resources of the rivers Douro, Tagus and Guadiana, with a special emphasis on the vulnerability of Portugal (the downstream country). Observed and projected changes in rainfall were assessed, as were future projections for drought and discharges.

A dataset of downscaled and bias corrected rainfall and temperature (and subsequently potential evapotranspiration) from CMIP5 climate models (RCP8.5) was created using two different methods: change factor and quantile mapping. From the CMIP5 ensemble, fifteen model runs were chosen to represent the range of future climate projections available. To assess changes in future rainfall, a 30 year time-slice approach was compared with a transient approach. Two drought indices (DSI-12 and SPI-12) were used to assess drought evolution from 1961 to 2100. A spatially distributed, physically based hydrological modelling system (SHETRAN) was used to provide historical and future (2050s) natural discharges. A minimal calibration approach was followed using small quasi-natural sub-basins.

The majority of climate models projected reductions of annual rainfall in the three basins for the 2050s (for both downscaling methods) and almost all models projected rainfall decreases in spring and autumn. None of the models projected positive annual rainfall trends (1961-2100) and in spring, summer and autumn the majority of models showed negative trends.

The 15 climate models display a wide range of future drought projections: some showed litle or no change while others project decades of extreme drought conditions. It was also shown that SPI-12 is not an appropriate index to use in Iberian climates.

Most models project decreases in daily, seasonal and annual discharges for all basins, although some models project increases in high discharges. The magnitude of the decreases in discharge varies significantly for the different climate models throughout the seasons and basins. However, the Guadiana consistently shows the larger reductions in discharge and the higher probabilities of falling below the discharge limits set in the international agreement between Portugal and Spain.

Acknowledgements

I would like to thank my supervisors Christopher Kilsby and Hayley Fowler for their guidance and fruitful discussions throughout the last four years, as well as for providing the opportunity to attend several conferences and summer schools. I would also like to thank Dr Francesco Serinaldi for the advice and patience during long statistical discussions, Dr Stephen Birkinshaw for the help provided in setting up the hydrological model and Elizabeth Lewis for processing the soil data used in the hydrological model.

Thanks are due to the Portuguese Foundation of Science and Technology (FCT) for partially funding this PhD (grant SFRH/BD/69070/2010) and I acknowledge the World Climate Research Programme's Working Group on Coupled Modelling, which is responsible for CMIP, and thank the climate modelling groups for producing and making available their model output.

This PhD would never have happened without Professor João Corte-Real and Professor Manuela Portela, who directed me to Newcastle University, and I will always be grateful for the time and the consideration they have showed me. Also a special thanks to Cláudia Brandão and Dr Manuela Saramago from the Portuguese Water Institute for their initial support and recommendation letter to the FCT.

Lastly I would like to thank my family for their moral support and encouragement and Chris Parker, for his patience, and for always believing in me, even when I didn't.

Table of Contents

Table of Figures

Chapter 1. Introduction

1.1 Rainfall and droughts in Iberia

The Iberian Peninsula is located on the western extreme of Europe, between 36° and 44° north and between 10°W and 3°E (see Figure). It encompasses Portugal, Spain, Andorra and the British Overseas Territory of Gibraltar.

Figure 1.1 – Map of Europe with the Iberian Peninsula highlighted in green.

The spatial and seasonal distribution of rainfall and its large interannual variability in the Iberian Peninsula makes water scarcity an important issue both in Spain and Portugal. The mountainous northwest of Iberia has one of the highest mean annual rainfalls of Europe (2200mm/year) but areas of the southeast coast of the peninsula receive less than 300mm/year (Trigo and DaCamara, 2000; Trigo *et al.*, 2004). Furthermore, almost all of the rainfall occurs between October and May (Trigo *et al.*, 2004).

In Portugal the last 2 decades have been dry, with the exception of the extremely wet hydrological years (October to September) of 1996, 1998 and 2001 (Andrade *et al.*, 2011) and in the south of Portugal the frequency of moderate to extreme droughts is approximately every 3.6 years (Santos *et al.*, 2010). The 2004/05 drought that affected Western Europe was particularly severe in the Iberian Peninsula where rainfall between October 2004 and June 2005 was roughly 45% less than the 1961-1990 mean. In Iberia's southern half the event was even worse with a 60% drop in rainfall and for many stations it was the driest year on record, including Lisbon (since 1865) and Madrid (since 1859) (García-Herrera *et al.*, 2007).

Droughts in Iberia are responsible for losses in crop yields, especially in non-irrigated agriculture, and soil degradation in semiarid areas due to loss of vegetation cover. Severe

droughts also cause major socio-economic impacts (Santos *et al.*, 2007). Water restrictions (impacting quality of life and tourism), complete destruction of crops in some areas, numerous livestock deaths and widespread forest fires have all been felt in Iberia in recent years. There is an apparent increase in the frequency and the area affected by droughts, and studying climate variability may contribute to a better management of these extreme climatic occurrences (Santos *et al.*, 2010).

Increases in water consumption in agriculture, tourism and industry have exacerbated the problem of water resources management in Iberia, and the transboundary character of many of its rivers adds to the difficulty of discharge management, especially during flood and drought periods (López-Moreno *et al.*, 2007).

1.2 Douro, Tagus and Guadiana basins

Portugal and Spain share five river basins which cover 40% of Iberia (see Figure 1.1). Around 40% of Portuguese water resources flow from Spain which, when considering the storage capacity in the Spanish territory (see Table 1.1), places Portugal in a vulnerable position.

Figure 1.1 – International Iberian basins (Almeida *et al.*, 2009). This figure uses the Portuguese names of the rivers (see Table 1.2 for clarification)

Table 1.1– Storage capacity in the international Iberian basins (adapted from (Almeida *et al.*, 2009).

River basin	Spain	
	hm^3	hm^3/km^2
Minho	2 880	0.18
Lima	170	0.13
Douro	1 670	0.10
Tagus	11 140	0.20
Guadiana	9 220	0.17
River basin	**Portugal**	
	hm^3	hm^3/km^2
Minho	0.2	0
Lima	400	0.34
Douro	1 080	0.06
Tagus	2 750	0.11
Guadiana	3 610*	0.31

*$3150hm^3$ are from the Alqueva dam

The three main international Iberian rivers: the Douro, the Tagus and the Guadiana will be the focus of this PhD. Under natural conditions, i.e. without water transfers, around 70% of the total outlet flow of these rivers has its origin in Spain (INAG, 2001). The main physical characteristics of these rivers are summarized in Table 1.2.

Table 1.2 – Summary of physical characteristics of the three studied basins: river length, basin area and annual discharge (INAG, 1999a; INAG, 1999b; INAG, 2001).

River	Length (km)	Basin area (km^2)	Annual discharge (hm^3)
Douro Spanish: Duero Portuguese: Douro	927	97 603 (19% in Portugal, 81% in Spain)	14 800
Tagus Spanish: Tajo Portuguese: Tejo	1 100	80 629 (30% in Portugal, 70% in Spain)	9 629
Guadiana Spanish: Guadiana Portuguese: Guadiana	810	66 800 (17% in Portugal, 83% in Spain)	2 680

The Douro is the largest basin in Iberia. It rises in the Urbión Mountains in central Spain, crosses the Numantian Plateau and flows westward into northern Portugal and then to the Atlantic Ocean. Along the river there are numerous hydroelectric power plants and the middle

Douro is extensively used for irrigation. In Portugal, the principal crop of the Douro valley is grapes, which are used to produce Port wine (UNEP, 2003).

The Tagus River rises in the Sierra de Albarracin at an altitude of 1590 meters, flows westward into Portugal and then to the Atlantic Ocean. It is the longest river on the Iberian Peninsula and its basin supplies water to two European capitals (Lisbon and Madrid) with a total of 11 million people. Several dams exist for irrigation and hydroelectric power production, creating large artificial lakes (UNEP, 2003b).

The Tagus River acts as a natural border between “wet Iberia” in the north and “dry Iberia” in the south, with its northern tributaries having considerably higher discharges than the southern tributaries (Portela *et al.*, 2009). Water quality is considered poor in the middle and lower parts of the basin due to deficient effluent treatment in small towns, intensive farming, illegal waste water dumping and gravel extractions (Beguería *et al.*, 2009).

The Tagus-Segura water transfer started in 1978 and was built to transfer up to 1 100hm^3/yr from the headwaters of the Tagus to the Mediterranean basins of the Jucar and the Segura, mainly to supply water to the irrigated areas in the south-east of Spain. The volume of water transferred annually is shown in Figure 1.2. This volume has to be approved by the Spanish government on a yearly basis (or on a seasonal/monthly basis in dry years). The 2005/2006 drought caused several public demonstrations in both the Tagus and the Segura basins, respectively against and in favour of this water transfer system (Beguería *et al.*, 2009).

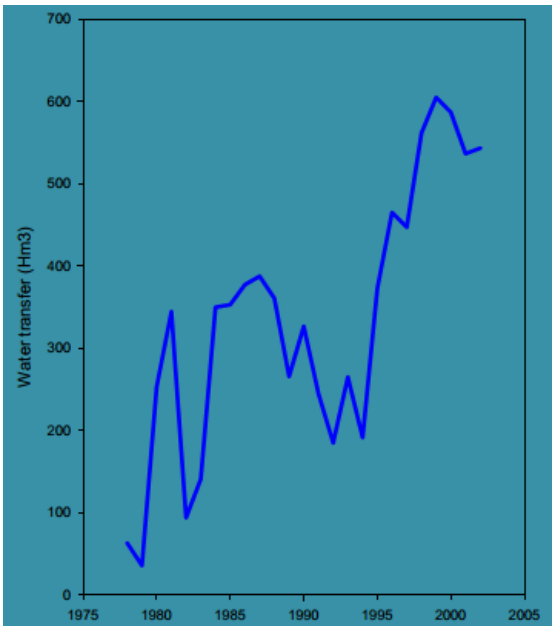

Figure 1.2 – Volume of water transferred annually from the Tagus River through the Tagus-Segura water transfer (Beguería *et al.*, 2009).

The headwaters of the Guadiana are one of the driest places in Europe, with mean annual rainfall of 415mm and PET above 800mm/yr (Kilsby *et al.*, 2007). The Guadiana flows westwards through the south of Spain and turns south when it crosses into Portuguese territory. It then flows to the Atlantic (Gulf of Cadiz) with several of its sections forming the border between the two countries. The land use is predominantly rural and due to widespread agricultural activity and high summer temperatures, algal blooms are frequent and eutrophication affects several artificial lakes (UNEP, 2004).

The upper Guadiana basin consists of streams closely connected to aquifers with both stream flows and groundwater levels in decline in line with a dramatic increase of groundwater abstraction for irrigation. Degradation of protected wetlands has occurred due to declining groundwater levels, problems with water salinity and with invasive species from the Tagus basin that resulted from occasional water transfers between the two basins (Conan *et al.*, 2003)

The Guadiana has the biggest reservoir in Europe: Alqueva. It was built with the objective of being a strategic water reserve for the south of Portugal, providing water for irrigation, urban and industrial consumption, energy production and regularization of flows. When the entire irrigation project is completed, the Alqueva dam will supply water for the irrigation of 112,240ha (INAG, 2001). It will also supply water for consumption for around 200,000 people (EDIA, 2010). Spain's storage capacity and water consumption for agriculture in the Guadiana basin was negligible before 1954. Between 1954 and 1963 the increase of storage capacity in the Spanish side of the Guadiana basin was around 4,000hm^3. This remained almost constant until 1988 when, in three years, the storage capacity was doubled. Significant uptake of water for irrigation purposes started at the beginning of the 1980s (Brandão and Rodrigues, 2000).

Figure 1.3 shows the mean monthly river flows for the Douro, Tagus and Guadiana. The seasonality of flows, with high winter discharges and low summer discharges, is typical of Iberia and is mainly a result of the seasonality of the rainfall exacerbated by the high temperatures (and therefore PET) of the summer months. The highest mean discharges are seen in the Douro, followed by the Tagus and then the Guadiana. However the highest maximum flow values are recorded in the Tagus. Iberian rivers tend to show high coefficients of variation in flow, which increase from north to south: around 100% for the Guadiana and 50% for the Douro (Gámiz-Fortis *et al.*, 2008).

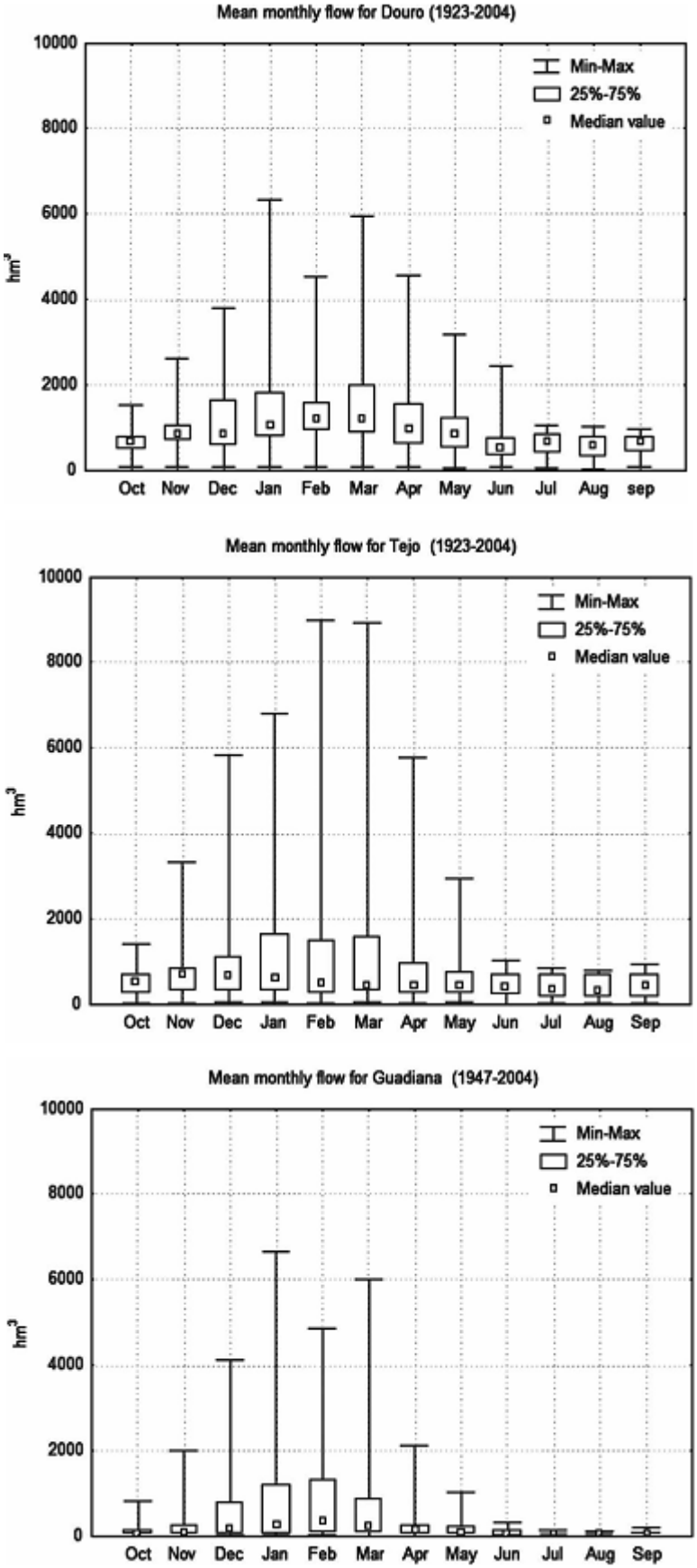

Figure 1.3 - Box plots of mean monthly river flows for Douro (top), Tejo/Tagus (middle), and Guadiana (bottom) (Gámiz-Fortis *et al.*, 2008). These mean river flows were calculated for different periods: 1923-2004 for the Douro and the Tagus and 1947-2004 for the Guadiana.

1.3 The Albufeira Convention

The first water treaties between Portugal and Spain date back to the 19th century and several treaties were later signed in the 1920s and 1960s. In 1993 the Spanish Government released its National Hydrological Plan that included a new transfer of 1 billion cubic metres of water between the Douro River and the Spanish Mediterranean region. Since environmental impacts and Portuguese interests were not considered, the Portuguese Government reacted and negotiations followed that led to the signature of a new water treaty in 1998: the Albufeira Convention. This convention seeks to balance environmental protection with sustainable use of water resources within the framework of International and EU Law (UN, 2013).

The Albufeira Convention came into effect in January 2000. It was based on the recommendations of the 1997 New York Convention and was influenced by the principles included in the main international treaties related to transboundary waters and by the philosophy of the EU Water Framework Directive (Almeida *et al.*, 2009).

The Albufeira Convention regulates: exchange of information on the state of water; uses of water and water infrastructure; the assessment of transboundary impacts; coordination of programs for the protection of aquatic systems; sustainable use of water; prevention and control of droughts, floods and pollution accidents. It also establishes minimum annual discharges for the international rivers (except the Lima) at determined locations. However, the discharge minima do not have to be complied with if the year is considered “exceptionally dry” (refer to section 7.1.2 for definitions of “exceptionally dry” periods).

In February 2008 a more detailed flow regime for the Douro, Tagus and Guadiana was defined (as a revision of the convention), which included different minimum flows for different times of the year. These limits and more information on the technical aspects of the convention are presented in section 7.1.2.

1.4 Aims and objectives

This thesis aims to undertake an impact assessment of climate change on the water resources of the rivers Douro, Tagus and Guadiana using different methodologies and accounting for uncertainty in future climate projections. It is hoped that, besides contributing to the advancement of scientific knowledge of the impacts of climate change in this area, the findings of this project will also guide stakeholders in government and industry to plan mitigation and adaptation strategies.

The objectives of this thesis are:

- To perform a thorough statistical analysis of historical rainfall and assess the effects of short term variability in the study of long-term changes. This provides the necessary context to the analysis of future rainfall changes.
- To collate rainfall and temperature outputs from climate models (CMIP5 model runs for RCP8.5) and develop a downscaled dataset using different downscaling methods and covering the climate models' uncertainty space.
- To assess future changes in rainfall projections, comparing a 30 year time-slice approach with a transient approach.
- To consider the value of using simple, rainfall based, drought indices to assess the impact of climate change in the Douro, Tagus and Guadiana basins.
- To set-up, calibrate and validate a physically based, distributed hydrological model for the Douro, Tagus and Guadiana rivers.
- To use the hydrological model and climate scenarios developed in this thesis to examine the impact of climate change on the discharge of the Douro, Tagus and Guadiana rivers both at the border between Portugal and Spain and at the outlets of the rivers.
- To assess the implications of these changes to future discharge in relation to the Albufeira convention discharge limits.
- To compare the results of a relatively simple methodology, based on drought indices, which requires only rainfall inputs and can be performed within a few weeks, with a data-intensive, physically based, distributed hydrological modelling approach which takes several months to set up and run.

1.5 Project limitations

Considering the availability of data, and the need to keep the project to a manageable size, only naturalized discharges will be modelled. Therefore, the complex system of hundreds of dams with multiple uses and thousands of water abstractions in these basins will not be modelled. Also, the extremely complex aquifer systems present in these basins will be highly simplified in the hydrological model.

Furthermore, the future projections for rainfall and temperature (and subsequently potential evapotranspiration) are based on downscaled climate model outputs. These climate model projections and downscaling processes have associated errors and uncertainties which are discussed in Chapter 4.

1.6 Thesis outline

This thesis is divided into seven chapters. *Chapter 1 - Introduction* started with a brief explanation of the problem of drought and water resources management in Iberia. It introduced the three international river basins that have been studied in this PhD and the Albufeira Convention. This was followed by the aims and objectives of this thesis and the project limitations. It finishes with the thesis outline.

Chapter 2 - Review of hydroclimatology in Iberia describes the climate in the Iberian Peninsula and its atmospheric and oceanic influences, focusing particularly on a literature review of the interannual variability of rainfall. There is also a review of the interannual variability of discharges in the Douro, Tagus and Guadiana rivers which sets the context for the hydrological modelling presented in *Chapters 6 and 7*.

Chapter 3 – Historical Rainfall Analysis presents an analysis of changes in rainfall in the Douro, Tagus and Guadiana basins for 1961 to 2009, where both change points and trends have been analysed. This provides the historical context necessary for the interpretation of future changes in rainfall.

Chapter 4 – Climate Models, Downscaling and Future Rainfall introduces the climate models used in this study and presents a critical review of the downscaling methods used. It also analyses the projected changes in rainfall between the recent past (1961-1990) and the 2050s (2041-2070) for the three river basins. It concludes with a transient analysis of rainfall changes between 1961 and 2100 and a comparison of the results from the two methods.

Chapter 5 – Drought starts with a literature review of drought in Iberia. It then introduces the two rainfall-only based drought indices used in this study (SPI and DSI) to analyse droughts in the three studied river basins. It then evaluates the evolution of drought in the basins between 1961 and 2100 using downscaled climate model outputs from Chapter 4.

Chapter 6 – Hydrological Model Set Up starts with a brief literature review of hydrological models and a description of the model used in this study (SHETRAN). The data and the methodology used for the calibration and validation of the model are then described. The effects of the model calibration on the discharge of the three main rivers are also analysed.

Chapter 7 – Hydrological Model Results starts with a review of studies of hydrological impacts of climate change in Iberia, followed by the technical details of the Albufeira convention. Then the results of the hydrological modelling for the historical period and for the future are

presented. The impacts of future discharge changes in the Albufeira Convention are also considered.

The thesis ends with *Chapter 8 – Conclusions* where the main conclusions are presented and discussed and possible future work is proposed.

Chapter 2. Review of Hydroclimatology in Iberia

This chapter starts with a review of the atmospheric influences in the Iberian climate. Particular attention is given to the North Atlantic Oscillation due to its important role in explaining Iberian rainfall. This is followed by a brief summary of oceanic influences on the Iberian climate.

The climate of the Iberian Peninsula is described in detail in section 2.2. An extensive literature review on the interannual variability of rainfall in the region is also presented in this section, and *Chapter 3 – Historical Rainfall Analysis* will expand on, and critically assess, most of the work introduced here. This chapter finishes with a review of the interannual variability of discharges in the Douro, Tagus and Guadiana rivers which sets the context for the hydrological modelling presented in *Chapters 6* and *7*.

This chapter is intended as a characterization of the study area and its hydroclimatology, and does not encompass all literature review. The introductions of the subsequent chapters will have specific literature reviews relevant for that chapter. Therefore the introduction of *Chapter 3 – Historical Rainfall Analysis* will briefly consider the detection of changes in rainfall time-series. The introduction of *Chapter 4 – Climate Models, Downscaling and Future Rainfall* includes the literature review of the uncertainty in climate models and the issues regarding how to combine them, as well as a review of downscaling methods. The introduction of *Chapter 5 – Drought* reviews the definitions of drought, the most common drought indices used and the literature of droughts in Iberia. The introduction of *Chapter 6 – Hydrological Model Set Up* considers the different types of hydrological models, their uncertainties and their applicability to climate change studies and the introduction of *Chapter 7 – Hydrological Model Results* encompasses the few existing studies of hydrological impacts of climate change in Iberia and the technical details of the Albufeira convention.

2.1 Overview of climate in Europe

2.1.1 *Large-scale atmospheric influences*

Natural variability is particularly high in Europe, with European climate influenced by large scale circulations of both the atmosphere and the ocean (Woollings, 2010). Climate in Europe is strongly seasonally dependent and has four distinct seasons: winter (December to February), spring (March to May), summer (June to August) and autumn (September to November).

During the summer, the Azores high-pressure system covers most of the North Atlantic. In the winter this anticyclone weakens and moves towards the equator and the low pressure Icelandic and Aleutian centres prevail in the north of the Atlantic. Due to the Coriolis Effect, the air flows clockwise around the Azores high pressure centre and counter clockwise around the Icelandic/Aleutian low-pressure centres. For this reason, in the mid-latitude Atlantic, the air flows from the west into Europe independently of the season. The pressure gradient between the two pressure centres determines the velocity of the westerly winds, with higher values attained during the winter (5m/s). The westerlies reach a maximum speed (up to 40m/s) at around 12km in the troposphere forming the westerly jet stream that flows from North America to Northern Europe (Hurrell and Deser, 2009).

The uneven solar heating of the planet is the origin of the Hadley cells that lead to subtropical jet streams and also the origin of the midlatitude transient eddies that lead to eddy-driven jets. Contrary to what is normal in other regions, during the European winter these two types of jet stream are separate from one another: in the latitude of northern Africa there is a subtropical jet stream and further north an eddy driven jet stream (Woollings, 2010).

European climate is particularly influenced by the Atlantic storm track. The path of the storms (atmospheric disturbances that last for days) travelling between North America and Europe is similar to the westerly jet stream (Hurrell and Deser, 2009; Woollings, 2010). Jet streams and storm tracks have the same origin (uneven heating of the planet) and they can be considered a complex self-maintaining system. The North Atlantic storm track is weaker during the summer, and points towards the British Isles independently of the season (Woollings, 2010).

During winter, in the troposphere of the northern hemisphere, there are two low pressure areas/troughs: northeast of Canada (the Icelandic/Aleutian low-pressure centres) and east of Asia, and two high pressure areas/ridges: west of Europe (the Azores high-pressure system) and western North America. These different pressure centres are shaped by the stationary waves that are formed by the different heating behaviour of ocean and continents and the existence of the Rocky and Himalayan mountain ranges. During summer, due to the more

uniform distribution of heat in the atmosphere, the pressure differences are milder (Hurrell and Deser, 2009).

Although these stationary waves are geographically bounded, they are not constant in time due to internal chaotic processes and different atmospheric heating patterns. One of the results of this variability are teleconnections, i.e. some regions will be affected by abnormal climate (e.g. climate drier than average) while other distant regions will be affected by the inverse anomaly (e.g. climate wetter than average) simultaneously. In the north Atlantic the most important teleconnection is the North Atlantic Oscillation – NAO (Hurrell and Deser, 2009). Another important teleconnection over the North Atlantic is the East Atlantic pattern but its correlation with rainfall in Iberia is very low or inexistent (Climate Prediction Center, 2011) and therefore only the NAO will be further analysed.

2.1.1.1 The North Atlantic Oscillation

The NAO index is defined as the anti-correlated pattern in sea level pressure (SLP) between the Azores and Iceland. This difference in SLP induces a north-south movement of the eddy driven jet (Woollings, 2010). During the positive phase of the NAO, the SLP is higher than average south of 55°N and lower than average throughout the Arctic (see Figure 2.1), with the main SLP anomalies occurring near Iceland and in the Iberian Peninsula (Hurrell and Deser, 2009).

The NAO is present all year but is much stronger during the winter, when it presents a northwest-to-southeast orientation. The NAO is weaker during the summer, when it is displaced towards the north and east. During spring and autumn it has an intermediate strength, presenting a south centre of action near the Azores in the spring and southwest-to-northeast orientation during autumn. Despite this relatively stable yearly spatial pattern, the NAO is highly variable, either considering a seasonal or a decadal time scale, and can change from a positive phase to a negative phase from one month to the next. The residence time and the amplitude of each phase define the longer-term time-average behaviour (Hurrell and Deser, 2009).

Figure 2.1 shows the four SLP weather regimes occurring in the North Atlantic during winter. The period and dataset do not seem to influence the spatial characteristics of these regimes (Casou *et al.*, 2004) but the period of analysis influences their frequency (Hurrell and Deser, 2009).

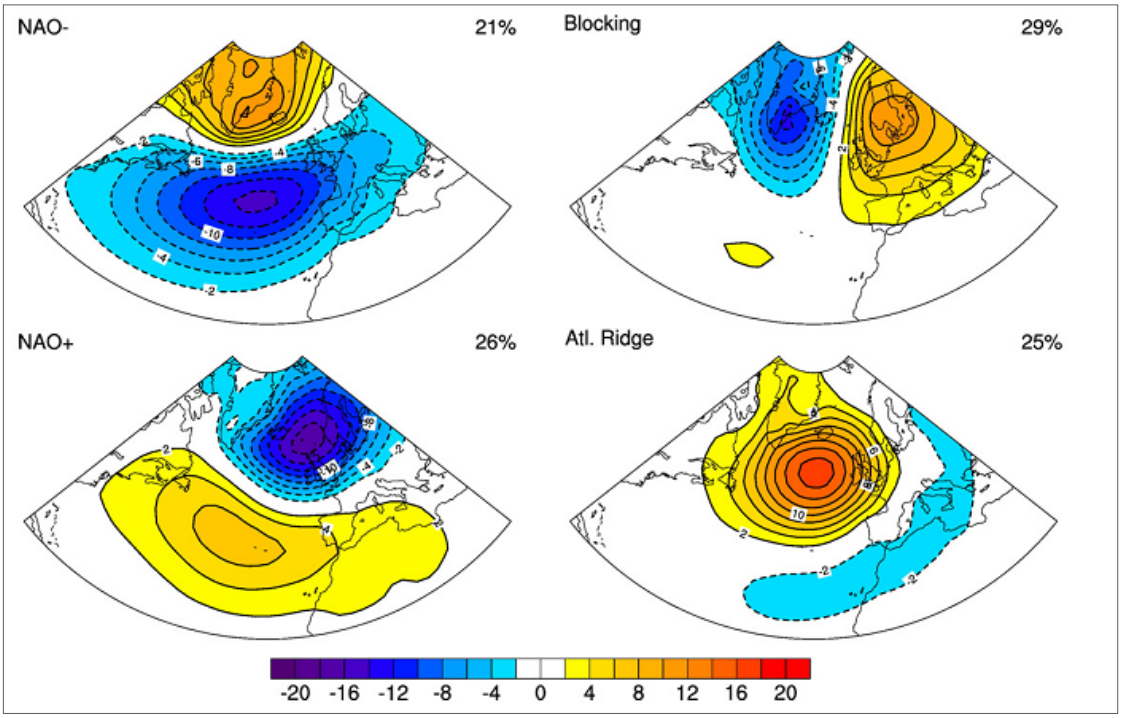

Figure 2.1 - Winter climate regimes in sea level pressure (hPa) over the North Atlantic based on daily data (1950 to 2006). The percentages convey the frequency of occurrence of each regime. The contour interval is 2 hPa (Hurrell and Deser, 2009).

The maps on the left in Figure 2.1 correspond to the negative and positive phases of the NAO. The upper right map describes a "blocking regime" where an anticyclone over Scandinavia blocks the prevailing westerly winds. This type of regime can persist for several days (sometimes weeks) and because it induces clear skies and often easterly winds, it causes cold snaps in the winter and heat waves in the summer (Woollings, 2010). The last map depicts a strong anticyclonic ridge off Western Europe which portrays the northward extension of the Azores high (Casou *et al.*, 2004).

It is evident from the percentages of each climate regime in Figure 2.1 that even though the NAO is the prevailing atmospheric circulation pattern over western Europe, the majority of winters cannot be defined just by the NAO (Hurrell and Deser, 2009).

The distribution of the winter NAO index is negatively skewed and negative NAO events exhibit enhanced persistence on the 10-day time scale when compared to positive NAO events. However, the NAO exhibited a positive trend from winter (DJF) 1957/58 to winter 2000/01 which resulted from an increase in regime loading/relative occurrence and also from a movement toward more positive values of the NAO index which is a change in the regimes themselves, with the centre of each regime shifted to higher values of the NAO index (Woollings *et al.*, 2010).

The 2007 IPCC report (Solomon, 2007) suggests that the NAO inter-decadal variability could be due to tropical and extratropical ocean influences, land surface forcing and other external factors. Woollings (2010) notices the lack of agreement in the scientific community over the reasons for the negative tendency of the NAO in the 1960s and the positive tendency in the 1990s; furthermore, he states that climate models are, in general, unable to simulate changes in the NAO as large as the ones observed and consequently the reliability of climate models for simulating the dynamics of the jet stream should be questioned.

Although normally the NAO is interpreted as a variation pattern in sea level pressures or as geopotential height anomalies, it can also be interpreted as the signal of combined variations in the strength and orientation of the Atlantic storm track and the associated eddy-driven jet (Woollings *et al.*, 2010). As can be seen in Figure 2.2, when the NAO index is positive a strong subpolar eddy-driven jet oriented southwest–northeast towards Europe coexists with a subtropical jet that develops over the subtropical North Atlantic. In this situation the surface westerlies are strong (Hurrell and Deser, 2009). When the NAO index is negative these two jet streams merge, forming one continuous jet across the Atlantic (Woollings *et al.*, 2010).

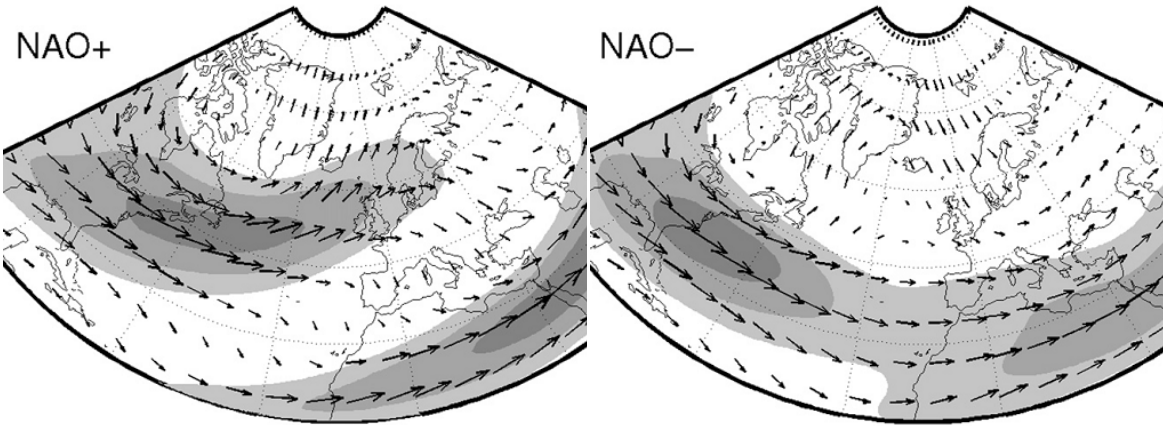

Figure 2.2 – Composites of the winter (DJF) 300-hPa wind field during positive and negative NAO days, using a threshold of one standard deviation of the standard NAO index. Isotachs are shaded at 20, 30, and 40 m/s (Woollings *et al.*, 2010).

The positive and negative phases of the NAO generate different intensities and positions of the jet stream affecting the storm track in the North Atlantic and the transport of heat and moisture. This affects temperatures and rainfall in western and central Europe (NOAA, 2008). During a positive phase of the NAO in the winter, the westerlies grow stronger, bringing warm moist maritime air over the North of Europe (IPCC, 2007) and therefore raising the temperatures and increasing the rainfall in the north of Europe and lowering the temperatures and decreasing the rainfall in the south of Europe (NOAA, 2008). Strong negative phases of the NAO have the opposite effect in the north and south of Europe due to a

weakening of the westerlies and their displacement towards the Iberian Peninsula (see Figure 2.3 for a schematic of impacts of positive and negaitive phases of the NAO).

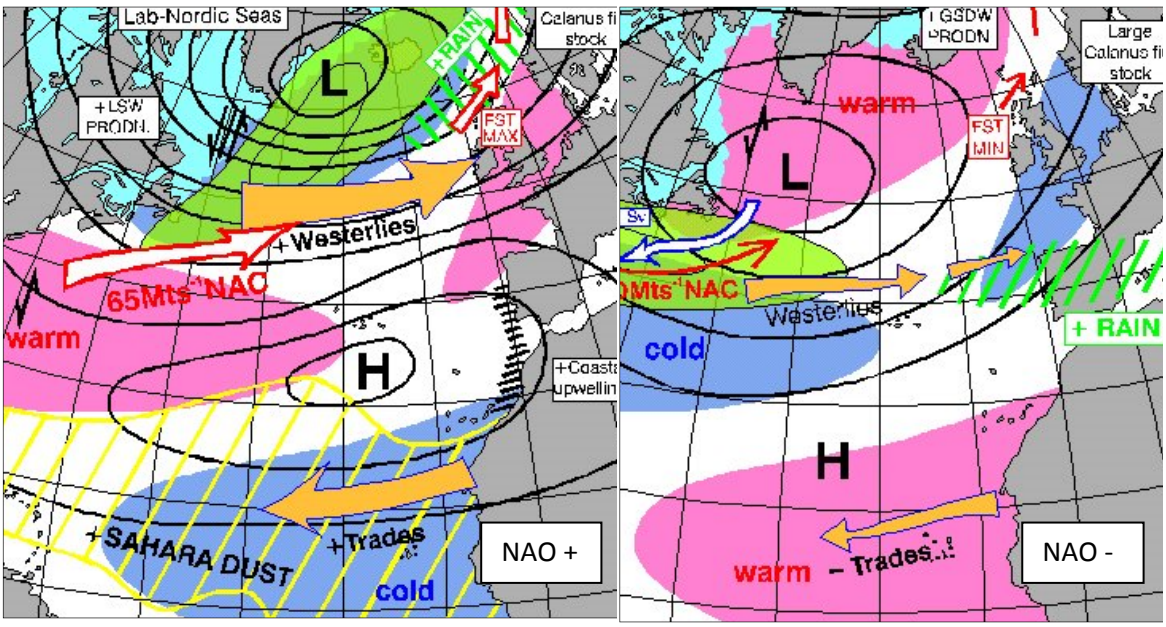

Figure 2.3 – Impacts of the different phases of the NAO (NAO+ in the left map and NAO- in the right map) in the North Atlantic and Western Europe for the winter (Dickson, 2010).

Figure 2.4 shows the impacts of the NAO on Europe for the winter months between 1958 and 1995. The maps show rainfall anomalies for winter months with high and low NAO index and their differences (significant at 1% level). For high NAO indices, Southern Europe has large areas with significant negative rainfall anomalies, which are especially strong in the Iberian Peninsula. The significant positive anomalies in Northern Europe are restricted to small areas in the UK, Scandinavia and the Benelux countries (Trigo *et al.*, 2004). For low NAO indices roughly the same areas are affected but with the inverse rainfall signal.

Rainfall anomalies between high and low NAO index periods calculated with NCEP-NCAR and with CRU datasets correspond very well in magnitude and geographical distribution (see Figure 2.4 c & f), both showing a maximum difference located over western Iberia of more than −2.5 mm/day (Trigo *et al.*, 2004).

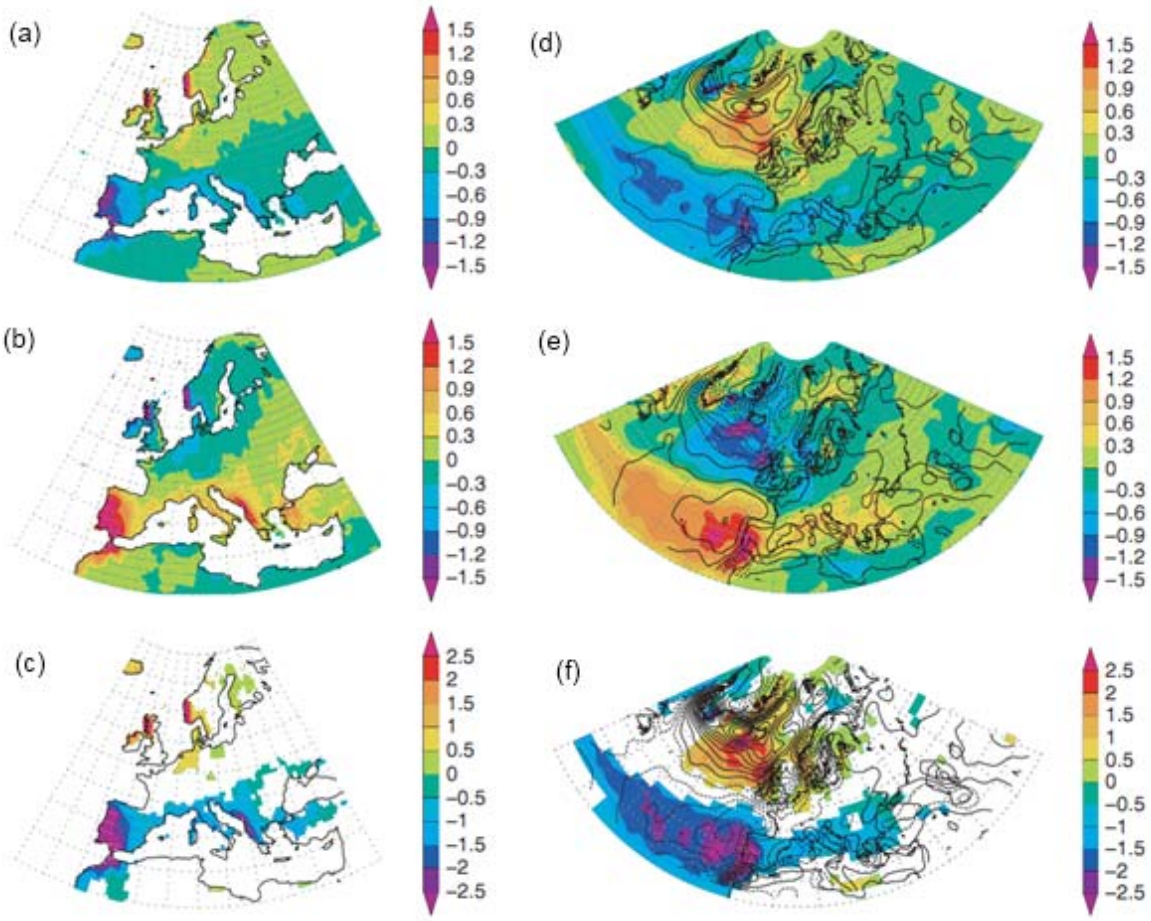

Figure 2.4 – Rainfall anomalies (mm/day) from CRU data (left) and NCEP-NCAR data (right) for winter months. (a) and (d) high NAO index >1.0, (b) and (e) low NAO index <−1.0 and (c) and (f) their differences (represented only if significant at the l% level) (Trigo *et al.*, 2004)

2.1.2 *Oceanic influences*

Europe is considerably warmer than other regions at the same latitude mainly due to the Gulf Stream and its North Atlantic Drift which bring warm water to the shores of Western Europe (see Figure 2.5.). This warm current is part of the Meridional Overturning Circulation (MOC) which is not well represented in current coarse-scale global climate models since many important physical processes occur at very small scales in the ocean (Woollings, 2010).

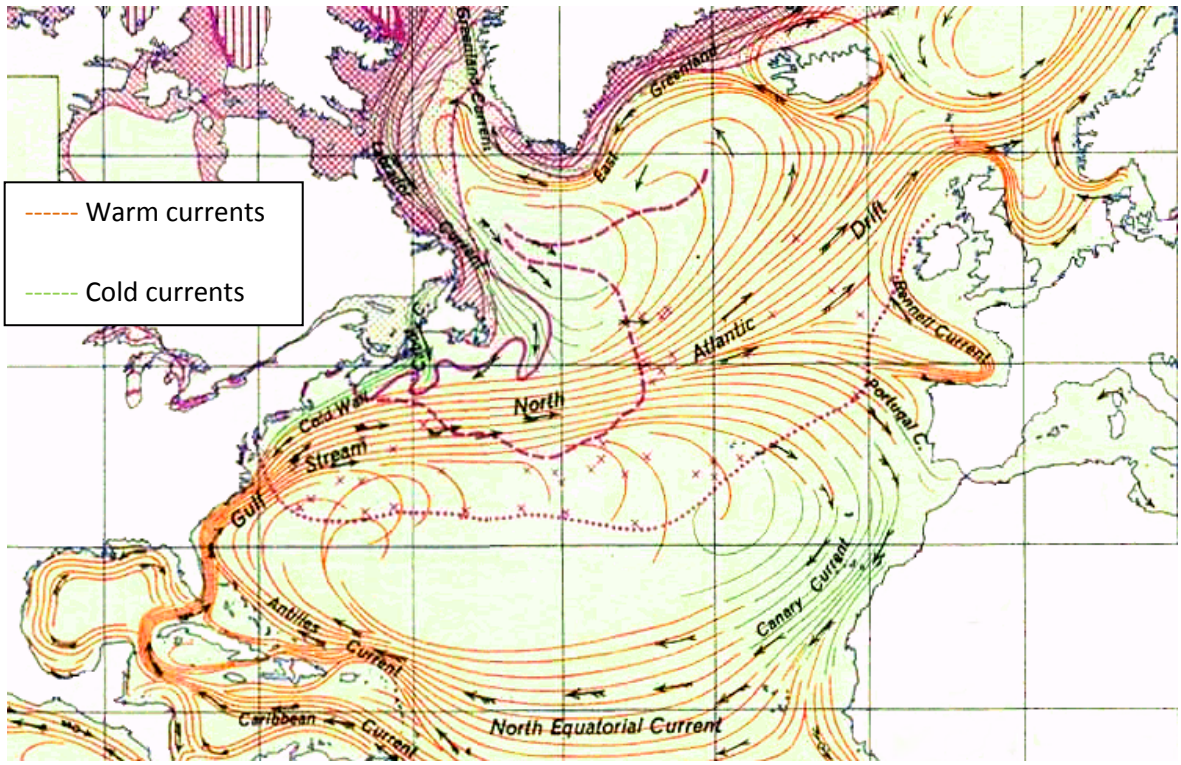

Figure 2.5 – Ocean currents atlas for the North Atlantic showing the Gulf Stream and the North Atlantic Drift (US_Army, 1943).

The North Atlantic has normal temperature oscillations (around one degree) between cold and warm phases that last from 20 to 40 years. This phenomenon is called the Atlantic Multidecadal Oscillation (AMO) and affects the climate of North America and Europe, with a positive AMO (warm ocean) increasing the rainfall in Northern Europe in summer (NOAA, 2005). Computer models are not yet able to simulate the behaviour of the AMO (NOAA, 2005). Nevertheless, no relevant connection has been found between the AMO and climate in Iberia.

2.2 Iberian climate

2.2.1 *The Iberian Peninsula*

The location of the Iberian Peninsula at the transition of the subtropical fringe and between the Atlantic Ocean and the Mediterranean Sea makes its climate a complex system, which is amplified by the effect of mountain ranges and a high mean altitude (González-Hidalgo *et al.*, 2010a), as can been seen in Figure 2.6.

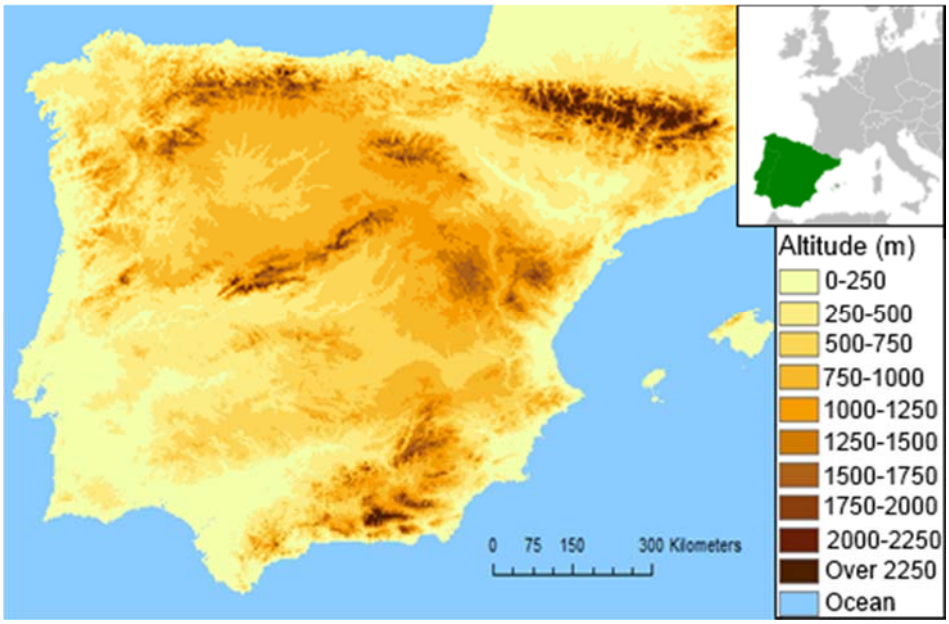

Figure 2.6 – Altitude map of the Iberian Peninsula.

The geographic position of Iberia and its large differences in altitude, give it a wide range of climatic conditions. Most areas are hot and sunny in summer, but in winter temperatures vary considerably, with coastal areas being milder. While in the north of Portugal and the northwest of Spain the climate is strongly influenced by the Atlantic, particularly in autumn and winter, in the South and Northeast of Spain the climate has a Mediterranean influence.

The Portuguese and Spanish meteorological institutes have divided Iberia according to the Köppen-Geiger climate classification system, producing the map in Figure 2.7. Regarding dry climates, hot and cold steppe (BSh and BSk) are widespread in the southeast of the Peninsula and the Ebro Valley. Also, small areas in the southeast of the Iberian Peninsula have been classified as hot and cold desert (BWh and BWk).

However, most of Iberia is classified as having a temperate climate (type C). The temperate with dry and hot summer climate type (Csa) covers approximately 40% of the peninsula, being particularly prevalent in the south and in the central plateau. The temperate with dry and temperate summer climate type (Csb) is common in the northwest of Iberia, most of the west

coast of Portugal, and several mountainous regions. The temperate without a dry season and with hot summer (Cfa) and temperate without a dry season and with temperate summer (Cfb) climate types are associated with mid-altitudes of several mountain ranges. The cold (type D) and Polar (type E) climates of the Köppen-Geiger climate classification in Iberia are present only in small areas and at high altitudes.

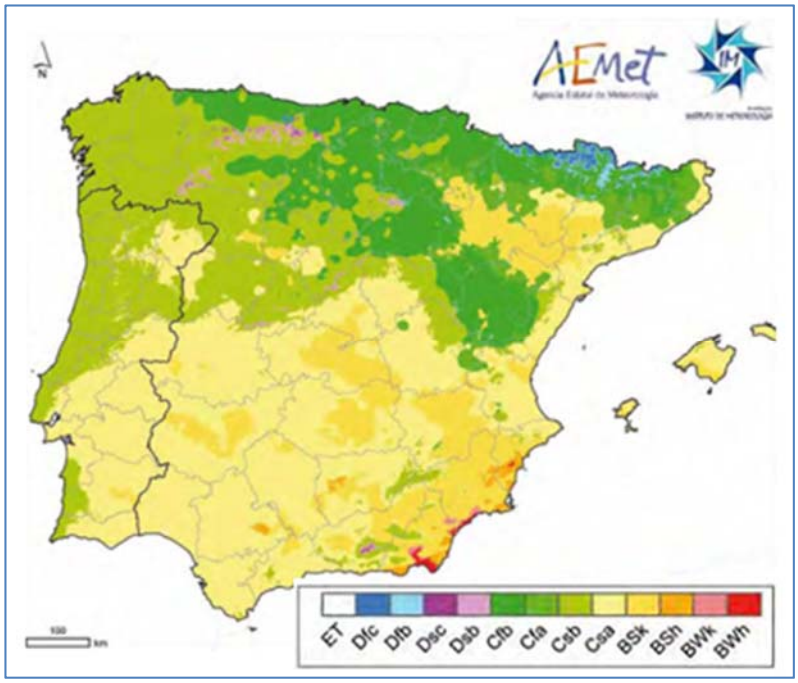

Figure 2.7 – Map showing the Köppen-Geiger climate classification for the Iberian peninsula and the Balearic Islands (IM and AEMET, 2011)

These different classifications reflect the significant variation in temperature and especially rainfall in the Iberia Peninsula.

2.2.2 *Temperature and rainfall variability*

Iberian mean annual temperatures vary from values below 2.5°C in the Pyrenees to values higher than 17°C in the south of Spain. Temperatures reach their maximum in the summer, especially in July and August, in some areas of the south of Spain. Minimums are felt in the winter between December and February at high altitudes (IM and AEMET, 2011) as can be seen in Figure 2.8.

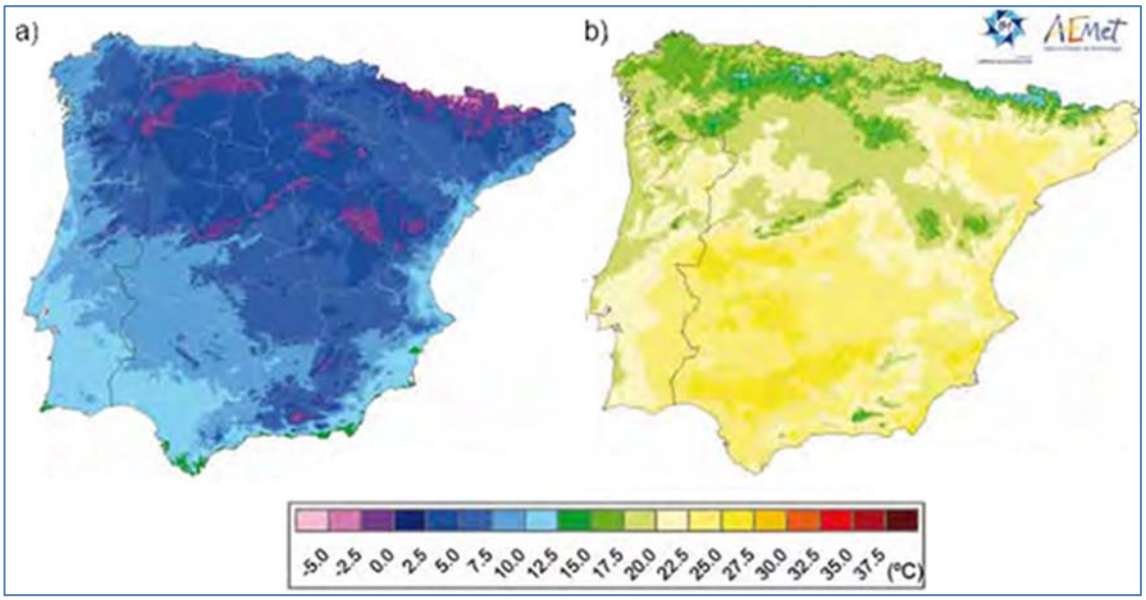

Figure 2.8 – Mean temperatures for Iberia (a) in the winter and (b) in the summer (IM and AEMET, 2011)

The rainfall regime in the Iberian Peninsula is highly variable in space and time. In the mountainous northwest the annual average rainfall is higher than 2200mm/year (see Figure 2.9), being one of the highest in Europe (Trigo and DaCamara, 2000). In contrast, some areas of the southeast coast of the peninsula have less than 300mm/year of rain (Trigo *et al.*, 2004).

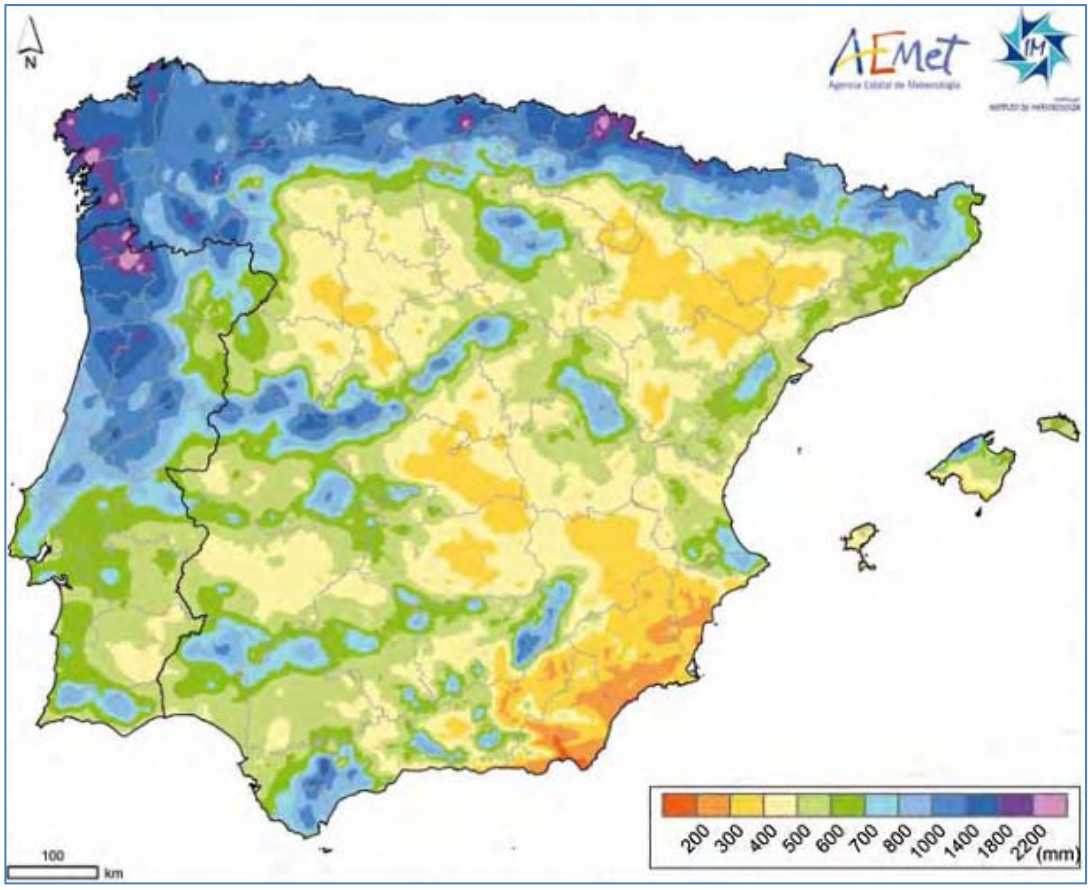

Figure 2.9 – Mean annual rainfall for Iberia (IM and AEMET, 2011)

December is the wettest month in Iberia with more than 300mm of rainfall falling in the northwest. The driest month is July, with monthly averages below 5mm occurring in some areas of the south of Portugal and Spain (IM and AEMET, 2011).

On the northern coast, rainfall is mostly due to meridional fluxes that the local orography forces to ascend and consequently produce rainfall. In the centre and west of Iberia rainfall is mainly produced by westerly air flows and is clearly influenced by the NAO. The Mediterranean coast is protected from the Atlantic influence by the central Spanish plateau, the Pyrenees, and also, by higher land that flanks this coast. In this region rainfall is mainly produced by easterly air flows and by convection (Rodrigo and Trigo, 2007).

The wet season in Iberia, when almost all the rainfall occurs, is between October and May (Trigo *et al.*, 2004). In the central and western regions of Iberia the maximum rainfall occurs from November to February and in the eastern parts there is an absolute maximum in autumn and a secondary maximum in spring (Paredes *et al.*, 2006). In parts of central Spain (see Figure 2.10) the maximum rainfall is in spring while summer is the wettest season in only a small area in the Catalan Pyrenees (Río *et al.*, 2010).

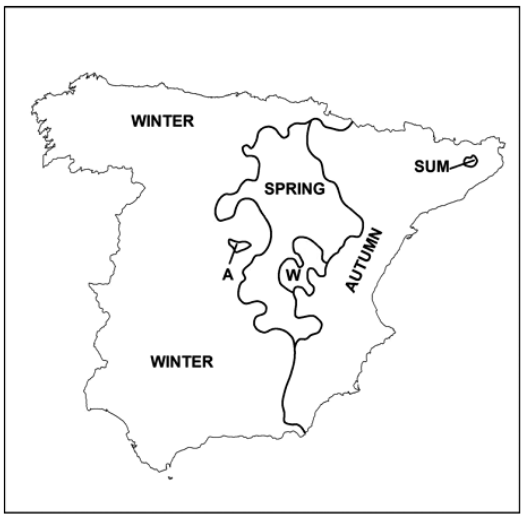

Figure 2.10 – Season with maximum rainfall (1961-2006) within different areas of Spain (Río *et al.*, 2010).

In the winter, the rainfall is controlled by the position and intensity of the Icelandic low and associated westerlies. This rainfall is increased by the passage of cold fronts associated with families of transient depressions, especially when the Icelandic low is strong and shifted south during a negative NAO. However, in the winter, most of the Iberian Peninsula can also be affected by northward extensions of the Azores anticyclone which steers polar continental mild and dry airflow (of tropical maritime origin) into Portugal (Trigo *et al.*, 2004). Also,

mesoscale convective systems produce high rainfall rates in the eastern part of Iberia (Paredes *et al.*, 2006).

The Azores anticyclone dominates the large-scale atmospheric circulation in Iberia during the summer. In its north-westerly position, it produces northerly or north-easterly winds that bring warm and dry air into Portugal (continental or maritime modified by continental influence origins). Regionally reinforcing this circulation pattern is the normal development of a thermal low, centred over the Iberian Peninsula (Trigo and DaCamara, 2000). The few rainfall episodes that occur in summer are normally explained by convective mesoscale systems (Rodrigo and Trigo, 2007). Due to the scarce summer rainfall in the Iberian Peninsula, trends and their significance are difficult to calculate and to assess, therefore the majority of papers dealing with Iberian rainfall do not present analysis for the summer season (Rodrigo and Trigo, 2007).

The marked seasonal character of the rainfall regime in Iberia makes spring and autumn transition periods between winter and summer. Early autumn is influenced by local convective storms, but from October onwards the westerly circulation types prevail (Rodrigo and Trigo, 2007).

2.2.3 *Interannual variability and trends in rainfall*

In Iberia a few daily events can significantly change monthly, seasonal and annual rainfall making the interannual variability very high (González-Hidalgo *et al.*, 2010a). This strong interannual variability, with very wet and very dry years occurring frequently, represents a major problem for water management, particularly in areas where demands on water supply (especially from domestic and agricultural sectors) are higher than water availability (Paredes *et al.*, 2006).

Contrary to the spatial distribution of rainfall and its seasonal variability, interannual variability cannot be explained by broad characteristics of the global circulation and regional climate factors, like the latitude, orography, oceanic and continental influences (Trigo and DaCamara, 2000). Large interannual variations in the flow regimes of all Iberian rivers, especially those located in the southern, drier areas, are driven by temporal rainfall variability. A small number of large-scale atmospheric modes, and in particular the NAO, can explain most of the rainfall occurring in Iberia during the wet winter season and several studies have shown that river flows tend to be lower (higher) when the NAO index is in its positive (negative) phase. However the strength of the correlation between the NAO and local (or regional) climate variables in Europe has recently been shown to be non-stationary (Trigo *et al.*, 2004).

In Iberia monthly and annual rainfall values may conceal very different rainfall regimes on the daily scale. The occurrence, or not, of a day with high rainfall can change the character (dry or rainy) of any given month, season, or year, especially in the southern and eastern sectors of Iberia. Rodrigo and Trigo (2007) studied daily rainfall at 22 sites (15 meteorological stations in Spain and 7 in Portugal) between 1951 and 2002. They calculated annual and seasonal total rainfall (P), number of wet days (N), rainfall intensity (I), the rainfall 95th percentile (P95), and percentage of rain falling on days with rainfall above the 95th percentile (%). The annual and seasonal trends were analysed, using the Mann–Kendall statistic, and a linear regression model. A t-test was applied to the difference between the means of two sub periods (1951–1976 and 1977–2002). The 95th percentile was determined by fitting an appropriate gamma distribution to the daily data.

Variations in total rainfall can be caused by a change in the frequency of rainfall events, or the intensity of rainfall per event, or a combination of both. Rodrigo and Trigo (2007) found a decreasing trend in the intensity of daily rainfall in some stations, but no significant change in the number of wet days, concluding that there is a decreasing trend in the amount of rainfall on wet days. In winter, several northern and southern stations revealed a decreasing trend in P, I, and P95. In spring some southern stations showed decreasing trend in P, I, and P95, showing also a decrease in I and P95 in summer. Some northern and southern stations in autumn had a decrease in I. Significant trends for extreme rainfall (measured by P95 and %) were only found in a few stations.

In some of the locations where a decreasing trend in the daily intensity of rainfall was found, the trend can be related to the predominance of the positive phase of the NAO during the later time period. Figure 2.11 shows the spatial pattern of correlation coefficients between the NAO index and daily rainfall indices for winter, the only season where the correlation was significant (Rodrigo and Trigo, 2007).

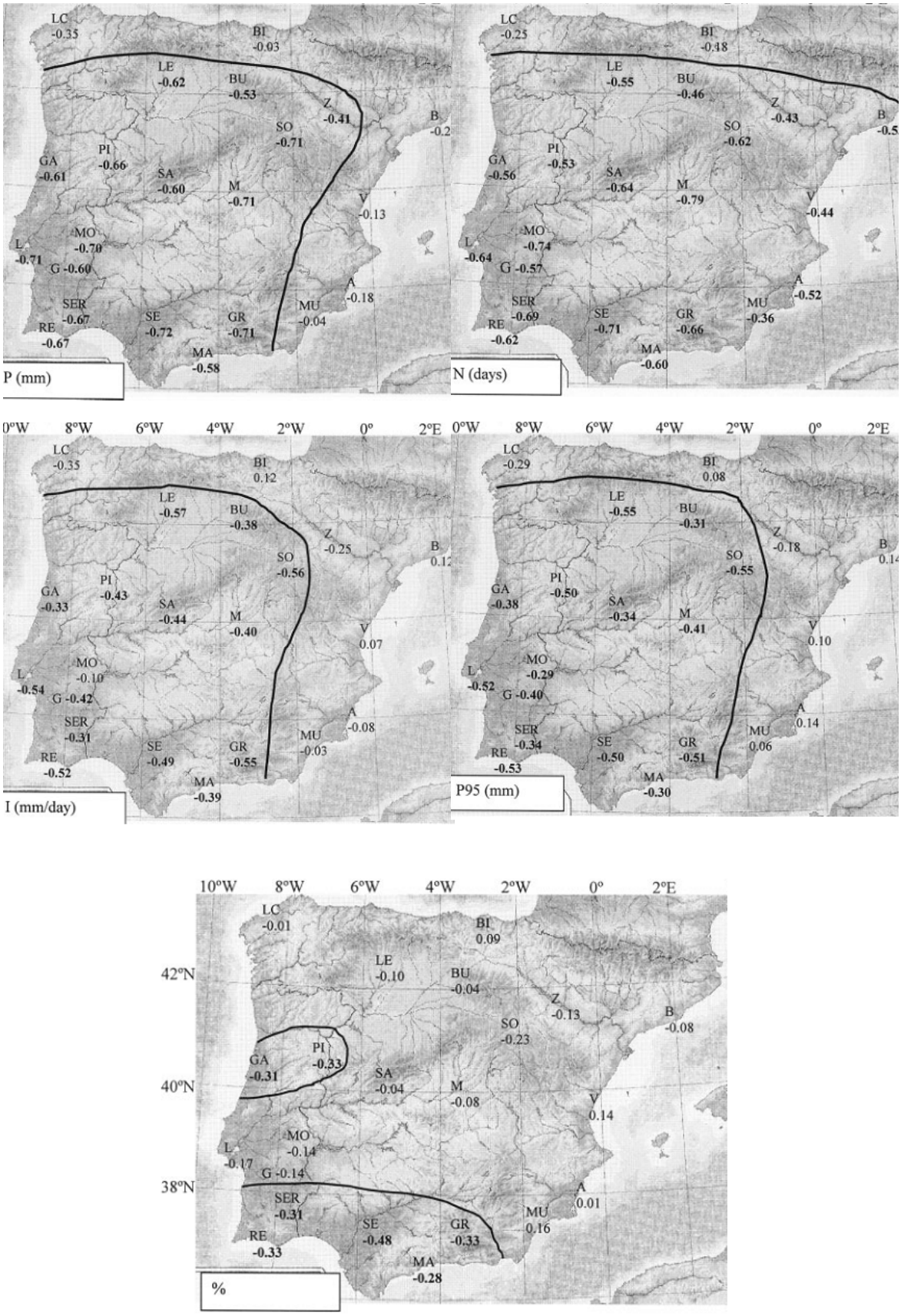

Figure 2.11 – Correlation coefficients between NAO index and winter rainfall indices: annual and seasonal total rainfall (P), number of wet days (N), rainfall intensity (I), the 95th percentile (P95), and percentage of rain falling on days with rainfall above the 95th percentile (%). Numbers in bold represent coefficients significant at the 95% confidence level. The continuous line divides areas with significant correlations from areas where the correlation is not significant (Rodrigo and Trigo, 2007).

The negative correlation coefficients for total winter rainfall were only significant in central and western areas of Iberia. The decreasing trend (mostly non-significant) detected in many southern and central stations may be partially related to the NAO influence; however, the significant decrease in BI (Bilbao) does not seem to be related to NAO fluctuations. In terms of the number of wet days, the significant coefficients extend to the Mediterranean coast. So the positive phase of the NAO is related to a decrease in the number of wet days all over the country, except in the north coast. The area where intensity (I) is directly influenced by the NAO is the central and western part of the Peninsula, indicating that, although the number of wet days may be related to the NAO on the Mediterranean coast, other mechanisms are responsible for the daily intensity in this area. The 95th percentile figure (P95) shows a spatial pattern similar to that corresponding to P and I. Only the south-western stations (and GA – Gafanha and PI - Pinhel in Portugal) showed significant correlations between the NAO index and %. If we accept that % is a measure of extreme events, these results seem to indicate that the NAO index governs rainfall fluctuations (number of wet days, intensity) over a large part of the Peninsula, but only in southern areas does it seem to influence the extreme episodes significantly (Rodrigo and Trigo, 2007).

Trigo and DaCamara (2000) state that rainfall regimes in Portugal are not controlled only by the NAO. They characterized the daily atmospheric circulation affecting Portugal using a set of indices associated with direction and vorticity of geostrophic flow over an area covering the Iberian Peninsula. Studying the winter in the cities of Coimbra (Central Portugal) and Mertola (South Portugal) on a daily basis between 1957 and 1986 they found the most frequent circulation weather type (CWT) to be the anticyclonic, which was associated with very dry conditions. Almost two thirds of the observed rainfall in winter was due to cyclonic (C), westerly (W) and south-westerly (SW) CWTs (which occurred in less than one third of all observed days). Homogeneous distribution of rainfall over Portugal was related to the cyclonic CWT, while the CWTs with an Atlantic origin (W, SW and NW) explained the decrease in rainfall from North to South. For spring and autumn similar results were obtained. Trigo and DaCamara (2000) also concluded that dry (wet) months were associated with low (high) monthly frequency of wet CWTs. In Figure 2.12 it is clear that the interannual behaviour of precipitation and wet CWTs is extremely similar (correlation coefficient of 0.88).

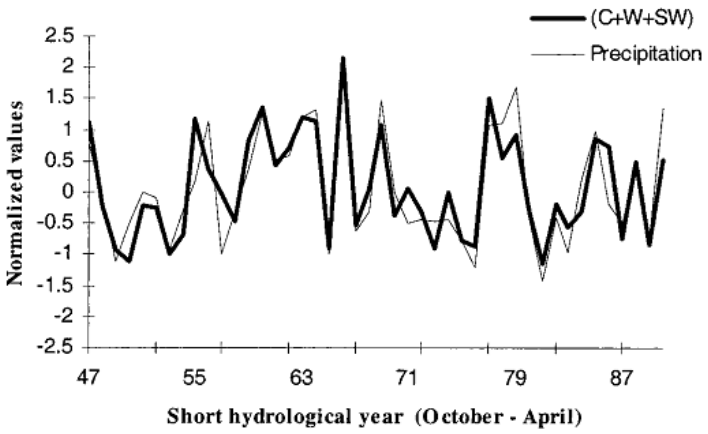

Figure 2.12 – Total number of days from the classes cyclonic (C), westerly (W) and southwesterly (SW) and normalized values of rainfall for the period between 1945 and 1990 using a short hydrologic year (Trigo and DaCamara, 2000).

Several studies have shown a decline in winter/spring rainfall during the twentieth century in the northern Mediterranean Basin; in the western sector this trend is especially visible in March (Paredes *et al.*, 2006; Río *et al.*, 2010; Gonzalez-Hidalgo *et al.*, 2010b; Paulo *et al.*, 2012) when water is most needed for spring plant growth. Paredes *et al.* (2006) used daily rainfall data to perform a sub-monthly analysis, concluding that the trend was roughly confined to the month of March and that the regions affected by significant changes were the central and western sectors of the peninsula (see Figure 2.13).

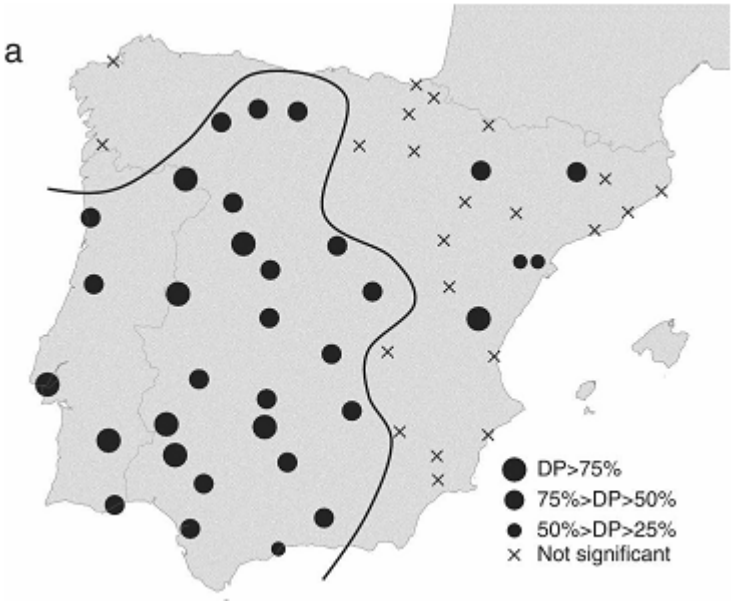

Figure 2.13 – Decreasing rainfall (DP) trends in March (1941–97). The dots represent stations with significant (0.10 level using Mann-Kendall test) declining rainfall, the different sizes of black dots depict the relative change in rainfall. The cross signs correspond to non-significant or positive trends (Paredes *et al.*, 2006).

The magnitude of the March rainfall monotonic decrease was about 50% (40 mm) over four decades, starting in the early 1960s (Paredes *et al.*, 2006). Figure 2.14 shows that March has the highest decrease in rainfall of all months. The small increases in January and December are offset by corresponding decreases in February and September. Therefore the annual decrease of average rainfall in this region is related to the strong decrease observed in March so the inclusion of this month in winter or in spring seasonal averages will impact dramatically on the computation of trends for those seasons (Paredes *et al.*, 2006).

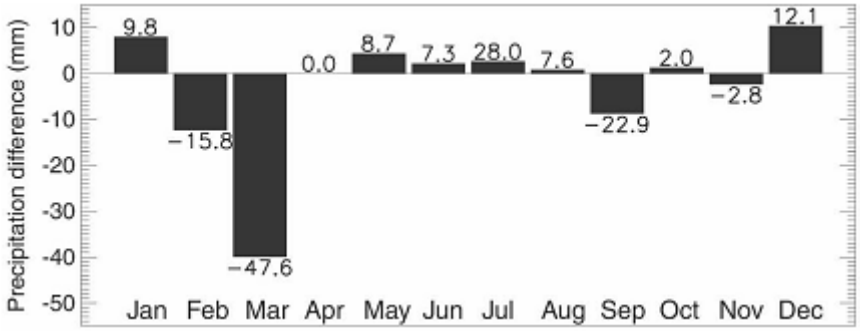

Figure 2.14 – Absolute rainfall change (mm) between the 1941–70 and the 1971–97 normal periods and corresponding relative change (%), indicated over (or below) each column (Paredes *et al.*, 2006).

Using circulation weather type (CWT) classifications, Paredes *et al.* (2006) found that, for March, three CWTs (C, W, and SW) account for most of the rainfall (between 50% and 75%) although only 28% of the days were classified as belonging to one of these types (which is consistent with the results of Trigo and DaCamara (2000) for winter). These "wet" CWTs showed a decreasing trend in frequency of occurrence for the month of March, while the dry anticyclonic CWT showed an equivalent increase. This shows that low pressure systems and their associated fronts have become less frequent in March over the Iberian Peninsula during the four decades starting in the early 1960s.

The analysis of the CWTs also shows that for the stations with strong decreasing rainfall trends in March, the rainfall is always dominated by types C and W (and to a lesser extent SW or NW types) confirming that the air masses with Atlantic origin account for the bulk of March rainfall. Rainfall in the stations without significant rainfall trends is mostly associated with Mediterranean airflows and, as expected, the frequency of such CWTs in March does not present a significant trend in the last four decades (Paredes *et al.*, 2006).

When analysing rainfall trends for March in Europe from 1960 to 2000 using the CRU monthly rainfall dataset, Paredes *et al.* (2006) found that the Mediterranean Basin and in particular the Iberian Peninsula showed a large continuous negative trend (see Figure 2.15). Northern Europe showed significant positive trends, which extend from Ireland and Scotland to the

Scandinavian Peninsula. Analysing CWTs for the UK, Paredes *et al.* (2006) found significant decreases in the dominant dry CWT (anticyclone) and increases of wet CWTs C, W, and SW, exactly the opposite of the results for the Iberian Peninsula.

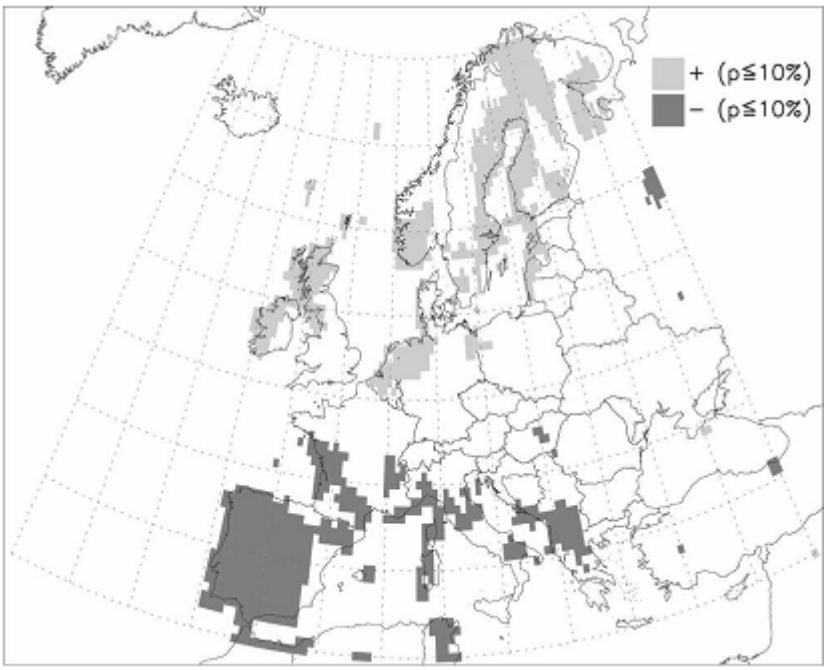

Figure 2.15 – Rainfall trends for Europe in March from 1960 to 2000, using CRU monthly rainfall dataset. The trends were assessed using the Mann-Kendall test and only the significant values (0.10 level) are shown. Light (dark) cells corresponding to positive (negative) trends (Paredes *et al.*, 2006).

These opposing results for north and south Europe suggest a change in the Atlantic storm track behaviour. Indeed Paredes *et al.* (2006), studied the average number of cyclones detected in March for the period 1960–2000 and found a strongly significant decline of cyclones centres from the Azores to Iberia and a significant positive trend over the northern Atlantic (between Greenland and Scandinavia). The NAO index for March presents a significant positive trend over the time period, which explains the storm track behaviour and the declining (increasing) frequency of wet CWTs over Iberia (United Kingdom/Ireland). Furthermore, in Iberia the region displaying the maximum correlation values between NAO and March rainfall is roughly the same one that presents the largest changes in rainfall.

González-Hidalgo *et al.* (2010a) conducted a similar analysis of trends in Spanish rainfall over the 1964-2005 time period. To do this they compiled the MOPREDAS database by collating all the data from the Spanish meteorological institute (AEMET), submiting it to quality control (suspicious data identification and inhomogeneity detection) and missing data reconstruction to achive 2670 monthly series from 1964 to 2005. The data was then interpolated to a regular grid (1/10°) and trends were analysed (using least squares methods and Mann-Kendall test for

significance). The trend analysis showed a high spatial and temporal variability on a monthly scale with consecutive months exhibiting different trends and the spatial distribution of signals varying significantly from month to month. Therefore caution must be exercised when interpreting seasonal or annual trend analyses for Iberia.

The trends detected were only significant for three months: March, June and October. The rainfall decrease detected in March affects 68.9% of Spain with likely probability ($p < 0.10$) and 57% with extremely likely probability ($p < 0.05$) and is especially evident along the central and southwest Iberia where the decrease reached up to −22% per decade (see Figure 2.16). In June there was also a negative trend in rainfall ranging from −5to −15% per decade and affecting 31.8% of Spain ($p < 0.10$). In October there was a positive trend that affects with very likely probability ($p < 0.10$) 33.7% of land, with increases between +15% to +10% per decade (González-Hidalgo *et al.*, 2010a)

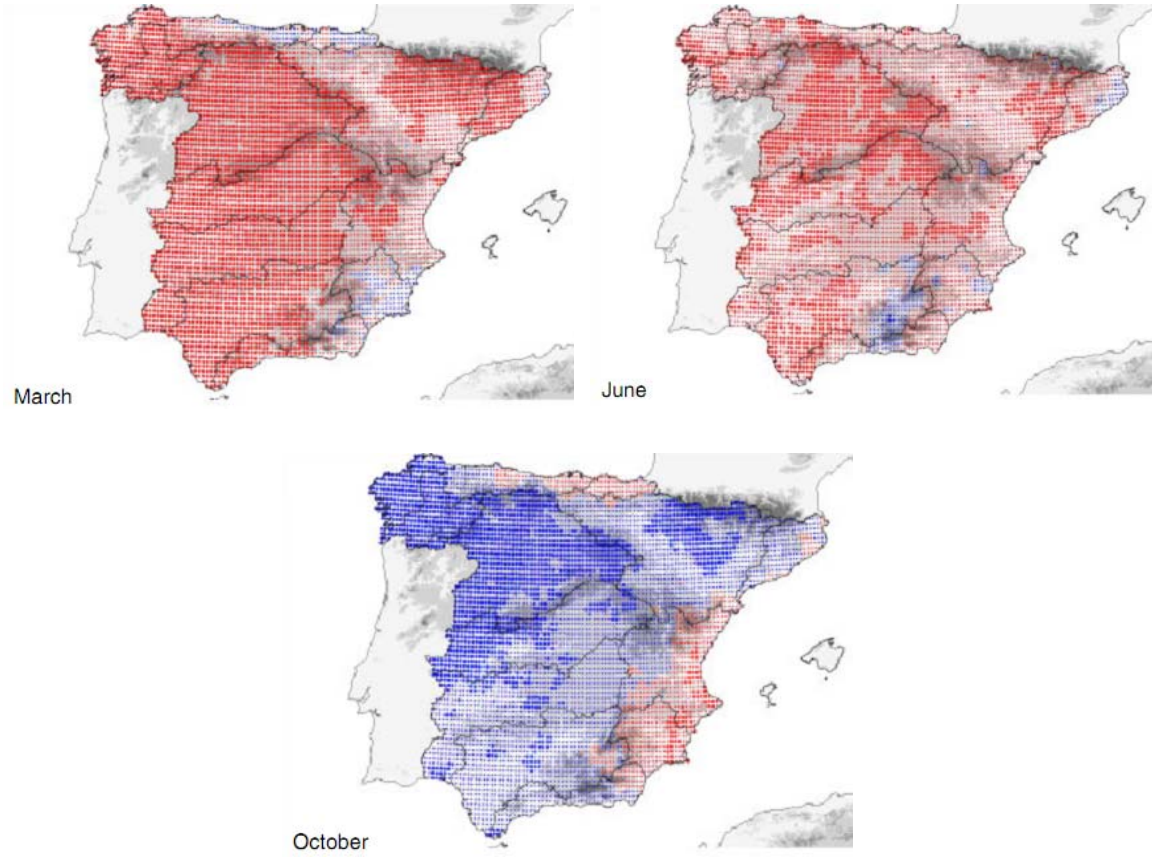

Figure 2.16 – Monthly distribution trends for March, June and October (months with significant trends). Dot sizes represent two different p levels: $p > 0.10$ (smaller dots) and $p < 0.10$ (bigger dots), blue represents positive trend and red negative trend (adapted from González-Hidalgo *et al.*, 2010a)

Río *et al.* (2010) have also analysed 553 monthly series from the Spanish meteorological institute (AEMET) for the period 1961–2006. These stations were selected based on

homogeneity (non-parametric Kruskal–Wallis test), length and completeness of records (less than 3% of missing values). For trend analysis, both linear and non-parametric models were used. The least squares method was used to calculate the magnitude of the trends, and the Mann-Kendall test was used for significance analysis.

Figure 2.17 shows the percentage of Spain with significant positive and negative trends per month, per season and per year from Río *et al.* (2010). Rainfall was found to have significantly decreased in February (in more than 60% of Spain), March (>10%) and June (>40%). Positive trends were mainly detected in August (>5%) and October (>20%). These monthly trends are shown spatially in Figure 2.18. Winter and summer showed significant decreases in rainfall in around 30% of Spain, spring in less than 5% while autumn showed a significant increase in less than 5% of the country. On a yearly scale the rainfall was showed to be significantly decreasing in more than 10% of the country.

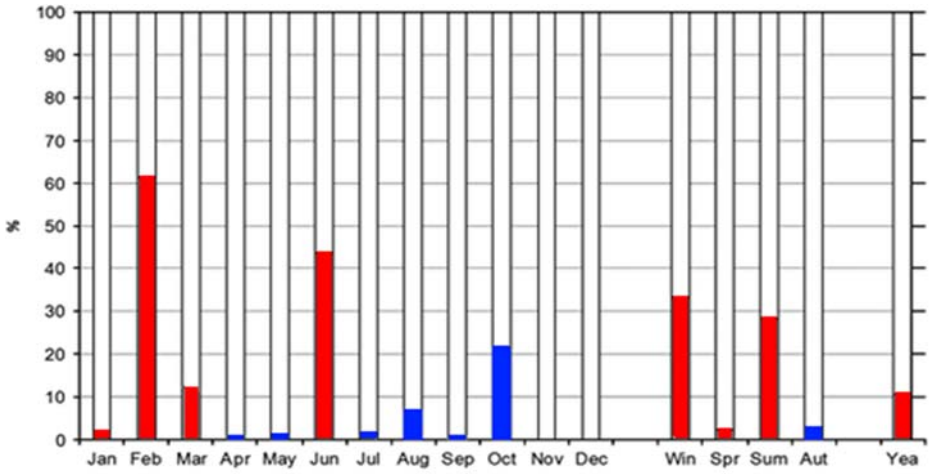

Figure 2.17 – Percentage of Spain with negative (red) and positive (blue) trends in rainfall for the period 1961–2006 at a confidence level of 95% (Río *et al.*, 2010).

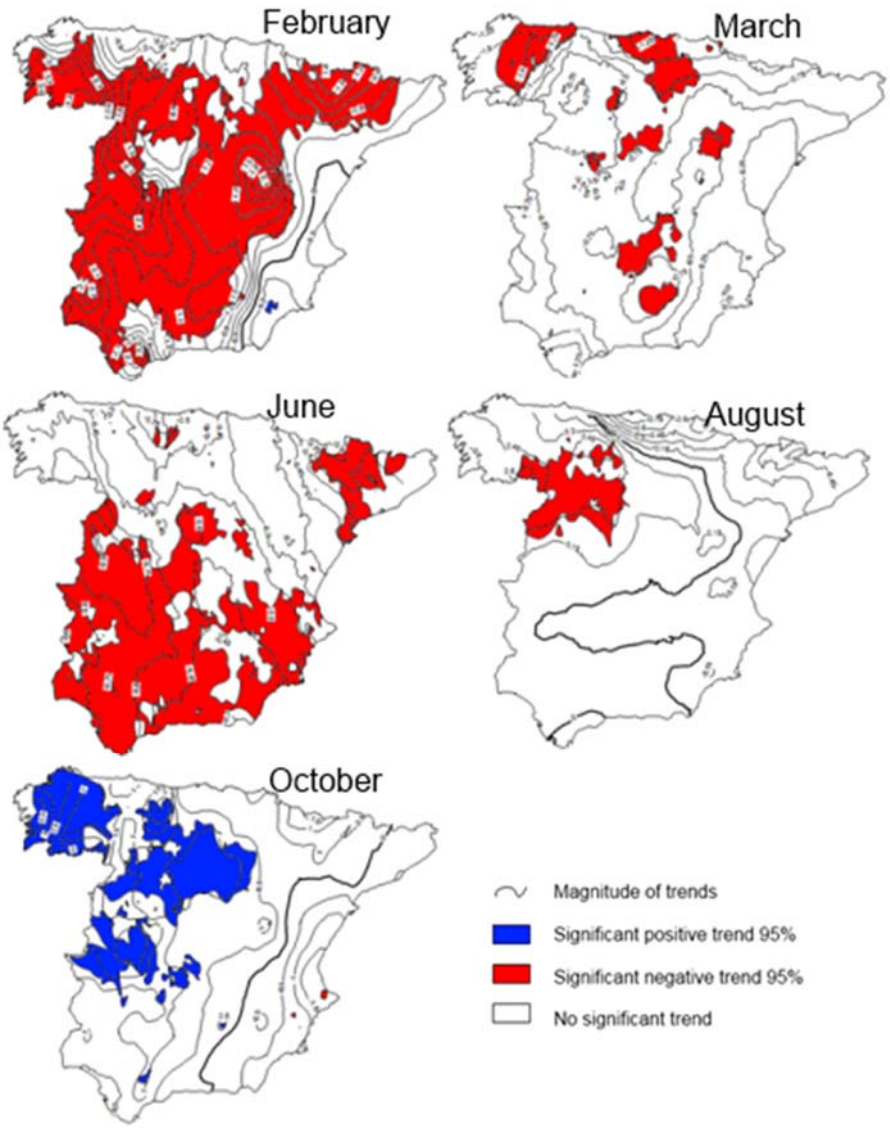

Figure 2.18 – Spatial distribution of rainfall trends in Spain from 1961 to 2006 for months with significant trends in considerable parts of the country, generated with geostatistical techniques. Areas superimposed to the contour maps shaded in blue (red) represent zones with significant positive (negative) trends at a confidence level of 95% (Río *et al.*, 2010).

According to Río *et al.* (2010), there has been a recent shift to February of the strong decrease of March rainfall stated by several authors for the second half of the 20th century. Also they point out that a change in the seasonal rainfall regime in Spain will happen if the current trends of increasing rainfall in autumn and summer in the north-western territories (where winter is the wettest season) and increasing rainfall in spring and winter in eastern areas (where autumn is the wettest season) continue.

The magnitude of the trends was not presented in Río *et al.* (2010) which hinders a comparison of this study to that of González-Hidalgo *et al.* (2010a). It is however interesting that they analyse almost the same period of AEMET data (1961–2006 and 1964-2005) and arrive at significantly different conclusions, especially considering the month where the

decrease in rainfall is more widespread (February or March) and the different geographic location of the June rainfall significant decrease.

Costa and Soares (2009) analysed 107 daily rainfall series of stations located in the South of Portugal and selected 15 stations with homogeneous daily records in the period 1955-1999 for temporal pattern analysis using six rainfall indices described in Table 2.1.

Table 2.1 – Acronyms and definitions of the six rainfall indices used by Costa and Soares (2009).

Acronyms	Explanation	Units
SDII	Ratio between the total rain on wet days and the number of wet days (R ≥1 mm).	mm
R5D	Highest consecutive 5-day precipitation total.	mm
R30	Number of days with daily precipitation totals above or equal to 30 mm.	Days
CDD	Maximum number of consecutive dry days (R <1 mm).	Days
FDD	Number of dry spells (consecutive period with at least 8 dry days, R <1 mm).	Freq.
AII	Ratio between the total rain on dry days and the number of dry days (R <10 mm).	mm

With the exception of the AII Index, there was no spatial consistency and/or significant trend in the rainfall indices calculated. From 1955 to 1999 the AII index showed a negative trend, meaning that the aridity increased over most of the study region (Costa and Soares, 2009).

Using a moving window technique with a life span of 5 to 10 years, Costa and Soares (2009) showed an increase in the rainfall intensity (R5D index). The rainfall intensity on wet days (SDII) and the frequency of extremely heavy rainfall events (R30) showed cyclic patterns and different trend signals at the local scale. An analysis of the standard deviations showed that extreme rainfall variability is higher in recent times.

In the southern half of the Iberian Peninsula, the 2004/05 drought was particularly severe with rainfall dropping to 45% of the normal rainfall between October 2004 and June 2005 and many stations having their driest year on record (García-Herrera *et al.*, 2007). According to García-Herrera et al. (2007), from November to January a positive NAO (0.7, 1.2 and 1.5 respectively) was responsible for the lower than average rainfall. In February it was due to a negative EA pattern (-1.7). In March none of these teleconnection patterns can explain the low rainfall levels; a negative NAO index (-1.8) increased the number of cyclones in lower latitudes, but an Atlantic block of anomalous intensity and southward extension induced the low rainfall records. Also, with the important exception of October 2004, almost no storm tracks hit Iberia during this winter, which can be explained by a very high frequency in blocking events and the positive NAO.

2.2.4 *Interannual variability of discharge*

Lorenzo-Lacruz *et al.* (2012) studied stream flows in the Iberian Peninsula between 1945 and 2005 and found decreasing trends in annual, winter and spring flows and increasing trends in the summer. The decreasing trends are stronger in the south/south-west basins and there is a strong SW-NE gradient. They are closely related to rainfall decreases observed in March and February and decreases in winter snow accumulation, and may have been exacerbated by:

- filling of reservoirs in the wet season;
- increases in forested land and expansion of irrigated areas (irrigated area in Spain increased from 1.3 million ha in 1940 to 3.7 million ha in 2004, representing 80% of total water consumption);
- population increases (from 26.0 million people to 44.1 million in Spain, and from 7.7 million to 10.5 million in Portugal for the period 1940 to 2005);
- growth in tourism, especially in the south of Iberia.

The positive trends in the summer are related to reservoir operations. Inter-basin water transfers have also affected basins by disrupting the natural water balance and creating new hydrological cycles, especially in the Tagus-Segura area.

Trigo *et al.* (2004) found high anti-correlations between winter month discharges (DJFM) in the Douro, Tagus and Guadiana rivers and the NAO index (the highest being found in the period 1973 to 1998: −0.76 for the Douro, −0.77 for the Tagus and −0.79 for the Guadiana) that tended to increase from north to south. Although the anti-correlation values are highly significant, the river flows of Guadiana and Tagus did not reduce as much as would have been predicted from the high NAO index values in the 1980s and 1990s. This could be due to the large increase in storage volume capacities of the large Spanish dams constructed in the middle and upper sections of both rivers (Trigo *et al.*, 2004).

The irregular spatial and temporal pattern of rainfall over Iberia has resulted in a complex network of dams and channels to optimize the storage and use of available water resources (especially in the southern basins) with the number of major reservoirs increasing from 58 in 1900 to 1195 in 2000, resulting in a total storage capacity of 56 500 hm^3 (Lorenzo-Lacruz *et al.*, 2012)

2.3 Summary

A characterization of Iberian climate was performed. Special attention was given to rainfall due to its spatial, seasonal and interannual variability. The Iberian rainfall spatial distribution was described, with its wet northwest – dry southeast gradient. The seasonal rainfall patterns of the study area were also characterized, with its wet winter and dry summers. Furthermore, the high interannual variability of rainfall was described. Studies performing trend analysis of Iberian rainfall were introduced, with a focus on the negative trend found by several authors for March's rainfall. The impact of the North Atlantic Oscillation on Iberian rainfall, droughts and the discharges of the Douro, Tagus and Guadiana was also explored. And the next chapter, *Chapter 3 – Historical Rainfall Analysis,* will build on the rainfall characterization and its correlation with the North Atlantic Oscillation.

Chapter 3. Historical Rainfall Analysis

This chapter presents an analysis of changes in rainfall records from the basins of rivers Douro, Tagus and Guadiana for the period 1961 to 2009 (therefore extending the period of analysis of the previous studies introduced in Chapter 2). Another distinctive point, related to those previous studies, is the inclusion of change point analysis (to detect abrupt changes in rainfall) as well as trend analysis (both performed using non-parametric tests: Pettitt, cusum and Mann-Kendall) and the assessment of field significance.

After a brief introduction (section 3.1), the rainfall and NAO index datasets used are characterized in section 3.2. Section 3.3 describes the applied testing strategy, which accounts for changes (at a point or trend) as well as autocorrelation and spatial correlation and the correlation and synchrony of changes between rainfall and the NAO index.

Significant results for autocorrelation, change points and trends (in the mean and variance) and correlations with the NAO Index are discussed in Section 3.4. A detailed analysis of the changes occurring in the months of February, March and October is also presented. The chapter ends with the identification and interpretation of the important results and their implications for the rest of the thesis.

The work presented in this chapter was performed with the guidance of Dr Francesco Serinaldi and was published in the International Journal of Climatology under the title “Analysis of time variation of rainfall in transnational basins in Iberia: abrupt changes or trends?” (DOI: 10.1002/joc.3669)

3.1 Introduction

The detection of changes in rainfall time series is of great importance for establishing the validity of the data set for frequency analysis or use in subsequent water resource and hydrologic modelling studies. Rainfall time series often show complex variability and the effects of autocorrelation and seasonality can be easily confused with changes in the mean or variance. Such changes may be in the form of trends over some period in time or of a more abrupt nature (a change point) and a detection methodology must be carefully designed to take account of both of these mechanisms. In order to reliably interpret such variability and/or changes, knowledge of the underlying processes and potential causes of variability are invaluable.

The motivation for this chapter was to understand the nature of spatio-temporal variation in rainfall over Iberian basins over the historical period (1961 to 2009) with a view to characterising the rainfall regime to allow further modelling and provide a context for study of future climate change. Our objectives were:

- To investigate the nature of time variations in rainfall in Iberia, distinguishing between abrupt changes (change points/step changes) and trends if present;
- To demonstrate the use of a range of statistical tests for change points and trends, identifying instances of agreement and discrepancy;
- To demonstrate the effects of space and time correlation in limiting the detection of change points and trends.

A full geographic context is used across three important transnational basins: Douro, Tagus and Guadiana. Both changes in the mean and in the variance of rainfall will be analysed because changes in the variance are important for extreme events. The impact of the changes' shape on the quantification of the magnitude of the change is studied due to its importance to water resources management. Comparisons with a large scale circulation index are carried out in order to give a climatological context.

Fatichi *et al.* (2009) point out that stochastic behaviour of a time series can sometimes be interpreted as an apparent deterministic trend due to long-range dependence (also referred to as long term memory or long-term persistence). However, due to the short time-series available and the motivation for this analysis, long-range dependence will not be analysed.

There are several statistical tests that can be used to assess changes. In this study only non-parametric tests will be considered in order not to have to assume a specific distribution for the data. The tests chosen for step change analysis were the Pettitt test and the cusum test,

for trend analysis the Mann-Kendall test was used. All of them are widely used in the literature.

3.2 Data

3.2.1 *Rainfall data*

The dataset used consists of daily rainfall series from 81 gauges, 25 in Portugal and 56 in Spain, evenly distributed over the Douro, Tagus and Guadiana basins. The 81 gauges were chosen considering both the need for a homogenous spatial coverage and the percentage of missing data for each record. The analysed period was 1961 to 2009 which was chosen to provide the maximum amount of gauges with complete records. Many Spanish gauges have gaps in the 1930s, 1940s and 1950s (possibly due to disruptions caused by the Spanish civil war) and most Portuguese gauges do not have complete records after 2009 due to budget cuts that prompted the lack of regular maintenance of the monitoring network. Most chosen gauges had less than 6% of missing data (see Figure 3.1) and the density of selected stations in Portugal and Spain is similar (although slightly higher in Portugal).

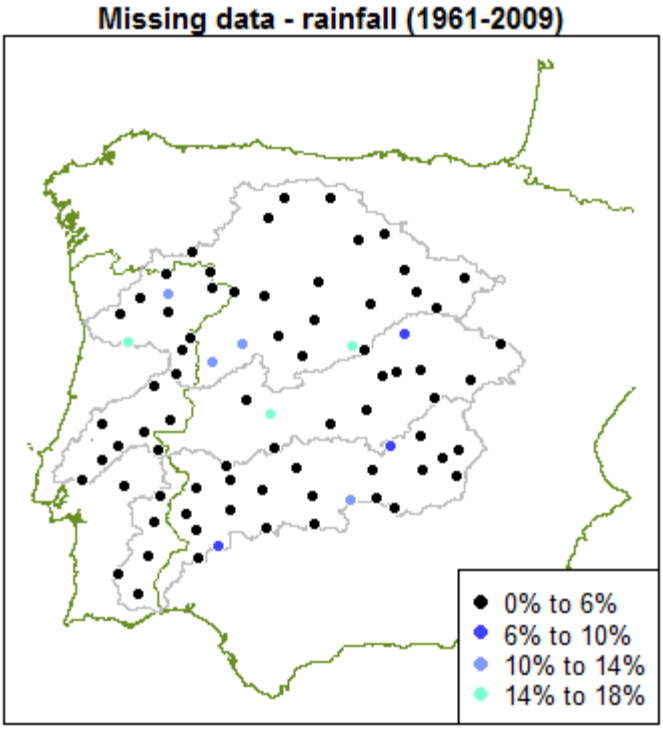

Figure 3.1 - Map of Portugal and Spain with the location and percentage of missing data of the gauges used in this study. The three basins studied are delimited in grey.

Data from the Spanish meteorological institute (AEMET – Agencia Estatal de Meteorologia) were retrieved from ftp://ftpdatos.aemet.es/ on the 10th of February 2010. Data from fifteen stations inside the relevant catchments were available. The second dataset from AEMET was requested and kindly sent by AEMET via email. The stations whose data were requested were selected based on their location (in order to have a good distribution of stations inside each

catchment area), by the length of the record, and by the size of data gaps. The two AEMET datasets were combined into a Spanish dataset.

For Portugal, data from the water institute (INAG) were retrieved from http://snirh.pt/ on the 25th of March 2010. Data from 384 stations inside the relevant catchments were available for download. In order to select the stations with the longest records and with the best quality of data, the Portuguese reference rainfall gauges from "boletim de precipitação" were initially chosen. This is a selection of gauges used by INAG to characterize the precipitation in the country. From the "boletim de precipitação", 26 stations are inside the relevant catchments and were therefore chosen.

Infilling had to be applied to all the stations that had missing data. From the nearest stations with data available, the best correlated station was used for infilling (i.e. the station with the highest monthly correlation that had available data for the necessary period was chosen). The infilling was done by applying a correction factor (ratio of the annual average rainfall of each station), calculated for the overlapping period of data. The data subjected to quality control was not only the stations selected for the dataset but also the ones used for the purpose of infilling.

The following quality control procedures were performed:

- Histograms with the distribution of daily precipitation were plotted for every station, all the distributions were exponential;
- Annual maxima of daily precipitation were plotted for every station; all were within plausible bounds.
- Bar plots of the mean rainfall per day of the month were plotted, to check if accumulated precipitation was written on the last day of the month instead of daily precipitation. Mean precipitation and a 99% confidence interval (using Student-t) were also plotted. All stations behaved as expected (with the bars for each day of the month falling inside the 99% confidence interval), except for stations 2450 and 2290 in Spain and 08K/01UG in Portugal (see Figure 3.2). However the results are satisfactory enough not to discard these stations especially because the worse station (08K/01UG) was only used to infill 0.12% of data from station 08J/04G.

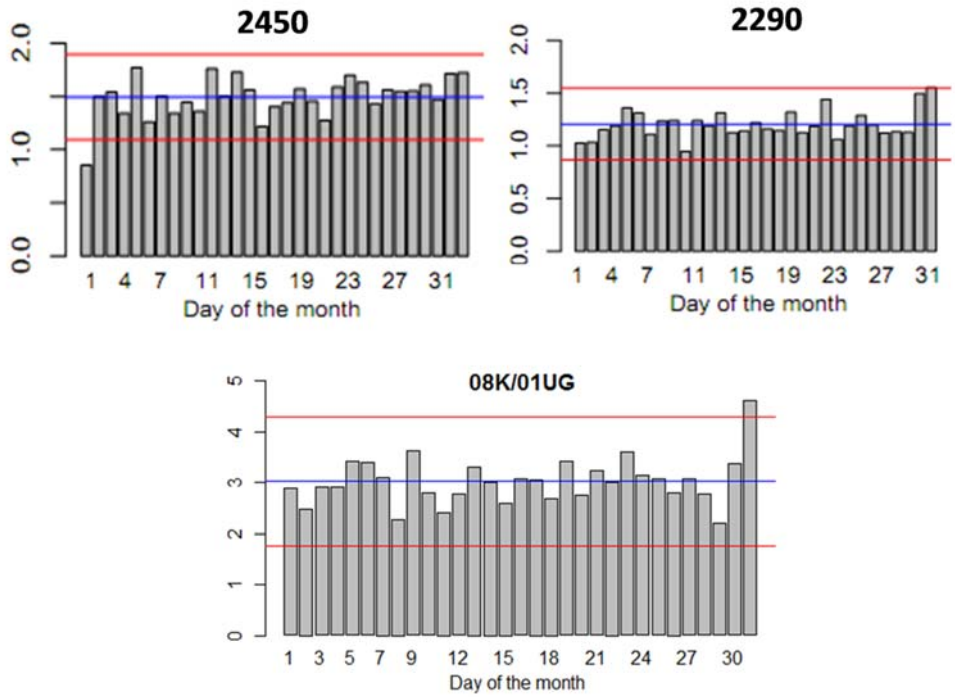

Figure 3.2 - Bar plots of the mean rainfall per day of month for stations 2450 and 2290 in Spain and 08K/01UG in Portugal. The blue lines show the mean precipitation and the red lines delimit the Student-t 99% confidence interval.

Finally, the daily data were aggregated to monthly values and the series were split by months.

The mean rainfall of each gauge, for each month, is shown in Figure 3.3.

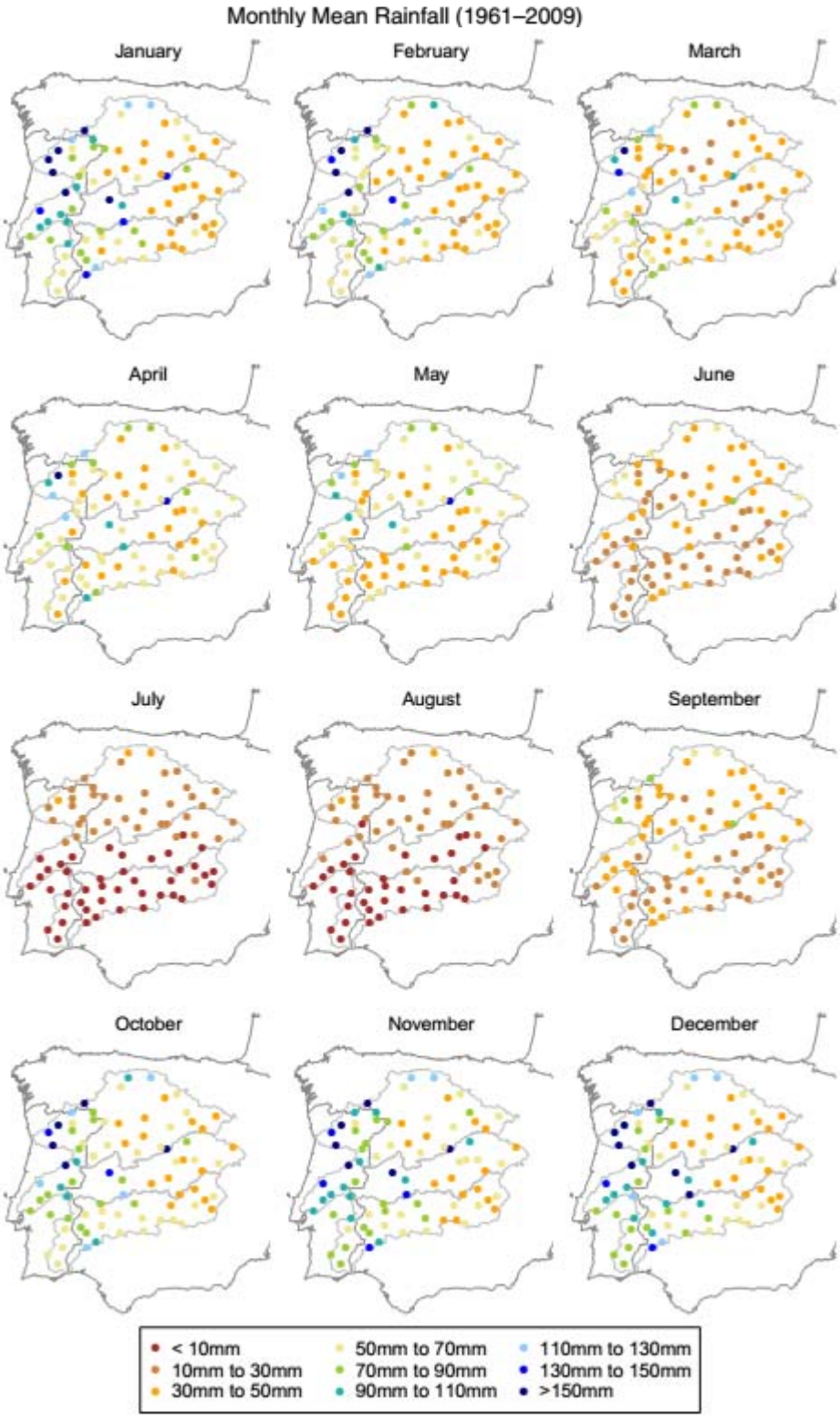

Figure 3.3 - Mean monthly rainfall from 1961 to 2009 for the selected gauges.

3.2.2 *NAO index*

The NAO is a shift of atmospheric mass between the Icelandic Low and the Azores High. Therefore the sea level pressures (SLP) of these two places are negatively correlated (r=-0.63) and the difference between them can be used as an index of the NAO (Osborn *et al.*, 1999). Alternatively, the sea level pressure of Lisbon or Gibraltar can be used instead of the Azores, or a principal component analysis (PCA) can be used to define the NAO. A number of different NAO series are available, however Osborn *et al.* (1999) showed that they are highly correlated, with inter-series correlations being typically around 0.9.

The NAO indices based on PCA are calculated using gridded SLP data. This means they can represent the full NAO spatial pattern better than the difference between two points (because the NAO centres of action move during the annual cycle) but it also means that their time-series cannot be extended long into the past. Besides having less information, another disadvantage of using the difference between two stations is that the Iceland and the Azores, Lisbon or Gibraltar stations are affected by local weather that is not related to the NAO (Osborn (2006) and Hurrell and Deser (2009)).

The length of record is not an issue in considering which NAO index to use for the period of 1961 to 2009. Therefore the NOAA's PCA NAO index (ftp://ftp.cpc.ncep.noaa.gov/wd52dg/data/indices/tele_index.nh) was used in this study.

3.3 Methodology

First a change point analysis was performed in order to detect abrupt changes in the rainfall series. Contrary to the slow changes that translate into trends, change-points in rainfall are normally related to either climate regime shifts or changes in the monitoring procedure or equipment. To detect change points both the Pettitt and the Cusum tests were used because different tests can give different results and there is not a unique widely accepted test for change point detection.

Secondly a trend analysis was performed to detect slow changes or tendencies in the data, using the Mann-Kendall test. This is the most popular test for trend detection (Fatichi *et al.*, 2009). Also, it has a similar power for trend detection to the widely used Spearman's test, being practically indistinguishable (Yue *et al.*, 2002a). Therefore only the Mann-Kendall test was used.

All these tests are non-parametric, which means that there are no assumptions about the distribution of the populations. However they all assume temporal/serial independence of the data, which was checked using the autocorrelation function (ACF).

Owing to the statistical nature of these tests, the results are never free of error, and the probability of wrongly rejecting the null hypotheses (which is no changes in rainfall) is given by the significance level chosen for the test (0.05 in this study). In other words, when performing one of these tests in the time series from one gauge there is a 5% chance of detecting a change that does not exist. However, these tests were not performed just one time; there are 81 gauges, so each test was performed 81 times. Therefore the probability of detecting one false change (in any of the 81 gauges) is higher than 5% and is given by what is called "field significance". Because our gauges are spatially correlated, field significance had to be calculated using bootstrap resampling.

Correlations, change point and trend tests were also used to study the relationship of the rainfall series to the NAO Index. All these tests and techniques are described in the following subsections.

3.3.1 *Change point analysis*

Both the Pettit (Pettitt, 1979)and the Cusum test are nonparametric/distribution free tests used to detect change in the median or mean at an unknown point in time (WMO, 2000). The method adopted for the cusum test analysis was based on Smadi and Zghoul (2006) where the cusum test is used to identify the time of change and a bootstrap procedure is used to find the

critical values under the null hypothesis (no abrupt changes). The code used for both the Pettitt and the cusum tests was provided by Dr Serinaldi and is presented in appendices A, B and C.

First, a step change analysis was performed on the means, by applying the cusum and the Pettitt test to all stations and all months. It was assumed that only one change point could be present in a series, to avoid fragmentation of the time-series into small segments where a trend analysis would not be meaningful. The same tests were used to check for change points in the variance, which was done by applying the tests to the squared residuals calculated by fitting the time series with a locally weighted scatterplot smoothing (LOESS) function (Villarini *et al.* (2009) and Villarini *et al.* (2011)).

3.3.2 *Trend analysis*

The Mann-Kendall test (Mann, 1945; Kendall, 1948) was used to assess the existence of statistically significant trends in the data. This is a non-parametric test widely used for trend detection. Initially the test was applied to all data. Afterwards, for the gauges that presented change points, the Mann-Kendall test was applied before and after the change point. This was done in order to see how the existence of a change point in the time series affected the existence of a trend.

Linear regression was used in order to calculate the magnitude of the significant trends. Fitting a linear model implies the assumption of a linear trend, while the Mann-Kendall test is devised for detecting a monotonic trend that is not necessarily linear. However some lenience has to be exercised in order to be able to calculate the magnitude of trends. The implications of this assumption will be discussed in the results and discussion section.

The trend analysis for the variance was done by applying the Mann-Kendall test to the squared residuals calculated by fitting the time series with a LOESS function (similar to the change point analysis for variance).

3.3.3 *Autocorrelation function*

All the statistical tests chosen assume the independence of the data. Therefore the serial independence of the monthly rainfall data was checked using the lag-1 of the ACF (denoted as the ACF1). For each month, the ACF1 coefficients for all the gauges were plotted along with the 95% confidence interval (figures not shown), and the number of gauges outside the confidence intervals was counted for each month.

3.3.4 *Field significance*

When analysing a number of gauges, a simultaneous evaluation of multiple hypothesis tests is performed and therefore the problem of test multiplicity or field significance arises (Wilks, 2006). The significance level (α) chosen for this study is 0.05, so for any specific gauge, there is a 5% probability that the null hypothesis is falsely rejected. However, because the analysis is being performed multiple times, even if the null hypothesis is true in all gauges (*K* gauges), on average $K\alpha$ of them will be erroneously rejected. It is therefore necessary to account for a global significance level (in order to be able to accept or reject the null hypothesis that all *K* local null hypotheses are true), or in other words, the field significance (Wilks, 2006).

Field significance is usually calculated using a binomial probability distribution. If each test is independent and *X* is the number of times we accept the null hypothesis using *K* individual α level hypothesis tests, then *X* follows a binomial probability distribution with parameters *K* and α (Douglas *et al.*, 2000). A bootstrap approach must be used when there is the need to account for spatial correlations (Yue *et al.*, 2003; Kenawy *et al.*, 2011).

Field significance was calculated for the ACF1 values and for the test statistics of the Pettitt test, the cusum test and the Mann-Kendall test.

3.3.5 *Bootstrap*

As previously mentioned the bootstrap resampling has been applied to assess the field significance for spatially correlated time series. In bootstrap resampling the data were sampled simultaneously across the gauges to preserve the spatial correlation while removing the temporal correlation and any possible trend. For each bootstrap replication, the significance of the ACF1 was tested and the Pettitt, cusum and Mann-Kendall tests were applied to each series. The number of series failing to pass the tests at 5% nominal level was recorded. Repeating the resampling procedure 10 000 times allowed defining the sampling distribution of the number of successes (rejections of the null hypothesis) in a multiple testing exercise under spatial dependence. The sampling distribution was then used to define the critical values (95^{th} percentile for the 5% field significance level) for testing the significance of the number of successes recognized in the set of the observed time series. A more detailed explanation of the procedure can be found in Douglas *et al.* (2000).

3.3.6 *Rainfall-NAO relationship*

The relationship of the rainfall series to the NAO Index was also investigated by (a) using monthly mean correlation between the rainfall of each gauge and the NAO index; (b) performing the change point and trend analysis for the monthly NAO index using the Pettitt,

Cusum and Mann-Kendall tests (as done for the rainfall data) to check for the synchrony between changes in the NAO index and changes in the rainfall data.

3.4 Results and discussion

3.4.1 *Autocorrelation*

The binomial distribution approach was initially used to calculate field significance of the ACF1. In a repeated testing procedure, the test results can be interpreted as the outcomes of a sequence of Bernoulli trials, where the outcome 1 (success) is the rejection of the null hypothesis and 0 (failure) is the lack of rejection. With 81 trials, the minimum number of locally significant results to ensure 5% field significance is 7 successes (using the binomial distribution). Since zero or one gauge exhibit significant ACF1 values for most of the months, the series could be considered temporally independent when field significance is accounted for.

However, February had 21 gauges showing significant ACF1, April had 11 and May had 9. One possible explanation was the effect of spatial correlation or cross correlation. If spatial correlation exists, then each test is not independent and the binomial approach cannot be applied to calculate field significance (Douglas *et al.*, 2000). Cross correlations for each pair of gauges and for each month were calculated to understand its variability and the possible impact on the field significance. The spatial correlations, quantified by Pearson correlation coefficient, were very high reaching the value 0.8 for the wet winter months.

When correlation is present, the null hypotheses are rejected too often because the effective sample size of a dataset is reduced. For example, if a trend is found at one gauge it is more likely to find trends at nearby gauges (Douglas *et al.*, 2000). Therefore, spatial correlation would easily explain 11 (9) gauges exhibiting significant ACF1 in April (May). However, more analysis was required to be able to confirm February's data serial independence.

For the month of February, the bootstrap resampling was applied to obtain the sampling null distribution of the number of successes (failures to reject the hypothesis ACF1 = 0) under spatial dependence. The 95th (99th) percentile of the resulting bootstrap distribution was 17 (37). The February exceedance number (19) is only marginally above the 95th percentile and well below the 99th percentile. Therefore we concluded that when accounting for spatial correlations, the hypothesis of temporal independence cannot be rejected for the February data.

The value of the exceedance number calculated using the bootstrap approach (17) was more than double the one calculated using the binomial test (7), which shows the importance of considering the spatial correlations between the gauges. The differences between the bootstrap and the Binomial distributions used to calculate the critical number of exceedances

are highlighted by the probability density functions (PDFs) and cumulative distribution functions (CDFs) plotted in Figure 3.4.

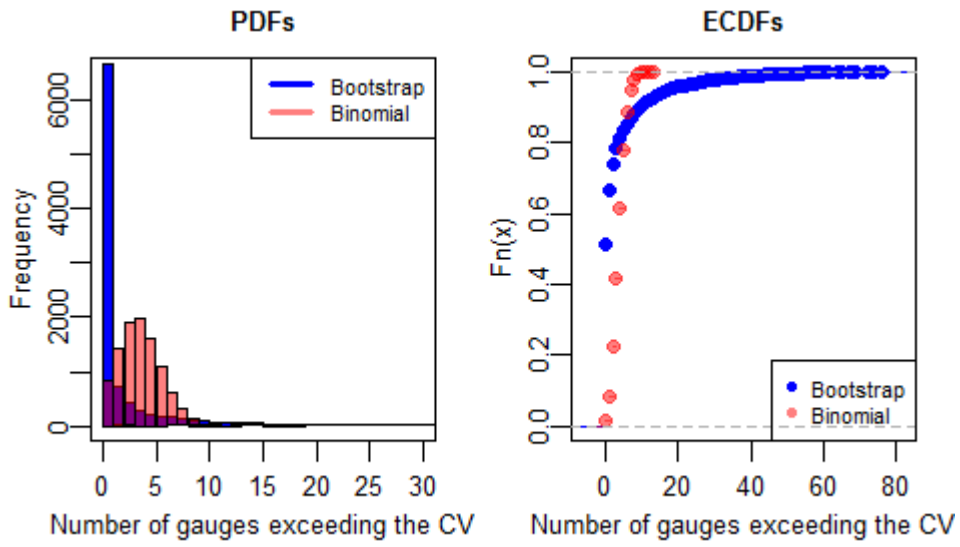

Figure 3.4 – PDFs (with the x-axis limited between 0 and 30 to make it more readable, left) and CDFs of the bootstrap and Binomial distributions (right) used to calculate the critical value (CV) corresponding to the null hypothesis ACF1 = 0.

3.4.2 *Change point analysis*

Regarding the analysis of the change points in mean, February, March and June presented significant change points when accounting for field significance using the Pettitt test. However, for the cusum test only February presented significant change points when accounting for field significance (see Figure 3.5).

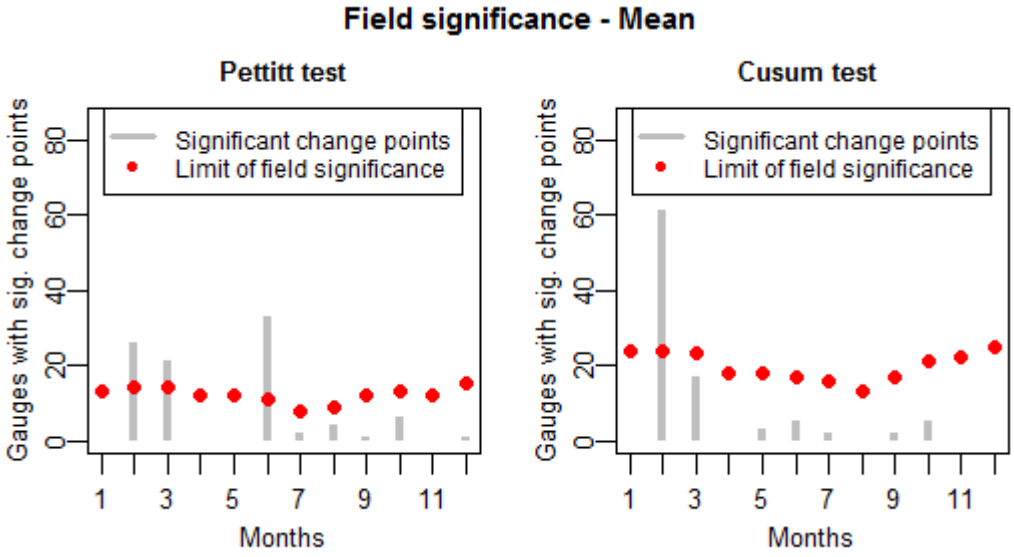

Figure 3.5 – Number of gauges with significant change points (with a significance level of 0.05) in the mean calculated using the Pettitt test (left) and the cusum test (right). Limits of field significance were calculated using 10000 resamples.

In terms of the variance analysis, using the Pettitt test, February presented significant change points when accounting for field significance. Using the cusum test there were no significant change points, although February is very close to the limit of field significance (see Figure 3.6).

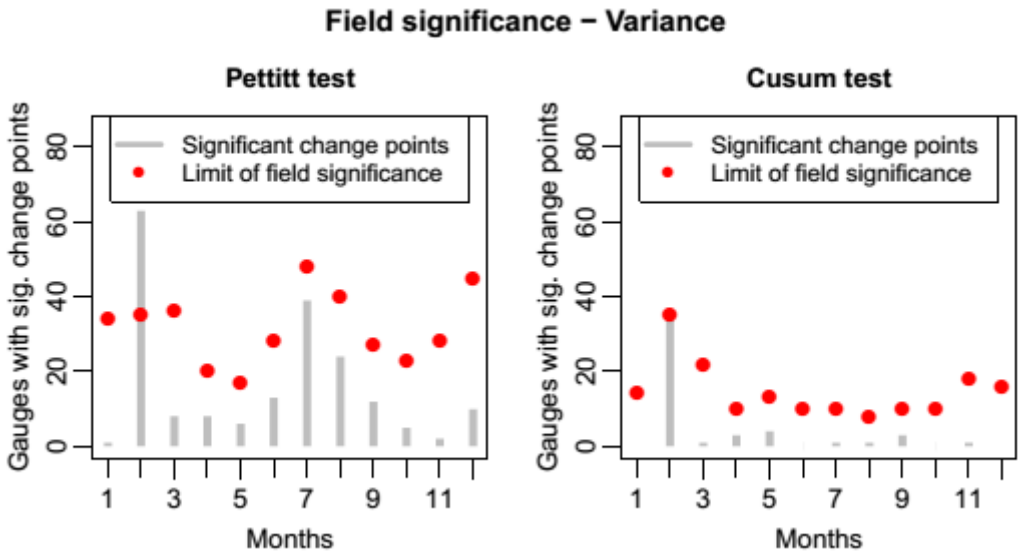

Figure 3.6 - Number of gauges with significant change points (with a significance level of 0.05) in the variance calculated using the Pettitt test (left) and the cusum test (right). Limits of field significance were calculated using 10000 resamples.

As explained before, for the cusum test the p-values are calculated using the bootstrap approach. For the cusum test, for variance, another methodology was also tested, using the R package "changepoint" (available at http://cran.r-project.org/), where an asymptotic distribution is used for the calculation of the p-values. The results obtained with this methodology were identical to the Pettitt test results. Therefore the differences in results of these two tests (Pettitt and cusum) should not be ascribed to the tests *per se* but in the methods used for the calculation of their p-values. Further analysis on the behaviour of the different tests/procedures applied was considered to be outside the scope of this study, therefore the results of both tests will be considered.

As the Pettitt test showed more months with significant changes than the cusum test, maps were plotted for all months to check the existence of spatial clusters that might be significant. Regarding the result of the Pettitt test applied to the mean (see Figure 3.7), only February, March and June had enough significant change points to check for spatial patterns. In these months all the change points detected were negative. In February and March no clustering is visible, but in June most of the gauges with change points are located in the Tagus and Guadiana basin. The northeast of the Douro basin seems to have a cluster of positive change points in October, but the number of gauges (five) is too small for it to be considered.

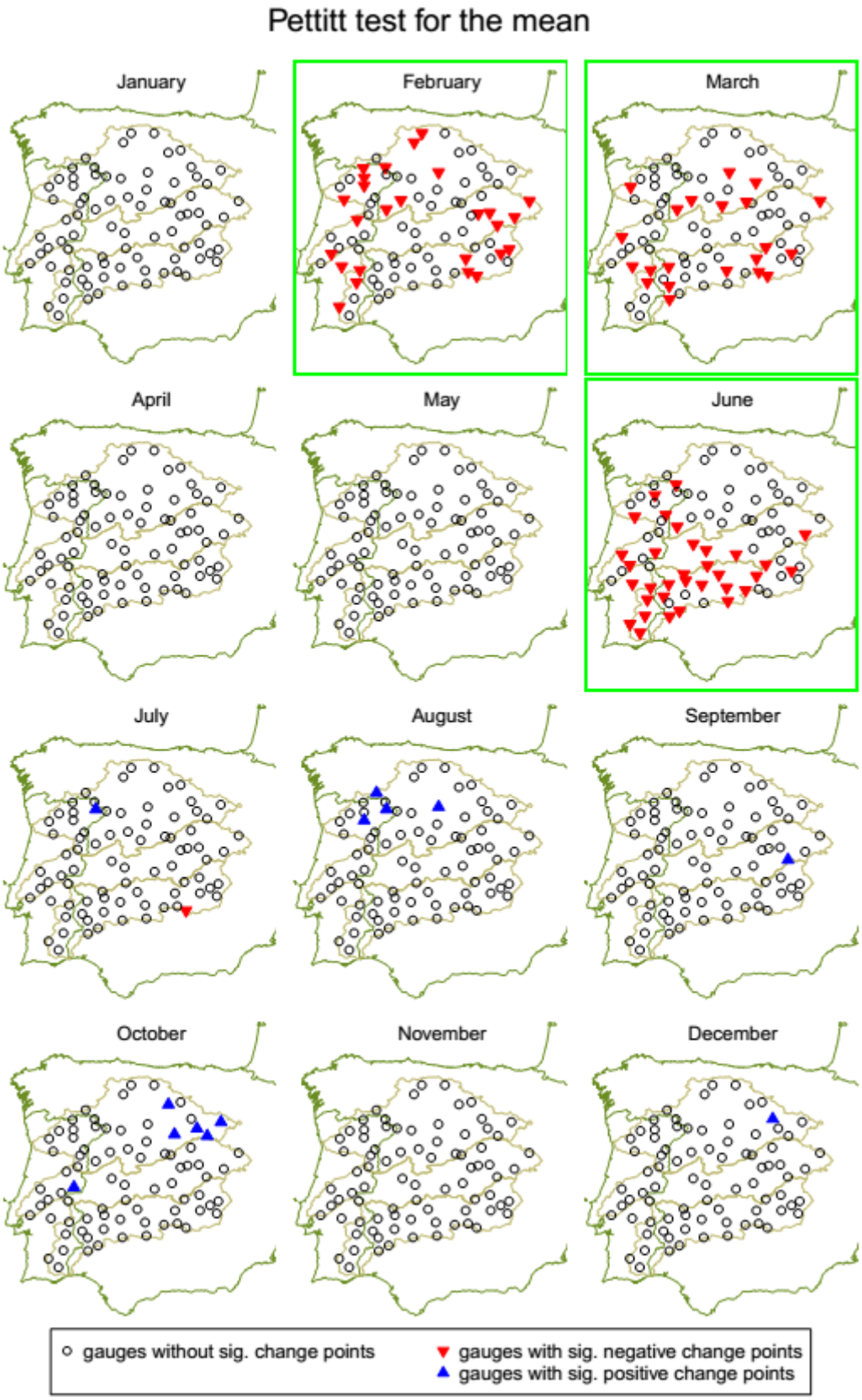

Figure 3.7 – Change points in the mean calculated using the Pettitt test, for all months and for all gauges (the significance level is 0.05). Months for which the number of gauges showing significant change points is above the field significance are highlighted in green.

Regarding the result of the Pettitt test applied to the variance (see Figure 3.8), almost all the study area is affected by negative change points in February. This decrease in the variance in February is noticeable just by looking at most of the time-series from the 81 gauges (see Figure 3.9). In July and August, and to a lesser extent in September, there are numerous gauges with significant change points spread throughout the entire study area, but some correspond to an increase in variance while others correspond to a decrease.

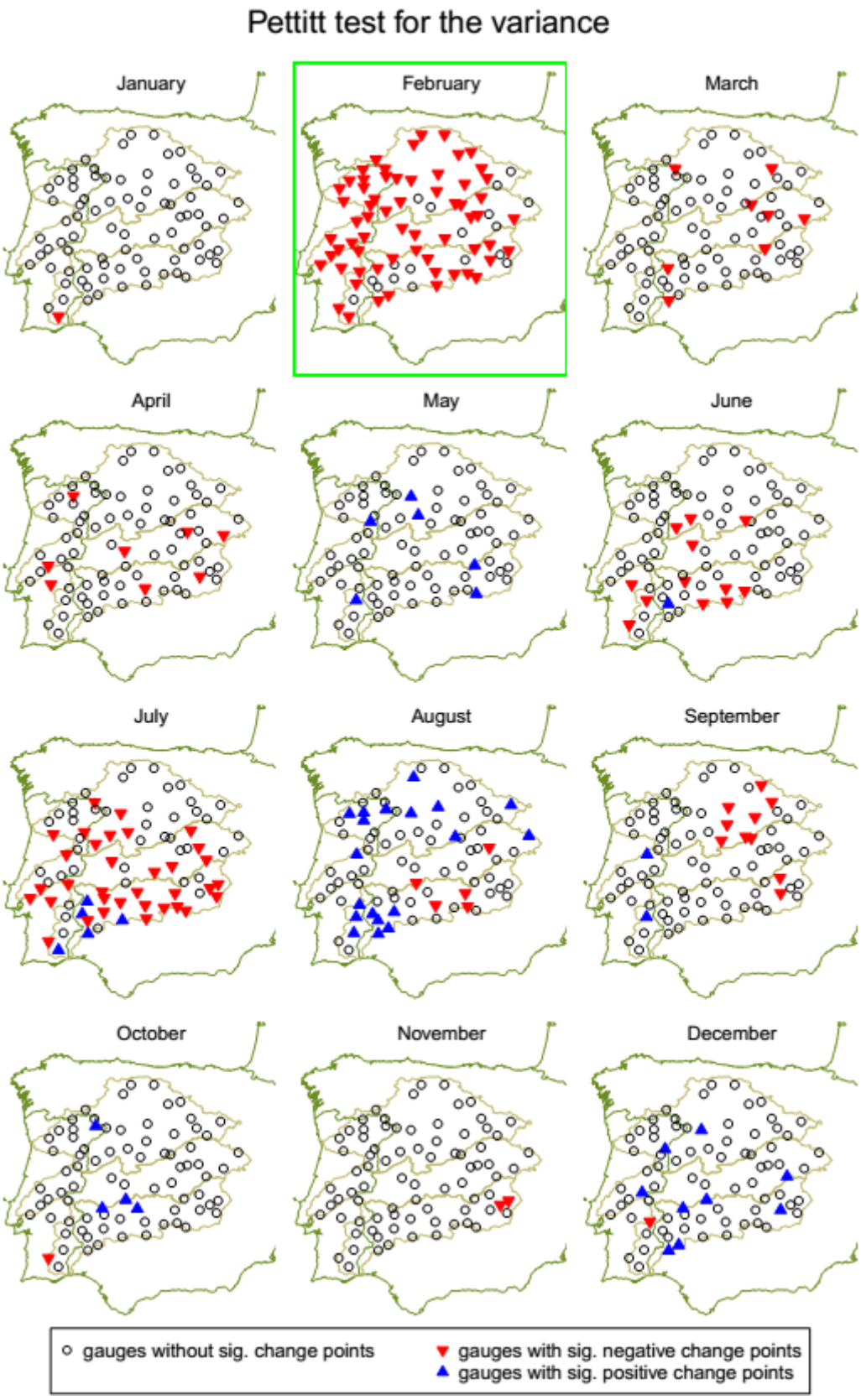

Figure 3.8 – Change points in the variance calculated using the Pettitt test, for all months and for all gauges (the significance level is 0.05). Months for which the number of gauges showing significant change points is above the field significance are highlighted in green.

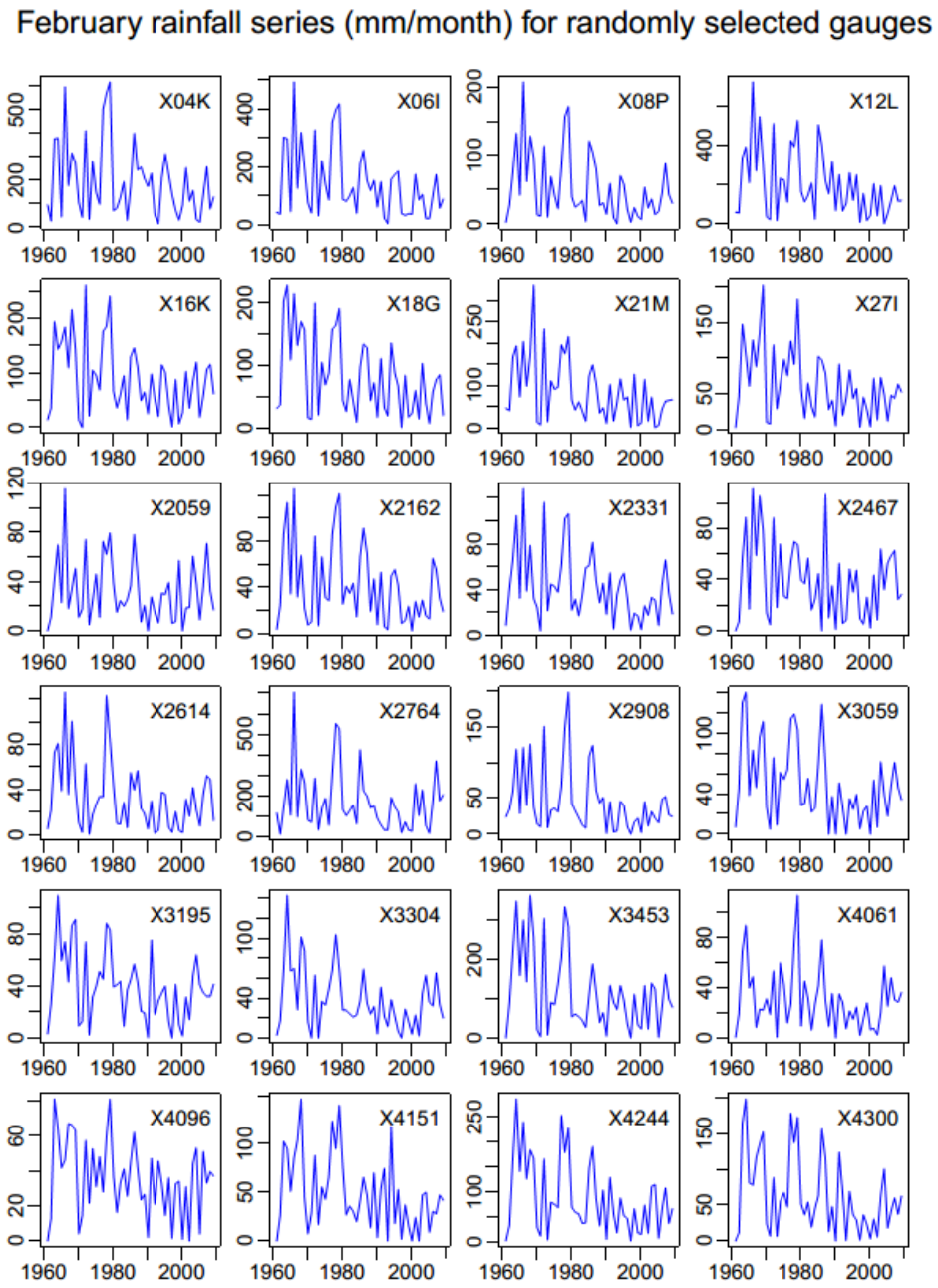

Figure 3.9 – February rainfall (mm) time-series for randomly selected gauges (1961-2009).

3.4.3 *Trend analysis for the mean*

The results for the significant (0.05 significance level) and non-significant trends detected using the Mann-Kendall test are shown In Figure 3.10. It is interesting to note that all gauges present negative trends (whether significant or not) in the months of February and March, and almost all gauges in the months of January, June and November. In October all gauges presented a positive trend.

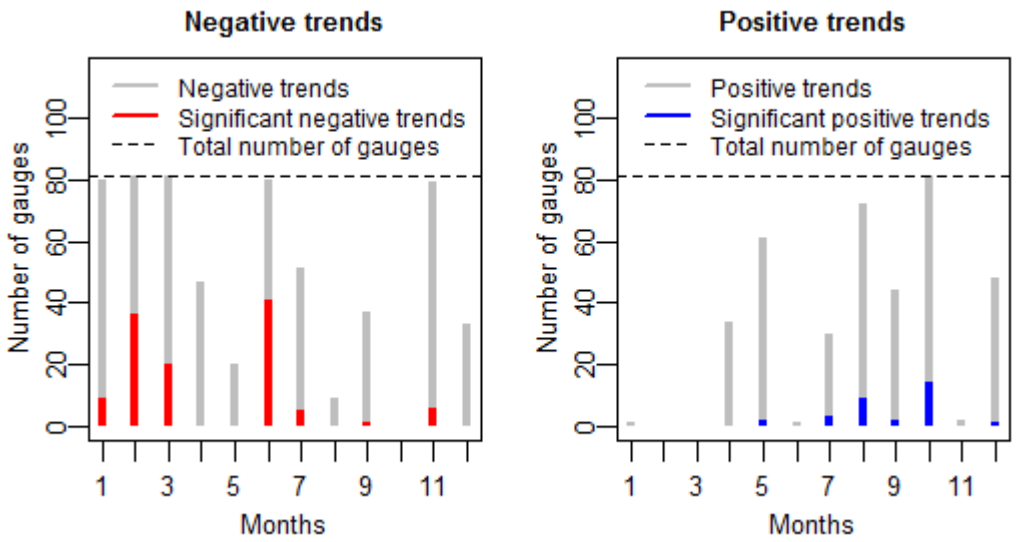

Figure 3.10 – Number of gauges with significant and non-significant trends (significance level of 0.05) calculated per month, using the Mann-Kendall test. Negative trends are shown on the graph on the left and positive trends are showed on the right.

The months of February and June (and to a lesser extent, January, March, July, September and November) presented negative trends that are statistically significant at a 0.05 significance level. Statistically significant positive trends were found mainly in August and October, but also a few in May, July, September and December.

These results agree with the results of Río *et al.* (2010), who found significant (0.05 significance level) negative trends in Spain mainly in February and June but also in March and January. Positive trends were found in August and October and to a lesser degree in April, May, July and September.

González-Hidalgo *et al.* (2010a) found significant (0.1 significance level) negative trends in the Spanish side of Douro, Tagus and Guadiana catchments mainly in March and June, with small areas also occurring in January, February, April, July, August, September and December. Positive significant trends were found in October with small areas also occurring in April, June, July and August. The main difference with González-Hidalgo *et al.* (2010a) is that the large negative trend is found in March, instead of February as in Río *et al.* (2010) and in the present analysis.

The comparisons of results are hindered by the fact that these studies only considered the Spanish side of the catchments and the period of analysis is also not exactly the same: 1961 to 2006 for the first study, 1964 to 2005 in the second and 1961 to 2009 in the present analysis.

However when field significance is considered (see Figure 3.11) only February and June have trends above the limit of field significance. Trends detected in other months are therefore probably due to random fluctuations rather than systematic trends. Nonetheless maps were

plotted for all months to check for the existence of spatial clusters that might be significant (see Figure 3.12).

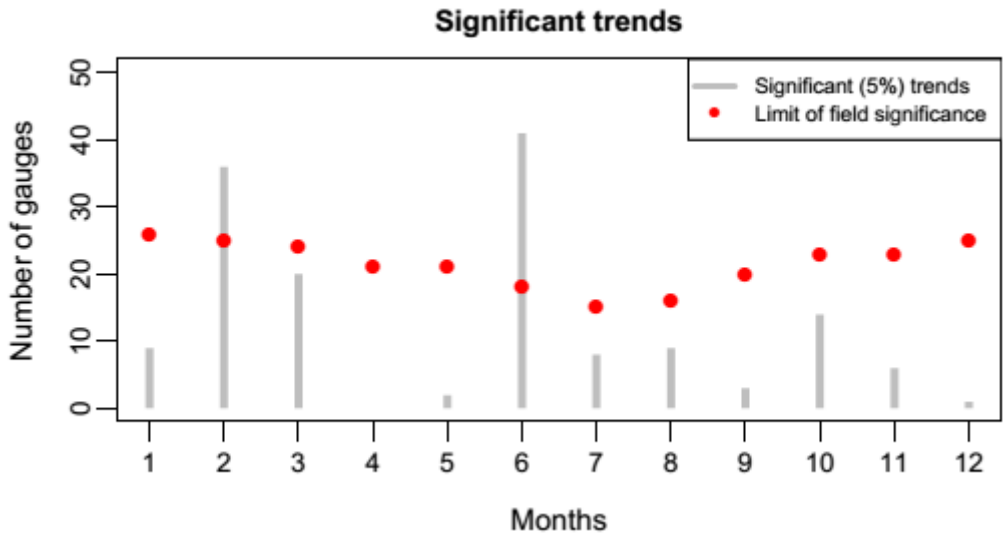

Figure 3.11 - Significant trends for the mean (positive and negative), with a significance level of 0.05, calculated using the Mann-Kendall test. Limits of field significance were calculated by resampling 10000 times.

In February no clustering is visible, but in June most of the gauges with trends are located in the western Douro, western Tagus and in the Guadiana basin. Although the number of gauges with significant trends for all the other months is below the limit of field significance, spatial clusters seem to be present in the months of March (Guadiana basin) and October (Spanish side of Douro and Tagus basins). Therefore, it seems logical to perform a field significance test on smaller regions containing large numbers of stations that exhibit significant trends. However, it should be noted that the clustering is an inherent property of spatially correlated data, and sub-regions should be determined with a physically based justification before performing the local analysis, as a *post hoc* domain selection could give biased results (Daniel *et al.*, 2012). In the present analysis, the sub-regions correspond to the drainage basins, which are hydrologically coherent physical units. When the field significance analysis is performed just for the Guadiana, the limit of field significance for March is 9 gauges. This area presented 11 gauges with significant negative trends, therefore being above the field significance limit. When the field significance analysis is performed in the month of October on the Spanish side of the Douro and Tagus basins, the limit of field significance is 10 gauges. This area presented 13 gauges with significant positive trends, therefore being above the field significance limit. These results show the importance of plotting the data on a map to check for spatial clusters on physically coherent units before discarding results based on field significance analysis, even though the possible shortcomings of a post hoc selection must be always kept in mind.

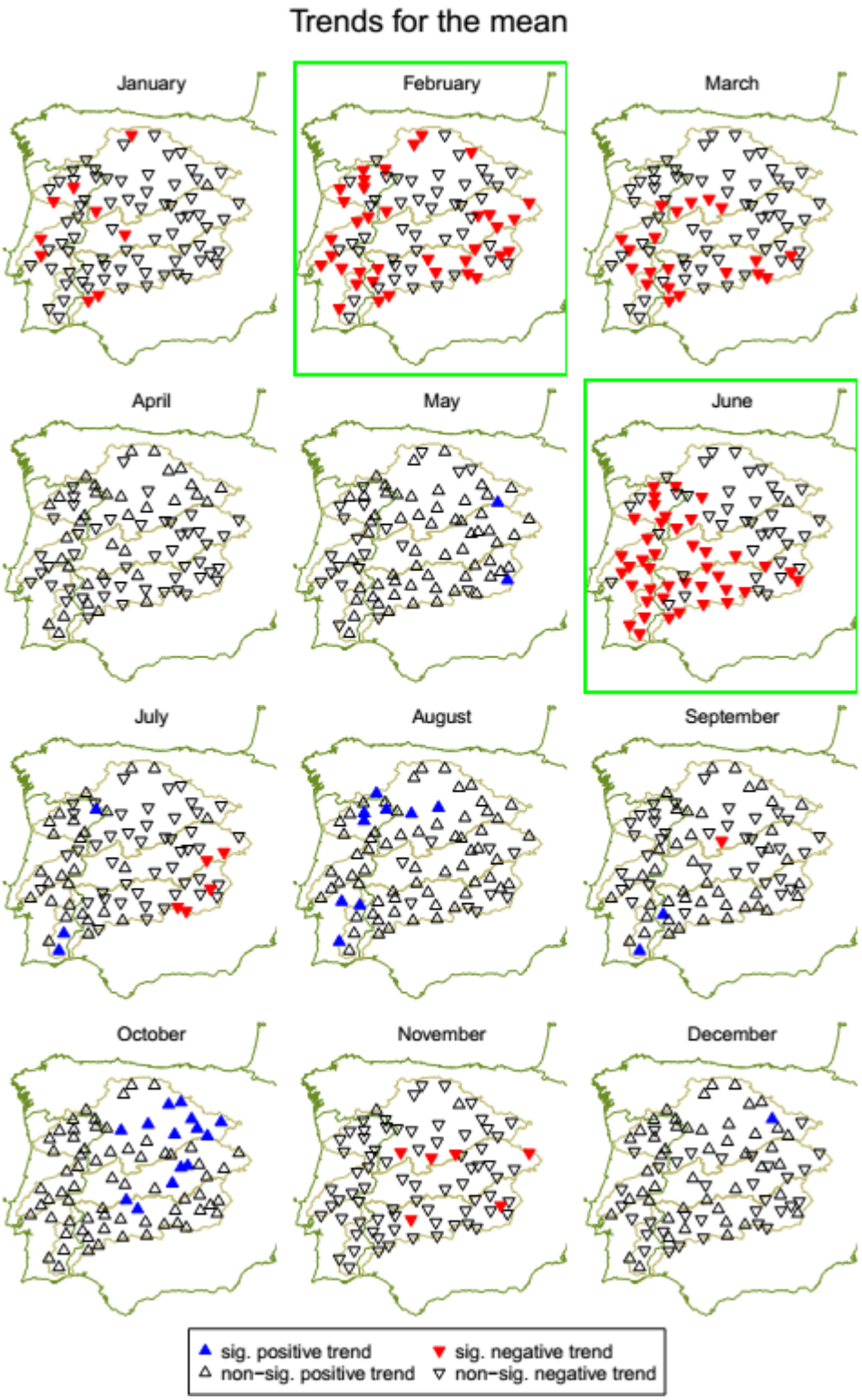

Figure 3.12 – Trends calculated for all months and for all gauges (significant trends are significant at a 0.05 significance level). Months for which the number of gauges showing significant change points is above the field significance are highlighted in green.

For the gauges that presented change points, the Mann-Kendall test was applied to the record before and after the change point, following the method applied by Villarini *et al.* (2011). This was done in order to see how the existence of a change point in the time series affected the existence of a trend. When testing for trends before and after the change points in the mean

identified by the Pettitt test, no significant trends were found. Therefore one might assume that for the gauges with change points, changes in rainfall in Douro, Tagus and Guadiana, from 1961 to 2009 occurred in the form of step changes instead of slow changes that could be perceived as trends. However if we analyse the gauges that have significant trends but no significant change points (for example for February) and apply the Mann-Kendall test before and after 1985 (because in February the change points in the mean using the Pettitt test are all between 1978 and 1991) the result is also zero significant trends. So, although no change point has been detected for these gauges, just by reducing the length of the records, the trends are no longer significant. As this is a shortcoming of this method, further development is warranted and discussed later.

Considering that the results of the Pettitt and cusum tests can be affected by the presence of a trend and that the Mann-Kendall results can be affected by the presence of a change point, it is not possible to draw any definite conclusion about the type of change occurring just by performing these tests. Moreover, it should be noted that the abrupt change is a limit type of a generic monotonic trend, and Mann-Kendall and Pettitt test statistics are strictly related, so that the results can be ambiguous especially for short and noisy series (Rougé *et al.*, 2013). We cannot also exclude regime shifts evolving over a few years, which can be recognized as abrupt changes only in long time series. This difficulty of defining the type of change that is occurring is not only due to the power of the statistical tests that were applied but also to the possible presence of temporal patterns that can be more complex than those described by a single change point or a monotonic trend.

In Figure 3.13 the changes in the rainfall record of a gauge in the Spanish Guadiana (AEMET gauge X4016) for February are shown as an example. It can be seen that both the change point interpretation and the linear trend interpretation seem to be reasonable but a more flexible LOESS curve points out that the behaviour might not be that simple, as the underlying pattern can be non-monotonic. The result in terms of magnitude of the change can be completely different depending on the type of change assumed. Using the example shown in Figure 3.13, if the change is perceived as a change point, its magnitude (computed as the difference in means before and after the change point) is -26.3mm. If the change is perceived as a linear trend, its magnitude (computed as the difference between the last and first prediction value when a linear regression is fitted) is -47.3mm. This analysis also reinforces the notion that extrapolation of the results of linear regression analysis for the future is without justification as the change might be occurring as a result of a regime shift that can evolve in some years, producing mixed non-monotonic patterns further complicated by the intrinsic fluctuations of the rainfall process.

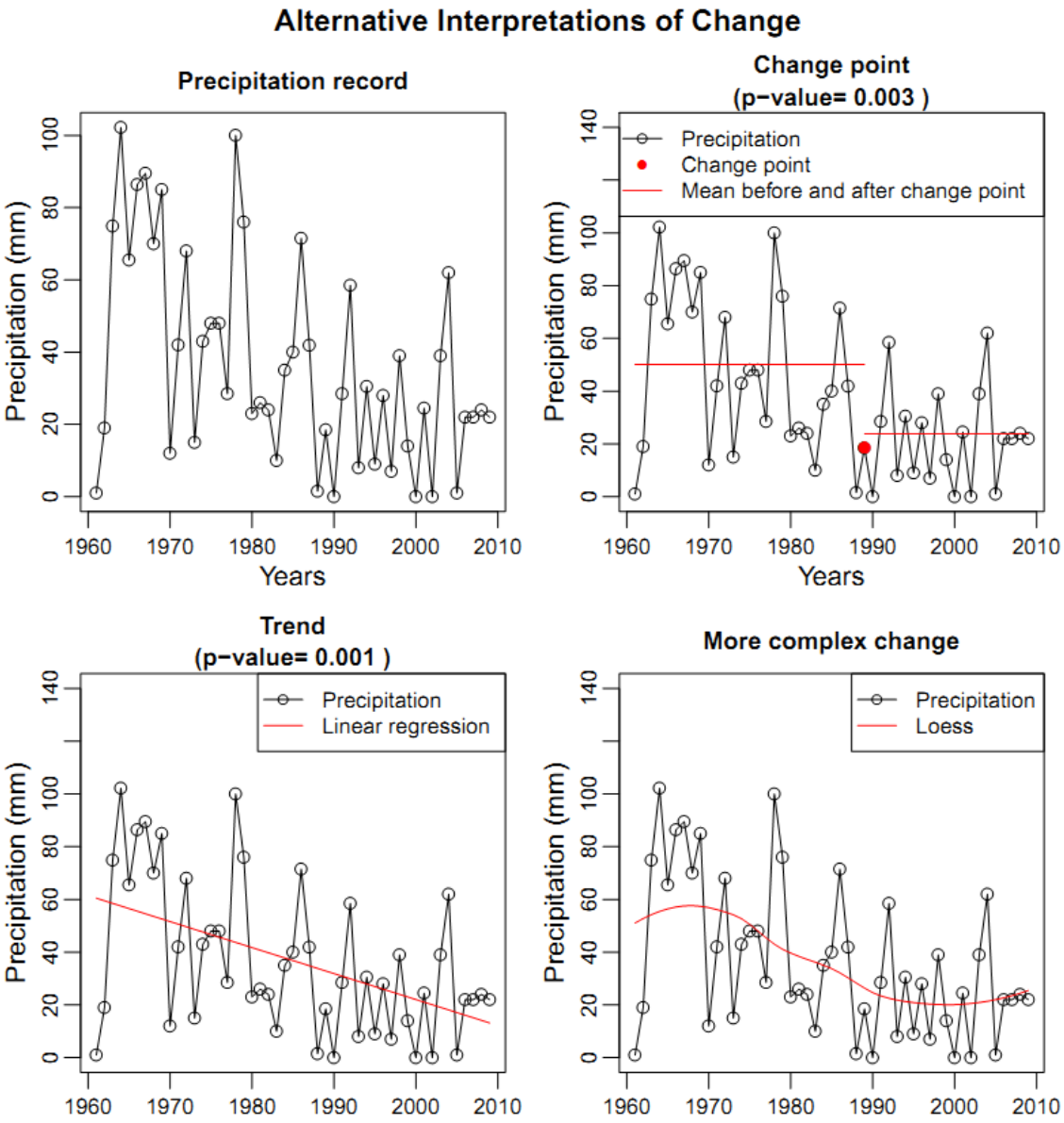

Figure 3.13 – Rainfall series for February, gauge X4016 (top left). In the top right corner the change is interpreted as a change point in the mean (with a significant p-value of 0.003 calculated using the Pettitt test). In the bottom left corner the change is interpreted as a trend (with a significant p-value of 0.001 calculated using the Mann-Kendall test) and a linear trend has been plotted. In the bottom right corner the change is shown using a local polynomial regression fitting (loess). This gauge did not present a significant change point in the variance.

3.4.4 *Trend analysis for the variance*

The results for the significant (0.05 significance level) and non-significant trends in the variance detected using the Mann-Kendall test are shown in Figure 3.14. It is interesting to note that, in February, all gauges present negative trends (whether significant or not), and almost all gauges in the months of January, March, June, July and September. In December almost all gauges show a positive trend.

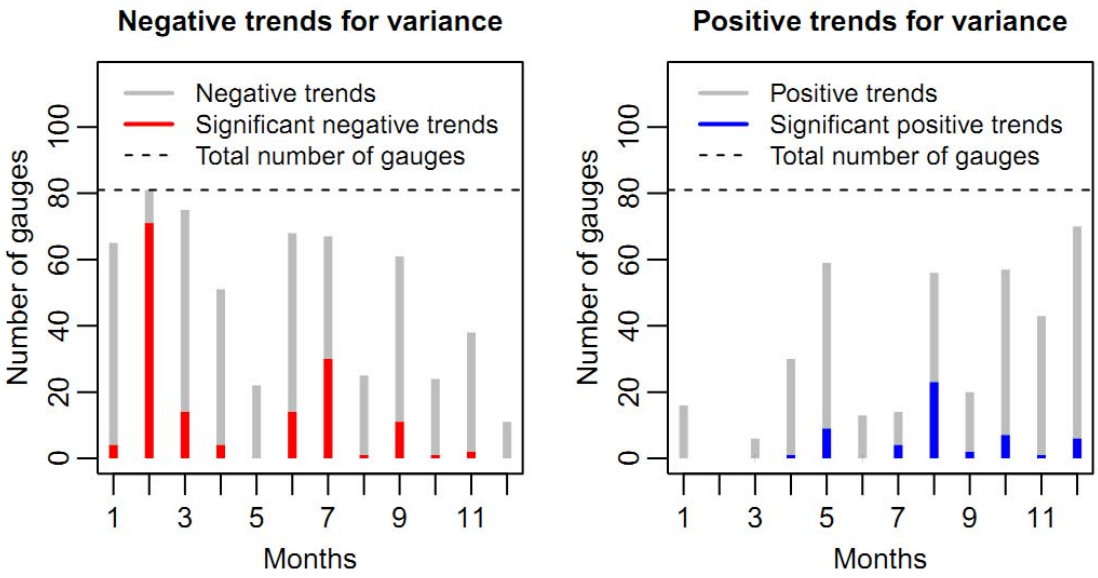

Figure 3.14 – Number of gauges with significant and non-significant trends for variance (significance level of 0.05) calculated per month, using the Mann-Kendall test. Negative trends are shown on the graph on the left and positive trends are shown on the right.

However, when field significance is considered only February has trends above the limit of field significance. The summer months (and especially July and August) present a high number of gauges showing a significant trend, however they also have a high limit of field significance (see Figure 3.15). These months are very dry throughout the basins with a baseline of low (sometimes zero) rainfall punctuated by a few high rainfall years. When LOESS is fitted to these datasets sequences of identical values are transformed into increasing/decreasing patterns and therefore (artificial) trends are detected.

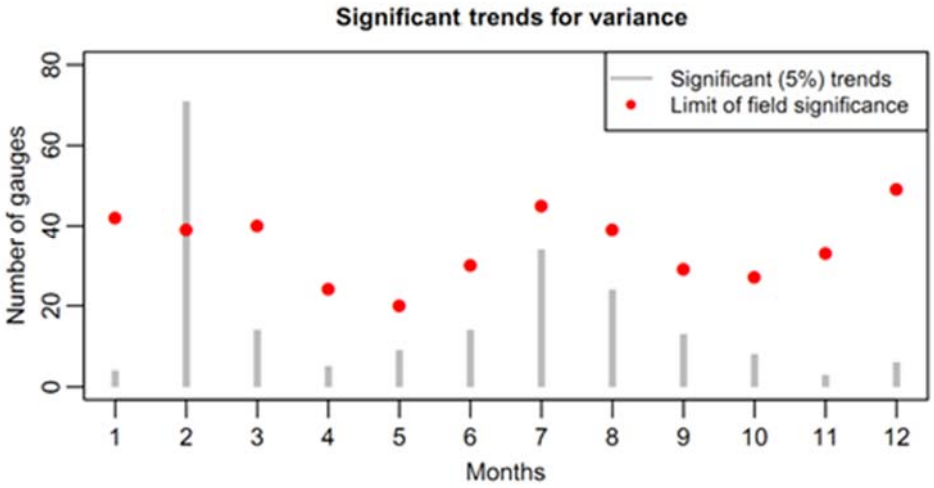

Figure 3.15 - Significant trends for the variance (positive and negative), with a significance level of 0.05, calculated using the Mann-Kendall test. Limits of field significance were calculated by resampling 10000 times.

Maps were plotted for all months to check for the existence of spatial clusters that might be significant (see Figure 3.16). No spatial clusters were found for months below the limit of field

significance, with the possible exception of negative trends on the Spanish side of the Guadiana in July. However, for the reasons explained in the previous paragraph, this apparent cluster was not taken into account.

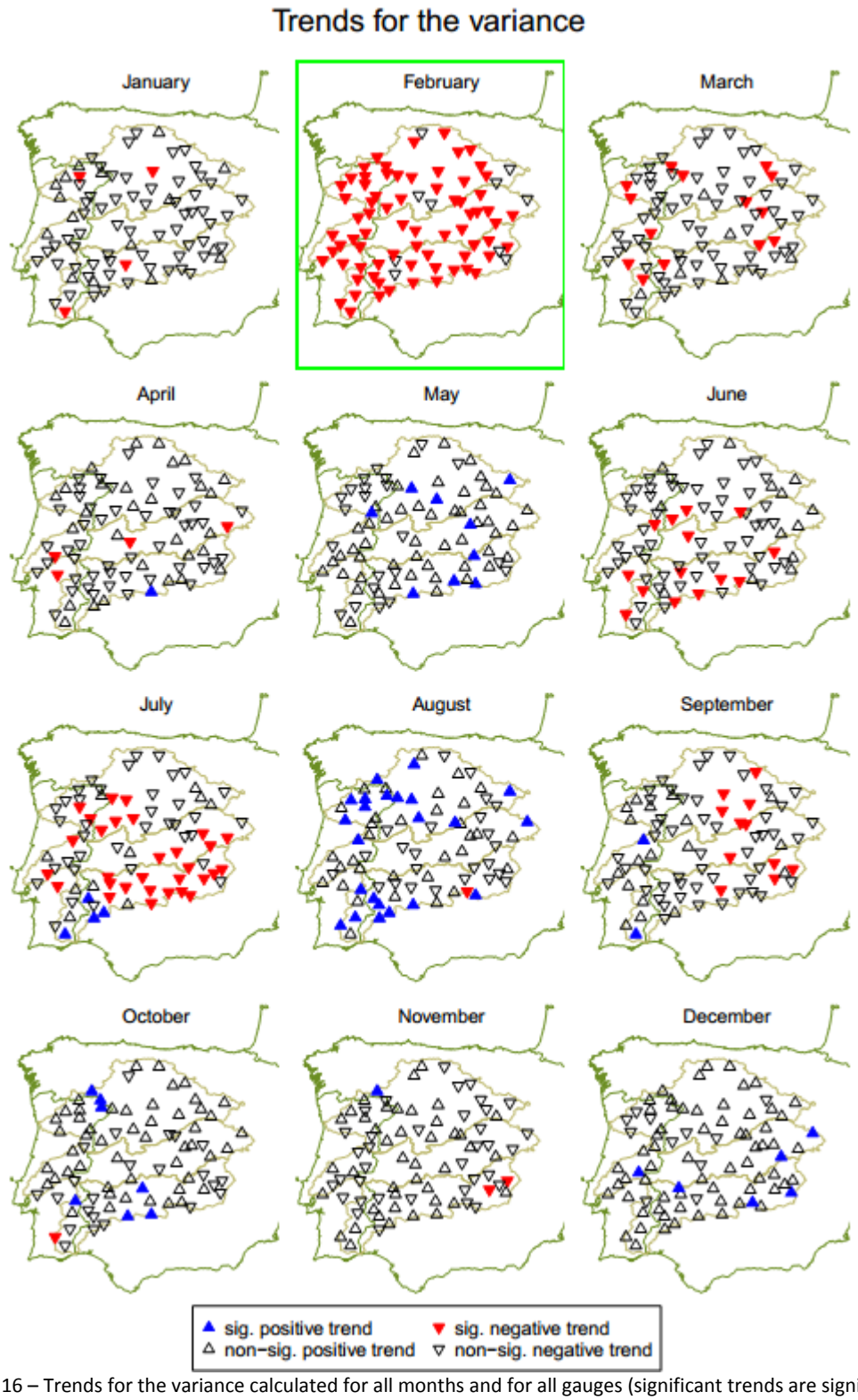

Figure 3.16 – Trends for the variance calculated for all months and for all gauges (significant trends are significant at a 0.05 significance level). The month for which the number of gauges showing significant trends is above the field significance is highlighted in green.

3.4.5 *Analysis of individual months*

From a water resources point of view the months of October to May are the most important for Iberia. They are the months with higher rainfall (see Figure 3.3), and although evapotranspiration is high in the spring and autumn, which translates into lower discharges, the rain in these seasons is very important for agriculture. Also, problems of water scarcity occur regularly in years with dry springs and autumns, and dams which have flood defence purposes are not allowed to fill their reservoirs before May.

As can be seen in Table 3.1, when accounting for field significance, February is the only month that shows a change with all the tests used, except for the cusum applied to the variance (where it is very close to the field significance limit).

Table 3.1 – Months with change points and trends detected by Pettitt, cusum and Mann-Kendall test applied to the mean and the variance, when accounting for field significance.

Test used	Months with significant changes
Pettitt – Mean	Feb, Mar, Jun
Cusum – Mean	Feb
Pettitt – Variance	Feb
Cusum Variance	- *
Mann-Kendall - Mean	Feb, Mar**, Jun, Oct ***
Mann-Kendall - Variance	Feb

* The number of gauges in February was very close to the limit of field significance
**For the Guadiana basin
***For the Spanish side of Douro and Tagus

Several authors have identified March as a month with decreasing trends in rainfall in Iberia. In this study, the number of gauges with significant trends in March is below, but close, to the limit of field significance and when the trends are calculated for the Guadiana basin they become significant. March also showed significant change points in the mean when using the Pettitt test.

October will also be considered for further analysis because it shows positive trends in the mean in the Douro and Tagus basins that might be important.

June shows significant changes in the mean (Pettitt) and shows significant trends for mean; however these are negative trends/change points in a month that is already relatively dry especially in the Tagus/Guadiana region where these changes are taking place.

Therefore a closer analysis will be performed for the months of February, March and October in order to find a possible physical explanation for the change points and trends. As pointed out in the introduction, several authors have identified the NAO as the main large-scale atmospheric mode that explains the rainfall variability in the winter months in Iberia.

Therefore the correlations between the rainfall data and the NAO index were calculated. Figure 3.17 shows the monthly variation of the temporal correlation between the monthly series of the NAO index and the rainfall amount for the three basins. The months December, January, February and March have the higher negative correlations, with February being the highest (between -0.6 and -0.7). This is consistent with the links identified between NAO index and Iberian rainfall in the winter by Trigo *et al.* (2004).

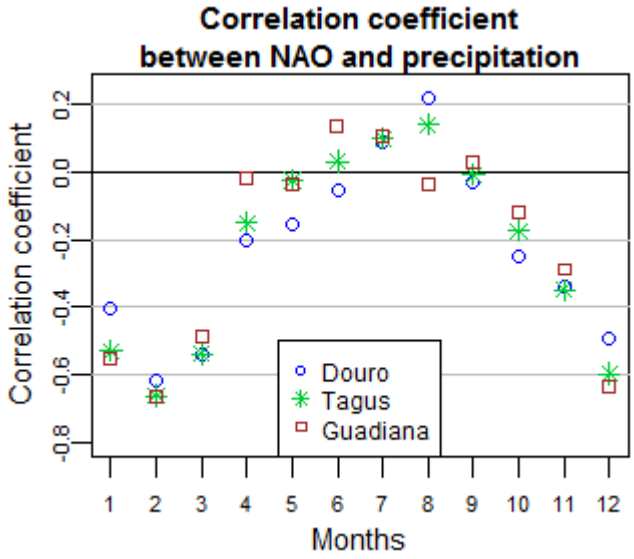

Figure 3.17 – Pearson correlation coefficients between the rainfall series and the NAO index, per month, averaged per basin.

3.4.5.1 The case of February

The overwhelming majority of gauges showed a change in the month of February, in the mean or the variance, either as a change point or as a trend (plots of rainfall series for February are presented in Figure 3.9). Regarding change points, the Pettitt test identifies the change more often as a change in the variance than in the mean, while the cusum test does the opposite.

The changes in the mean, as trends or change points, are very relevant as they range from 39% decrease to 149% decrease (relative to the mean) in the rainfall over the period 1961 to 2009 (see Figure 3.18). This decrease in rainfall ranges from 13.9mm to 240.0mm in absolute values. The Guadiana basin and the Portuguese side of the Douro and Tagus basins are the most affected by decreasing trends, while change points cover almost all gauges. Considering that the data come from two different countries (and in Spain from different autonomous regions), an undocumented change in monitoring procedures/equipment is unlikely to explain the change points that occurs both in the Portuguese and the Spanish datasets in the same month.

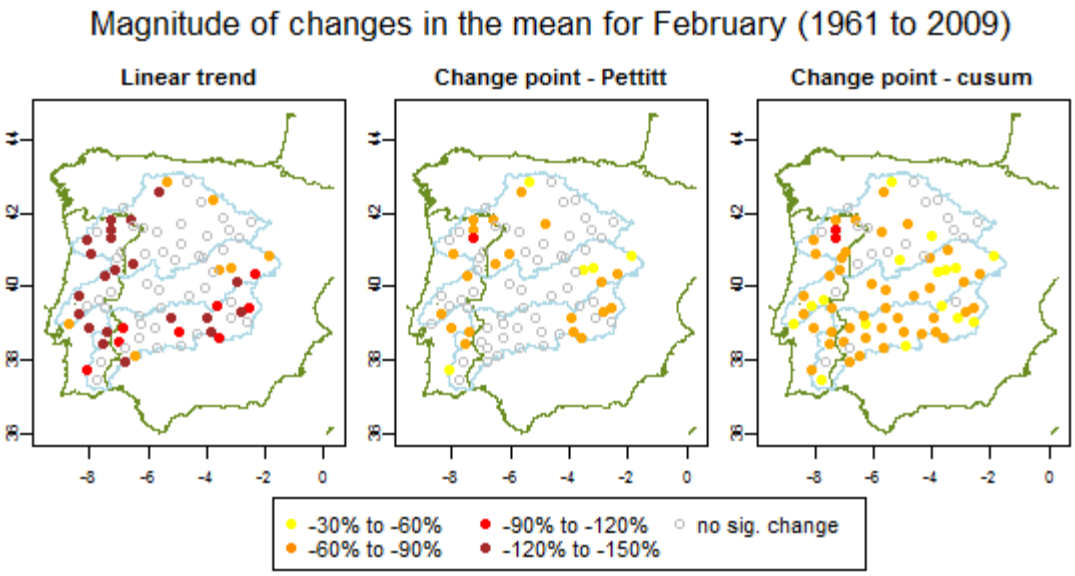

Figure 3.18 – Magnitude of the changes in March rainfall (in percentage relative to the mean) for each gauge, for the period 1961 to 2009, when interpreting the change as a linear trend detected by the Mann-Kendal test (left), a change point in the mean detected with Pettitt test (middle) or a change point in the mean detected with cusum test (right). The significance level is 0.05 for all tests.

A graph was plotted showing the years when the significant (0.05 significance level) change points occurred, both in the mean and in the variance for both statistical tests (Figure 3.19). When accounting for the result of both tests, there seem to be two years that concentrate the majority of the significant change points in the mean: 1978 (mainly the cusum test) and 1986 (both tests). In the variance these years seem to be 1978 (cusum test) and 1985 (Pettitt test).

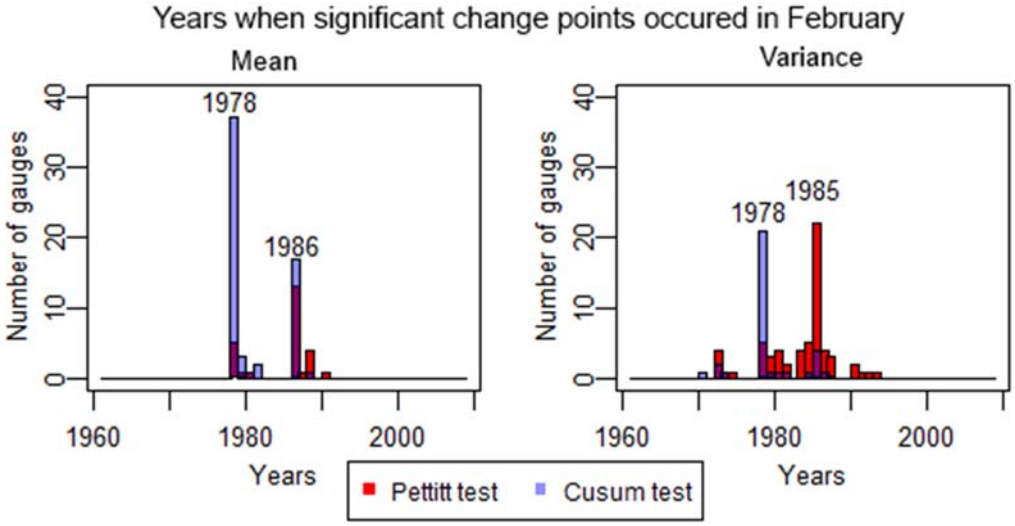

Figure 3.19 – Years when the significant change points occurred in the mean (left) and in the variance (right) in February. The significance level is 0.05 for the Pettitt test (red) and for the cusum test (blue).

According to NOAA's Climate Prediction Center (2011), in the winter of 1978/1979 the NAO changed from a predominantly negative phase (that had lasted since the mid-1950s) to a positive phase that lasted until the winter of 1994/1995 which was only interrupted by two

predominately negative winters: 1984/1985 and 1985/1986. This could represent a physical explanation for the change points in rainfall data detected by the Pettitt and Cusum tests.

When analysing the NAO index for the month of February (1961-2009), the Mann-Kendall test shows a significant increasing trend (with a p-value of 0.02), which might be the cause of the decreasing trends present in the rainfall records. Both Pettitt and cusum tests show a significant change point in the NAO for the year 1987 (seeFigure 3.20) with a p-value of 0.01 for both tests. By performing a one-tailed Pettitt test one can conclude that the change point corresponds to an increasing change. The 1978 change points in the rainfall records correspond to an extremely negative NAO (see Figure 3.20), while the 1985/1986 change points in rainfall are adjacent to the change point in the NAO index (1987).

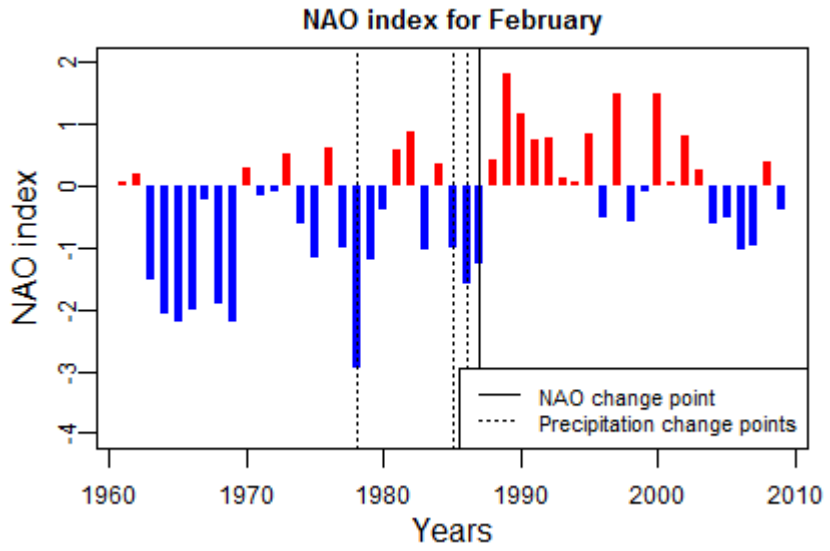

Figure 3.20– NAO index for the month of February (from 1961 to 2009) with its change point highlighted with a solid line (p-value of 0.01 for both Pettitt and cusum tests). Dotted lines denote the years where most gauges show a significant change point in the rainfall record for the month of February.

A positive NAO index induces a northern movement of the eddy driven jet (Woollings, 2010), therefore steering the Atlantic storm track towards the North of Europe. Consequently a positive trend in the NAO index could perhaps explain the negative trend in the rainfall variance since the stronger systems associated with the storm track are no longer present in Iberia, leaving only the weaker systems (instead of a combination of strong and weak systems) to influence the amount of rainfall.

3.4.5.2 The case of March

For the month of March, if the trend analysis is performed only for the period 1961 to 2000, almost all gauges show significant negative trends (see Figure 3.21). This concurs with various papers that described a decreasing trend in Iberia in March (Paredes *et al.*, 2006; Río *et al.*,

2010; Gonzalez-Hidalgo *et al.*, 2010b; Paulo *et al.*, 2012). However that trend, although still present, is no longer significant for the majority of gauges when the analysis is performed from 1961 to 2009.

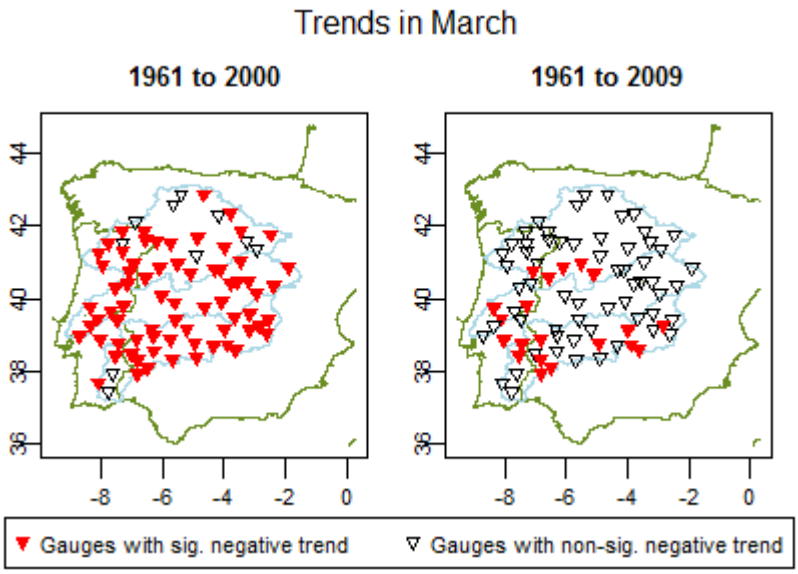

Figure 3.21 – Maps of significant and non-significant (0.05 significance level) trends (in the mean) for the month of March in the study area. On the left the trends were calculated for the period 1961 to 2000 and on the right the trends were calculated for the entire record (1961 to 2009).

When analysing the entire record, the changes in the mean for March, although not as widespread as the changes in February, are still relevant as they range from a 45% decrease to a 123% decrease in the rainfall over the period 1961 to 2009 (see Figure 3.22). This decrease in rainfall ranges from 17.7mm to 90.1mm in absolute values. The Guadiana basin and the southern gauges of Douro show the most change points. In terms of trends the same area plus the Portuguese side of Tagus is affected. Although the results of the cusum test were not above the limit of field significance, they are in agreement with those from the Pettitt test which do exceed the limit of field significance (see Figure 3.22).

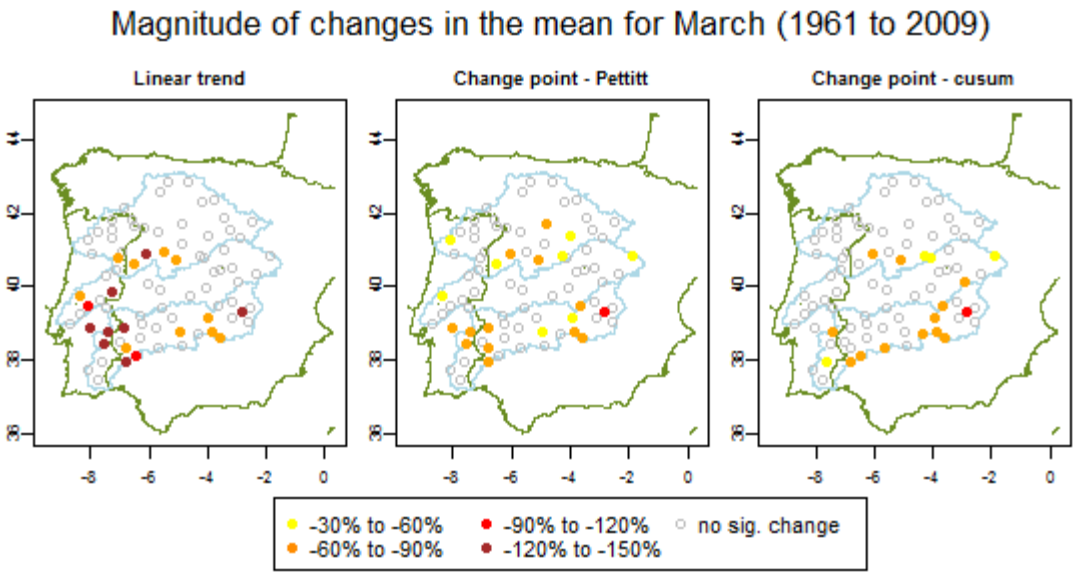

Figure 3.22 – Magnitude of the changes in October rainfall (in percentage relative to the mean) for each gauge, for the period 1961 to 2009, when interpreting the change as a linear trend detected by the Mann-Kendall test (left), a change point in the mean detected with Pettitt test (middle) or a change point in the mean detected with cusum test (right). The significance level is 0.05 for all tests.

Looking at the behaviour of the NAO index for the month of March (see Figure 3.23) there is an apparent monotonic trend from the beginning of the study period until the nineties that is no longer visible after the year 2000. If a Mann-Kendall test is performed at a 0.05 significance level, there is a significant trend for the NAO in the period 1961-2000 (with a p-value of 0.002) but not for the period 1961-2009 (p-value of 0.055). This might explain the trend in the rainfall record for the 1961-2000 period. No change points were found in the NAO index for March, either using the cusum or the Pettitt tests, at the 0.05 significance level.

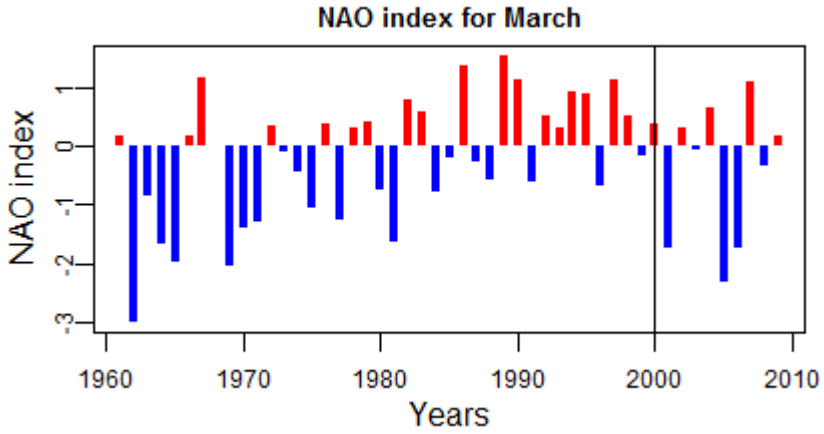

Figure 3.23 – NAO index for the month of March with the year 2000 highlighted with a vertical line.

3.4.5.3 The case of October

When performing the trend analysis for the mean, a spatial cluster of significant positive trends in the month of October in the Spanish side of Douro and Tagus catchments was identified. The magnitude of the linear trends identified ranges from 63% to 119% (see Figure 3.24). This increase in rainfall ranges from 22.2mm to 111.5mm in absolute values. The number of gauges with significant change points was much smaller than the number of gauges with significant trends. Therefore for the case of rainfall in October, interpreting the change as a trend might be reasonable.

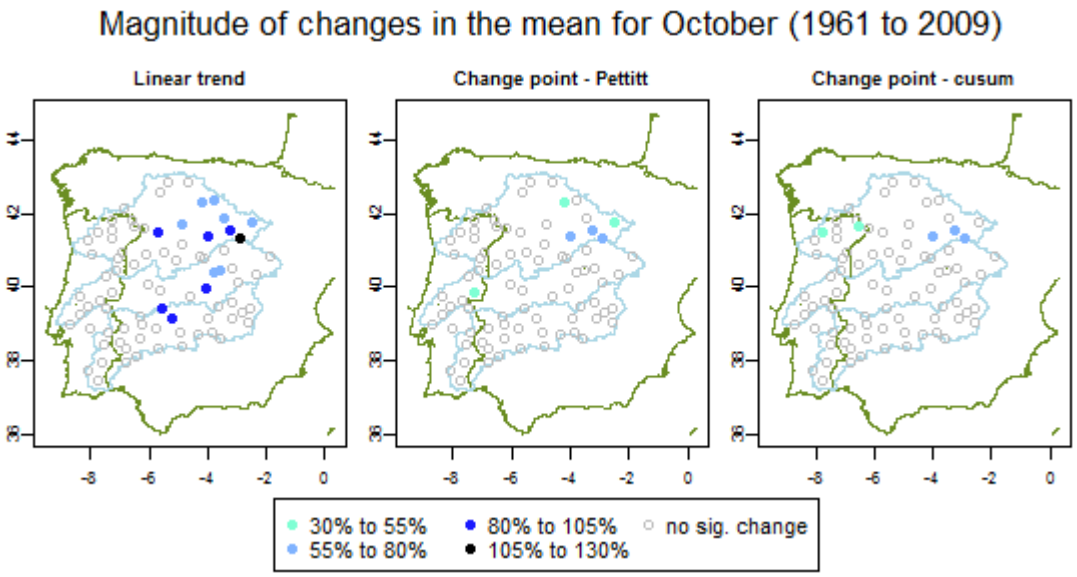

Figure 3.24 – Magnitude of the changes (in percentage relative to the mean) for each gauge, for the period 1961 to 2009, when interpreting the change as a linear trend detected by the Mann-Kendall test (left), a change point in the mean detected with Pettitt test (middle) or a change point in the mean detected with cusum test (right). The significance level is 0.05 for all tests.

The NAO index for the month of October (see Figure 3.25) shows a monotonic decreasing trend (with a p-value of 0.016 for the Mann-Kendall test), which could explain the increasing trend in the rainfall in the Spanish side of Douro and Tagus catchments. However, since the correlation between rainfall and NAO for the month of October is low (see Figure 3.17) other factors could be causing this increase in rainfall. As expected, no change points were found for the NAO, either using the cusum or the Pettitt tests at the 0.05 significance level.

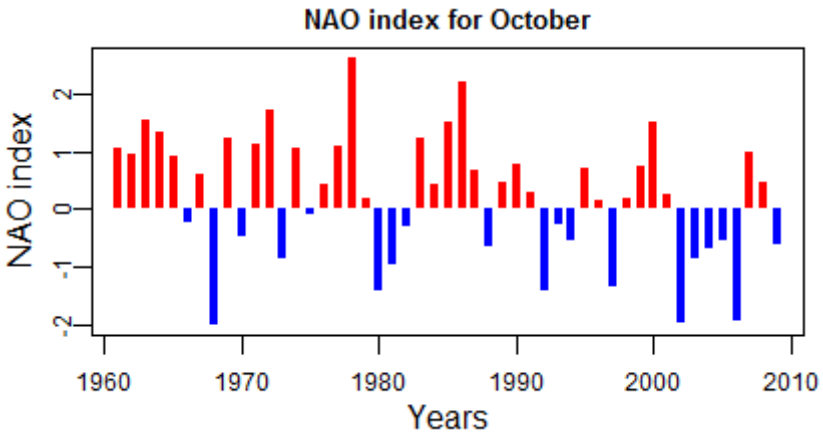

Figure 3.25 – NAO index for the month of October.

3.5 Conclusions

In this chapter, the problem of quantifying the spatio-temporal variation of rainfall in Iberian basins for the period 1961-2009 was addressed. The analysis allowed the highlighting of both methodological aspects related to the statistical inference and empirical results concerning the analysed data. From a methodological point of view, an attempt to distinguish between abrupt changes (change points) and trends was made. However this differentiation was not always possible in the short, noisy series analysed because the pattern of change can be more complex than these two simplistic ways of describing change. Performing the Mann-Kendall test before and after the change points did not help this differentiation because it was not possible to separate the effect that the change point might have on the trend from the effect of reducing the length of the record.

The danger of overestimating changes in rainfall by assuming that they take the form of linear trends was demonstrated. The analysis points out that Mann-Kendall test is devised to detect a monotonic change which in the limit case can be abrupt and is hardly ever linear. Moreover, it is well-known that the progressive Mann-Kendall test can be used to detect a change point (thanks to the similarity between the Mann-Kendall and Pettitt test statistics). Therefore, possible regime shifts that evolve in some steps can be recognized as a monotonic S-shaped trend. When both trend tests and change-point tests recognize a possible change, its quantification must be made with care, as the widely used linear trend could provide a poor and rough assessment and, in principle, is not coherent with the multiple alternative hypotheses (different admissible monotonic patterns) implied by nonparametric tests.

The effects of space and time correlation were also studied. The problem of performing multiple tests on data that exhibits spatial correlation is well known in the literature, but is often overlooked in empirical studies. In agreement with previous studies, the present analyses show that the impact of the spatial correlation can dramatically influence the results, thus leading to very different conclusions about the presence of time correlation, trends, and change points. As an example, when calculating the critical number of gauges whose ACF1 could be significant at 5% nominal significance level in February the result was seven gauges using the binomial approach (which does not account for spatial correlation). When this calculation was done using a bootstrap approach (which accounts for spatial correlation) the result was 17. This large difference can lead to opposite conclusions on the overall significance of the ACF1 values. Also, plotting the data on maps to assess the existence of spatial clusters across physically coherent areas that were not accounted for in the field significance analysis

proved to be important. The possible shortcomings of a *post hoc* domain selection were recognized as well.

Focusing on the empirical findings, the results of two statistical tests for change point analysis were used. Although they presented some discrepancy, significant change points in the mean were identified in February, March and June – all of them negative. February also shows negative change points in the variance.

Significant trends in the mean were identified in February (negative), June (negative), and also March for the Guadiana basin (negative) and October for the Spanish side of the Douro and Tagus Basins (positive). Significant trends in the variance were identified in February (negative).

Correlations between rainfall and the NAO index did not vary much from basin to basin. However, they showed a very strong seasonal pattern, with the months of December, January, February and March showing relatively strong negative correlations (correlation coefficients around -0.6) and zero or weak positive correlations for the months of June to September.

By month, those presenting the most interesting changes are February, March and October. February is the month where more changes are present, either as a trend or as a change point (with the Pettitt test identifying the change more often as a change in the variance and the cusum test identifying it more often as a change in the mean). The changes in the mean for February range from a 39% decrease to a 149% decrease in the rainfall over the period 1961 to 2009 (depending on the gauge and on the type of change considered). Most change points in February occur in the year 1978, which corresponds to the year where the NAO index was more negative, and in the years 1985/1986 which is adjacent to the change point in the February NAO index (1987).

For March, if the trend analysis is done for the period 1961 to 2000 (which was done to compare our results with previous studies), almost all gauges show significant negative trends. However those trends are no longer significant for the majority of gauges when the analysis is performed over the longer period from 1961 to 2009. When analysing the entire record, the changes in the mean for March range from a 45% decrease to a 123% decrease. The NAO index for March shows a significant increasing trend (Mann-Kendall test at the 0.05 significance level) for the period 1961 to 2000 that loses its significance for the period 1961 to 2009. This might explain the behaviour of the rainfall trends for March.

October showed positive significant trends in the Spanish side of Douro and Tagus catchments that ranged from 63% to 119%. This might be explained by a monotonic decreasing trend (with

a p-value of 0.016 for the Mann-Kendall test) in the NAO index for the month of October. As the number of change points in the rainfall data was below the limit of field significance (and the NAO did not present any change points), in this case, interpreting the change as a slowly varying trend might be reasonable.

Therefore, this work has extended previous studies on Iberian rainfall (Paredes *et al.*, 2006; Rodrigo and Trigo, 2007; Costa and Soares, 2009; Río *et al.*, 2010; González-Hidalgo *et al.* (2010a); Gonzalez-Hidalgo *et al.* (2010b)) in several important respects: by updating rainfall data to 2009, by covering three major transnational basins, using data from Spain and Portugal which are normally considered separately, by using a portfolio of statistical tests, allowing for the detection of change points as well as trends, by considering the effects of field significance and by showing the overestimation of changes in rainfall that can come from assuming the change is happening as a linear trend.

Also, this thorough analysis of historical rainfall provides the necessary context to the analysis of future rainfall changes projected by climate models presented in the next chapter and the changes in drought and discharges in subsequent chapters. The effects of short term variability in the study of long-term changes (demonstrated in the analysis of March rainfall) were especially relevant for the interpretation of these future changes.

Chapter 4. Climate Models, Downscaling and Future Rainfall

This chapter starts with a brief literature review of the sources of uncertainty in climate models, of the challenges in combining outputs from multi-model ensembles and of downscaling techniques (with a focus on the techniques that will be used in this study).

After introducing the datasets used, the selection procedure of climate model outputs is presented where the objective was to select the smallest possible number of models that allowed the capture of the full range of uncertainty for temperature and rainfall mean changes. The downscaling methods used (change factor and bias correction through empirical quantile mapping) are also extensively explained.

In the results section, a comparison is made between monthly rainfall from climate models and observed rainfall for the period 1950 to 2003. The models' dispersion is considerable large, but in most cases it encompasses the observed data.

For the 2050s, the majority of models projected a reduction in rainfall in the three basins for all months (using both downscaling methods) but there is a significant spread between different models. The range of annual rainfall changes was between -33% and +7% in the Douro, -33% and +10% in the Tagus and -41% and +10% in the Guadiana.

The magnitude of linear long-term trends (1961-2100) was also calculated for annual and seasonal bias-corrected rainfall. Only three significant positive trends were identified and all of them in the winter. Annual changes ranged between -6% per decade and no significant change. This analysis showed that a considerable part of the climate model disagreement in the projection of future rainfall changes for the 2050s was due to the choice of 30 year intervals within possibly cyclic patterns of rainfall.

Reductions in rainfall were projected for spring and autumn by almost all models, both downscaling methods and both methods of analysing future rainfall changes (differences between 30 years periods and trends in transient rainfall) pointing to a possible lengthening of the dry season in these three basins.

The chapter ends with conclusions where the main results of all these different methods are collated and their implications are discussed.

4.1 Introduction

4.1.1 *Climate models*

Outputs from a new generation of Atmosphere-Ocean General Circulation Models (GCMs) are available from the fifth phase of the Climate Model Intercomparison Project (CMIP5) and will feature in the Intergovernmental Panel on Climate Change Fifth Assessment Report (AR5). The CMIP5 provided a framework for coordinating climate change experiments from climate modelling groups around the world. The objectives of this project were to evaluate how realistic the models are in simulating the recent past, to provide projections of future climate change and to understand some of the factors responsible for differences in model projections (WCRP, 2012).

There are three main reasons for uncertainty in climate projections: greenhouse gases emissions, model-responses and natural variability (Deser *et al.*, 2012). Uncertainties in forcing (emission/concentration of greenhouse gases) are circumvented by making predictions conditional on an emission/concentration scenario (Knutti *et al.*, 2010b). Model-responses are imperfect due to limited theoretical understanding with many small scale processes being parameterized in a simplified form and some processes missing or being only approximated (Knutti *et al.*, 2010b).

Natural variability is largely a consequence of the chaotic nature of large-scale atmospheric circulation patterns and therefore its related uncertainties are unlikely to be reducible. Deser *et al.* (2012) showed that natural variability (or "initial conditions" uncertainty) can contribute significantly to uncertainty in rainfall and temperature predictions even for timescales of more than 50 years, and suggested that it might explain the disagreement in future projections between different GCMs. Regional averaging might not reduce this type of uncertainty (because some local areas have lower natural variability than others) and downscaling, whether statistically or dynamically, adds local detail but cannot mitigate these uncertainties (Deser *et al.*, 2012).

The spread of future projections is not decreasing although models are getting better at reproducing the mean state of climate and past trends. However, because some of the datasets used for climate model calibration are also used for their validation, it is unclear if the convergence to observations is due to model improvements or if it is a by-product of the model calibration. The inclusion of more processes and therefore more degrees of freedom might also play an important role in explaining this spread (Knutti, 2010).

Climate models from CMIP5 are more heterogeneous in structure than those from previous generations of CMIP; since some models now have interactive representations of biogeochemical cycles, gas-phase chemistry, aerosols, ice sheets, land use, dynamic vegetation, or a full representation of the stratosphere which makes a model average difficult to interpret and defend (Knutti *et al.*, 2010a). Furthermore, averaging across models might produce physically implausible results that do not resemble any of the models because spatially heterogeneous patterns between models are smoothed (Knutti, 2010).

Besides averaging, another common way of using different climate model outputs is to build a probability density function (PDF) of change from the ensemble of models. However, this means assumptions are being made that the models are independent, distributed around a "perfect model" and sample the range of uncertainty (Knutti, 2008). In a multi-model ensemble like the CMIP5, where models are not independent, model agreement might not be an indication of likelihood but a consequence of shared process representation and/or calibration on particular datasets (Knutti *et al.*, 2010a). Also the sampling of models is not random or systematic (Knutti, 2010) and it is hard to verify (or falsify) that the ensemble spans the full uncertainty range (Masson and Knutti, 2011).

A general all-purpose metric that allows a user to evaluate climate models has not been found, and different metrics produce different rankings of models. Consequently, excluding or weighting models might lead to overconfidence in the projections and unjustified convergence (Knutti *et al.*, 2010a).

However, analysing the way different GCMs simulate important atmospheric physical processes for the studied area (like the North Atlantic jet stream/storm track for the case of Iberia) can give a better understanding of model performance and perhaps reasons for their lack of agreement. The atmospheric component is very diverse among CMIP5 models; some have spectral and others have grid point dynamical cores, horizontal resolutions vary from approximately 80Km to 310Km while vertical resolutions range from around 20 to 80 levels and only around half the models have a well resolved stratosphere (Zappa *et al.*, 2013). Zappa *et al.* (2013) found that although CMIP5 models still underestimate the intensity of cyclones (both in winter and summer) they capture the meridional tilt of the North Atlantic stormtrack in winter better than the CMIP3 model set (see Figure 4.1). Notwithstanding this improvement, the CMIP5 models ability to simulate the North Atlantic stormtrack is very diverse and they clustered the models into three groups regarding their ability to simulate the position of the North Atlantic stormtrack in winter (compared to ERAI): a group that shows small biases (EC-EARTH, GFDL-CM3, HadGEM2-ES and MRI-CGCM3), a group with a southward

displaced stormtrack and a group which displays a stormtrack that is too zonal (and MIROC5 where the stormtrack is southward displaced at 60W but it is well positioned at 0E). The different performance of these groups can be seen in Figure 4.2. Zappa *et al.* (2013) also showed that the bias in cyclone density was related to the model's ability to represent the Atlantic jet stream but the biases in cyclone intensity are probably dependent on the numeric parameterisations of the models.

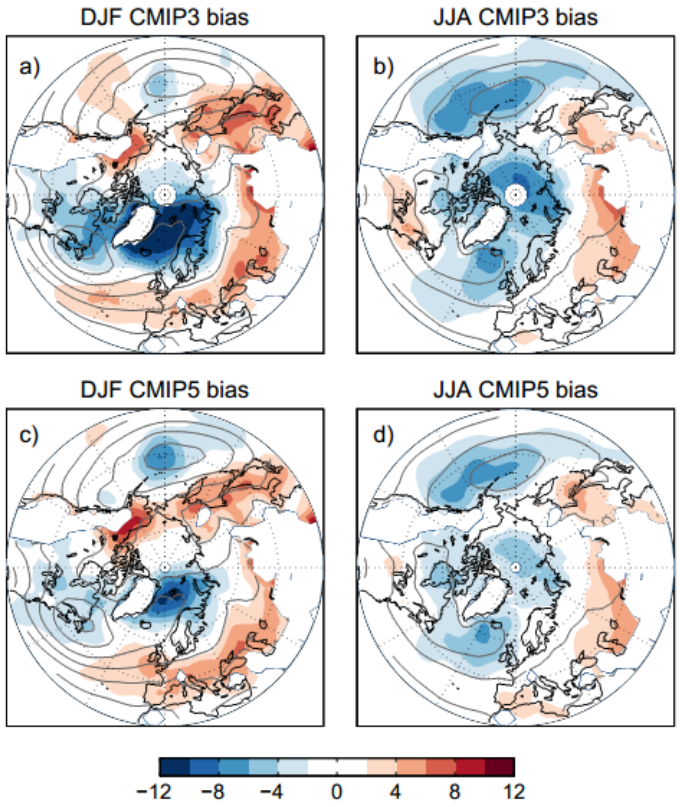

Figure 4.1 - Mean bias (in 10^{-1}hPa) with respect to ERAI reanalysis (shading) in 2–6 days bandpass filter standard deviation of mean sea level pressure of the control simulations of the CMIP3 (a–b) and CMIP5 (c–d) models in DJF (a,c) and JJA (b,d). The ERAI climatology is contoured with isolines every 1 hPa. High orography is masked (Zappa *et al.*, 2013).

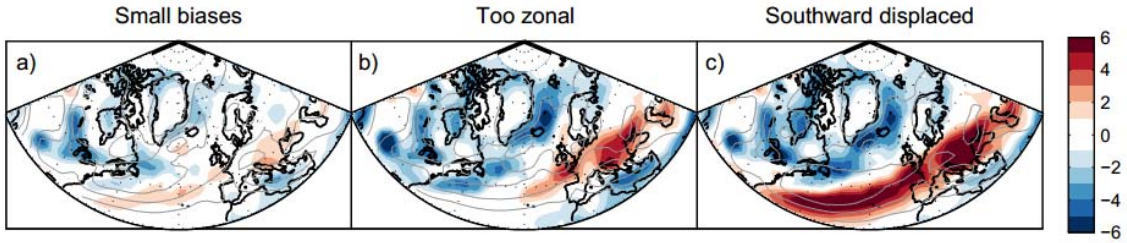

Figure 4.2 - Mean DJF track density bias (HISTORICAL - ERAI) of the CMIP5 models (in cyclones per month per unit area) separately computed for three groups of similar behaviour: the small bias group (a), the too zonal group (b) and the southward displaced group (c). The group mean climatology is contoured with isolines every 4 cyclones per month per unit area (Zappa *et al.*, 2013).

Small differences at the GCM scale can lead to completely different results on a local scale. For example, the CMIP3 models showed an increase in rainfall in the north of Europe and a

decrease in the south, with the latitude of the transition zone being pushed north during the summer and south during the winter. However, the latitude of this transition zone can differ by hundreds of kilometres between different GCMs which has deep implications for country-scale impact studies (Boé *et al.*, 2009).

The lack of consensus on how to combine GCM outputs highlights the need for robust adaptation. Sometimes using a few models to demonstrate alternative plausible outcomes (without probabilities being assigned) might be a useful and transparent way to test different adaptation strategies. However one has to consider that the extreme ends of the plausible range might not be sampled (for e.g. very high climate sensitivities are not present in CIMP3) and that the chosen outcomes might be perceived as equally probable (Knutti *et al.*, 2010b).

4.1.2 *Downscaling*

Due to their coarse resolution, and therefore the inability to resolve significant subgrid scale features, GCM outputs have to be downscaled when used to assess local/regional impacts of climate change (Fowler *et al.*, 2007). A downscaling procedure has to be able to reproduce observed conditions of the relevant variables at the appropriate time scale(s) for the impact being studied. Therefore, the validation and the correction of climate model outputs rely on the availability, length and quality of the observation records. The ability to represent the spatial variability of rainfall depends on the density of the monitoring network, furthermore rainfall is more difficult to model than temperature due to its nonlinear nature and high temporal and spatial variability (Maraun *et al.*, 2010). Moreover, downscaling GCM output does not take into account the feedbacks between the large and small scales and the implications of this are unknown (Maraun *et al.*, 2010).

Several downscaling techniques exist but they can be grouped into two main methods: dynamical and statistical. Dynamical downscaling consists of embedding a regional climate model (RCM) or a limited-area model within a GCM (Fowler et al., 2007). RCMs model the same atmospheric processes as GCMs but have a higher resolution and cover a sub-global domain (Maraun *et al.*, 2010). Sea surface temperatures are supplied by the GCM as are the boundary winds, temperature, and humidity. Due to their higher spatial resolution, RCMs show an improvement in the description of orographic effects, land-sea contrast, land surface characteristics and mesoscale circulation patterns. They also retain the spatial and temporal correlation between variables (Maraun *et al.*, 2010). However, dynamical downscaling is extremely computational intensive which limits the number of runs available and it inherits biases from the driving GCMs (Fowler et al., 2007).

RCMs represent rainfall better than their driving GCM (including extreme events), however they still tend to overestimate the number of days with light rain ("drizzle effect") and underestimate the occurrence of heavy precipitation. The latter deficiency is usually attributed to inadequate representation of convective processes and/or to insufficient resolution of the topography within the model. Precipitation is strongly dependent on several parameterization schemes and both the sub-daily precipitation and the diurnal cycle of convection are not well simulated. Very high grid resolution (≤5km) has been shown to improve the diurnal cycle of convection and short duration extreme precipitation events (Kendon *et al.*, 2012). Nonetheless, RCMs still tend to show a wet (dry) bias in dry (wet) months and a warm bias in hot and dry regions (Maraun *et al.*, 2010).

Bias correction has been used to transform the statistical properties of the modelled data (from an RCM or a GCM) to match the ones of the observed data. However, these statistical properties depend on the time-scale (for example daily and monthly means can show a different statistical behaviour); therefore the correction of the data is limited to the time-scale used. This means that, for example, when bias-correcting daily temperatures the correction might be detrimental for monthly temperature statistics (Haerter *et al.*, 2010). Bias-correction is based on empirical statistical relationships between model outputs and observations and often done on a quantile basis. Therefore, just like with statistical downscaling, an assumption has to be made that this correction remains valid for future climate conditions (Boé *et al.*, 2009).

Statistical downscaling is based on the establishment of empirical relationships between output variables from GCMs or RCMs and observed variables of the local climate. It is less computationally intensive and simpler than dynamical downscaling but it breaks down the physical relationships between different variables. By correcting some variables but not others the feedbacks between the variables are not properly taken into account (Ehret *et al.*, 2012).

The simplest statistical downscaling method is the change-factor (CF), perturbation or delta-change approach where the mean change between control and future GCM outputs is applied to observations (by adding or multiplying, depending on the variable). Its simplicity makes it possible to downscale several GCM/scenarios quickly but this method assumes that the GCM bias is constant in time and that variability, spatial patterns of climate and percentage of wet/dry days will remain the same (Fowler *et al.*, 2007).

The CF method cannot be used to simulate transient changes in climate because the mean changes are calculated for specific time slices. Another problem with the method is the inherent step change it introduces when applying different monthly change factors to the

data. However this method preserves spatial correlations between stations or grid points, which some complex statistical methods are not able to. This simple method also captures the full climate signal of the GCM/RCM while more complex downscaling methods capture only climate forcing shown by the chosen predictor(s) and grid box(es) (Diaz-Nieto and Wilby, 2005). The CF method is not suitable for the study of extreme events (since it assumes that changes in the mean and in the extremes are the same) but might be appropriate for studies where changes in average values are relevant such as regional water resources studies (Sunyer *et al.*, 2010).

Regression models, weather typing schemes and weather generators are more sophisticated statistical downscaling tools where the regional variable to downscale is a function of a large-scale climate variable present in the GCM. The function is typically calculated using observations or reanalysis data. The choice of large-scale variable (predictor) has to be made carefully: it has to be well represented by the GCM, be physically relevant and reflect the local climatic variability on a range of time-scales (Fowler *et al.*, 2007). Regression models directly quantify a relationship between the local scale variable of interest and large scale atmospheric variables. Weather generators are stochastic models that simulate weather data based on observed statistical properties and, in weather typing, days are grouped according to synoptic similarity into a number of weather types or states (Sunyer *et al.*, 2010). These methods assume that the relationship between the predictor and the predictand is (and will remain) stationary in time. Also, since only part of the regional/local climate's variability is related to large-scale processes, regression models and some weather typing schemes tend to underpredict climate variability (Fowler *et al.*, 2007). Generally speaking, regression-based methods and weather typing are not adequate for simulating extreme rainfall events (Sunyer *et al.*, 2010).

Both statistical and dynamical downscaling methods perform poorly for convective and for sub-daily rainfall and they all inherit GCM circulation errors like the insufficient number of blocking events over Europe which can cause drought and heat waves in the summer (Maraun *et al.*, 2010). Changes in extreme rainfall are harder to predict than changes in mean rainfall or changes in temperature, also downscaling methods perform worse for extreme precipitation changes, therefore changes in high flows are more uncertain than changes in mean or low flows (Boé *et al.*, 2009).

Boé *et al.* (2009) state that it is preferable to use a simple statistical method to downscale a large ensemble of GCMs in order to characterize the envelope of uncertainty than dynamically downscale a single GCM. Themeßl *et al.* (2011) studied the performance of seven empirical

statistical downscaling and bias correction methods to correct RCM daily precipitation outputs in Austria: multiple linear regression (MLR), multiple linear regression with randomization (MLRR), analogue method (AM), nearest neighbour analogue method (NNAM), local intensity scaling (LOCI) and quantile mapping (QM) using the empirical distribution. The direct approaches (QM and LOCI) and the non-linear resampling methods (AM and NNAM) performed well in correcting the entire distribution (mean, day-to-day variability and extremes), with QM performing slightly better. MLR and MLRR could not estimate non-normally distributed precipitation even when using objective predictor selection. The authors favoured the use of QM since it showed the best performance and because it is a simple non-parametric method. QM corrects the shape of the distribution (which means variability is corrected) but only maps modelled values to observed values, which means that for future climate simulations extrapolation may be necessary in order to deal with modelled values outside the observed range. This study did not account for the impact of decadal variability on model error statistics.

Lafon *et al.* (2013) compared the following different methods of bias correction for daily precipitation from one RCM for seven catchments in Great Britain with different climatic conditions: linear, non-linear, distribution-based quantile mapping and distribution-free quantile mapping (empirical distribution). They concluded that although the first and second moments of the distribution could be robustly corrected, the third and fourth moments couldn't. The empirical quantile mapping with the highest number of quantiles gave the better correction but its sensitivity to the calibration period meant it was not a very robust technique. Over fitting to the calibration period can always be a problem with methods with many degrees of freedom (as QM), however, Gudmundsson *et al.* (2012) using observed daily precipitation for Norway for the 1960-2000 period, found it not to be a problem for QM if there was sufficient data for the calibration.

Rainfall and surface temperature are outputs from GCMs/RCMs and can therefore be directly downscaled from the climate models either dynamically or statistically using any of the methods mentioned above. Potential evapotranspiration (PET), which is a necessary input in hydrological models, is not an output of climate models which adds another layer of complexity to assessing its future changes.

Evapotranspiration is the water lost through evaporation from soil, plant surfaces and open water and plant transpiration and it is limited by soil water availability, radiation and the humidity of surrounding air. When soil moisture is not a limiting factor, the maximum evapotranspiration rate for the specific local environmental conditions occurs. This maximum

rate is called potential evapotranspiration (PET). Because PET is a theoretical concept with inherent direct monitoring difficulties, several equations have been developed to calculate PET from measurable variables. Some of these equation use radiation, wind speed, humidity and air temperature but the last two variables have been found to be the most relevant (Prudhomme and Williamson, 2013).

The Food and Agricultural Organisation of the United Nations (FAO) recommends the use of the Penman-Monteith (PM) equation for the calculation of PET, which is physical-based and incorporates the relevant meteorological variables. However due to the amount of data required for this method, PET is often calculated using simplified, empirical methods that require fewer input data (Kingston *et al.*, 2009).

Weiland *et al.* (2012) concluded that PM applied to Climate Forecast System Reanalysis data did not outperform other methods when compared to the CRU dataset (CRU TS2.1 and CRU CL 1.0) – which is also derived using a variant of the PM method – and in arid regions resulted in low PET values and consequently in discharges that were too high (Weiland *et al.*, 2012).

Ekström *et al.* (2007) found that PM calculated PET based on outputs from the climate model HadRM3H for the NW of England and for the Rhine basin showed biases that could not be corrected by a multiplicative adjustment. It also produced physically unrealistic future PET that could not be used for hydrological modelling.

Prudhomme and Williamson (2013) found that even the sign of future PET changes for the UK (using HadRM3-Q0 climate simulations) can depend on the method used for the calculation of PET and that PET increases projected for spring and summer were higher for temperature-based methods than for radiation-based methods.

Kingston *et al.* (2009) investigated the global response of six PET calculation methods to a 2°C increase in global temperature using outputs from five CMIP3 GCMs and found that the uncertainty in water surplus between PET methods from each GCM was of comparable magnitude to the uncertainty between GCMs for a given PET method. This means that the method used to calculate PET changes can significantly add to the uncertainty of the projections, especially in regions where precipitation is closely in balance with PET. Furthermore the authors questioned if it is preferable to calculate PET changes using more reliable physical-based methods (like the PM) based on variables that are not well simulated by the GCMs (cloud cover and vapour pressure) or use simpler empirical methods based on a more reliable GCM output (temperature).

4.1.3 *Studies of future climate in the region*

Both Portugal and Spain have national climate change impact studies. In Portugal the project SIAM - Scenarios, Impacts and Adaptation Measures (Santos *et al.*, 2002) assessed the impact of climate change in the country, dividing it into three regions: North, Centre and South. A second project (SIAM II) focused on the island territories. Four runs of the climate model HadCM3 (different initial conditions for A2 and B2 emission scenarios) and one of the HadRM2 model were selected from an ensemble of six climate models (RCMs and GCMs) and the downscaling method used was the change factor. The choice of climate models was based on similarity to observed climatic conditions in Portugal for the historical period. As discussed in section 4.1.1, there is no agreed metric to evaluate or exclude models, with different metrics producing different rankings of models. Furthermore, being able to produce similar conditions to the observed for a particular parameter, a particular time interval and a particular region does not mean that the relevant atmospheric physical patterns are well simulated (it might be a result of errors cancelling each other or random chance). Consequently, choosing one GCM and one RCM (from the same institution) does not allow a proper exploration of the range of uncertainty of future projections.

Nevertheless, the project results showed an increase in annual mean temperature of between 2.0°C and 3.0°C by 2050 (3.5°C and 5.0°C by 2100), with the Northern region showing smaller increases. Rainfall results showed a wide range of projections but the general trend indicating an annual decrease of up to 10% in the northern region, and up to 30% in the southern region (Da Cunha *et al.*, 2007).

In Spain, the project “Generación de Escenarios Regionalizados de Cambio Climático para España” (Brunet *et al.*, 2009), which is only available in Spanish, used several climate models and both dynamical downscaling (from the PRUDENCE project) and different statistical downscaling methods to provide future changes in meteorological variables. They projected annual temperature changes of 3-5°C (2045-2070) and 5-8°C (2071-2100) for the scenario A2 and approximately 2°C lower for the scenario B2. Both scenarios showed a higher increase in summer than winter months.

In terms of rainfall they also found a lack of agreement between models; with climate model deviations being of the same order of magnitude as the differences between historical and future rainfall. According to the authors, this is partly because of different downscaling techniques (with different RCMs showing different projections when run with the same GCM) and partly because of the position of the Iberian Peninsula; between the high latitudes in

Europe where GCMs show an increase in rainfall and the sub-tropical zone where a reduction of rainfall is expected.

Other studies concerning the future climate of the Douro, Tagus or Guadiana basins were not found.

4.2 Data

A gridded daily rainfall dataset for Iberia - IB02 - was used. This was produced by merging two datasets, a Portuguese dataset: PT02 (Belo-Pereira *et al.*, 2011) and a Spanish dataset: Spain02 (Herrera *et al.*, 2012). Both datasets have a resolution of 0.2° × 0.2° (see Figure 4.5) and used ordinary kriging based on a dense network of quality-controlled gauges (2000 in Spain and 400 in Portugal). The IB02 dataset covers the period from 1950 to 2003.

Gridded monthly PET from the Climatic Research Unit, version CRU TS 3.1 (Harris *et al.*, 2013) with 0.5° spatial resolution was also used. The method for PET calculation used in this dataset is the FAO grass reference evapotranspiration equation which is a variant of the Penman-Monteith (PM) method to use with gridded variables. The data-set covers the period from 1961 to 2009 and the mean annual values for Iberia are plotted in Figure 4.3. CRU's PET values range from 770mm and 1380mm and are of the same order of magnitude as the ones presented in the Portuguese National Water Plan (INAG, 2002) – 1025mm for Douro, 1124mm for Tagus and 1242mm for the Guadiana – and a little higher than the ones presented in the Spanish Water White Paper (MMA, 2000) which are shown in Figure 4.4. The Portuguese values were calculated using the PM method for the period 1941/42 to 1990/91. The Spanish values were calculated using the Thornthwaite method corrected by monthly factors in order to obtain values analogous to the results of the PM method for the entire Spanish territory for the period 1940/41 – 1995/1996. Both the different methods and the different time-periods could perhaps explain the differences between the Spanish dataset and the CRU dataset.

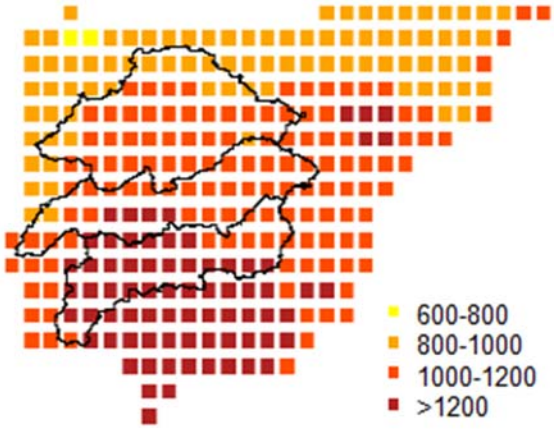

Figure 4.3 – Map of Iberia with mean annual PET (mm) from CRU dataset (1961-2009) and the studied basins in black.

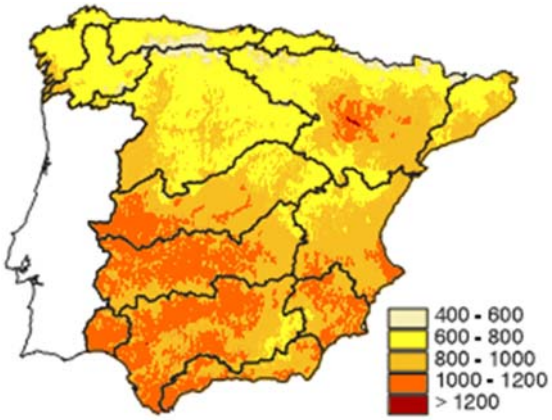

Figure 4.4 - Map with mean annual PET (mm) for Spain calculated for the period 1940/41 – 1995/1996 from the Spanish Water White Paper (MMA, 2000) with the main Spanish water basins in black.

Monthly rainfall and minimum and maximum monthly temperature outputs from the CMIP5 models were downloaded from http://climexp.knmi.nl. The data from all the GCMs were

available regridded to a common grid (2.5°). At the time of download (June 2012) 65 model runs were available with the required variables (see Table 4.1). The variables and the time-scale chosen (monthly) reflect the objective of using these GCM outputs to study water resources and drought for the Douro, the Tagus and the Guadiana basins. Four GCM grids were chosen (see Figure 4.5) in order to cover as much of the basins as possible but without incorporating grids that contained ocean (since that could skew the values of the grid's spatial mean).

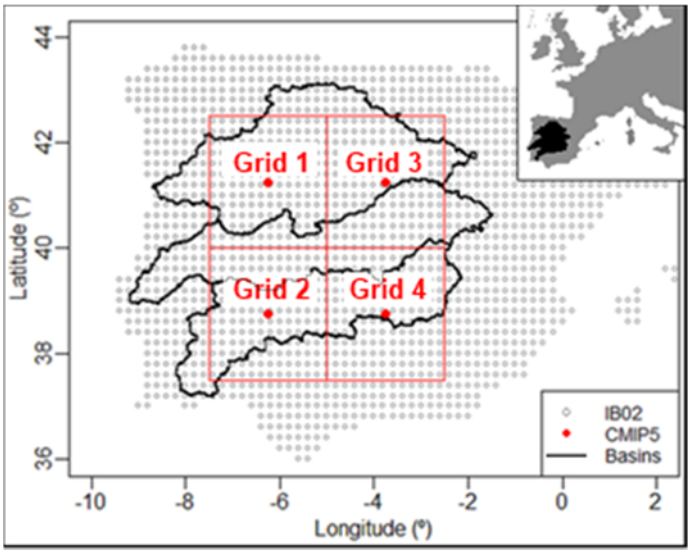

Figure 4.5 – Map of Iberia with the grid points for IB02 (gridded observed rainfall data) and the CMIP5 grids used in this study. The three studied basins are also highlighted in black.

Table 4.1 – GCMs (and their number of runs) from CMIP5 used in this study.

Model	Number of runs
ACCESS1-0	1
bcc-csm1-1	1
CanESM2	5
CCSM4	5
CESM1-BGC	1
CESM1-CAM5	1
CNRM-CM5	5
CSIRO-Mk3-6-0	10
EC-EARTH	5
FGOALS_g2	1
FIO-ESM	3
GFDL-CM3	1
GFDL-ESM2G	1

Model	Number of runs
GFDL-ESM2M	1
GISS-E2-R	3
HadGEM2-ES	4
inmcm4	1
IPSL-CM5A-LR	4
IPSL-CM5A-MR	1
MIROC5	3
MIROC-ESM	1
MIROC-ESM-CHEM	1
MPI-ESM-LR	3
MPI-ESM-MR	1
MRI-CGCM3	1
NorESM1-M	1

In terms of greenhouse gas scenarios, CMIP5 results are available for four representative concentration pathways (RCPs): RCP8.5, RCP6, RCP4.5 and RCP2.6. In this study RCP8.5 will be used, which has a rising pathway of radiative forcing of more than 8.5W/m^2 in 2100 (more

than 1370 CO2-equiv) being the highest emissions scenario of the four (Moss *et al.*, 2010). Sanderson *et al.* (2011) showed that RCP8.5 is similar to SRES A1FI and, although they are the higher emission scenarios considered by IPCC, they still assume emissions well below what the current energy mix would produce in the future (see Figure 4.6).

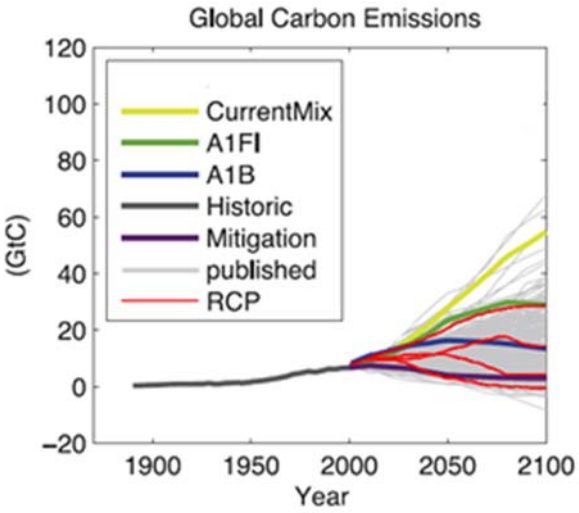

Figure 4.6 – Global anthropogenic emissions of CO_2 in the four RCPs, A1FI and A1B SRES scenarios, a current mix scenario (where the carbon intensity of energy supply is assumed to remain constant at 2000 levels), a mitigation scenario from Washington et al (2009) and other 600 published scenarios (adapted from Sanderson *et al.* (2011)).

4.3 Methodology

4.3.1 *Climate model selection*

Monthly maximum and minimum temperature time-series from each CMIP5 model run were averaged to create time-series of monthly mean temperature. Please note that monthly temperature will always refer to monthly mean temperature and monthly rainfall to monthly rainfall totals in this chapter.

A comparison between rainfall from the CMIP5 model runs and gridded observed rainfall (IB02) was performed by plotting monthly rainfall means against monthly rainfall coefficients of variation for each GCM. The observed gridded rainfall had to be spatially aggregated to the four GCM grids before plotting. The entire available observed rainfall record (1950 to 2003) was used and the same time-slice was used from all the GCMs.

For analysing future changes a sub-section of the GCM transient integrations had to be chosen because each run of the hydrological model used takes several weeks for any of the studied basins. Therefore running the hydrological model 65 times for each of the basins would take months.

The 2041-2070 period (thereafter referred to as the 2050s) was chosen as the period to analyse future changes (compared to the reference period 1961-1990) because it is a standard period used in hydrology and 40 years into the future is a relevant time-frame for water resources planning.

As discussed in this chapter's introduction there is no agreed general all-purpose metric that allows a user to evaluate climate models, neither is there a consensus on how to select/combine the output of different GCMs. Also, as expected, no relation was found between how well the models simulate historical rainfall in Iberia and the changes they projected for the 2050s. This is shown in Figure 4.7 where it can be seen that the correlations between the root mean square error (RMSE) of monthly CMIP5 rainfall for the period 1961-1990 (against aggregated IB02) and rainfall monthly change projected for 2050s range between -0.74 and 0.86 across the different model runs with the mean correlation in GCM Grid 1 being 0.34, 0.30 in Grid 2 and 0.29 in Grid 3 and 4.

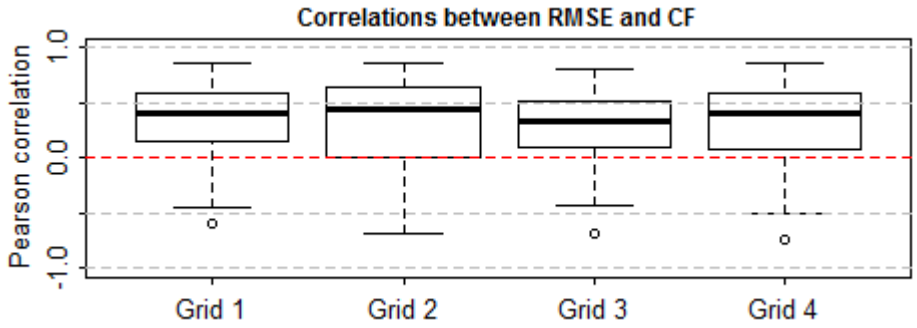

Figure 4.7 – Boxplots (whiskers showing 1.5 times the interquartile range and internal line indicating the median) showing the correlation between root mean square error (RMSE) of CMIP5 monthly rainfall for the period 1961-1990 and rainfall monthly change factor (CF) projected for 2050s by each model run for GCM gird 1 and 2.

In this study, the pragmatic decision was taken to select the smallest possible number of models that allowed the capturing of the full space of uncertainty for temperature and rainfall mean changes for the four GCM grids and the four seasons. Considering that only two variables were of interest (rainfall and temperature), the complications of a formal statistical method were not justified and the selection was ,made by plotting changes in mean temperature and rainfall for the four seasons and the four GCM grids (see Figure 4.8) and selecting model runs that would cover the full space of uncertainty. It was found that this could be achieved with the selection of 15 model runs, as shown in Figure 4.8 (the selected models are presented in Appendix C). The verification of the appropriateness of these 15 models to cover the whole range of mean future changes in rainfall and temperature are shown in Figure 4.9,

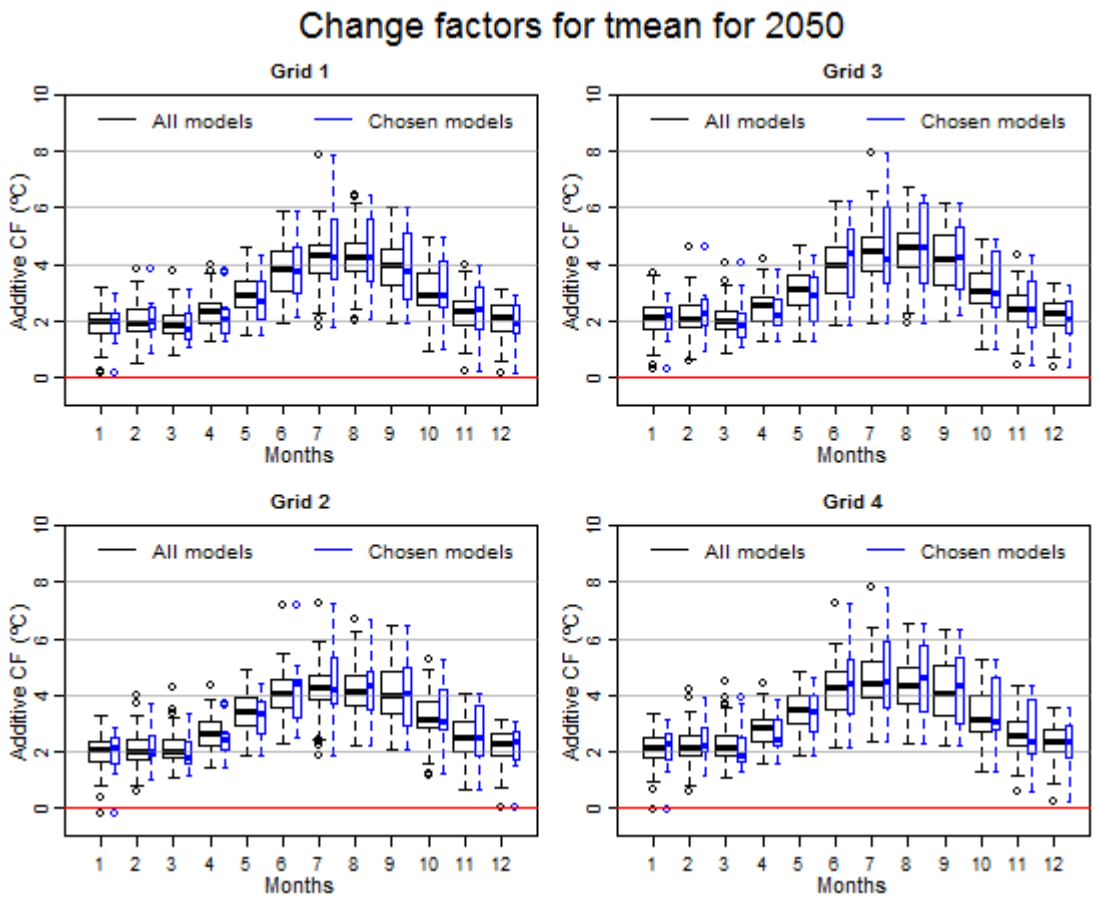

Figure 4.10 and Figure 4.14.

By choosing enough models to cover the space of uncertainty (available from CMIP5 model runs for RCP8.5) and by not assigning probabilities to any of the models, we hope to provide useful and transparent plausible future scenarios that can be used by others to test an array of adaptation alternatives, as suggested by Knutti *et al.* (2010b).

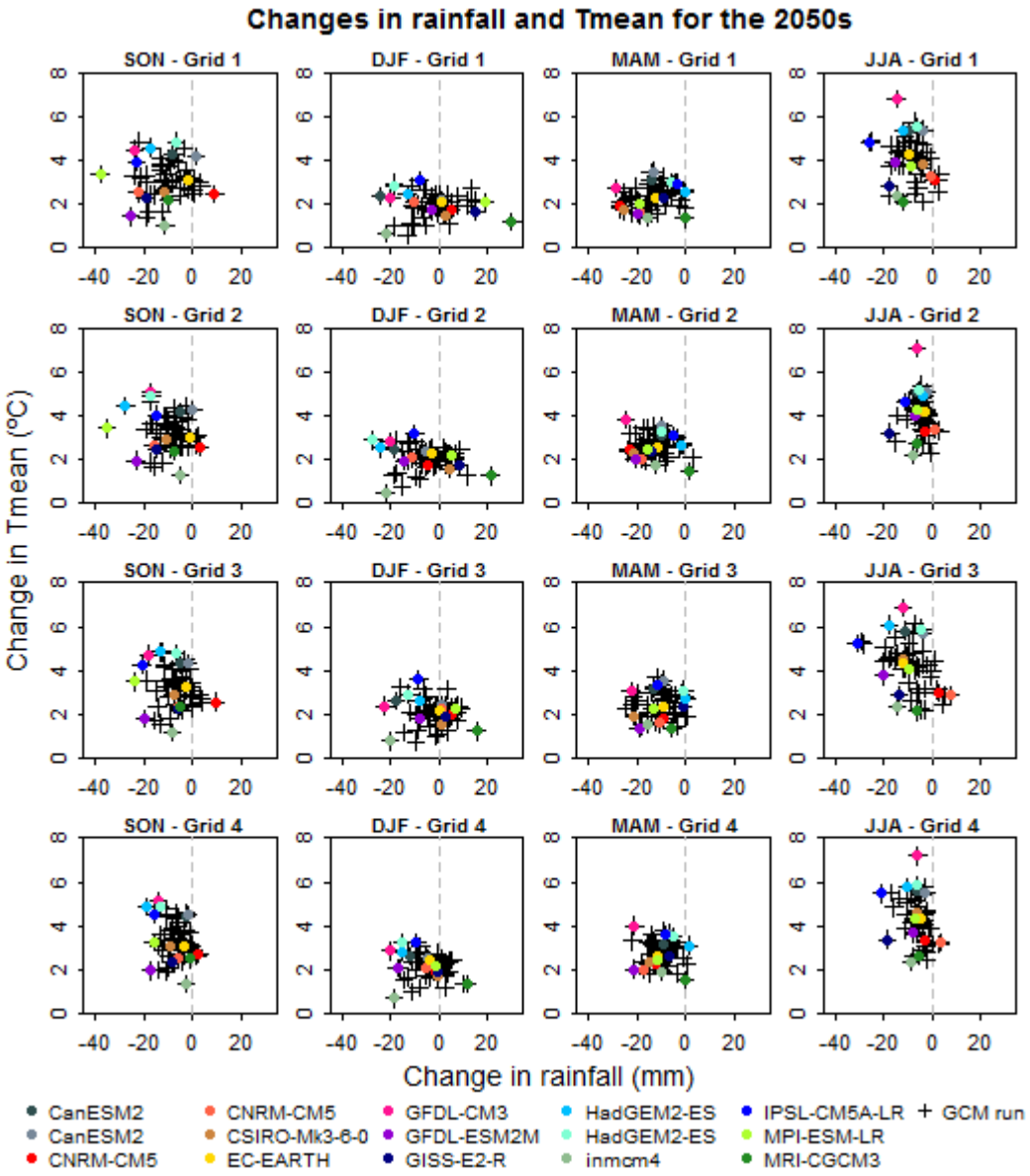

Figure 4.8 – Changes in mean temperature (°C) and rainfall (mm) between 2041-2070 and 1961-1990 per season (mean of the change of the three months in each season) and per GCM grid. All CMIP5 model runs are represented as black crosses. Chosen model runs are represented as colourful circles.

4.3.2 *Change factor*

As mentioned in this chapter's introduction, the simplest statistical downscaling method is the change-factor (CF) which was one of the downscaling methods used in this study. For each month of the year and each GCM grid, a rainfall change factor was calculated by dividing the mean future rainfall (2041-2070) by the modelled mean historical rainfall (1961-1990). The change factors for each month and each GCM grid were then applied to the time series of observed rainfall inside that GCM grid for that month:

$$CF_{m,g} = \frac{\bar{P}^{fut\ mod}_{\mathrm{m,g}}}{\bar{P}^{his\ mod}_{\mathrm{m,g}}} \qquad \mathrm{P}^{fut}_{\mathrm{i,m,g}} = \mathrm{P}^{obs}_{\mathrm{i,m,g}} \cdot CF_{m,g}$$

$CF_{m,g}$ – Rainfall change factor for month *m and* grid *g*

$\bar{P}^{fut\ mod}_{\mathrm{m,g}}$ – 30 years mean (2041-2070) modelled rain for month *m* and grid *g*

$\bar{P}^{his\ mod}_{\mathrm{m,g}}$ – 30 years mean (1961-1990) modelled rain for month *m* and grid *g*

$\mathrm{P}^{fut}_{\mathrm{i,m,g}}$ – Future rainfall for time step *i*, month *m* and grid *g*

$\mathrm{P}^{obs}_{\mathrm{i,m,g}}$ – Observed rainfall for time step i, month *m* and grid *g*

With this method, the future mean and variance will be different from the observed record, but the coefficient of variation, the skewness and the spatial correlation between grid points inside each GCM grid will remain the same as the historical observed rainfall.

Figure 4.9 shows the change factors calculated for rainfall for all the models and for the 15 chosen models. Figure 4.10 shows temperature change factors (additive instead of multiplicative change factors). It can be seen that for these two variables, the four grids and the 12 months, the chosen 15 model runs have a similar range to all (65) model runs, they also have a similar mean and inter-quartile range.

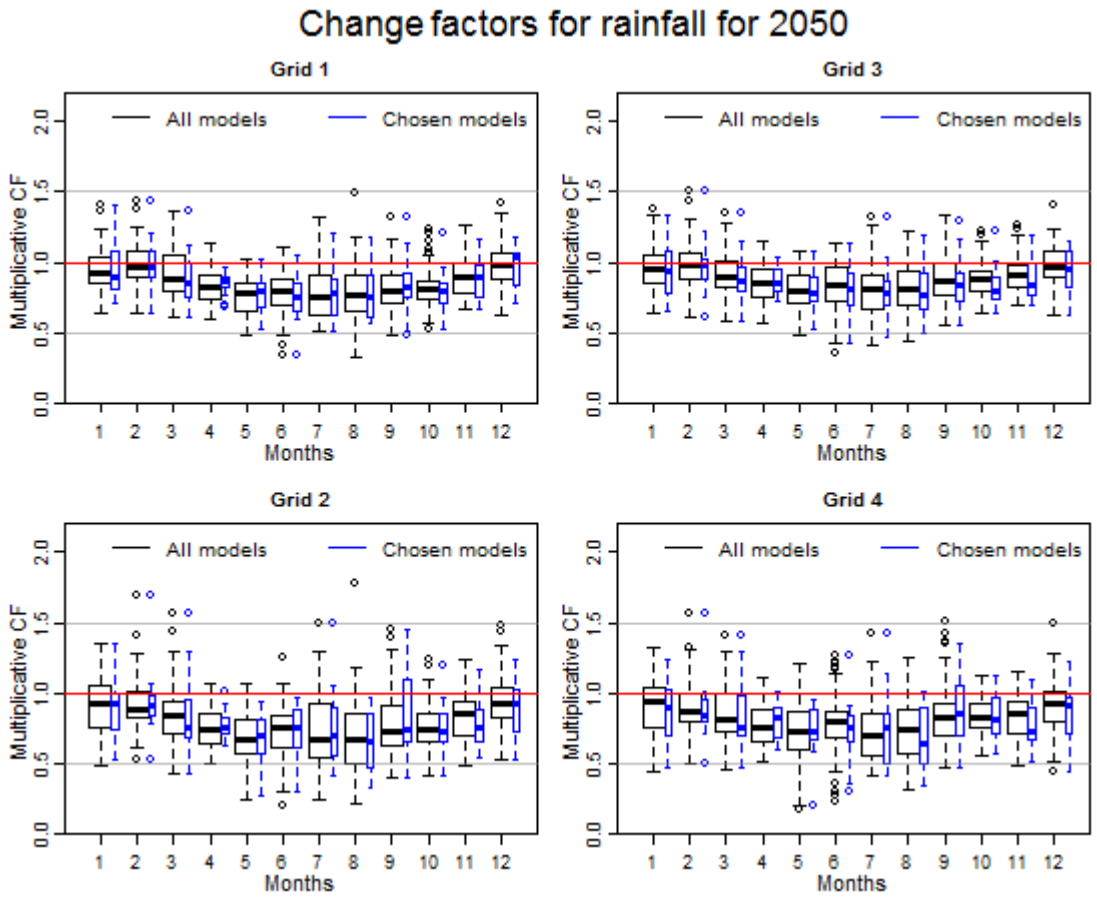

Figure 4.9 – Monthly rainfall change factors for the 65 CMIP5 model runs in black and the chosen runs in blue, for the four CMIP5 grids and for the 2050s (2041 to 2070).

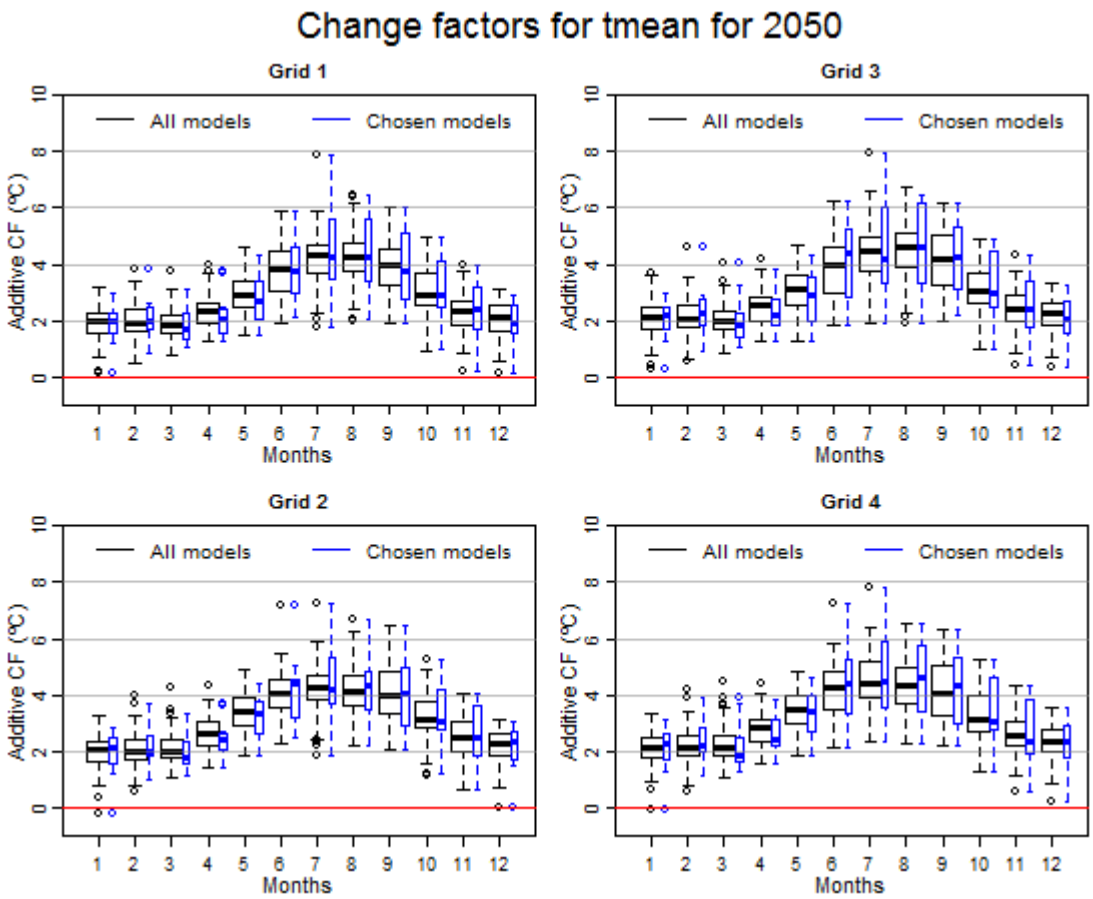

Figure 4.10 – Monthly mean temperature change factors for the 65 CMIP5 model runs in black and the chosen runs in blue, for the four CMIP5 grids and for the 2050s (2041 to 2070).

To calculate change factors for PET, historical and future GCM based PET was calculated by applying the Thornthwaite equation (Thornthwaite, 1948) using the SPEI package for R. This is a simple empirical method that correlates mean monthly air temperature and PET for any determined latitude. The PM method was not chosen because it requires time-series for several variables that are not well simulated by GCMs and is very sensitive to input data inaccuracy (Weiland *et al.*, 2012) which means the results might be physically unrealistic (Ekström *et al.*, 2007).The Thornthwaite method is a simplistic method of calculating PET but it only require temperature time-series which is a more reliable GCM output. However, as discussed in section 4.1.2 and according to Prudhomme and Williamson (2013), because it is a temperature-based method it might show higher PET increases than radiation-based methods.

Figure 4.11 shows that 1961-1990 PET calculated from GCM output using the Thornthwaite method varies considerably between different GCMs. However, despite the big inter-model spread, PET calculated from the CMIP5 models is consistently below the PET estimates taken from the CRU dataset where PM is used to calculate PET (spatially aggregated to the four GCM grids). This might be due to the different methods of calculating PET (and a possible slight overestimation of PET by the CRU dataset), due to poor GCM simulation of local temperatures

or a combination of both. However, since the PET calculated from the CMIP5 models was only used to calculate change factors that were later applied to the CRU PET dataset, the effects of any temperature bias in the GCMs were minimized.

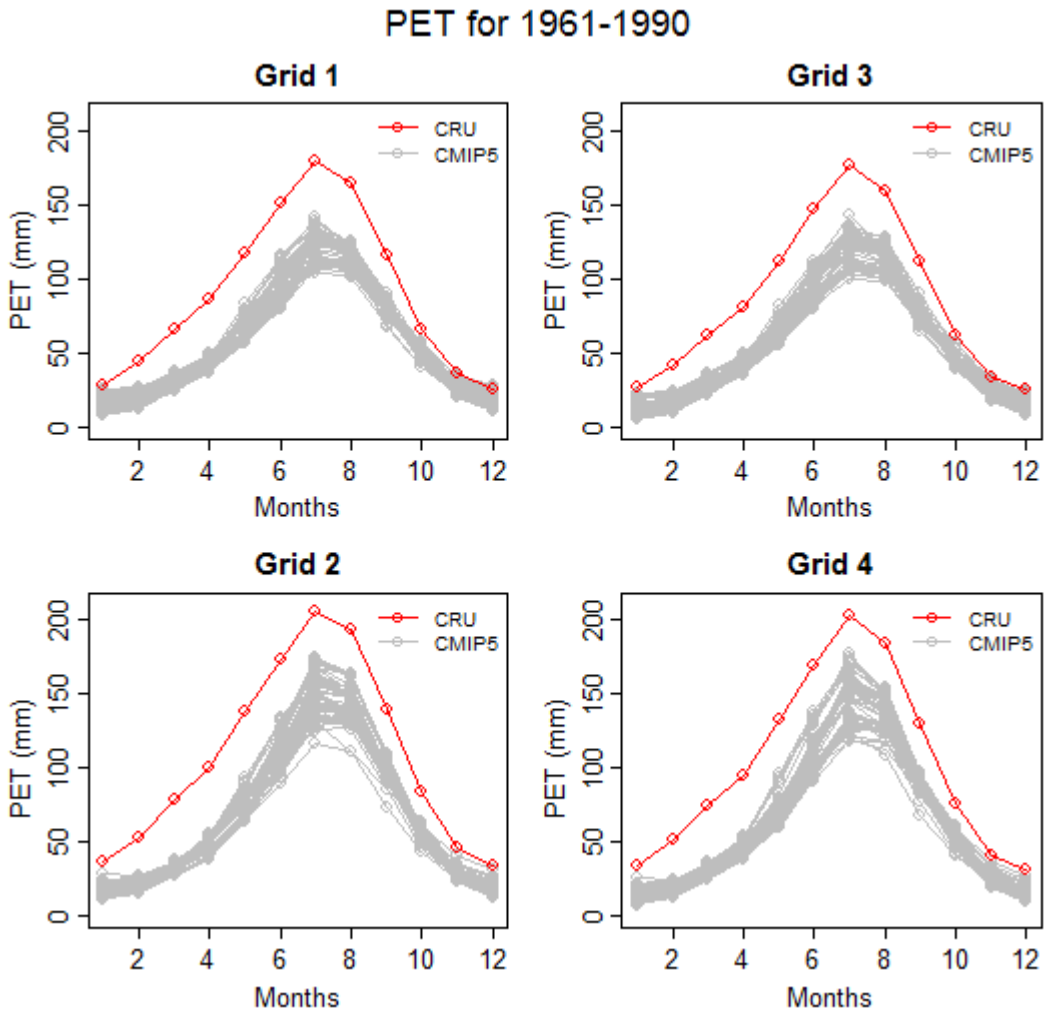

Figure 4.11 – PET calculated from GCM output using the Thornthwaite method (in grey) and PET from the CRU dataset spatially aggregated to the four GCM grids (in red) from the period 1961-1990.

To understand how important errors in PET might be for the simulation of future discharge (in *Chapter 6 – Hydrological Model Set Up*), the water balance for the areas must be taken into account. Figure 4.12 and Figure 4.13 show the water balance for Portugal and Spain (respectively). In both countries PET is above actual evapotranspiration (AET) for most of the year (April to October in Portugal and March to November in Spain). Potential errors regarding the PET calculation or calculation of PET increases should only be relevant for the wetter part of the year, where PET is similar to AET and energy is the limiting factor for evaporation.

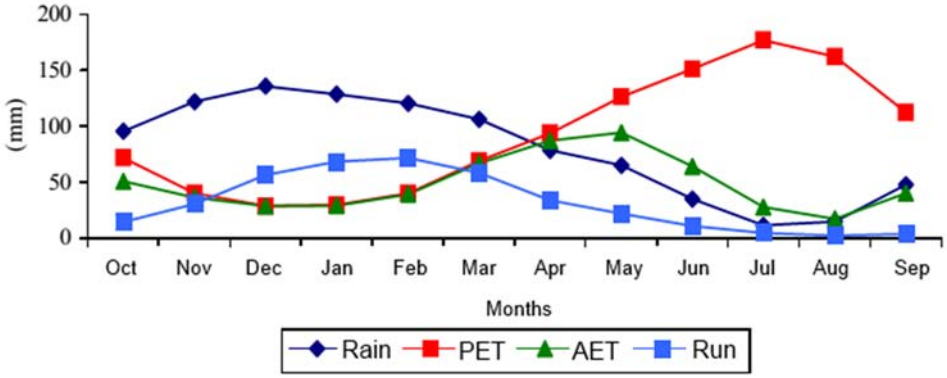

Figure 4.12 – Monthly water balance for mainland Portugal, showing rainfall, PET, AET and runoff for the period 1941/42 to 1990/91 (INAG, 2002).

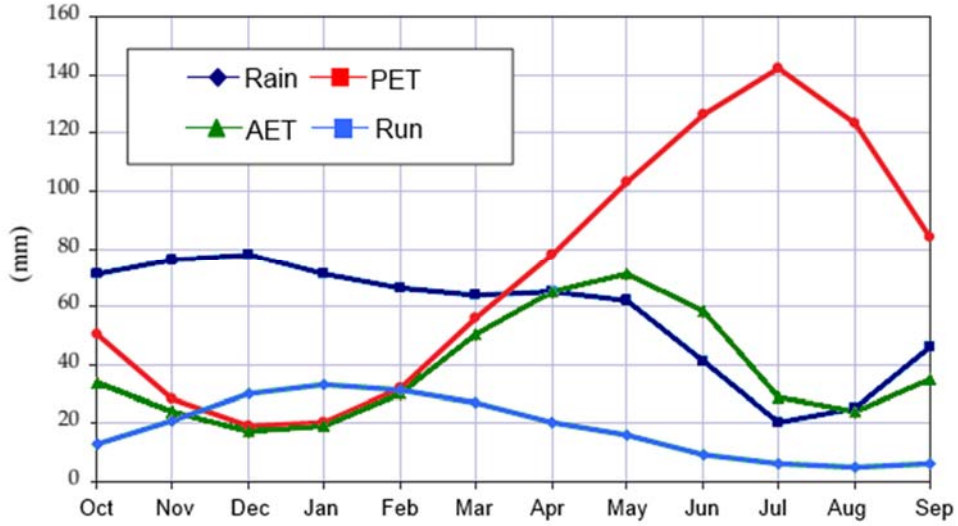

Figure 4.13 – Monthly water balance for Spain, showing rainfall, PET, AET and runoff for the period 1940/41 to 1995/96 (MMA, 2000).

After calculating historical and future PET from GCM outputs (using the Thornthwaite equation) the methodology described for rainfall was applied to calculate PET change factors (for each month and each grid). Lastly these PET change factors were applied to the PET gridded dataset from CRU.

Figure 4.14 shows the change factors calculated for PET for all the models and for the 15 chosen models. It can be seen that the chosen 15 model runs have a similar range to all (65) model runs for the four grids and the 12 months.

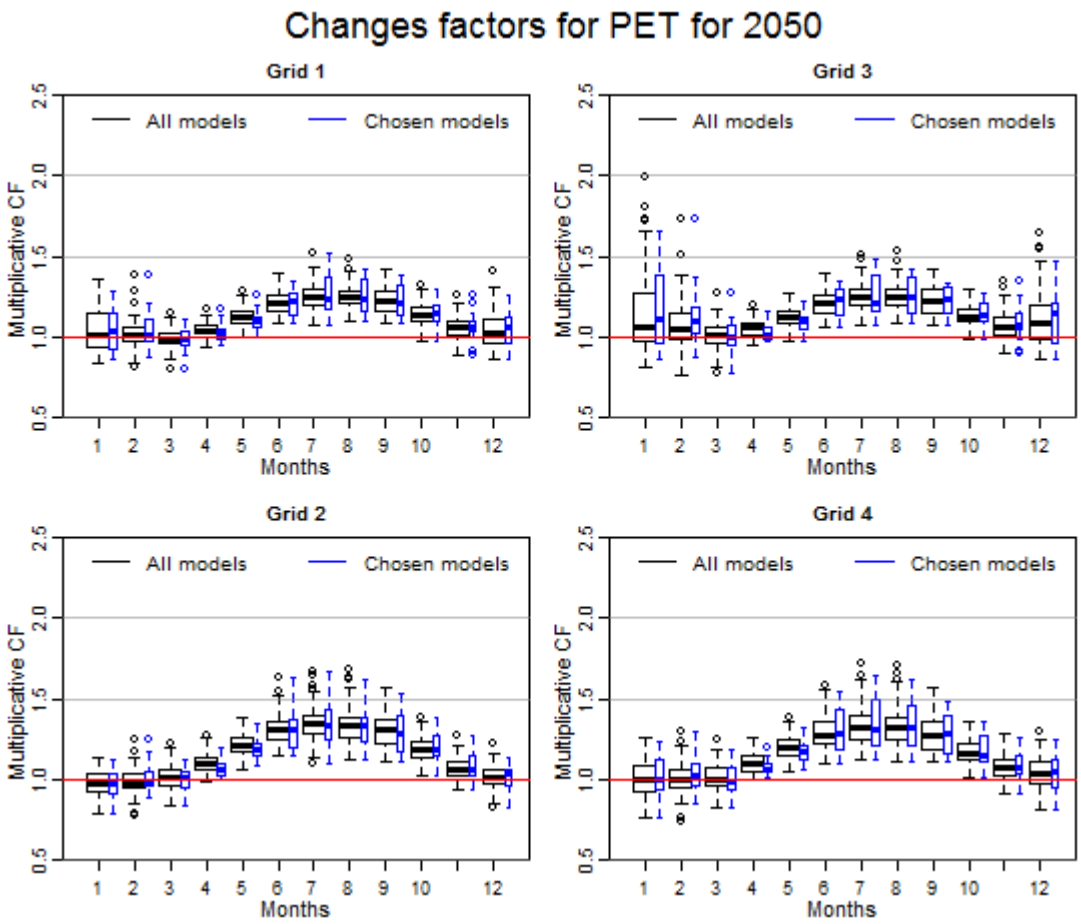

Figure 4.14 – Monthly mean PET change factors, for the 65 CMIP5 model runs in black and the chosen runs in blue, for the four CMIP5 grids and for the 2050s (2041 to 2070).

4.3.3 *Bias correction – empirical quantile mapping*

Another method used to downscale (and simultaneously correct) GCM outputs was a variation of empirical quantile mapping. This was used to provide transient future rainfall and to account for changes in variability which are vital for the assessment of droughts. Also, using more than one downscaling method allows at least a partial assessment of the uncertainties related with the choice of downscaling method. Empirical cumulative distribution functions (ECDFs) were calculated for rainfall from each GCM and for IB02 (spatially aggregated to the GCM grids) for the 12 months and the four grids for the period 1961-2003. Then for each GCM simulated rainfall value a correspondent observed value can be found by matching the quantiles. The period chosen (1961-2003) is the entire record of observed rainfall (IB02) and PET (CRU dataset).

An example, for January rainfall, is demonstrated in Figure 4.15 where a GCM simulated rainfall of 100mm corresponds to the quantile 0.674 using the ECDF calculated for the GCM.

The quantile 0.674 corresponds to a rainfall value of 110mm using the ECDF calculated for the aggregated IB02. Therefore the GCM value of 100mm can be corrected to 110mm.

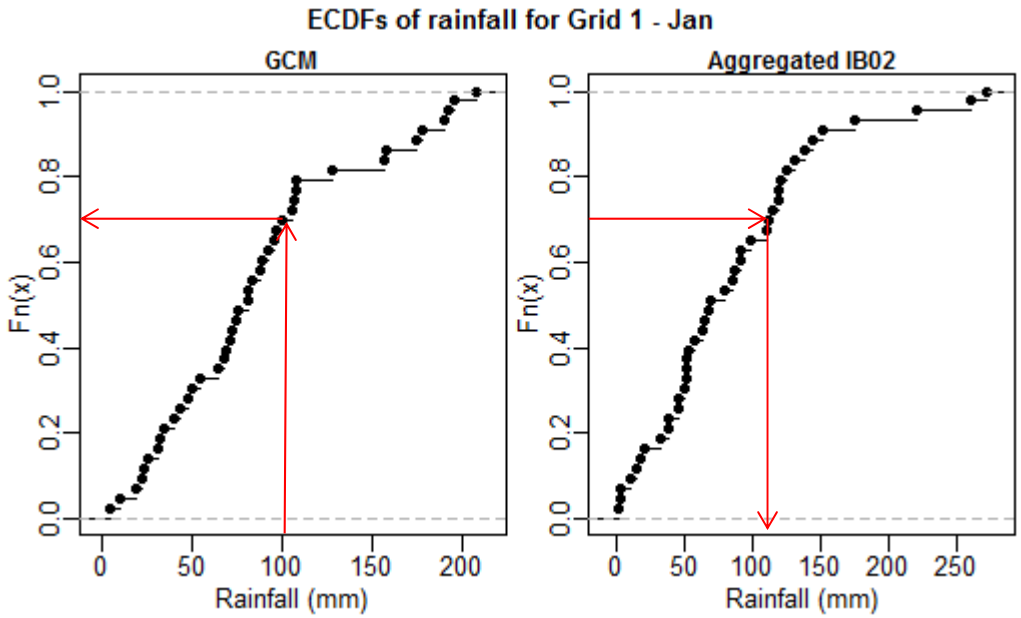

Figure 4.15 – Illustrative example of quantile matching between climate model and observed data for January rainfall.

Small variations in the calculation of the ECDFs exist for the application of this technique in order to increase the robustness of the method:

- Themeßl *et al.* (2011), using daily rainfall, calculated the ecdf using a 61-day moving average;
- Lafon *et al.* (2013), also using daily rainfall, divided the ranked rainfall into a number of discrete quantiles prior to the calculation of the ecdf
- Boé *et al.* (2007), again using daily rainfall, divided the data into 99 percentiles and applied linear interpolation between percentiles.

Figure 4.16 shows a comparison between rainfall ECDFs calculated for the period 1961-2003 (in black) and for the period 1950-2003 (in red). For the case of March, where the mean rainfall of the decade added is substantially higher than the rest of the record, the ECDFs are substantially different and any kind of smoothing would have little effect in improving the robustness of the method. In the case of May, where the mean of the decade added is similar to the rest of the record, it is not obvious if smoothing (by applying moving averages, discrete quantiles binning or linear interpolation) would increase the robustness of the method. Therefore, in order to conserve the structure of the observed monthly rainfall and to avoid introducing an artefact based on an arbitrary choice of number of bins/percentiles or time-steps incorporated into a moving average, the ECDFs were calculated using the monthly values of rainfall and the quantile matching was performed without interpolation.

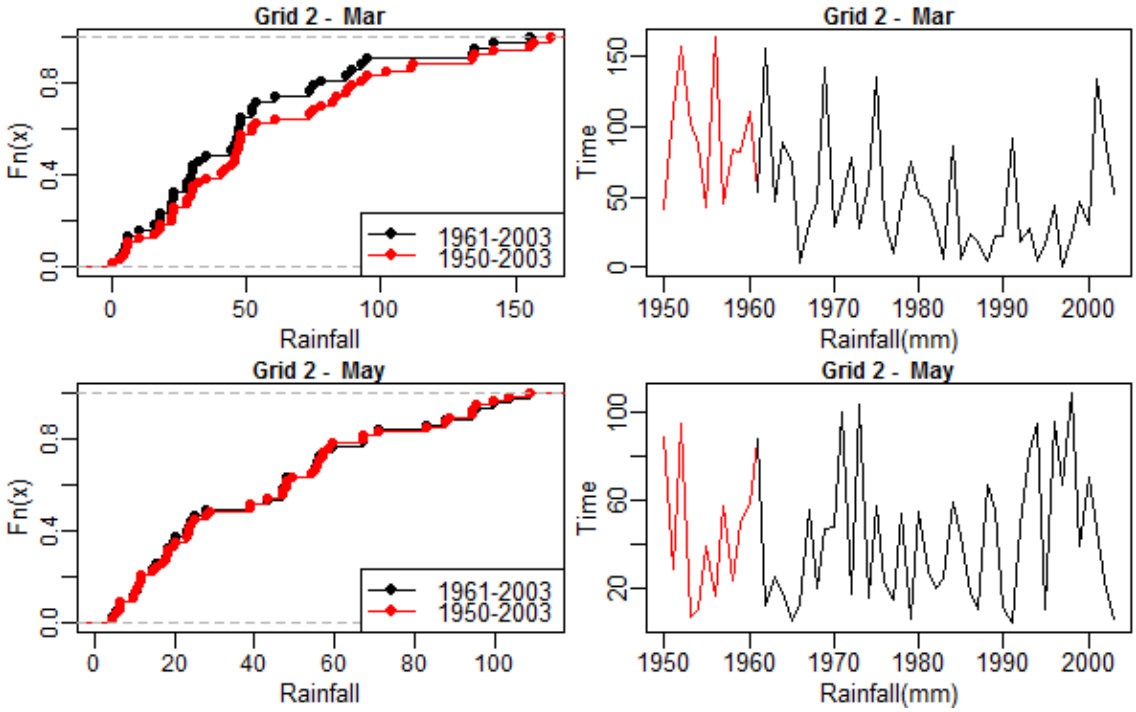

Figure 4.16 – ECDFs (left) and time-series (right) of monthly rainfall for grid 2 for March (top) and May

The quantile mapping describe so far is a standard bias correction method. In order to downscale the GCM data an extra step was added. For each month and each GCM, the quantile matching was used to identify the year of observed data (spatially aggregated monthly IB02) that had the same quantile as the GCM's year being downscaled for that month. Then the correspondent daily spatially distributed IB02 time-series for that year and that month was selected. Figure 4.17 shows a schematic of the process.

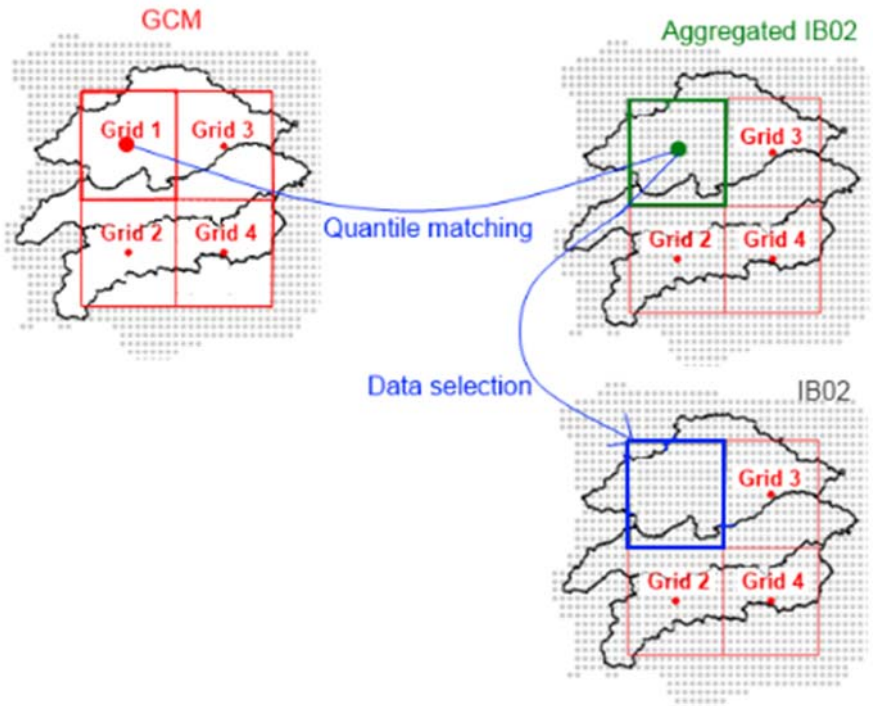

Figure 4.17 – Schematics of bias correction with simultaneous downscaling for GCM grid 1 using quantile mapping.

So, following the example set on Figure 4.15, for January and for grid 1, the year with a GCM rainfall value of 100mm corresponds (through quantile matching) to a year where the aggregated IB02 for January had a value 110mm. The rainfall time series for the January of that year was then selected from the daily distributed IB02. This method preserves the bias-corrected GCM monthly time-series, while assuming that inside each GCM grid the spatial and the daily rainfall distribution of the monthly total will remain the same as the observed.

Initially the method was applied simultaneously over the four GCM grids by doing the quantile matching between each GCM grid and each aggregated IB02 grid and selecting the year where the root mean square error for the four grids was smaller. However, due to the lack of correlation between the simulated rainfall in the four GCM grids (see Figure 4.18) the errors were substantial in the quantile matching with the observations, which then led to substantial errors in the reconstructed rainfall of each basin (see Figure 4.19 and Figure 4.20). Therefore a different methodology had to be applied; only one grid cell was used to identify the year for the quantile matching which kept the spatial correlation of the observed rainfall inside each basin and reduce the errors to zero over the period 1950-2003 (or close to zero in the case where there are years with the same amount of rainfall for a particular month, which only happened for the month of August in the Guadiana where two years had zero rainfall). Grid 1 was used for the Douro and the Tagus and grid 2 was used for the Guadiana. The choice of grids was done to capture the area that contributed more to the discharge of the basin (areas with higher runoff) which can be seen in Figure 4.21.

Since the bias correction was done for two GCM grids and for the period 1950 to 2003, boxplots were plotted (see Appendix D) for the reference period (1961 to 1990) to confirm that the bias corrected GCMs showed a rainfall distribution similar to the observed rainfall throughout the year for the three basins.

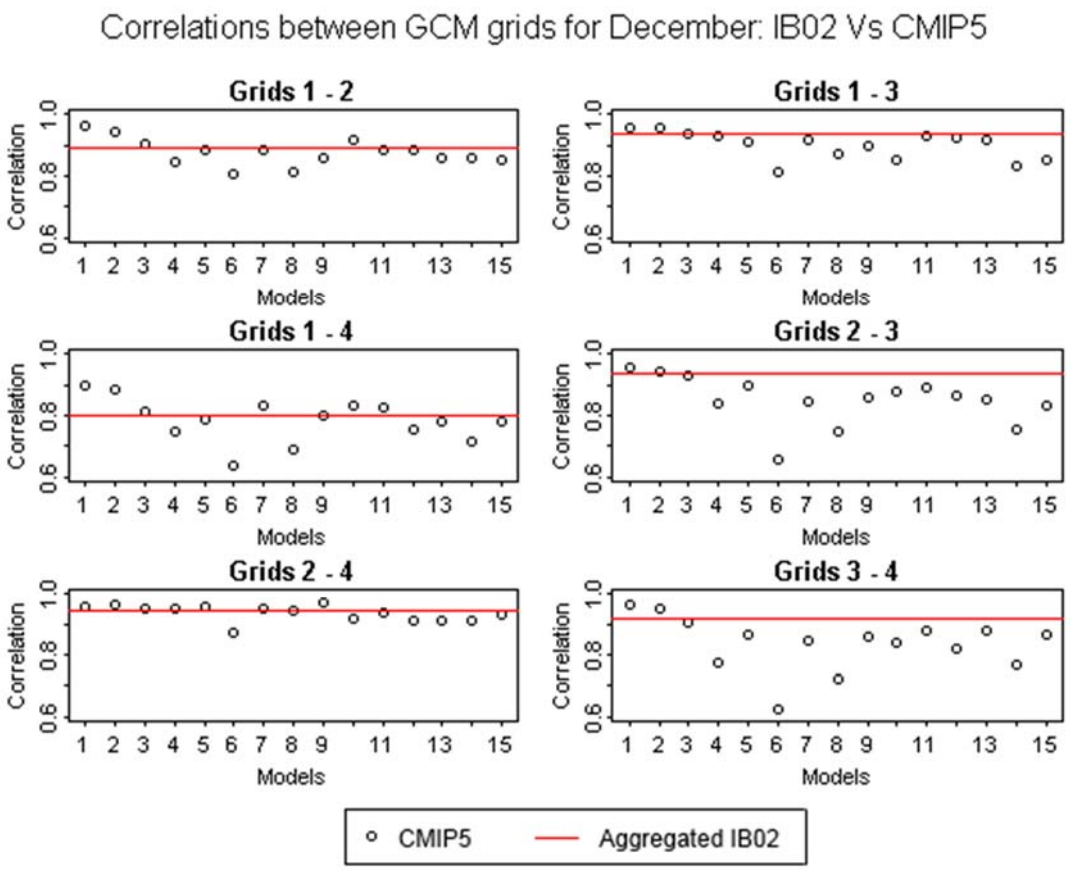

Figure 4.18 – Correlation between different GCM grids for December rainfall: CMIP5 models versus aggregated observed rainfall (aggregated IB02).

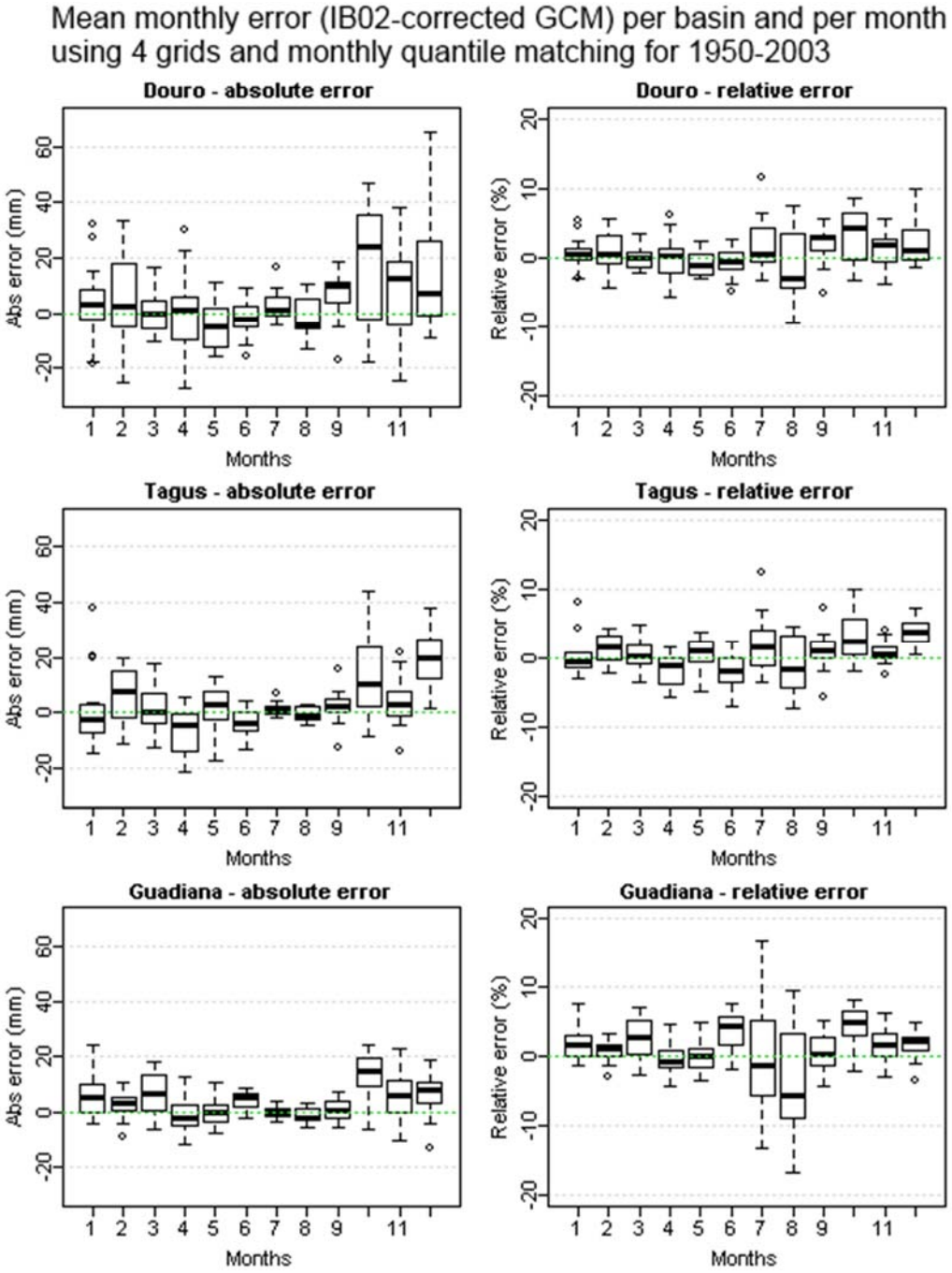

Figure 4.19 – Absolute errors (mm) and relative errors (%) of total basin rainfall per month using the four GCM grids for the quantile matching. The box-plots show the error dispersion between the 15 CMIP5 GCMs per month.

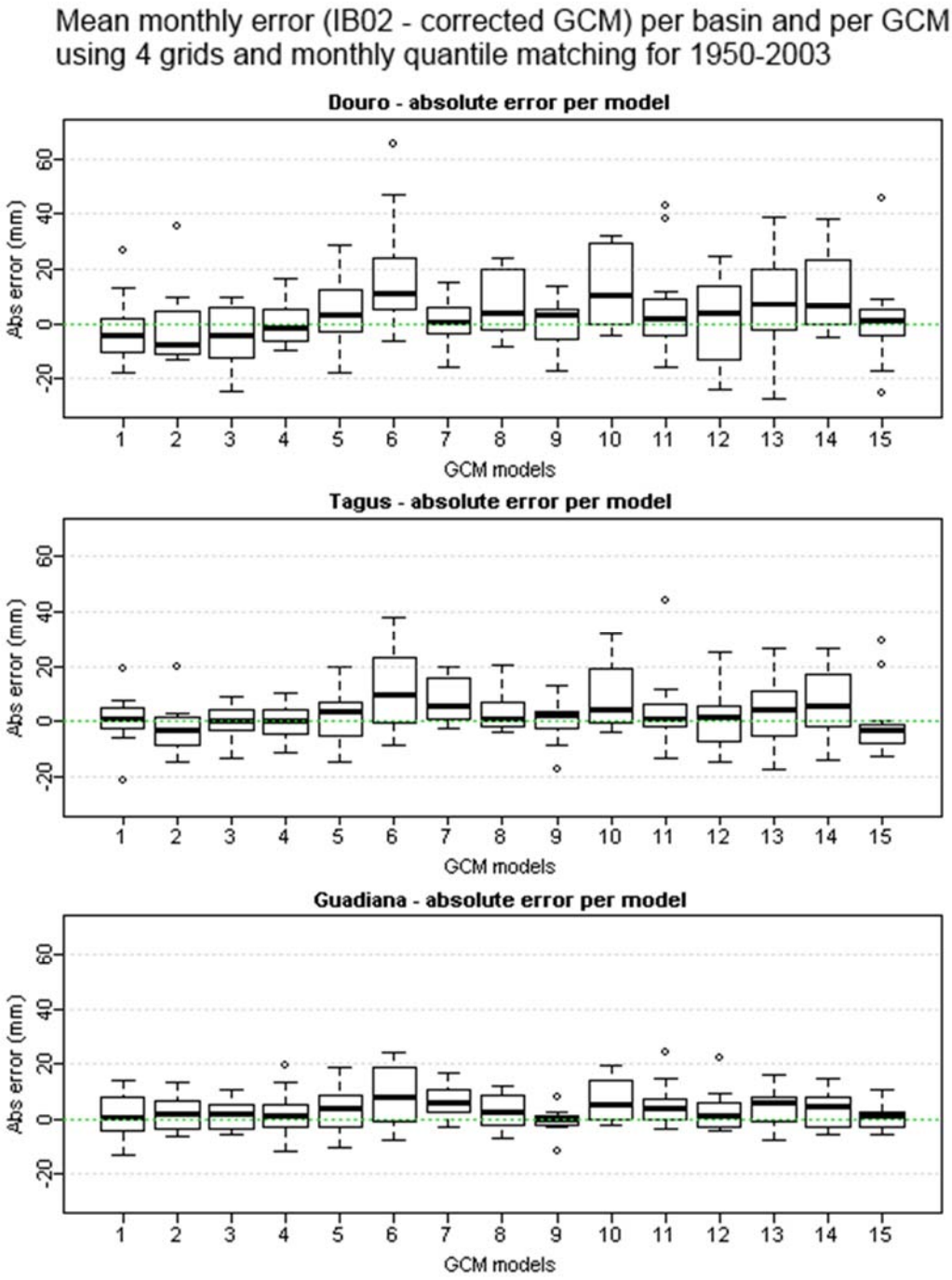

Figure 4.20 – Absolute errors (mm) of total basin rainfall per CMIP5 model using the four GCM grids for the quantile matching. The box-plots show the error dispersion the 12 months of the year per GCM.

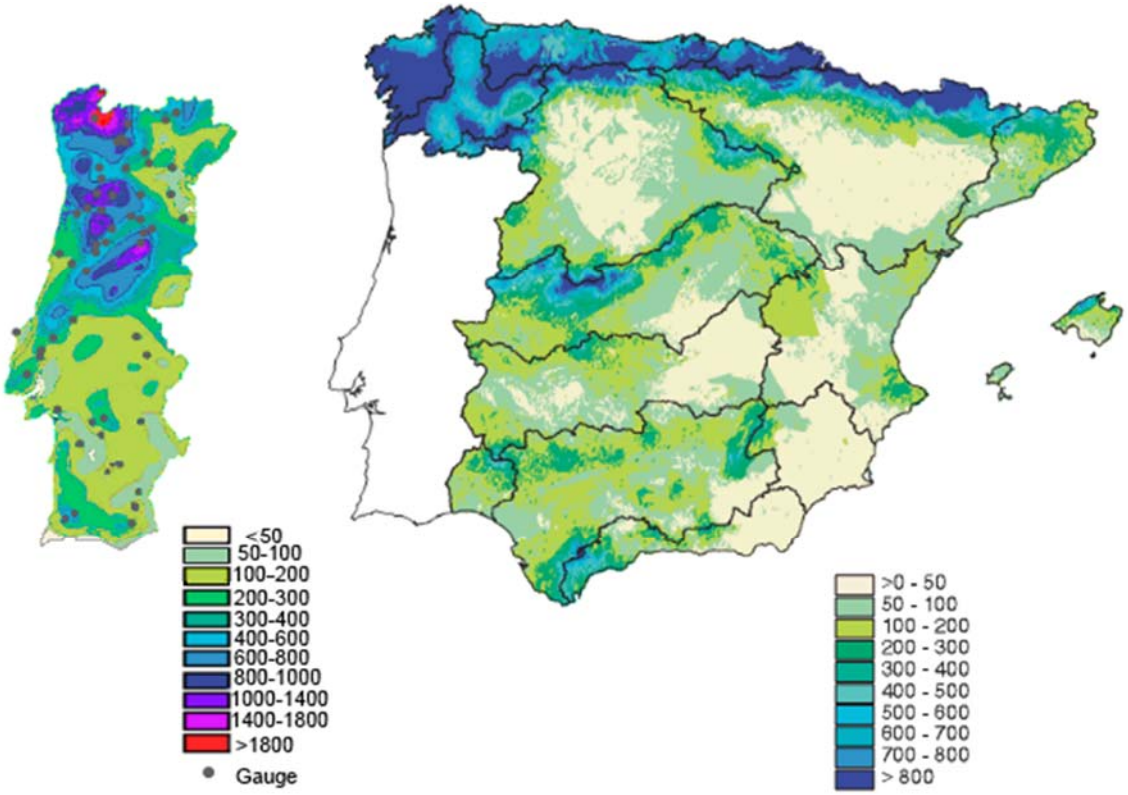

Figure 4.21 – Runoff maps (in mm) of Portugal on the left (adapted from Portela and Quintela (2002)) and Spain on the right (MMA, 2000)

As mentioned previously, one of the shortcomings of quantile matching is that it is restricted to producing events within the observed historical range. Rainfall higher or lower than the observed range during the future period was subsequently changed using a change factor approach. Figure 4.22 shows the percentage of years where the rainfall is outside the observed historical range for the 2050s (with reference to the 1961-2003 period).

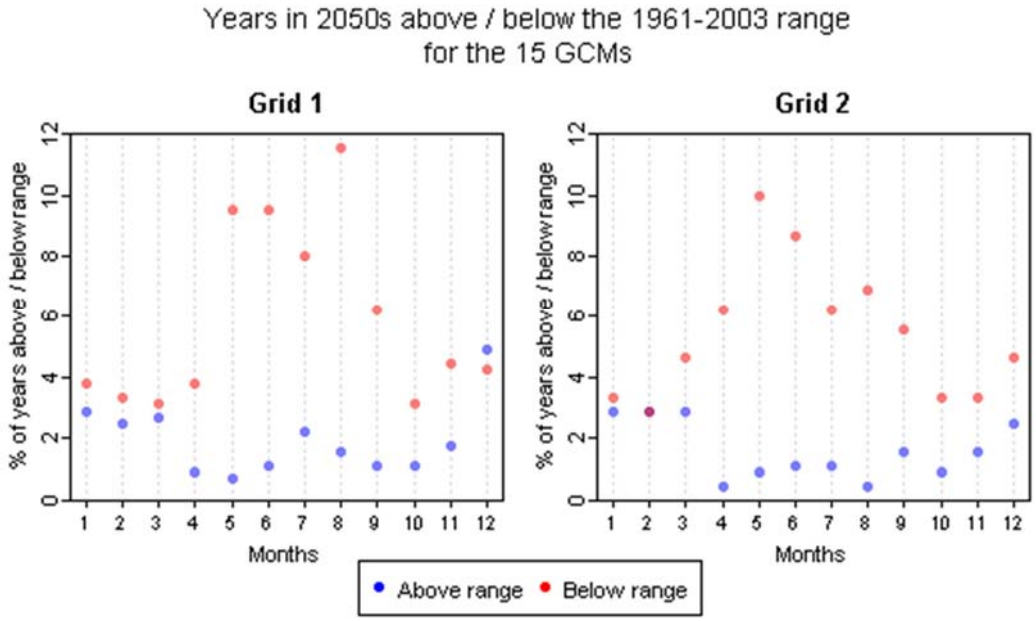

Figure 4.22 – Percentage of years above or below the historical range for the 2050's for the 15 GCM models used in this study.

The higher number of future years outside the historical range is seen in the summer with reductions in rainfall. Across the months, the mean number of years below the 1961-2003 range is 5.9% for grid 1 and 5.5% for grid 2. However, as can be seen in Figure 4.22, this percentage is considerably higher from April/May to September. In terms of increases in rainfall, the number of years above the 1961-2003 range are all below 3% except December for grid 1 which is 5%.

For the calculation of future PET, initially the same year that was selected for the rainfall was also selected for PET (in order to keep the physical relationships between the two variables). However the differences in PET between 1961-90 and the 2050's were negligible, therefore a change factor approach was also applied.

4.3.4 *Transient analysis*

Bias-corrected rainfall generated for 1961-2100 for each basin, each season and each model was plotted with 30 year rolling means and linear regressions. Trend significance was assessed using the Mann-Kendall test at a 5% level (Mann, 1945; Kendall, 1948). However some seasonal/annual rainfall in some models/basins could not be considered serially independent (using the lag-1 of the autocorrelation function at a 95% level). Yue *et al.* (2002b) showed that positive serial correlation increases the probability of detecting a significant trend using the Mann-Kendall test, and on the other hand, the existence of a trend influences the magnitude of the estimate of serial correlation. Therefore to assess the significance of trends the method described in Yue *et al.* (2002b) was also used, which consists of the following steps:

1. Calculate the slope of the trend;
2. If the slope differs from zero, the identified trend is assumed to be linear and is removed. The residual series is referred to as the detrended series;
3. Calculate the lag-1 serial correlation coefficient of the detrended series and remove the AR(1) process;
4. Combine the identified trend and the modified residual series;
5. Apply the Mann-Kendall test to the combined series to assess the significance of a trend.

This was done using the R package "zyp" and the results were very similar to the application of the Mann-Kendall test directly onto the bias-corrected rainfall.

The magnitude of the trend was calculated using linear regression and is presented in change per decade calculated as a percentage of the rainfall mean between 1961 and 2100.

4.4 Results and discussion

4.4.1 *Historical period*

A comparison between monthly rainfall outputs from CMIP5 runs and gridded observed rainfall (IB02) spatially aggregated to the CMIP5 grids are presented in Figure 4.23 to Figure 4.26 for the period from 1950 to 2003. The model dispersion is considerably large, but in most cases it encompasses the observed data range. In the northern grids (1 and 3) most models are too wet throughout the year (except for September for grid 1) while in the southern grids (2 and 4) the excess rainfall is mostly noticeable in the summer. Most models underestimate the coefficient of variation of the observed data, mainly from October to March in grid 1 and 3, October to December in grid 2 and July, August, November and December in grid 4.

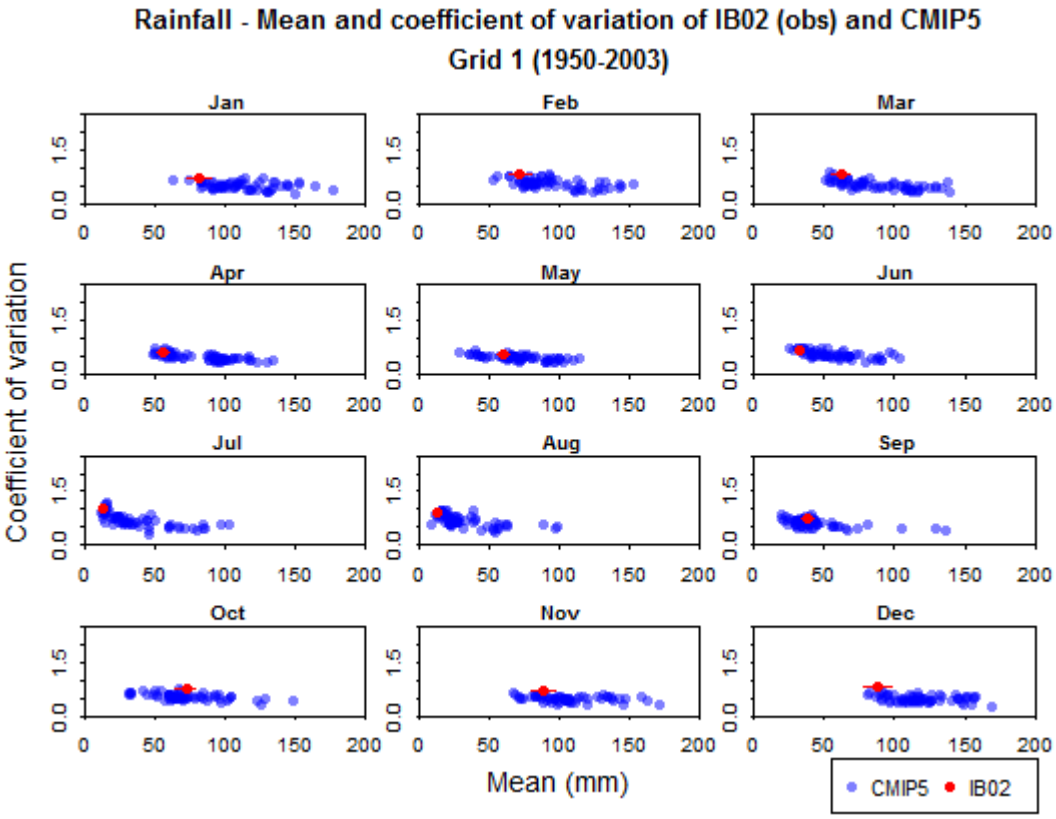

Figure 4.23 – Grid 1 monthly rainfall means and coefficients of variation for observations (IB02) in red and all CMIP5 model runs in blue for the period 1950 to 2003. Error bars (using jack-knife) of the observed rainfall are also plotted (although not always visible due to the scale of the plots).

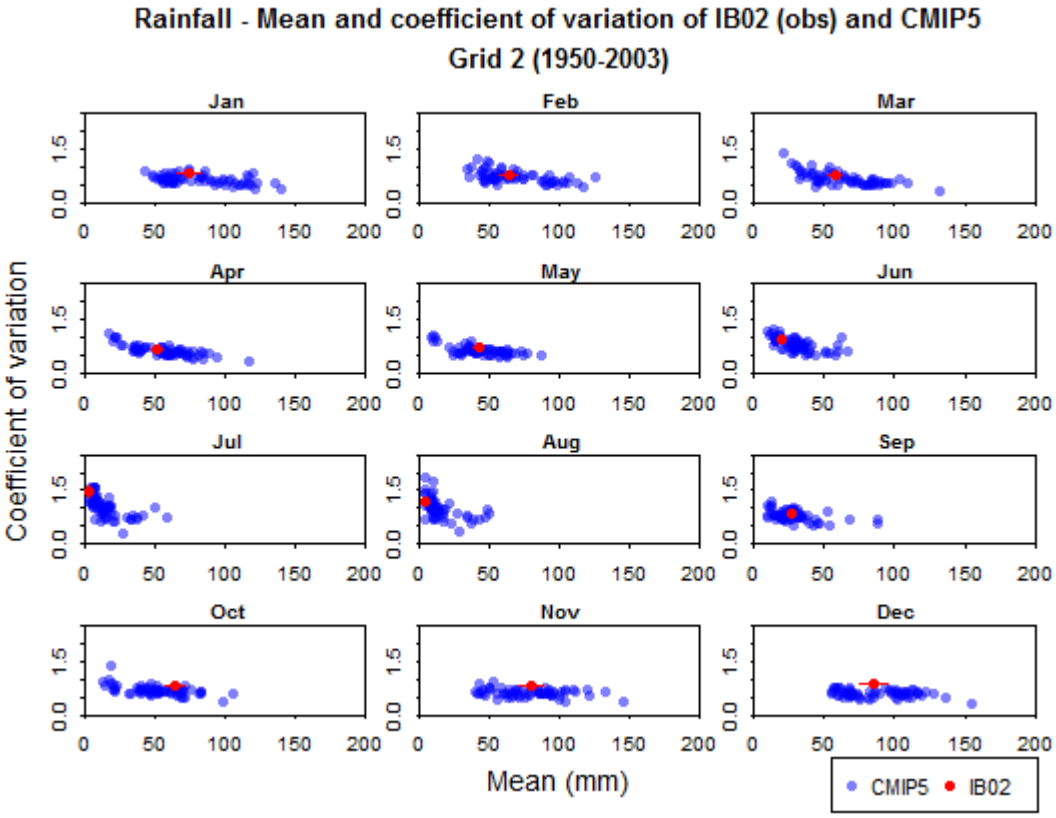

Figure 4.24 – Grid 2 monthly rainfall means and coefficients of variation for observations (IB02) in red and all CMIP5 model runs in blue for the period 1950 to 2003. Error bars (using jack-knife) of the observed rainfall are also plotted (although not always visible due to the scale of the plots).

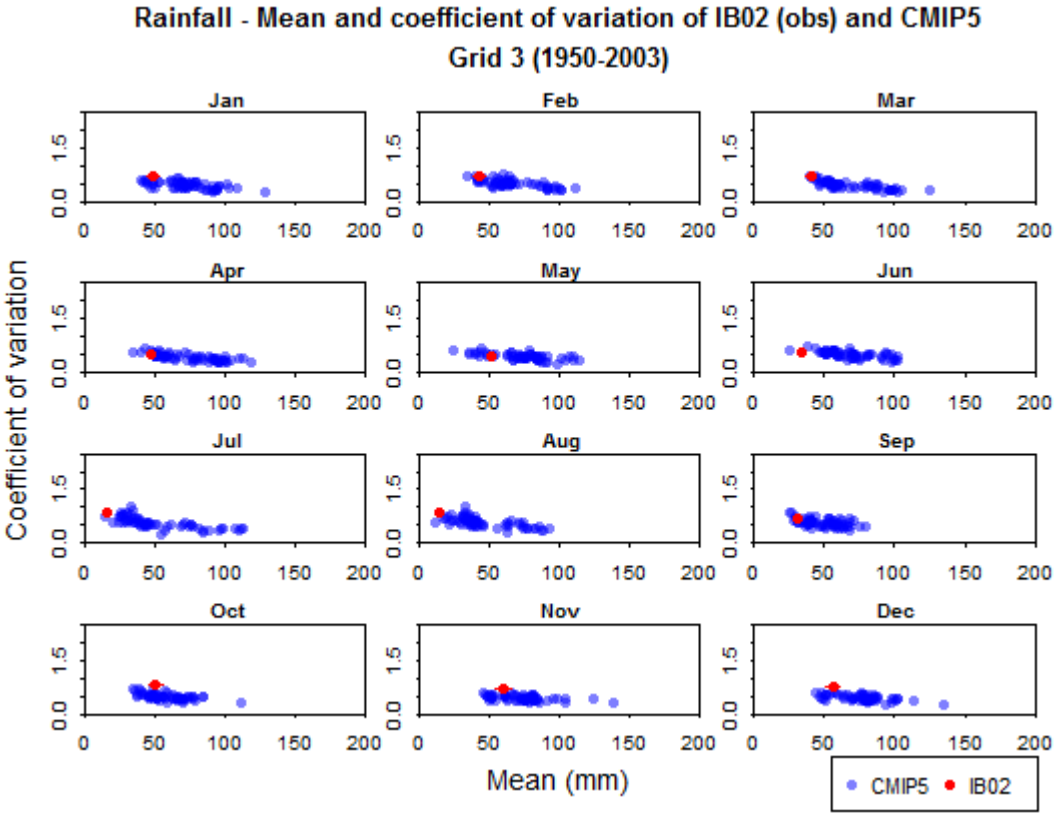

Figure 4.25 – Grid 3 monthly rainfall means and coefficients of variation for observations (IB02) in red and all CMIP5 model runs in blue for the period 1950 to 2003. Error bars (using jack-knife) of the observed rainfall are also plotted (although not always visible due to the scale of the plots).

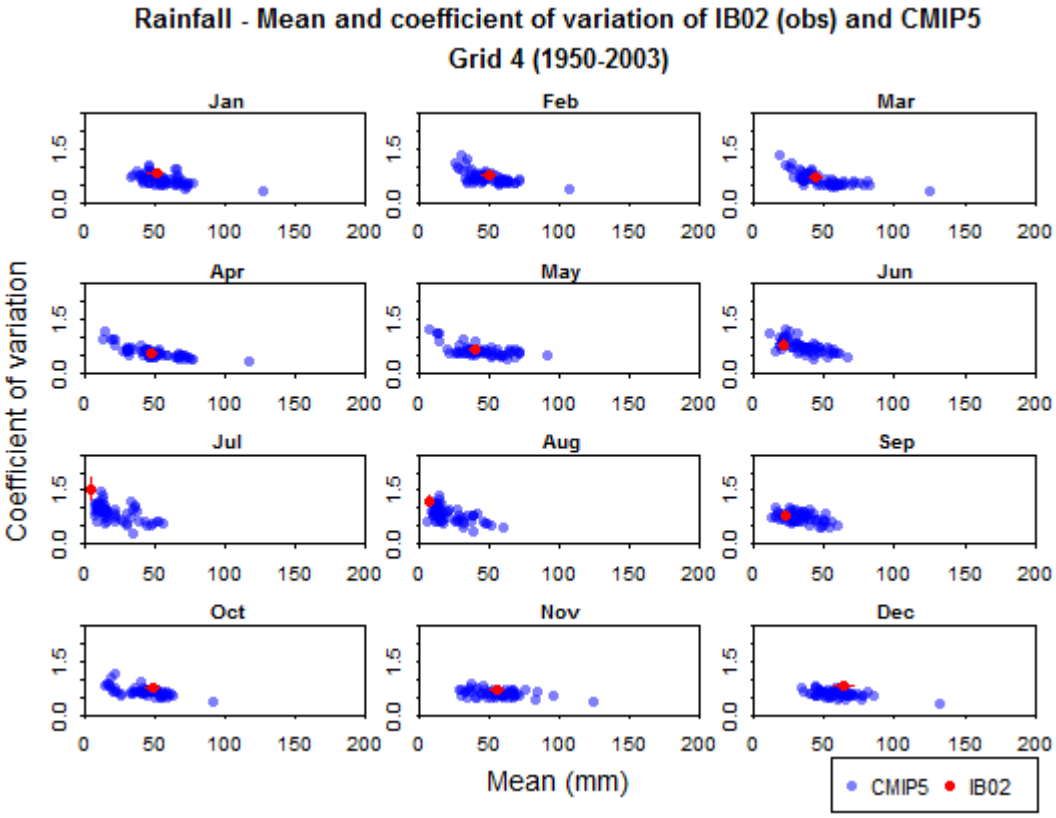

Figure 4.26 – Grid 4 monthly rainfall means and coefficients of variation for observations (IB02) in red and all CMIP5 model runs in blue for the period 1950 to 2003. Error bars (using jack-knife) of the observed rainfall are also plotted (although not always visible due to the scale of the plots).

4.4.2 *Future – the 2050s*

To show that no single model stands out as an outlier, boxplots with 2050s rainfall projected by the 15 GCM runs per month and per basin, downscaled using the change factor approach and the bias correction approach are presented in Appendix D.

Figure 4.27 shows the changes (between 1961-1990 and 2041-2070) in monthly and annual rainfall for the Douro basin (spatial mean), as absolute changes (in mm) and as relative changes (in percentage) for both downscaling methods and for the 15 selected models. Figure 4.28 shows the same for the Tagus basin and Figure 4.29 for the Guadiana basin. Due to the high inter-annual variability of this region (apparent in all months) most of these changes are not statistically significant. The number of models showing significant negative changes between 1961-1990 and 2050s using the Kolmogorov-Smirnov test at 0.05 significance level is presented in Table 4.2. No model showed significant positive changes for any of the months (or annual rainfall).

Table 4.2 – Number of models showing significant negative changes in rainfall between 1961-1990 and 2050s using the Kolmogorov-Smirnov test at 0.05 significance level per basin and per month (annual values also included).

Month	Douro		Tagus		Guadiana	
	Change Factor	Bias Correction	Change Factor	Bias Correction	Change Factor	Bias Correction
1	0	2	0	4	0	2
2	0	1	0	1	0	1
3	0	4	0	5	0	3
4	0	3	3	2	1	3
5	4	4	4	5	0	8
6	1	6	1	4	1	5
7	0	5	0	4	0	4
8	0	5	4	5	0	4
9	0	4	1	3	0	1
10	2	4	1	4	1	3
11	0	3	1	3	0	2
12	0	2	0	2	0	5
Annual	0	2	0	2	0	5

Both downscaling methods show similar projections for the 2050s, although the bias correction method tends to show a bigger inter-model dispersion which could perhaps be expected since more information is being retained from the climate models. The apparent big differences between the two methods in the relative changes in summer are, in reality, small differences in absolute terms which are amplified by the very low rainfall of these months.

Most models show a reduction in rainfall in all three basins, this is true for all months and for annual rainfall and for both downscaling methods. The exception is for December in the Douro and the Tagus for the bias correction method. However, the inter-model dispersion on a monthly level is considerably high, with some models showing increases in rainfall. This dispersion will be looked into in more detail in section 4.4.3.

The projected annual rainfall changes range between -33% and +7% for the Douro, -33% and +10% for the Tagus and -41% and +10% for the Guadiana. Especially relevant might be the reduction in rainfall projected by almost all models, and both methods, for spring and autumn months. In the spring months (MAM) the monthly decreases are as large as -43% for the Douro, -40% for the Tagus and -36% for the Guadiana. For the autumn months (SON) reductions are even larger: -56% for the Douro, -54% for the Tagus and -51% for the Guadiana.

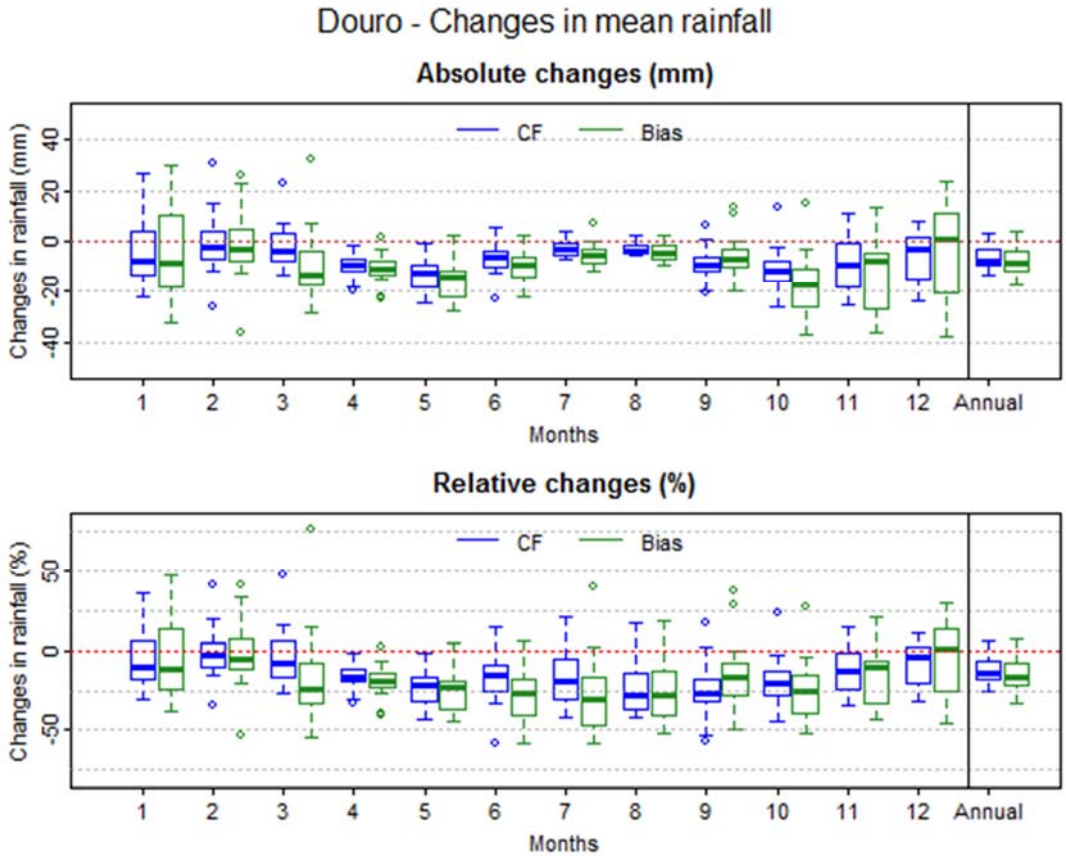

Figure 4.27 – Boxplots of Douro's absolute (top) and relative (bottom) changes in the basin's mean rainfall (between 1961-1990 and 2041-2070), per month, using the change factor and the bias correction methods.

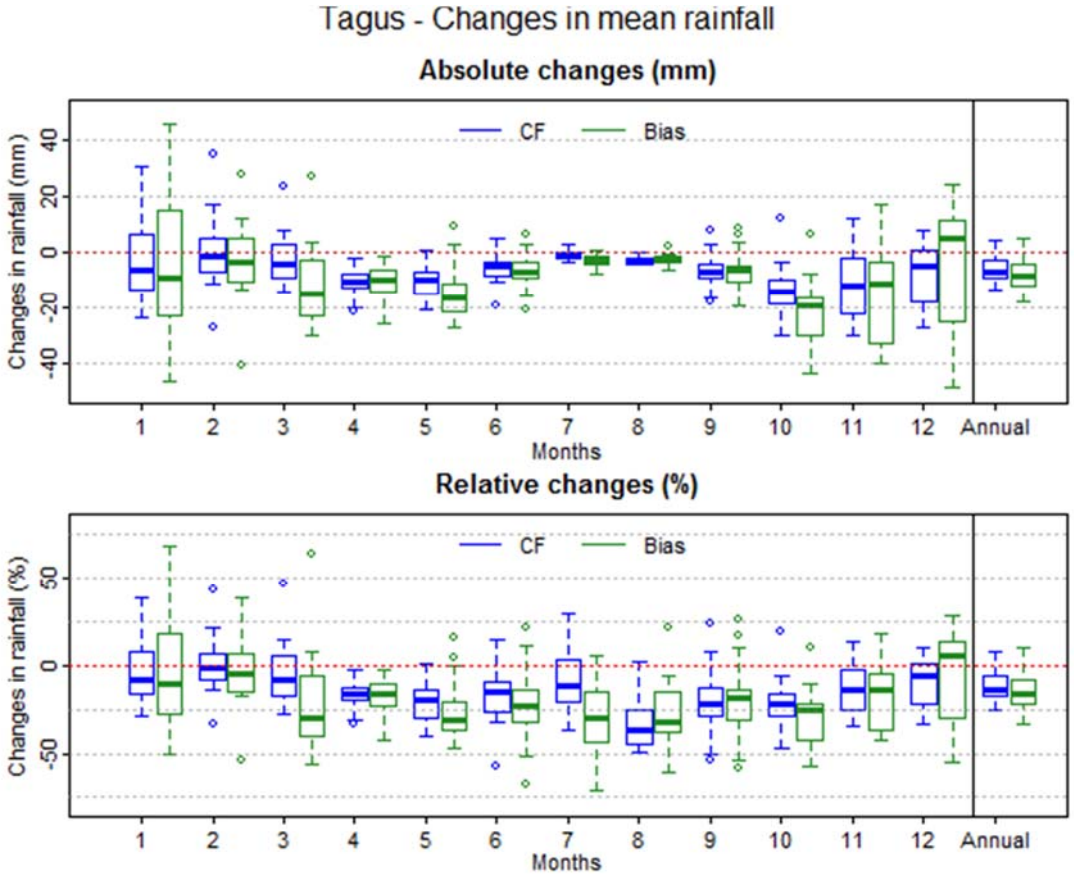

Figure 4.28 – Boxplots of Tagus's absolute (top) and relative (bottom) changes in the basin's mean rainfall (between 1961-1990 and 2041-2070), per month, using the change factor and the bias correction methods.

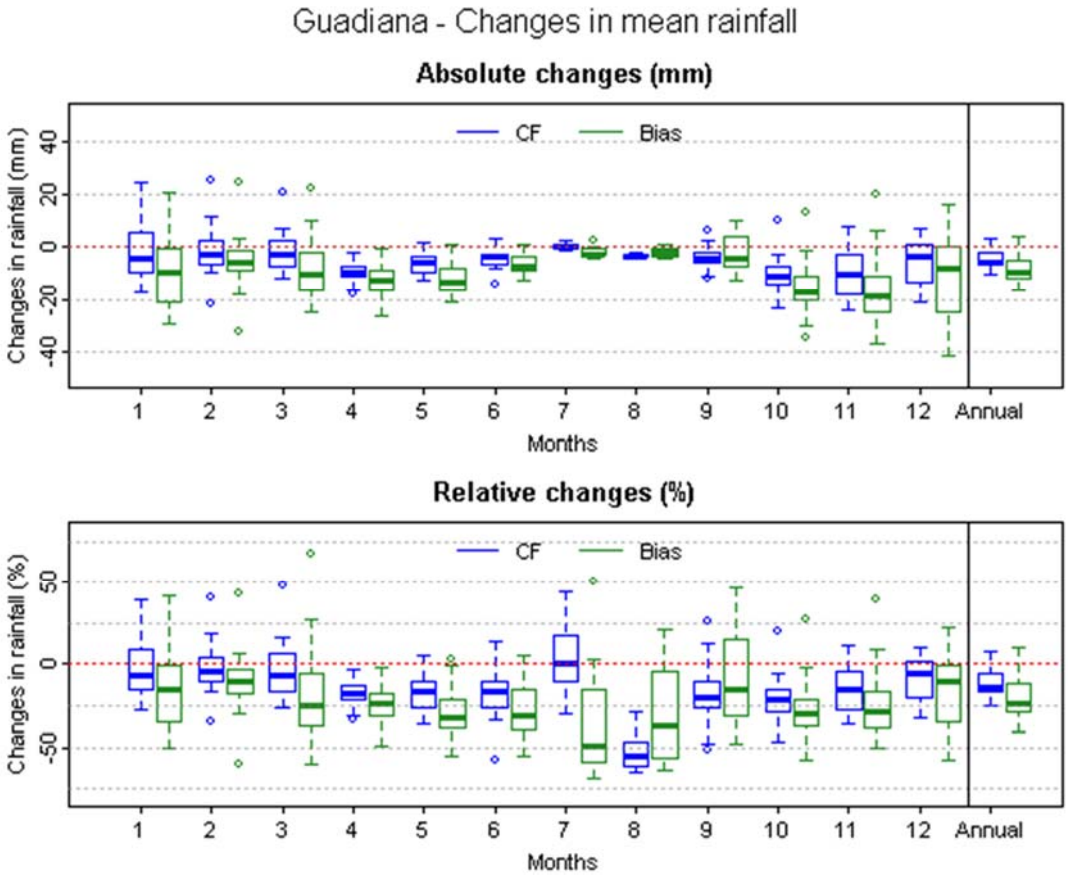

Figure 4.29 – Boxplots of Guadiana's absolute (top) and relative (bottom) changes in the basin's mean rainfall (between 1961-1990 and 2041-2070), per month, using the change factor and the bias correction methods.

4.4.3 *Transient analysis*

The previous analysis showed that the inter-model dispersion on a monthly level is high, with disagreement not just on the magnitude of the change but also, in most months, in the sign of the projected change. Since only one greenhouse gas representative concentration pathway is being used (RCP8.5), this disagreement must result from either structural uncertainties in climate model responses or from initial conditions uncertainty (natural variability).

Deser *et al.* (2012) showed that natural variability can contribute significantly to the disagreement between different GCMs even for timescales of more than 50 years, and particularly for regions dominated by large scale climate modes. A transient analysis of rainfall is therefore necessary to assess if the disagreement between the models is an artefact from the selection of a 30 year period that happens to slice through different parts of a natural cycle or pattern. However, only one of the downscaling methods used (bias correction through quantile mapping) is able to provide transient rainfall outputs so an inter-comparison between methods will not be possible. This should not affect the result significantly because the two methods resulted in comparable projected rainfall changes for the 2050s and the range of the

results of the change-factor method were, in general, encompassed in the range of the results of the bias correction-quantile mapping method.

Figure 4.30 shows boxplots of absolute changes in monthly rainfall for the Tagus for the 2050s (top panel; as in Figure 4.28) and the transient bias corrected rainfall for the GCM run that showed the highest 2050s decrease in rainfall (on the bottom left) and the GCM run that showed the highest 2050s increase in rainfall (on the bottom right). When assessing change between the 30 year periods (1961-1990 and 2041-2070) one model projects a January rainfall decrease of 46mm while the other projects an increase of 46mm. However, when looking at the linear trend between 1961 and 2070, one model projects a decrease of -29mm and the other an increase of 18mm. While there is still no agreement in the sign of the change, the difference in the magnitude of the projected change falls from 92mm to 47mm. The possibly cyclic behaviour of rainfall, shown more clearly in the bottom right graph, shows how choosing arbitrary 30 year periods can contribute to apparent model disagreement.

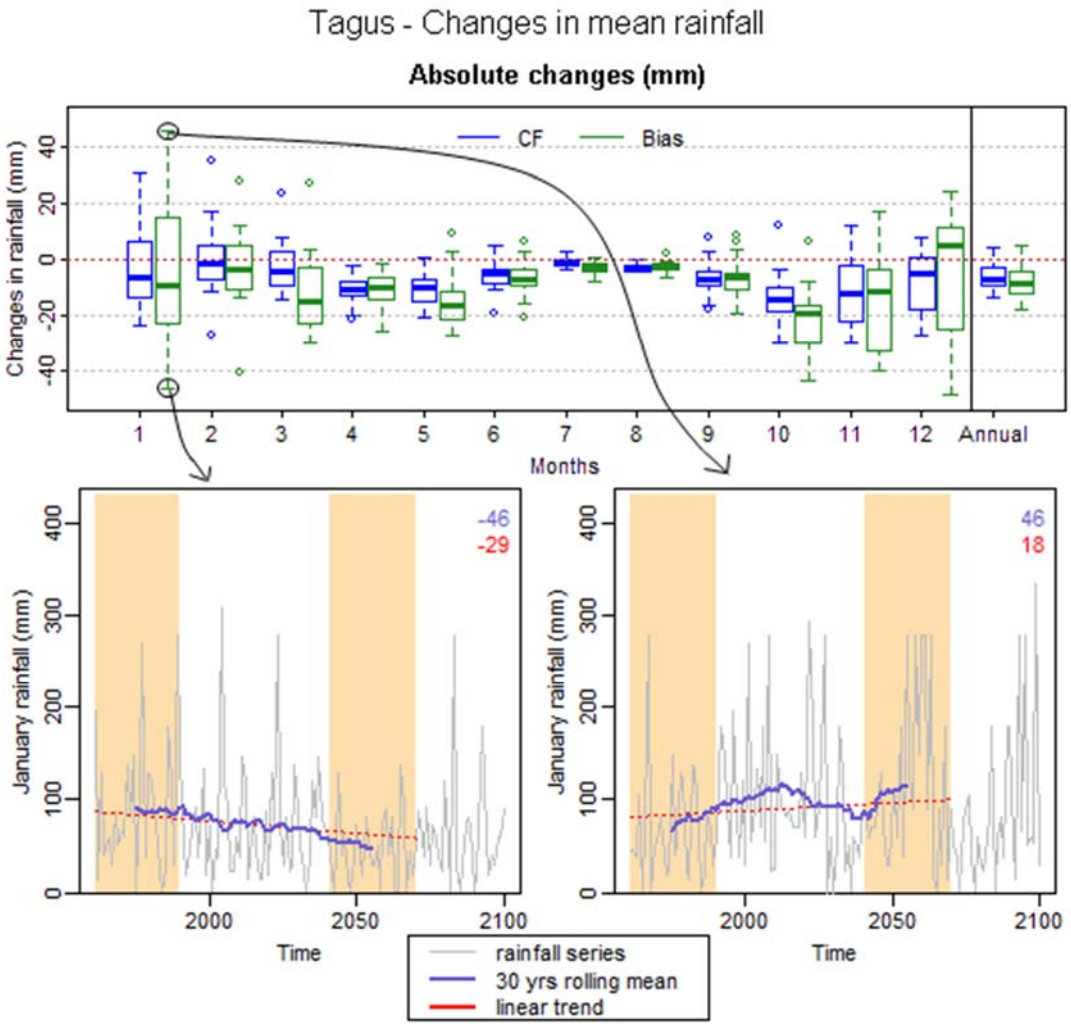

Figure 4.30 – Boxplots of Tagus's absolute changes in monthly rainfall for the 2050s, as in Figure 4.28 (top). Transient bias corrected rainfall for the GCM that showed the highest 2050s decrease in rainfall (on the bottom left) and the GCM that showed the highest 2050s increase in rainfall (on the bottom right) for January in the Tagus. A 30 year rolling mean starting in 1975 and finishing in 2055 is plotted in purple (the magnitude of change between the reference period and the 2050s is shown on the upper right corner in purple). A linear trend covering the period

1961 to 2070 is plotted in red (and its magnitude is shown on the upper right corner in red). The reference period (1961-1990) and the 2050s (2041-2070) are highlighted in orange.

Given the large apparent impact that the choice of 30 year period can have on the projected change signal, long-term trends for the whole time-series (1961-2100) were calculated for annual and seasonal bias-corrected rainfall for every basin and for every model to investigate the long term behaviour of rainfall. The results are summarized in Figure 4.31 and in Table 4.3.

The first striking result is the lack of positive trends in the Guadiana basin and the existence of only one (two) positive trends in the Tagus (Douro). This contrasts with the large range of model projections using 30 year time-slices shown in the previous section. The positive trends (2% or 3% per decade) are confined to the winter season (DJF), when most models show no significant trends in all basins and a few models show significant negative trends, especially in the Guadiana (up to -4% per decade in the Douro and the Tagus and up to -6% per decade in the Guadiana).

In spring (MAM) and autumn (SON), a few models show no significant trends but the majority show negative trends that reach -6% per decade in the Douro and -7% per decade in the Tagus and the Guadiana. This reinforces the possible problem of dry season lengthening identified in the previous section.

Summer (JJA) shows the highest percentage changes in all basins but, as explained before, it is a very dry season so these changes are small in absolute terms. Annual changes range between -5% and no significant change for the Douro and the Tagus, and -6% and no significant change for the Guadiana.

It is important to keep in mind that these are mean values of change per decade, associated with the calculation of long term linear trends; they do not imply a steady transition, and are themselves affected by the start and end point of the time series and the associated point in the natural cycles. This can clearly be seen in Figure 4.32 that shows the annual transient bias corrected rainfall for the Douro basin and in the figures in Appendix G that show annual and seasonal transient bias corrected rainfall for the three studied basins.

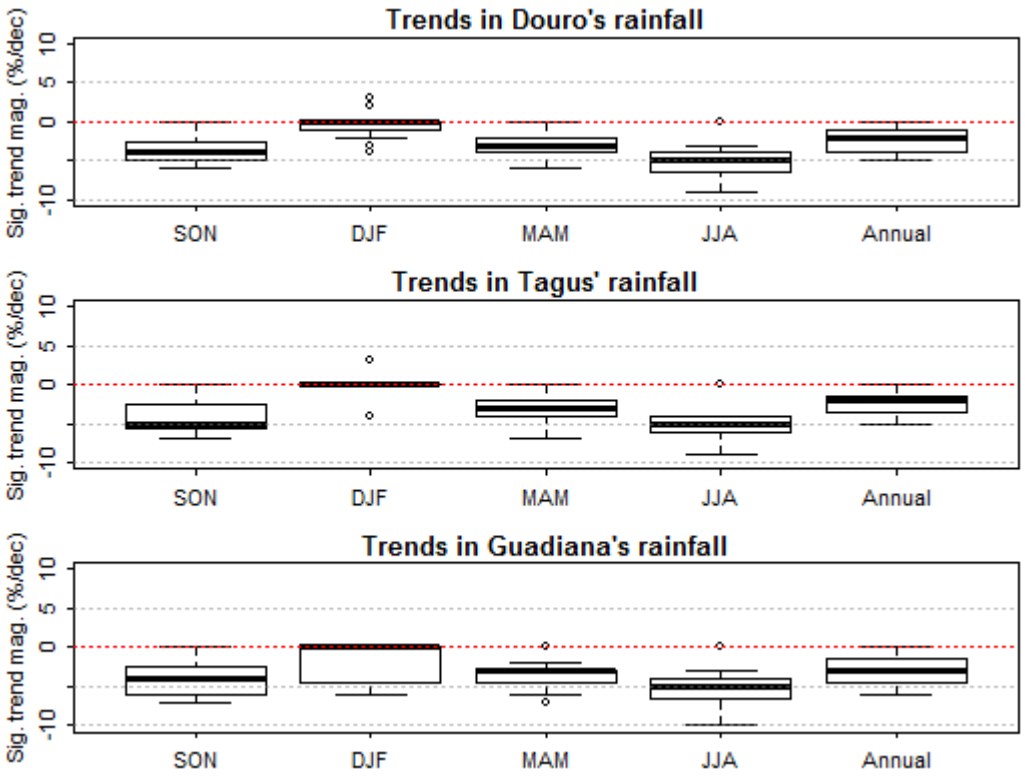

Figure 4.31 – Magnitude of linear trends (significant at a 5% level using Mann-Kendall test) of bias corrected rainfall for the Douro (top), Tagus (middle) and Guadiana (bottom) for the 15 GCMs and for the period 1961-2100. Magnitudes are presented in percentage of change per decade (relative to the 1961-2100 mean rainfall). Non-significant trends are presented as having zero magnitude.

Table 4.3 – Magnitudes of significant trends (at 5% level and assuming a linear trend) in rainfall for each basin, each model and each season. Values are expressed as change per decade as a percentage of the 1961-2100 mean.

	Models	1	2	3	4	5	6	7	8	9	10	11	12	13	14	15
Douro	Annual	-4	-3	-2		-1	-2	-1	-5	-4		-4	-2	-4	-3	
	SON	-5	-4	-5		-2	-3	-2	-6	-4	-4	-5	-3	-4	-6	
	DJF	-3							-4	-2	3	-4				2
	MAM	-3	-4	-2	-3	-3	-6	-2	-6	-4	-2	-2	-3	-4	-4	
	JJA	-4	-3	-7			-4	-5	-6	-5	-4	-7	-5	-9	-7	-4
Tagus	Annual	-4	-3	-2		-2	-2	-1	-5	-3		-4	-2	-4	-3	
	SON	-6	-5	-6			-4	-2	-6	-5	-3	-5	-3	-5	-7	
	DJF	-4							-4		3	-4				
	MAM	-4	-4	-3	-3	-3	-7	-2	-6	-4	-2	-2	-2	-4	-3	
	JJA	-4	-4	-8			-4	-5	-4	-6	-5	-6	-5	-9	-6	-4
Guadiana	Annual	-5	-3	-3	-1	-2	-2	-1	-6	-5		-5	-3	-4	-4	
	SON	-5	-4	-7		-2	-4		-7	-5	-3	-7	-3	-4	-7	
	DJF	-5							-6	-5		-6		-4		
	MAM	-4	-5	-3	-3	-3	-7	-3	-6	-5	-3	-2	-3	-3	-4	
	JJA	-5	-5	-10		-3	-5	-4	-5	-3	-5	-6	-7	-9	-10	-4

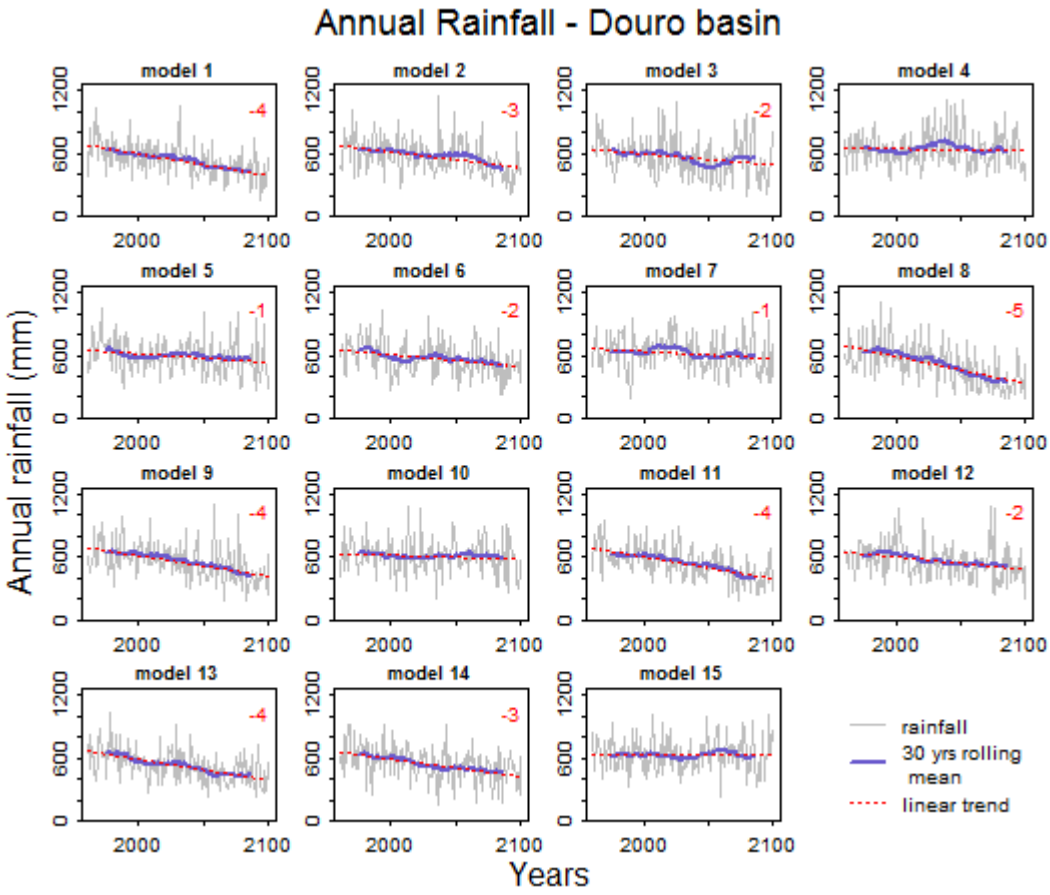

Figure 4.32 – Annual transient bias corrected rainfall for the Douro basin and for the 15 GCMs. 30 year rolling means are plotted in purple and linear trends in red. When the monotonic trend was significant at a 5% level (using Mann-Kendall test) its magnitude, assuming a linear trend, is presented in the upper right corner of the plot in percentage of change per decade (relative to the 1961-2100 mean rainfall).

4.5 Conclusions

This chapter started with the selection of climate model outputs to assess projected changes in rainfall and temperature (and consequently PET). The smallest possible number of models that allowed the capture of the full range of uncertainty for temperature and rainfall mean changes were selected in order to provide useful and transparent plausible future scenarios that can be used by others to test an array of adaptation alternatives, as suggested by (Knutti *et al.* (2010b)).

Two downscaling methods were used: change factor and bias correction through empirical quantile mapping. Both methods showed similar projected monthly rainfall changes for the 2050s (changes between 1961-1990 and 2041-2070). However, the bias correction method tended to show a bigger inter-model range.

Despite considerable disagreement between models on a monthly level, the majority of models projected a reduction in rainfall in the three basins for the 2050s, for all months and for annual rainfall, for both downscaling methods. The only exception is December in the Douro and the Tagus for the bias correction method.

The range of annual rainfall changes was between -33% and +7% in the Douro, -33% and +10% in the Tagus and -41% and +10% in the Guadiana. Almost all models projected rainfall decreases for the spring and autumn months using both downscaling methods. In the spring months (MAM) these decreases can reach up to -43% for the Douro, -40% for the Tagus and -36% for the Guadiana. For the autumn months (SON) it can reach -56% for the Douro, -54% for the Tagus and -51% for the Guadiana.

The magnitude of linear long-term trends (1961-2100) was calculated for annual and seasonal bias-corrected rainfall for every basin and every model. In the winter season (DJF) most models showed no significant trends in the three basins. Contrasting with the time-slice approach, the only significant positive trends identified were for winter in the Douro (two models) and the Tagus (one model). There were no significant positive trends in annual rainfall or in any other season.

In spring (MAM) and autumn (SON) the majority of models showed negative trends that reach -6% per decade in the Douro and -7% per decade in the Tagus and the Guadiana. Annual changes ranged between -5% (-6%) and no significant change for the Douro and the Tagus (Guadiana).

Reductions in rainfall were projected for spring and autumn by almost all models, both downscaling methods and both methods of analysing future rainfall changes (differences between 30 years periods and trends in transient rainfall). This agreement between different methods increases the confidence in a possible lengthening of the dry season in these three basins which could have series impacts for agriculture, water supply and forest fires in the region.

As reviewed in Chapter 2, the rainfall climatology in Iberia is the result of complex seasonal and inter-annual variability, driven largely by large scale circulation patterns like the NAO. Zappa et al. (2013) found that CMIP5 models' ability to simulate the North Atlantic stormtrack is very diverse and they underestimate the intensity of cyclones (see section 4.1.1). Therefore the ability of these climate models to project changes in circulation patterns is questionable. However, an overall drying regime is a component of most of the climate model projections and this may most obviously be associated with circulation pattern features such as the extension of the Azores High, a northward migration of the storm track or the weakening of the NAO. Whilst these changes may superficially explain (some of) the drying/change in rainfall regime, they are themselves only simple measures of the global/Atlantic circulation and not fundamental physical mechanisms. Nevertheless such attribution is beyond the scope of the present work.

The transient approach (linear trends between 1961-2100) showed that a considerable part of the climate model disagreement in the projection of future rainfall changes using the time-slice approach (changes between 1961-1990 and 2041-2070) was due to the choice of 30 year intervals within possibly cyclic patterns of rainfall. The transient approach allows the assessment of the long term direction of the changes projected by the climate models. However, from an impact and adaptation point of view, the results of the time-slice approach can also be important; if the disagreement between climate model projections for the 2050s was interpreted just as a result of model errors it could easily lead to the conclusion that there was no useful information coming from the climate models. However if it is interpreted as a superimposition of model errors, long term change and the cyclic patterns of rainfall due to natural variability, it provides the minimum range of future rainfall changes that should be considered in adaptation studies.

Chapter 5. Droughts

This chapter firstly examines different ways that are used in the literature and practise for defining and measuring a drought. This evaluation enabled the selection of two simple rainfall based drought indices to compare with results from the more sophisticated hydrological modelling presented in Chapter 6 and 7. The objective here is to compare a relatively simple methodology, which requires only rainfall as input and can be performed within a few weeks, with a data-intensive, physically based, distributed hydrological modelling approach which may take several months to set up and run and requires a number of variables as inputs.

Two drought indices were chosen: the Standardized Precipitation Index (SPI) and the Drought Severity Index (DSI). These indices were then fitted to the rainfall data for the 3 basins. Problems related with the distribution fitting that is required for the calculation of the SPI are mentioned both in the methodology and the first part of the results section.

In the second part of the results section DSI and SPI calculated with observed gridded rainfall were compared to DSI and SPI calculated using the downscaled rainfall from the climate models (as detailed in Chapter 4). This analysis showed that using the downscaled rainfall from the climate models results in overestimation of the length/severity of droughts for the historical period for some models, especially in the Guadiana basin.

A transient analysis is then performed using the downscaled climate model rainfall for 1961-2100. This examines both the evolution of the drought indices and the evolution of the mean area of basin in severe and extreme drought. A large range of possible future drought conditions was projected using both drought indices. Some climate models show little or no change in drought conditions from the present (or possibly cyclic behaviour) while others project decades of extreme drought conditions reaching up to 800% accumulated precipitation deficit.

The chapter ends with a discussion of the inadequacy of the SPI for Iberia and a summary of the range of future drought conditions that are projected from the different indices and methods analysed.

5.1 Introduction

There is no universally accepted definition of drought. It can be defined in terms of meteorological, hydrological, agricultural or socio-economic conditions and consequently a large number of different drought indices exist (Lloyd-Hughes and Saunders, 2002). The common ground between all definitions is the cause of drought – a deficit in precipitation. The problems arise in the determination of the time period over which this deficit accumulates and the relations between the deficit in rainfall with deficits in usable water sources and impacts therein (McKee *et al.*, 1993).

Drought is not a distinctive event; it might only be recognised several months after it starts, it might be interrupted by wet spells and depending on what type of drought is being considered it can terminate at different times (Phillips and McGregor, 1998). Bordi *et al.* (2009) define meteorological drought as abnormally low precipitation over a few months and hydrological drought as deficiencies in surface and sub-surface water supplies caused by a reduction in precipitation over the period of one year or more.

Hydrological drought (related to river flows, reservoirs and ground water) typically develops over a longer period than agricultural drought which is related to soil moisture; it is therefore advisable that drought indices can be calculated for different time-scales (McKee *et al.*, 1993). Drought characteristics are dependent on the time-scale: as it increases droughts become less frequent and their duration increases (McKee *et al.*, 1993).

The most commonly used indices in drought studies are the PDSI - Palmer Drought Severity Index and the SPI - Standardized Precipitation Index (Vicente-Serrano *et al.*, 2010). The PDSI is based on a soil water balance equation but requires large amounts of data and is strongly influenced by the calibration period (Vicente-Serrano *et al.*, 2010). The conventional PDSI uses the Thornthwaite equation (whose only variable is temperature) to calculate potential evaporation. Sheffield *et al.* (2012) argue that using the Thornthwaite based PDSI inflates the impact of climate change on future drought because possible changes in radiation, vapour-pressure deficit and wind speeds are ignored. Also they hypothesise that droughts are not caused solely by temperature increases (through increased evaporation) but that evaporation decreases during a drought (due to lack of rainfall) which drives short-term increases in temperature because there is less evaporative cooling. They argue that physically realistic hydrological modelling might be the best way to study the effects of climate change on future drought.

Precipitation deficiency is the main factor in a drought. Evapotranspiration can also be an important factor and some indices, notably the SPEI (Vicente-Serrano *et al.*, 2010), have been used in Iberia. However difficulties in the quantification of evapotranspiration have promoted the use of simple indices based just on precipitation and that have been found to compare well to complex hydrological indices (Lloyd-Hughes and Saunders, 2002). One of such indices is the SPI; it is based on a probabilistic approach, is comparable in time and space and can be calculated for specific time-scales. However the use of the SPI, or any other rainfall-only-based index, assumes that droughts are controlled by the temporal variability of precipitation, hence the variability of all other variables must be low and they must be stationary (Vicente-Serrano *et al.*, 2010). This means that the SPI is insensitive to future increases in drought conditions due to increased temperature, and consequently PET (Vicente-Serrano *et al.*, 2010). Nonetheless, Lloyd-Hughes and Saunders (2002) showed that the SPI-12 is well related to the PDSI for Europe.

Usually parts of Iberia experience drought conditions when others parts show positive SPI values (indicative of wet conditions) and only the most extreme droughts affect the entire peninsula (Vicente-Serrano, 2006a). Spatial patterns of drought in Iberia vary according to the time-scale studied and do not necessarily show climatic coherence because a localized extreme precipitation event can significantly influence the calculation of the drought index (Vicente-Serrano, 2006b). However, for SPI-12, Vicente-Serrano (2006a) found an optimum of four drought regions in Iberia (see Figure 5.1) where the central/western cluster (represented by black circles) includes the Douro, Tagus and Guadiana basins. In this cluster the 1940s, 1950s and 1990s saw the biggest drought events while the 1960s and 1970s were humid. Also, between 1910 and 1940, dry and humid periods were not as intense as between 1940 and 2000 which experienced a higher temporal variability (Vicente-Serrano, 2006a).

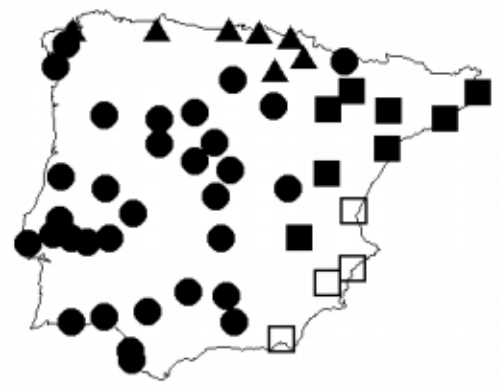

Figure 5.1 - Regional division of Iberia according to drought history for an optimum of 4 clusters (Vicente-Serrano, 2006a).

According to the Spanish Water Information System (Hispagua), the droughts of the 20th century in Spain exposed the divergence between water demand and water resources in Spain

and led to an increase in reservoirs and water transfers (Hispagua, 2013). The worst droughts of the last centuries in Spain were in 1941/1945, 1979/1983, 1990/1995. These droughts affected most of Spain with reductions in rainfall between 23% and 30%, resulting in runoff reductions of above 40% in most of the country and reaching 70% in the Guadiana and the Guadalquivir basins (JuntaDeAndalucia, 2013).

According to the Portuguese Institute for the Ocean and the Atmosphere (IPMA), the worst recent droughts in Portugal that affected agriculture and water resources and had significant social impacts were in 1943/46, 1965, 1976, 1980/81, 1991/92, 1994/95, 1998/99 and 2004/06. The last one had the biggest spatial extent (all territory) and was the most intense when considering the number of consecutive months in severe or extreme drought. The regions south of the Tagus are more prone to droughts and in the last decades of the twentieth century there has been an increase in the frequency of droughts, especially in the months from February to April (IPMA, 2013a).

Only two studies of future drought in the region could be found. Pulquério *et al.* (2014) used a generalized linear model to downscale daily rainfall from one GCM (HadCM3) and two scenarios (SRES A2 and B2) but only for the Portuguese part of the Tagus basin for the period 2010-2099. Subsequently they calculated SPI-12 using a gamma distribution but no details are presented about the calculation of the SPI (and the suitability of the gamma distribution to their data). They found an increase in magnitude of droughts under the A2 scenario that reached three-times the observed (1961-1990) by the end of the century. Under the B2 scenario they found a decrease in magnitude but an increase the number of events. However, the use of just one climate model does not allow the assessment of the range of possible futures and the choice of study area doesn't account for the majority of the basin (which is upstream in Spanish territory) therefore limiting the usability of their results.

In the other study found (Jenkins and Warren, 2014) SPI-6 and SPI-12 was applied to observed (1955–2003) and projected (2003–2050) precipitation for several countries around the world, including Portugal and Spain. The rainfall data used came from the Community Integrated Assessment System (CIAS) where a simple climate model emulates the a range of GCMs and emission scenarios and the downscaling model ClimGen uses pattern scaling to produce monthly precipitation data. As with the previous study, no details are presented about the calculation of the SPI and the suitability of the gamma distribution to their data. Nevertheless, using SPI-12 they found droughts could increase by 96% to 341% in Spain, while in Portugal there was no agreement in the direction of the change.

Some studies can be found about global or regional drought which also include the region. Heinrich and Gobiet (2012) used a subset of eighth RCM simulations driven by five different GCMs from the ENSEMBLES project for the period 1961-1990 and 2021-2050 followed by a daily quantile mapping correction of RCM output (using the E-OBS dataset). SPI-3, SPI-6, SPI-12, SPI-18 and SPI-24 were calculated using a gamma distribution which fitted well their aggregated rainfall data for most months for the calculation of SPI-3 to SPI-18 (but not for SPI-24). Besides SPI, the self-calibrated Palmer Z-Index (scZI) and the self-calibrated Palmer Drought Severity Index (scPDSI) were also calculated and multi-model mean change between baseline and future period were assessed for Europe.

For all the SPIs the most pronounced increases in mean dry event frequency, length, distance, magnitude, and area are obtained for the Iberian Peninsula with SPI-18 showing increasing mean dry event frequency by 19.8%, length by 26.5%, magnitude by 62.6%, and area by 51.1%, while distance decreases by 35.1%. Unfortunately, the range of changes projected by the different models is not presented. The results for changes in extreme dry events were even more pronounced.

5.2 Data

Two different rainfall datasets were used in this chapter, both of them previously introduced in Chapter 4:

- The observed gridded daily rainfall dataset IB02 with a resolution of 0.2° × 0.2°. It was constructed based on 2000 gauges in Spain and 400 in Portugal and is available for the period 1950 to 2003.
- Daily gridded rainfall obtained by downscaling 15 GCMs using empirical quantile mapping – (see section "4.3.3 - Bias correction – empirical quantile mapping" for more information). Since IB02 was used to downscale and bias correct the GCMs the two datasets have the same resolution. The GCM downscaled rainfall is available from 1961 to 2100.

5.3 Methodology

5.3.1 Standardized Precipitation Index – SPI

The Standardized Precipitation Index (SPI) was initially defined by McKee *et al.* (1993). The first step was to fit a Gamma distribution to monthly rainfall (aggregated to the desired temporal scale, for e.g. 12-month aggregated monthly rainfall for the calculation of SPI-12). Then transform it to a standard normal. Using this distribution, the probability associated to each aggregated monthly rainfall is its SPI. As the Gamma distribution is undefined for zero, when months with no rainfall exist, the probability of zero rainfall has to be added to the cumulative probability calculated by the Gamma distribution. McKee *et al.* (1993) defined drought as a period of continuously negative SPI, where SPI reached a value equal or inferior to -1.

The Portuguese Institute for the Ocean and the Atmosphere (IPMA) uses PDSI and SPI to characterize drought in Portugal. SPI-3 is used to characterize agricultural drought, SPI-6 to characterize the rainfall in autumn and winter, SPI-9 for medium duration droughts and SPI-12 for droughts that are associated with low reservoir levels, low river discharges and low aquifer levels (IPMA, 2013b).

The Spanish Meteorological Agency (AEMET) uses SPI to characterize drought in Spain. It uses the following SPI time scales: hydrological year (1st of September to 31st of August), 1 month, 3 months, 6 months, 1 year, 2 years and 3 years (AEMET, 2013). IPMA's and AEMET's drought classes are presented in Table 5.1. Following the Portuguese classification, in this study two thresholds will be used: SPI ≤ -2.00 to define extreme drought and SPI between -1.99 and -1.50 to define severe drought.

Table 5.1 – Drought classes used by the Portuguese Institute for the Ocean and the Atmosphere (IPMA, 2013c) on the left and the Spanish Meteorological Agency on the right (AEMET, 2013).

SPI values	Drought classes	Probability %
≥2.00	Extremely wet	2.3
1.50 to 1.99	Severely wet	4.4
1.00 to 1.49	Moderately wet	9.2
0.50 to 0.99	Slightly wet	15.0
-0.49 to 0.49	Normal	19.1
-0.99 to -0.50	Slight drought	15.0
-1.49 to -1.00	Moderate drought	9.2
-1.99 to -1.50	Severe drought	4.4
≤ - 2.00	Extreme drought	2.3

SPI values	Drought classes
2.00 to 3.00	Extremely wet
1.25 to 2.00	Very wet
0.75 to 1.25	Moderately wet
-0.75 to -0.75	Normal
-1.25 to -0.75	Moderately dry
-2.50 to -1.25	Very dry
-4.00 to -2.50	Extremely dry

Sienz *et al.* (2012) argued that the gamma distribution does not represent monthly rainfall well for considerable areas of the globe. However for longer time-scales (including 12 months) the Gamma distribution outperforms all other considered distributions (Weibull, Burr Type III, exponential Weibull distribution and generalized Gamma distribution). For SPI-1, the

inappropriate fit of the Gamma distribution led to overestimation of extreme dryness (and underestimation of extreme wetness) and hindered comparisons between different areas or periods. They therefore proposed the calculation of SPI using multiple distributions: selecting the distribution that fits rainfall better for each month and each location. They showed that the selection of the distribution had large impacts on the calculation of SPI and differences in SPI between using multiple-distributions and using the Gamma distribution ranged between 20% and 50% for the control period (depending on the area). However, the SPI calculate using multiple-distributions is not appropriate to compare different areas/periods so, when comparability is important, a single distribution should be chosen that produces accurate estimates in almost all areas and months (Sienz *et al.*, 2012).

When applying SPI in Europe, Lloyd-Hughes and Saunders (2002) showed that the Gamma distribution performed better that the normal distribution but none were adequate to describe rainfall in the north-west of Spain.

Because the Gamma distribution is not defined for values of zero, if present they have to be excluded before fitting this distribution. Posteriorly the probability of occurrence of zero rainfall has to be added to the cumulative rainfall distribution calculated using the Gamma before the normal transformation. This means that, if the probability of zero precipitation events is high, the SPI will not be normally distributed since it will have a lower bound. Therefore small rainfall amounts will correspond to high SPI values (Wu *et al.*, 2007). Another problem with using a Gamma distribution to calculate SPI in arid climates, or climates with dry seasons, is that if the time-series has a considerable amount of zeroes that have to be removed before the Gamma distribution is fitted there will be a limited sample size for the fitting (Wu *et al.*, 2007).

Guttman (1999), using data from the USA, compared the calculation of a single site SPI using several probability distributions (Gamma, Pearson III, Generalized Extreme Value, Kappa and Wakeby) with a regional calculated SPI based on a best fit analysis (L-moments) that was considered to be “the most accurate” SPI. He concluded that for dry events the SPI results did not depend much on the distribution used, however both Gamma and Pearson III fitted the data better than other distributions. Due to the higher flexibility of Pearson III (with its extra parameter) he advises the use of a Pearson III distribution, fitted with L-moments algorithm in the calculation of SPI. This distribution also showed the best results for wet events.

Vicente-Serrano (2006b) calculated the SPI for Iberia for the time-scales of scales of 1, 3, 6, 12, 24 and 36 months. Using L-moments they concluded that the Pearson III distribution fitted well to their gauge data. Depending on the time-scales the Pearson III parameters ranged from

values that indicate an exponential distribution to values that indicate a normal distribution as can be seen in Figure 5.2.

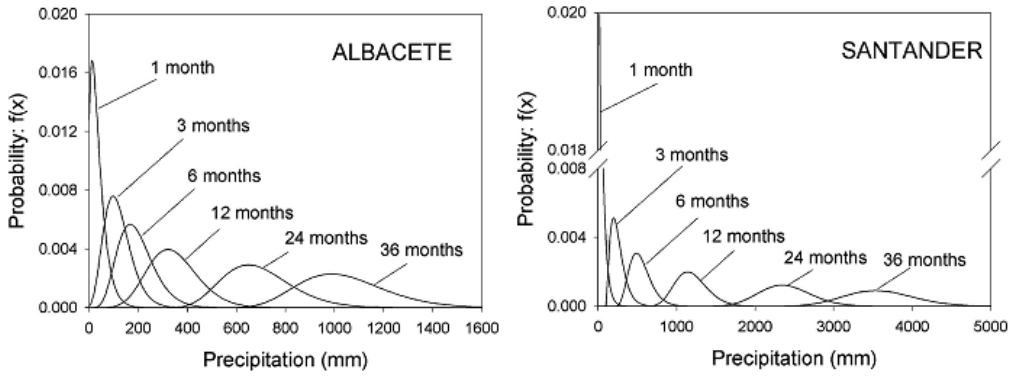

Figure 5.2 – Pearson III distributions used for SPI calculation in two stations in Iberia for different time-scales (Vicente-Serrano, 2006b).

Soľáková *et al.* (2013) compared a non-parametric approach to calculate SPI (where the cumulative distribution function is approximated by the Weibull plotting position) with two parametric methods of calculating SPI: using one probability distribution for all the months (with different parameters each month) or choosing different probability distributions each month. The probability distributions considered were: Burr, Erlang, Gamma, Generalized Gamma, Inverse Gaussian, Lognormal, Pearson, Weibull and Generalized Extreme Value, and the distribution was chosen using the Maximum Likelihood method. The SPI was calculated using 80 years of monthly rainfall from Roma Collegio Romano. For SPI-12 the mean differences between methods were very significant for drought severity (reaching up to 54%) but smaller for drought duration (up to 7.2%) or inter-arrival time (up to 1.2%).

A non-parametric approach would be the ideal method by which to calculate SPI, since it avoids the problem of finding a distribution that fits the rainfall data reasonably well. However, it is not clear how to extrapolate the empirical cumulative function to be able to calculate SPI for future rainfall when the range of future and historical rainfall is different. Therefore, in this study two distributions were fitted to the gridded monthly rainfall for the period 1961-1990: the gamma distribution, as originally proposed by McKee *et al.* (1993) and the Pearson III distribution as suggested by Guttman (1999) and Vicente-Serrano (2006b) for Iberia. Both distributions were fitted to 12-monthly aggregated rainfall based on L-moments using the R-package "lmomco". The distributions were then transformed to a standard normal distribution giving the value of SPI-12. The code developed for the calculation of SPI is presented in Appendix E.

To assess which distribution fitted the data better, a modified mean square error (MSE), as defined by Papalexiou *et al.* (2012) was used (see equations 5.1 and 5.2). Unlike the classical

MSE, the errors between the theoretical and the empirical values are independent of the magnitude of the rainfall. This means that errors in the lower tail (the important part of the distribution for drought assessment) have as much impact in the value of MSE as errors in the rest of the distribution.

$$\boldsymbol{MSE} = \frac{\mathbf{1}}{\boldsymbol{N}} \sum_{\boldsymbol{i=1}}^{\boldsymbol{n}} \left(\frac{\boldsymbol{F(x_i)}}{\boldsymbol{F_N(x_i)}} - \mathbf{1} \right)^{\mathbf{2}}$$

Equation 5.1

N – Sample size

$F(x_i)$ – Probability of value x_i using a theoretical distribution (Gamma or Pearson III)

$F_N(x_i)$ – Probability of value x_i using the empirical distribution defined as:

$$F_N(x_i) = \frac{rank(x_i)}{N+1}$$

Equation 5.2

For each grid point, this modified MSE was applied to the aggregated rainfall for each month and the 12 monthly MSEs were summed. Figure 5.3 a) shows which distribution fitted the rainfall data better for each IB02 grid point and Figure 5.3 b) shows boxplots of the sums of the modified MSEs per grid point using both the Gamma and the Pearson III distributions for all grid points inside the three studied basins. The Pearson III distribution is a better fit than the Gamma distribution in most grid points and overall it shows smaller MSEs, thus being the preferred distribution for the calculation of the SPI.

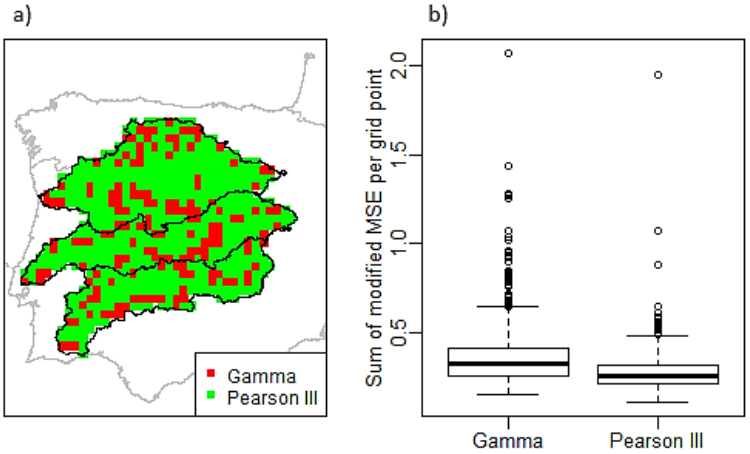

Figure 5.3 – a) Map of Iberia with rainfall grid points in red where the Gamma distribution is a better fit than the Pearson III and in green when the inverse is true. b) Boxplots of the sums of the modified MSE (see equation 5.1) per grid point for the Gamma and the Pearson III distributions.

However, for some grid points, and for some months, the SPI-12 calculated using the Pearson III distribution is minus infinity. This happens because the fit is not particularly good and the Pearson III distribution has a probability of zero for the lowest observed value of rainfall (see Figure 5.4 for an example). Also, due to the lack of an asymptotic behaviour, if the future is drier than the present, this distribution will produce minus infinity SPI values.

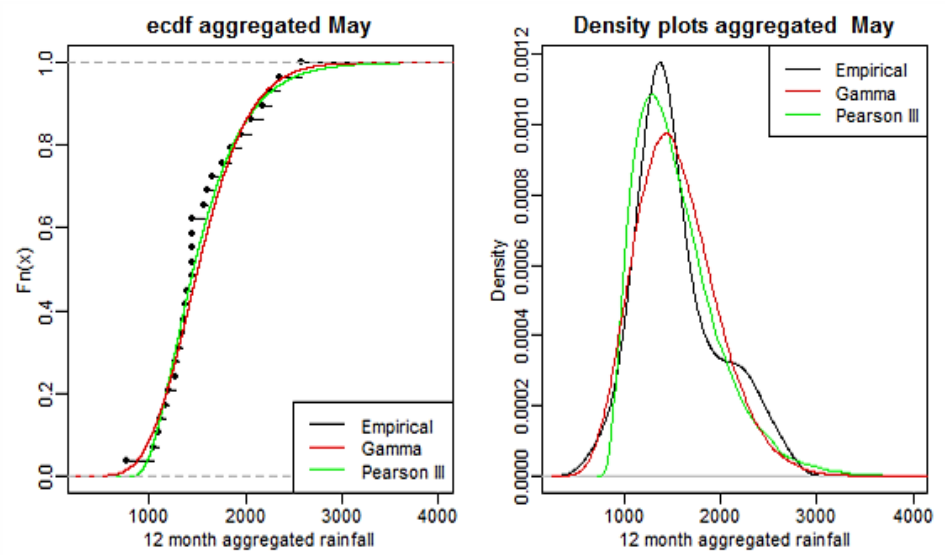

Figure 5.4 – ecdfs and density plots for a grid point in the Douro basin where SPI-12 calculated using the Pearson III distribution is minus infinity for the 12-month aggregated rainfall for May.

When calculating the SPI-12 for the gridded bias corrected downscaled GCM rainfall, minus infinity SPI-12 values are present, on average over the 15 GCMs, at around 10% of the grid points inside each basin. The percentages for each GCM and each basin can be seen in Table 5.2. However for the future, due to drier conditions, there are minus infinity SPI values on average in more than half the grid points for all three basins. In some models, like model 7 for the Guadiana, this does not happen. For other models, like model 8 for the Douro, 94% of the basin is affected. Therefore, the Pearson III distribution is not suitable for the calculation of SPI-12 in the Douro, Tagus and Guadiana basins.

Table 5.2 – Percentage of grid points and of months (considering all grid points) where SPI-Pearson III values are minus infinity. Percentages are presented per basin and per downscaled GCM for two periods: 1961-1990 and 1991-2100.

	Models	Grid points		Months	
		1961-1990	1991-2100	1961-1990	1991-2100
Douro	1	9.51	76.43	0.01	1.20
	2	1.90	53.61	0.00	0.42
	3	3.42	27.38	0.00	0.15
	4	0.76	20.53	0.00	0.10
	5	37.26	50.95	0.06	0.84
	6	3.42	47.15	0.00	0.42
	7	0.76	13.69	0.00	0.02
	8	14.07	94.30	0.01	3.59
	9	8.75	73.76	0.01	1.93
	10	4.18	66.54	0.00	0.73
	11	31.56	84.79	0.03	3.76
	12	7.22	72.62	0.01	1.04
	13	1.52	74.90	0.00	0.77
	14	2.28	38.78	0.00	0.53
	15	18.63	78.71	0.02	0.72
	Mean	**9.68**	**58.28**	**0.01**	**1.08**
Tagus	1	10.47	73.30	0.01	1.19
	2	15.18	73.82	0.01	0.82
	3	0.52	5.24	0.00	0.01
	4	3.14	43.98	0.00	0.47
	5	30.89	77.49	0.04	1.40
	6	5.24	64.40	0.00	0.92
	7	16.75	45.03	0.03	0.32
	8	20.94	96.86	0.02	3.78
	9	10.47	81.68	0.02	1.56
	10	8.38	80.63	0.01	0.57
	11	1.57	48.69	0.00	0.46
	12	11.52	80.10	0.01	1.01
	13	8.90	72.25	0.01	1.49
	14	12.57	47.64	0.01	0.68
	15	21.99	85.86	0.03	0.78
	Mean	**11.90**	**65.13**	**0.01**	**1.03**
Guadiana	1	2.94	77.06	0.00	1.26
	2	13.53	92.94	0.02	1.67
	3	5.88	46.47	0.00	0.58
	4	11.76	68.24	0.01	0.95
	5	29.41	66.47	0.03	0.62
	6	1.18	5.88	0.00	0.02
	7	0.00	8.82	0.00	0.01
	8	9.41	83.53	0.01	2.71
	9	19.41	90.59	0.02	3.84
	10	1.18	49.41	0.00	0.17
	11	61.76	98.24	0.12	5.83
	12	7.65	65.29	0.01	1.67
	13	5.88	79.41	0.01	1.26
	14	5.88	32.94	0.01	0.50
	15	24.12	87.06	0.02	1.91
	Mean	**13.33**	**63.49**	**0.02**	**1.53**

Since Pearson III is not suitable for the calclation of the SPI in the Douro, Tagus and Guadiana basins, a Generalized Gamma distribution was also considered, using the R-package “gamlss”. However the modified MSEs for some grid points were significantly higher than using the Gamma or Pearson III distribution fitted with L-moments using the R-package “lmomco” (see Figure 5.5). This is probably because the “gamlss” package uses maximum (penalised)

likelihood estimation to fit the distributions and "lmomco" uses L-moments. Unfortunately Generalized Gamma is not a choice of distribution available in the "lmomco" package.

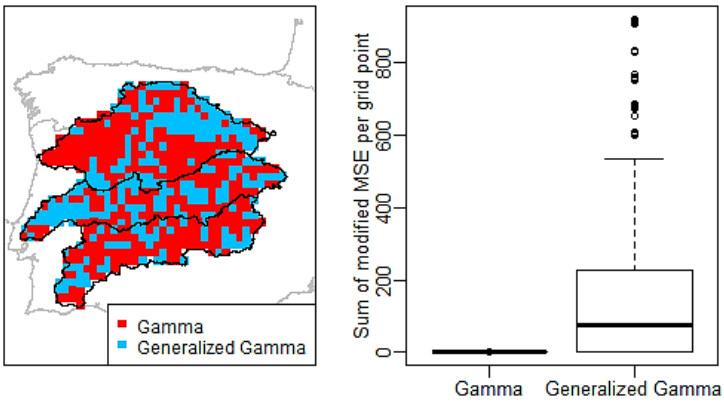

Figure 5.5 - Map of Iberia with rainfall grid points in red where the Gamma distribution is a better fit than the Generalized Gamma and in blue when the inverse is true (left). Boxplots of the sums of the modified MSE (see equation 5.1) per grid point for the Gamma and the Generalized Gamma distributions (right).

In the end, the Gamma distribution was used to calculate SPI-12 for the Douro, Tagus and Guadiana basins. However, for the historical period, the differences in maximum severity of drought and frequency of severe and extreme drought using SPI-12 $_{\text{Gamma}}$ and SPI-12$_{\text{Pearson III}}$ were assessed using the dataset IB02 to assess how the uncertainty in the choice of distribution may affect the results. Because IB02 dataset was used to downscale and bias correct the rainfall from the 15 climate models (using quantile mapping), this analysis was performed only in the IB02 dataset, which was assumed to also act as a proxy for the rainfall of the 15 models during the historic period.

Monthly basin rainfall was calculated by adding together the monthly rainfall from every grid point inside each basin. For the historical period, SPI-12 plots were performed for all basins using the IB02 dataset and the 15 models in order to compare the models behaviour with observations. For the 15 models, SPI-12 plots were also performed for the period 1961-2100 to assess future drought conditions.

The percentage of basin in severe (SPI< -1.5) and extreme (SPI< -2) drought was also calculated for the three basins using the gridded rainfall from the 15 models. Plots with 30-year rolling means of percentage of basin in severe and extreme drought are shown.

5.3.2 Drought Severity Index - DSI

The Drought Severity Index (DSI) was also used in this study. The concept was originally proposed by Bryant *et al.* (1992) and is based on cumulative monthly precipitation anomalies

(Blenkinsop and Fowler, 2007). The index was defined by Phillips and McGregor (1998) and, like the SPI, can be calculated for different time-scales.

DSI-3 is calculated using the following procedure:

- If the rainfall anomaly in month t is negative (i.e. rainfall is below the mean for that month) and rainfall in the three previous months is lower than its three-monthly mean, a drought sequence is initiated in month t;
- DSI-3 for month t is then a positive value equal to the precipitation anomaly in month t.
- The DSI for the following month (t+1) is the rainfall anomaly of month t plus the rainfall anomaly of month t+1, but only if the three-monthly mean total for the months t – 1,t and t+ 1 has not been exceeded. When this mean is exceeded the drought sequence terminates and DSI-3 is assigned a value of zero.
- To standardise the index, the absolute deficit (in mm) is divided by the station's mean annual rainfall and multiplied by 100. Therefore the final index value expresses the accumulated precipitation deficit as a percentage of the mean annual rainfall.

DSI-6, DSI-12 (or any other DSI) is calculated in the same way but using six months, 12 months (or any other time-scale required) instead of three months. The code developed for the calculation of DSI is presented in Appendix F.

DSI-3 is able to promptly detect rainfall deficits but tends to terminate the drought sequence too easily. Longer scale DSIs, like DSI-6 or DSI-12, show a greater resistance to the initiation and termination of a drought sequence. Droughts identified with DSI-6 are more persistent than with DSI-3, but have some lag (Phillips and McGregor, 1998).

In order to select the DSI scale that better correlates with SPI-12, the correlations between the magnitude of SPI (the sum of the SPI values of a drought) and the DSI-1 to DSI-20 values were calculated (see Figure 5.6 for an illustration of the methodology).

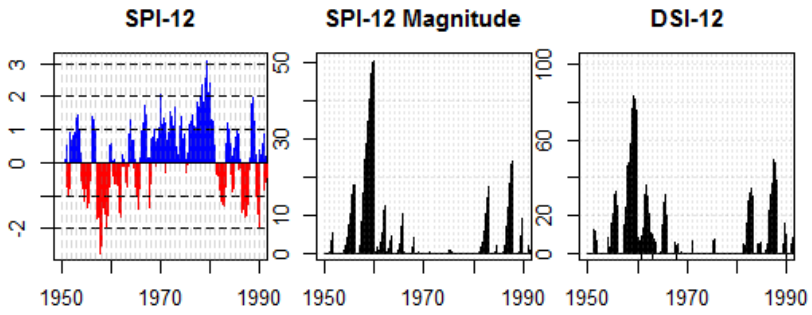

Figure 5.6 – Plots showing an example of SPI-12 (left), magnitude of SPI-12 (centre) and DSI-12 (right).

Figure 5.7 shows that, for most grid points inside the Douro, Tagus and Guadiana basins, DSI-12 is the DSI that best correlates with SPI-12 magnitude. The correlation coefficients are in general very high (Figure 5.7, right panel). Therefore 12 months was the scale used for DSI calculation.

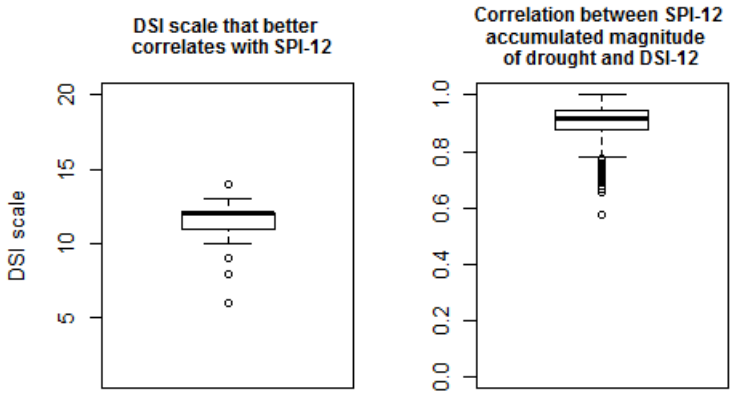

Figure 5.7 – Boxplots showing the DSI scale that best correlates with SPI-12 for each grid point inside the Douro, Tagus and Guadiana basins (left) and the Spearman correlation coefficient between SPI-12 and DSI-12 for each grid point inside the Douro, Tagus and Guadiana basins (right).

As with SPI, monthly basin rainfall was calculated by adding the monthly rainfall from the grid points inside each basin. For the historical period, DSI-12 plots were produced for all basins using the IB02 dataset and the 15 bias-corrected models in order to compare the models' behaviour with observations. For the 15 models, DSI-12 plots were also produced for the period 1961-2100 to assess future drought conditions.

The percentage of basin in severe (DSI> 50%) and extreme (DSI> 100%) drought was also calculated for the three basins using the gridded rainfall from the 15 models. Plots with 30-year rolling means of the percentage of basin in severe and extreme drought are shown.

5.4 Results

5.4.1 *Differences between SPI-12$_{Gamma}$ and SPI-12$_{Pearson\ III}$*

Using the IB02 dataset, comparisons were made between SPI-12 calculated by fitting a Gamma distribution and SPI-12 calculated by fitting a Pearson III distribution for all grid points inside each basin for the period 1961-1990. In terms of the frequency of severe drought, the range of the number of events per decade does not change with the distribution used. However, using the Gamma distribution there are more areas of the basins with a slightly higher number of events per decade (see Figure 5.8, left). For extreme drought, Pearson III tends to show a higher number of events (see Figure 5.8, centre). The maps in Figure 5.9 show the lack of spatial pattern in the differences of the frequency of severe and extreme drought inside the basins when using a Gamma or a Pearson III distribution.

The comparison for maximum severity (see Figure 5.8, right) is hindered by the existence of minus infinity SPI-12 values when using the Pearson III distribution. But even when not accounting for these values, the range of maximum severity of drought is larger using the Pearson III distribution. This means that some areas show more severe droughts using Pearson III than using Gamma. But again there is no spatial pattern (see Figure 5.10).

Most differences in maximum severity of drought between SPI-12 $_{Gamma}$ and SPI-12 $_{Pearson\ III}$ (not accounting for the grid points with minus infinity values) are between -1 and 1. However they reach a maximum of 5.5 (SPI-12 $_{Gamma}$= -2.4 and SPI-12 $_{Pearson\ III}$= -7.9) which corresponds to a 70% difference in maximum severity of drought.

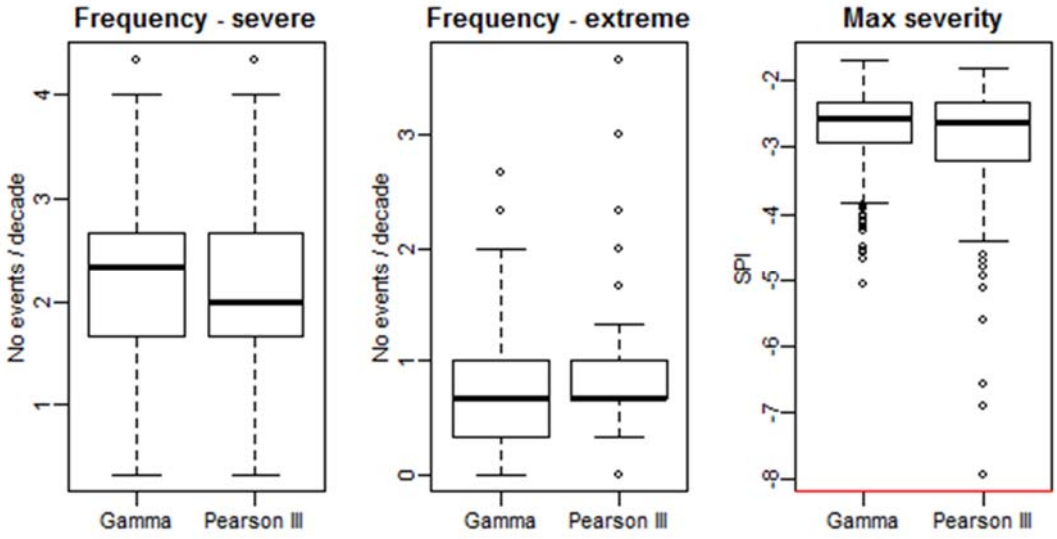

Figure 5.8 –Number of events per decade for severe drought (for all grid points inside the Douro, Tagus and Guadiana basins) using Gamma and Pearson III distributions (left). Number of events per decade for extreme drought using Gamma and Pearson III distributions (centre). SPI-12 maximum severity of drought (for all grid points inside the Douro, Tagus and Guadiana basins) using Gamma and Pearson III distributions (right). Note that minus infinity SPIs for Pearson III are not plotted. The period of analysis is 1961-1990.

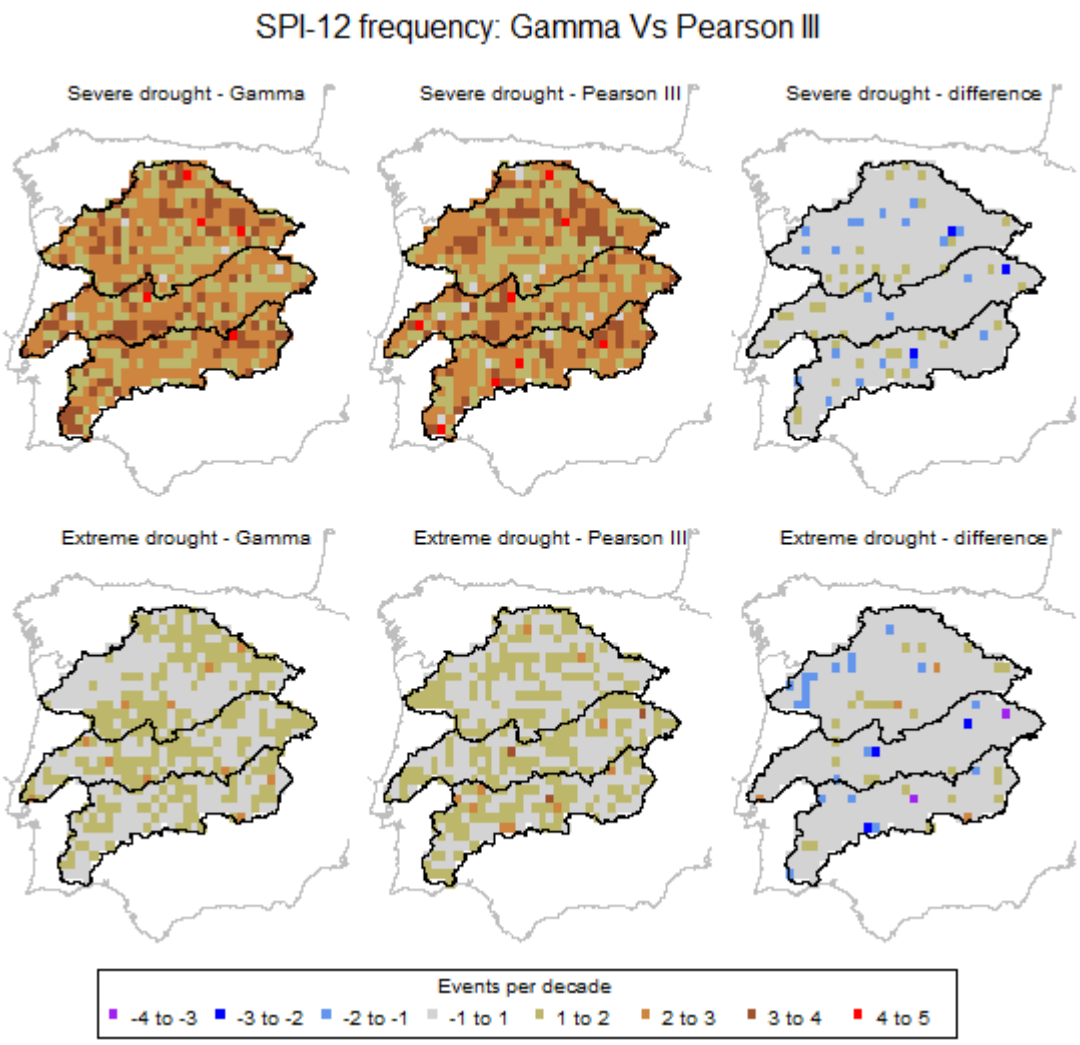

Figure 5.9 – Maps of Iberia showing SPI-12 drought frequency in number of events per decade (for the Douro, Tagus and Guadiana basins) using Gamma (left) and Pearson III (centre) distributions and the difference between the two distributions (right) for severe drought (top) and extreme drought (bottom).

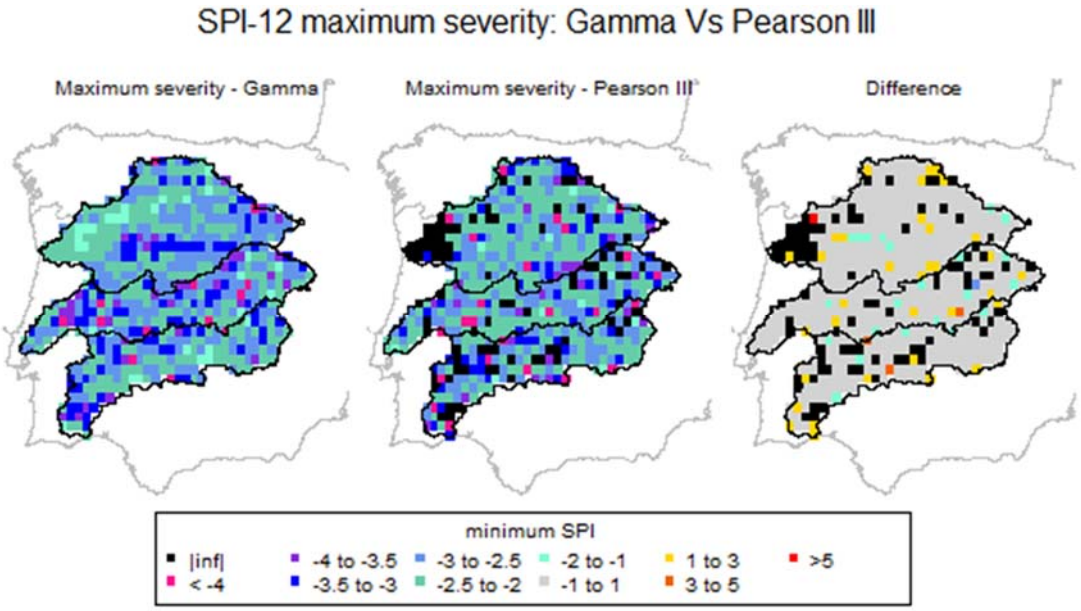

Figure 5.10 – Maps of Iberia showing SPI-12 maximum severity of drought (for the Douro, Tagus and Guadiana basins) using Gamma (left) and Pearson III (centre) distributions and the difference between the two distributions (right). Black squares are grid points where SPI is minus infinity (or when the difference between $SPI\text{-}12_{Gamma}$ and $SPI\text{-}12_{Pearson\ III}$ is infinite because $SPI\text{-}12_{Pearson\ III}$ is minus infinity)

5.4.2 Historical period

A comparison between the DSI-12 values calculated from monthly rainfall from the gridded observation dataset IB02 and from the 15 downscaled and bias corrected climate models was made for the 1961-2003 period (all available data) for the three basins. For this period some models seem to be performing quite well, but most models are overestimating the duration /severity of droughts which might affect the confidence in these models projections for future drought. This overestimation happens with models 3, 5, 6, 7 and 8 in the Douro basin (see Figure 5.11), and 3, 5, 6, 7, 8,9, 11 and 13 for the Tagus (see Figure 5.12). In the Guadiana most models overestimate the duration/severity of droughts; nonetheless models 1, 2, 12 and 15 perform better (see Figure 5.13). Table 5.3 synthesises the results.

Table 5.3 – Summary of drought results for the historical period (1961-2003): frequency of severe drought (number of droughts with DSI-12>50% per decade), maximum duration of severe drought (in months) and maximum severity (maximum value of DSI-12 reached).

	Freq.	Max dur.	Max sev.		Freq.	Max dur.	Max sev.		Freq.	Max dur.	Max sev.
	Douro				**Tagus**				**Guadiana**		
obs	1.66	24	90.2	**obs**	1.66	12	84.6	**obs**	0.48	4	60.2
1	0.95	4	59.8	**1**	1.19	20	79.0	**1**	0.71	16	72.4
2	0.71	6	60.8	**2**	0.71	2	52.5	**2**	0.95	10	74.3
3	0.95	38	166.0	**3**	1.66	51	229.3	**3**	0.95	72	207.9
4	0.24	22	96.6	**4**	1.66	21	98.7	**4**	2.38	26	113.8
5	0.95	53	139.5	**5**	1.66	29	128.8	**5**	1.43	56	161.7
6	0.71	44	185.9	**6**	2.14	47	218.8	**6**	0.48	44	176.8
7	0.24	55	206.0	**7**	0.71	42	177.6	**7**	1.43	60	241.5
8	0.71	36	124.2	**8**	0.95	53	178.2	**8**	1.19	46	180.9
9	1.66	27	90.1	**9**	1.66	37	138.6	**9**	0.95	36	109.7
10	0.48	13	73.7	**10**	0.71	25	98.4	**10**	1.66	26	107.3
11	0.95	13	80.9	**11**	0.95	26	121.8	**11**	1.43	33	102.5
12	0.95	4	67.3	**12**	0.71	5	68.2	**12**	0.48	8	67.6
13	1.19	22	82.1	**13**	1.19	25	115.8	**13**	0.95	32	109.6
14	0.48	20	99.4	**14**	0.24	20	108.4	**14**	2.38	20	106.9
15	0.24	10	75.8	**15**	0.24	12	78.6	**15**	0.00	0	49.5

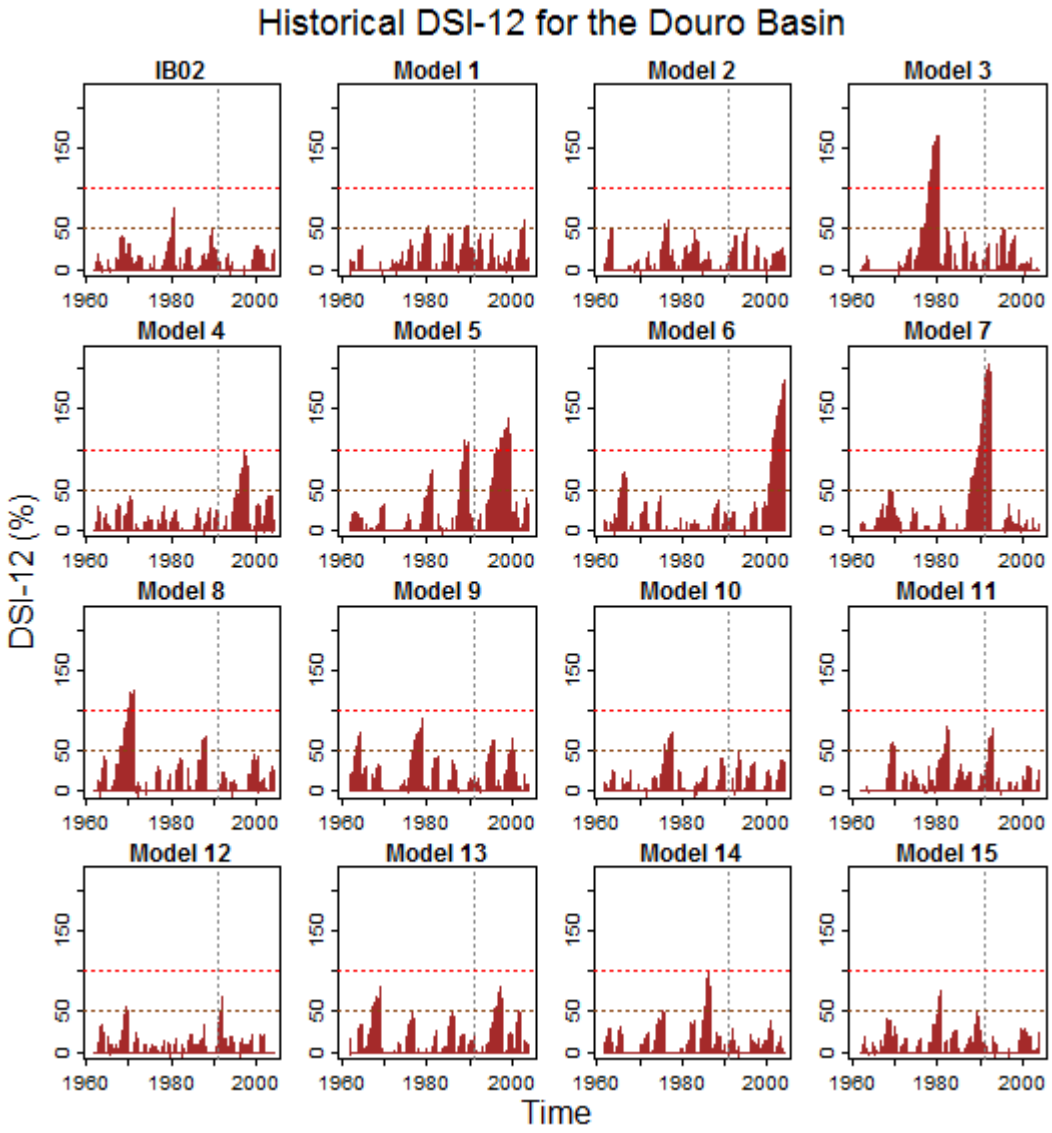

Figure 5.11 – DSI-12 plots for the 1961-2003 period and for the Douro basin using monthly rainfall from the gridded observation dataset IB02 and from the 15 downscaled and bias corrected climate models. The vertical dotted line separates the DSI-12 reference period (1961-1990) from the rest of the record, while the horizontal lines define severe (brown) and extreme (red) droughts.

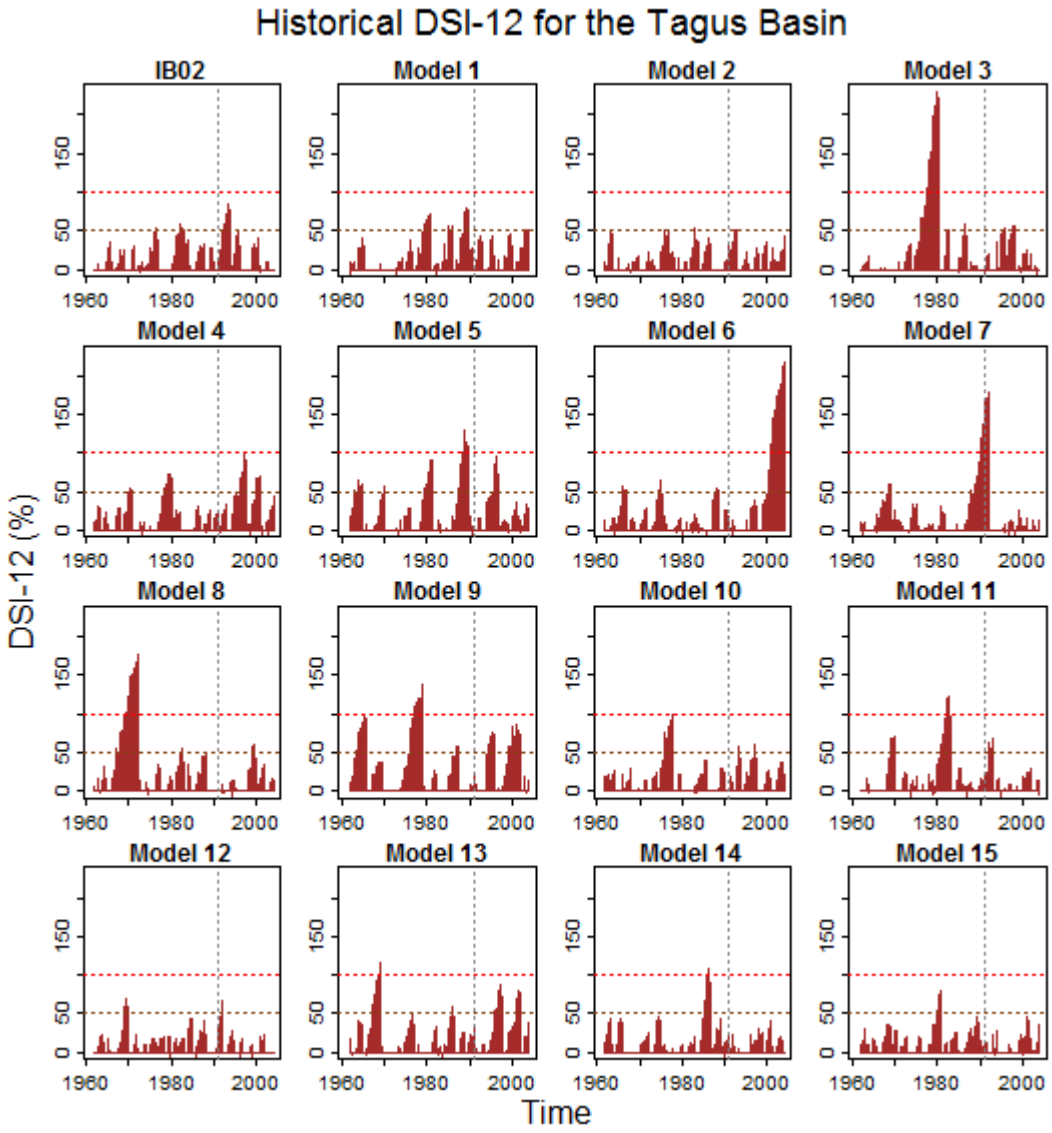

Figure 5.12 – DSI-12 plots for the 1961-2003 period and for the Tagus basin using monthly rainfall from the gridded observation dataset IB02 and from the 15 downscaled and bias corrected climate models. The vertical dotted line separates the DSI-12 reference period (1961-1990) from the rest of the record, while the horizontal lines define severe (brown) and extreme (red) droughts.

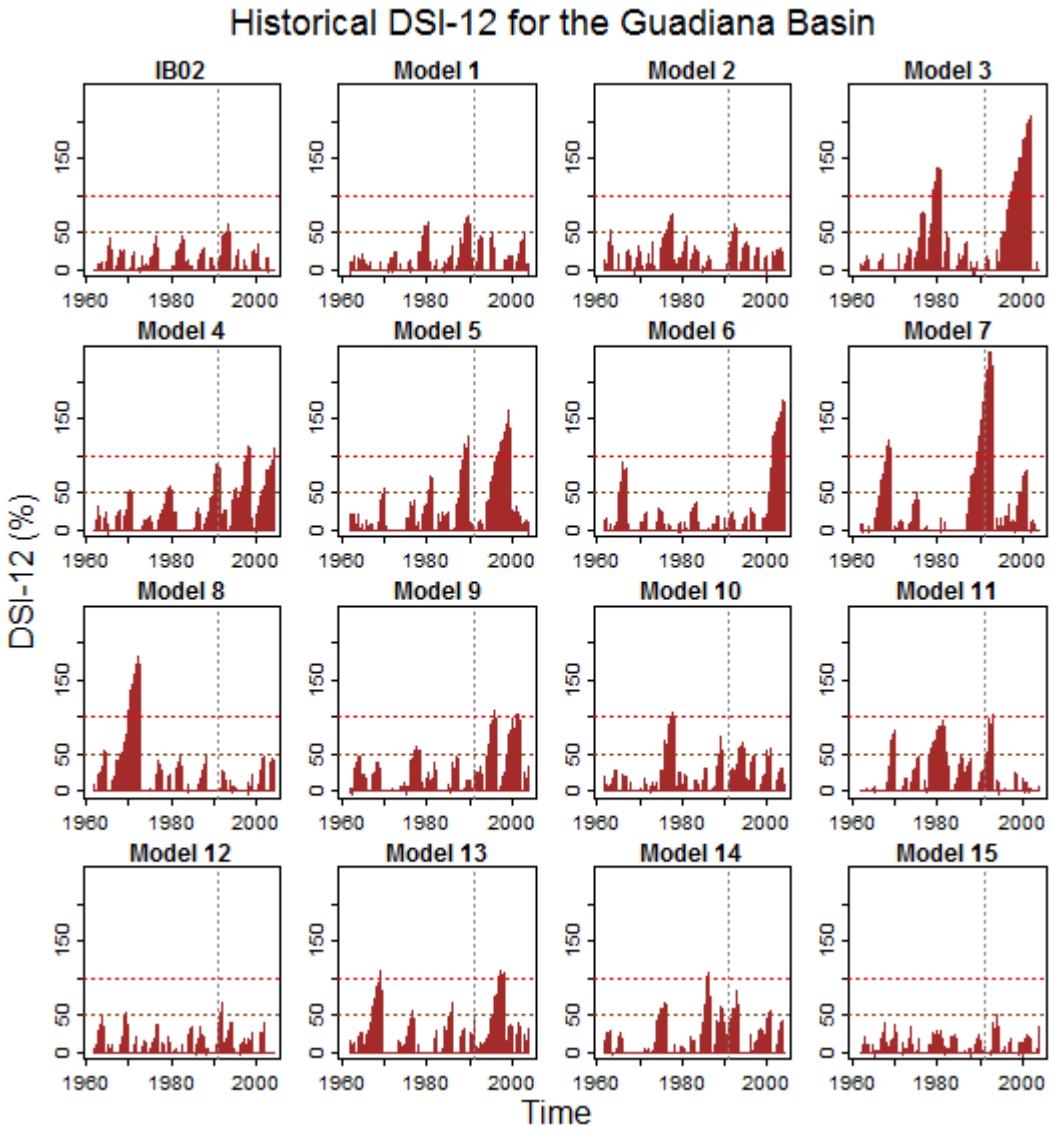

Figure 5.13 – DSI-12 plots for the 1961-2003 period and for the Guadiana basin using monthly rainfall from the gridded observation dataset IB02 and from the 15 downscaled and bias corrected climate models. The vertical dotted line separates the DSI-12 reference period (1961-1990) from the rest of the record, while the horizontal lines define severe (brown) and extreme (red) droughts.

SPI-12 plots were also produced for the three basins (see Figure 5.14, Figure 5.15 and Figure 5.16) using the same datasets. For the period 1961-2003, model 6 performs particularly badly for all basins (and model 7 is also particularly bad for the Douro), reaching SPI values around -6, which is associated with a very small probability (9.8×10^{-10}) of occurrence.

Even during the 1961-1990 period, which is the reference period used to fit the Gamma distribution to the data, four models in the Douro basin show SPI-12 below -3 (meaning less than 0.0013 probability of occurrence). The Tagus has one model with SPI-12 below -3 and the Guadiana has six models. The worst case is model 9 for the Guadiana which reaches a SPI-12 of -3.8 for the 12 month aggregated November rainfall. This has an associated probability of occurrence of just 7.2×10^{-5}. Figure 5.17 shows that the Gamma distribution does not fit well

the 12-month aggregated Guadiana rainfall for model 9, especially for the month of November, which results in the probability of low rainfall being too low. The same problem happens, to a lesser extent, in other models and basins. Also, in all basins, some models seem to have periods of negative and positive SPI-12 that are too long, meaning the drought or wet conditions are too persistent within the models. This means that, when using SPI-12, errors related with distribution fitting will be added to errors from climate model.

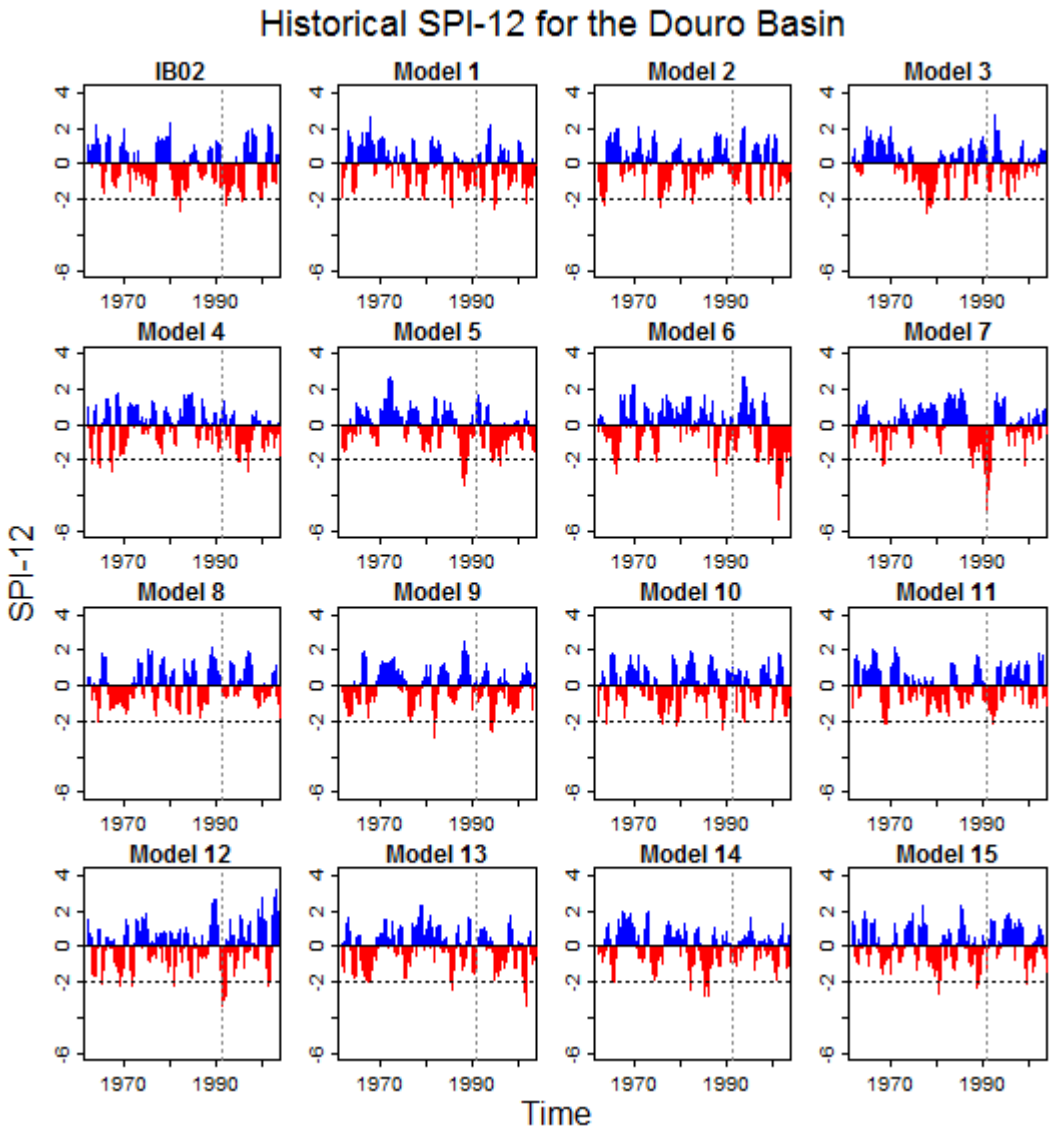

Figure 5.14 – SPI-12 plots for the 1961-2003 period and for the Douro basin using monthly rainfall from the gridded observation dataset IB02 and from the 15 downscaled and bias corrected climate models. The vertical dotted line separates the SPI-12 reference period (1961-1990) from the rest of the record, while the horizontal line defines extreme droughts.

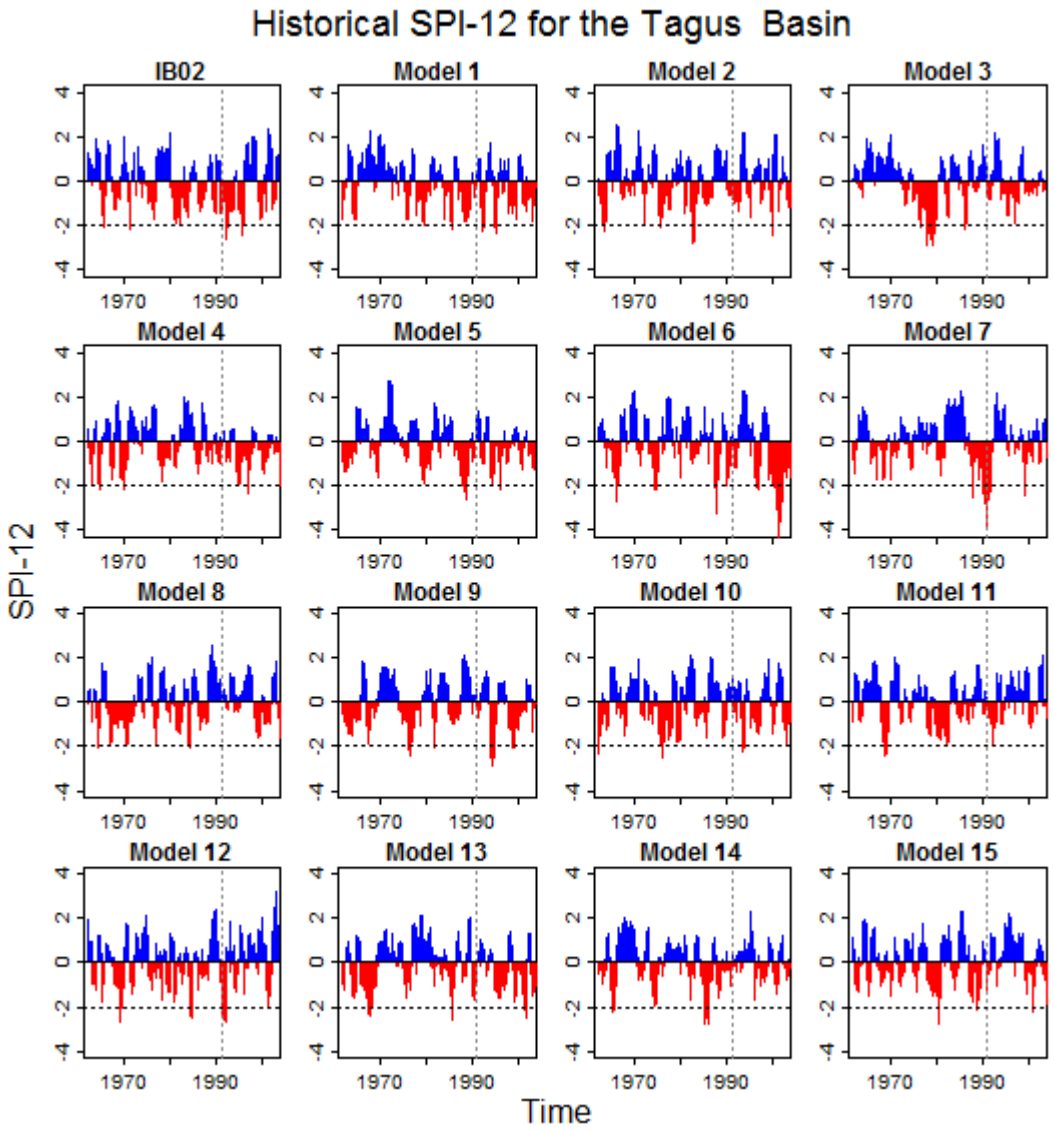

Figure 5.15 – SPI-12 plots for the 1961-2003 period and for the Tagus basin using monthly rainfall from the gridded observation dataset IB02 and from the 15 downscaled and bias corrected climate models. The vertical dotted line separates the SPI-12 reference period (1961-1990) from the rest of the record, while the horizontal line defines extreme droughts.

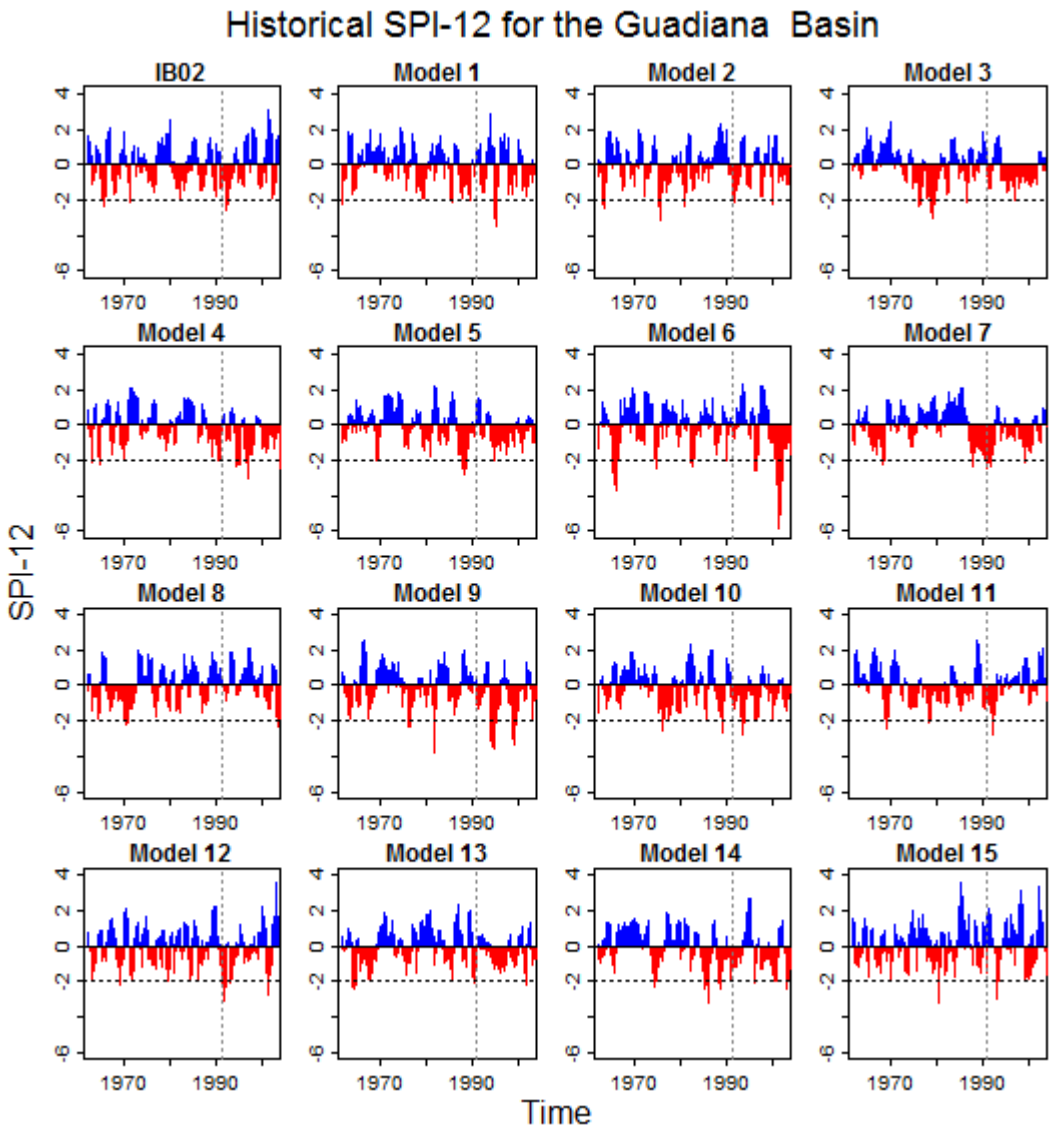

Figure 5.16 – SPI-12 plots for the 1961-2003 period and for the Guadiana basin using monthly rainfall from the gridded observation dataset IB02 and from the 15 downscaled and bias corrected climate models. The vertical dotted line separates the SPI-12 reference period (1961-1990) from the rest of the record, while the horizontal line defines extreme droughts.

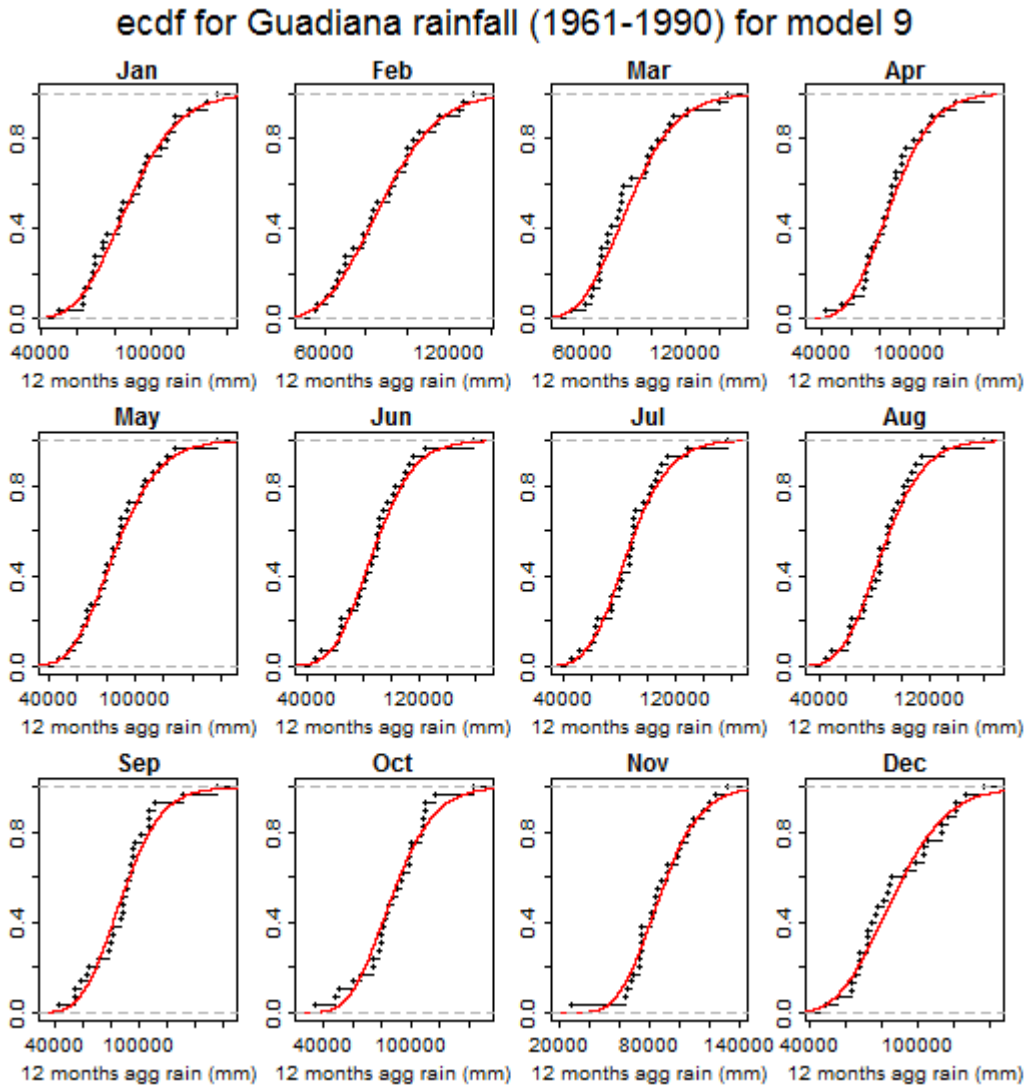

Figure 5.17 – ecdf plots of 12 month aggregated Guadiana rainfall (in mm) from model 9 (used for the calculation of SPI-12) with the ecdf of the fitted Gamma distribution in red. The period 1961-1990 was used since it is the period used for the calculation of the reference SPI-12.

5.4.3 Transient analysis

The DSI-12 projections for the future from the 15 models are very diverse (see Figure 5.18, Figure 5.19 and Figure 5.20). All models show an increase in drought conditions but some project small increases (like models 4, 5, 7, 10 and 15, for the Douro and Tagus and models 7, 10 and 15 for the Guadiana) while most models ((1, 2, 3, 8, 9, 11, 13 and 14) project multi-year droughts reaching up to 800% accumulated precipitation deficit.

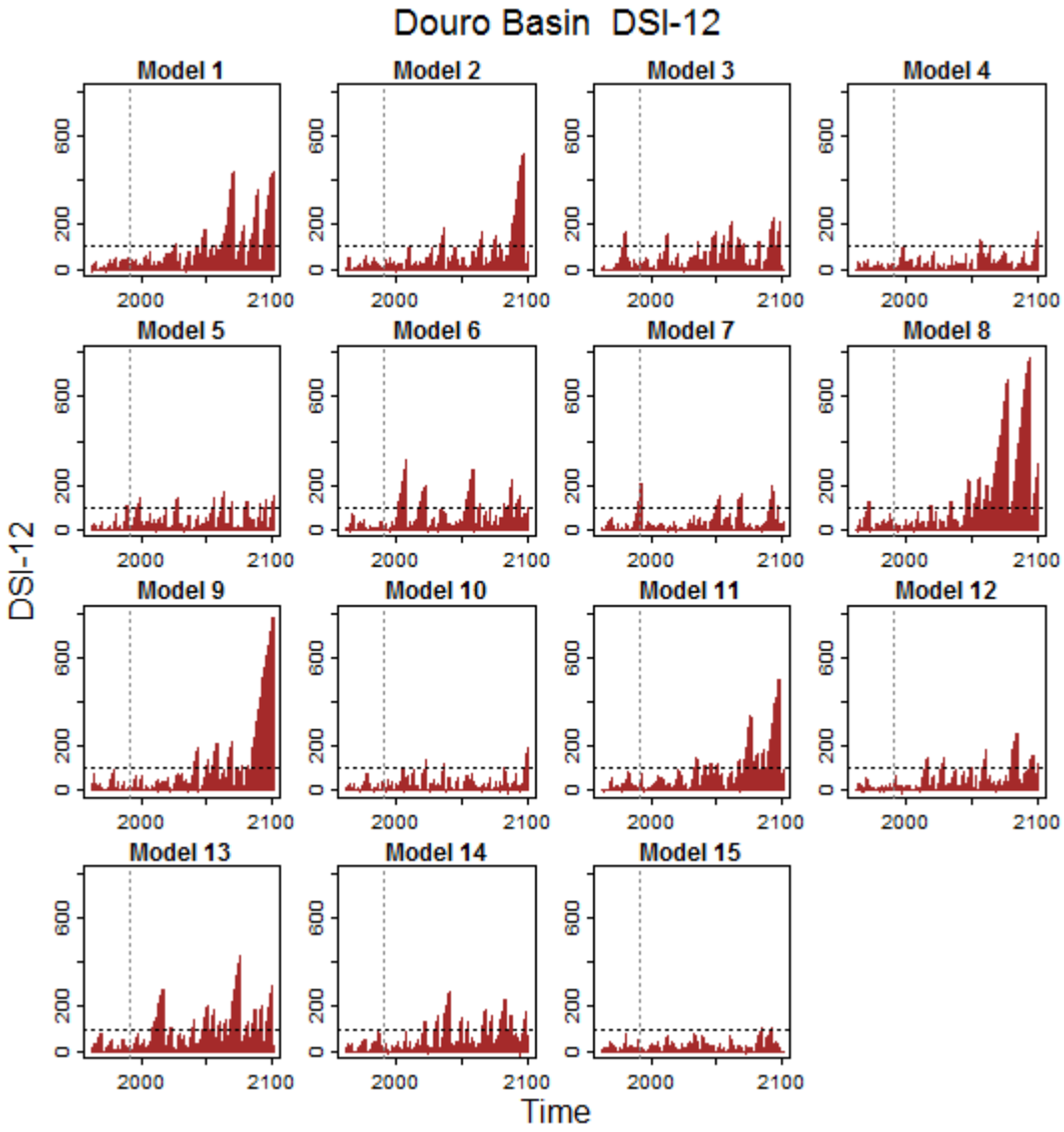

Figure 5.18 – DSI-12 plots for the 1961-2100 period and for the Douro basin using monthly rainfall from the gridded observation dataset from the 15 downscaled and bias corrected climate models. The vertical dotted line separates the DSI-12 reference period (1961-1990) from the rest of the record, while the horizontal line defines extreme droughts.

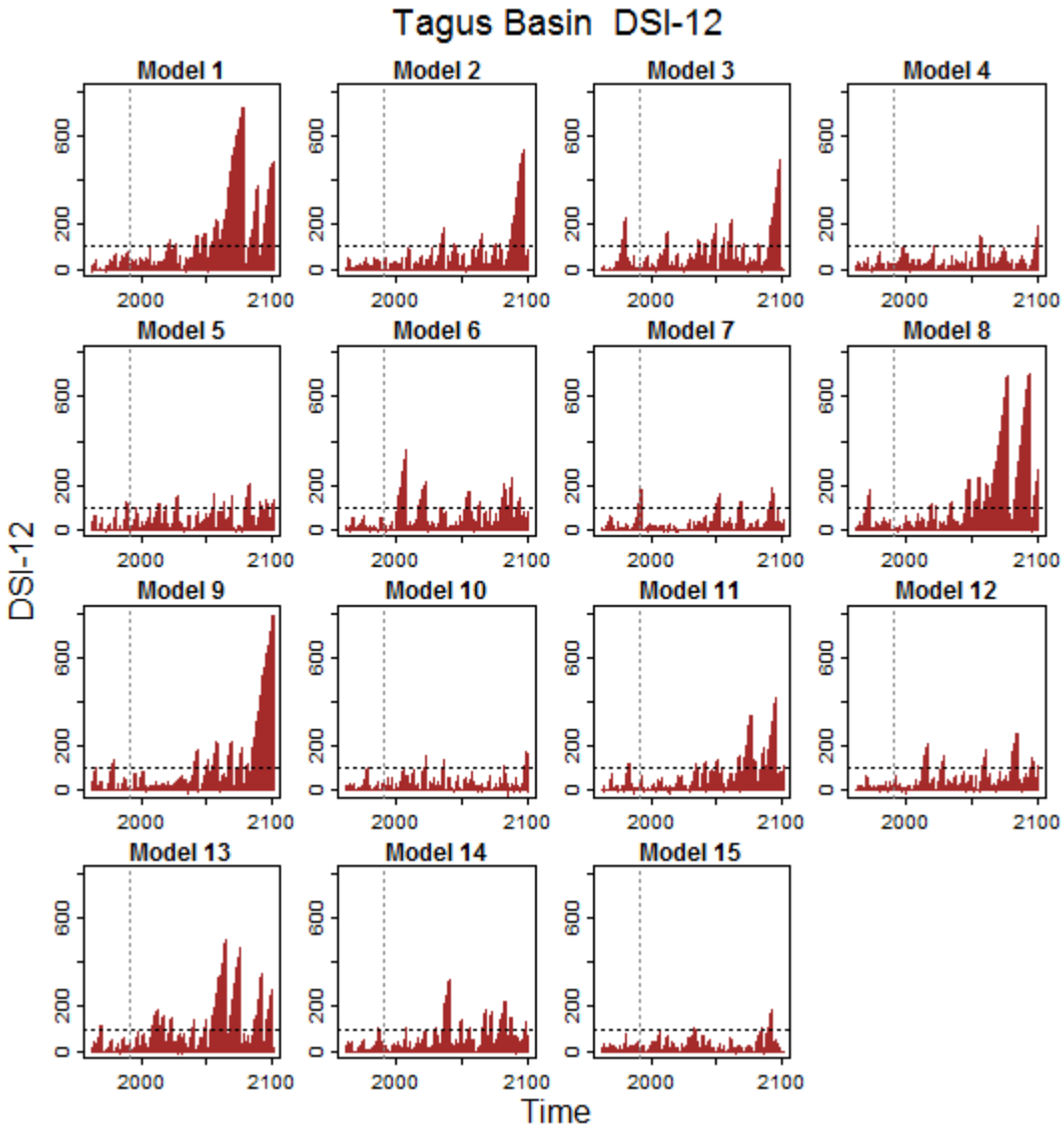

Figure 5.19 – DSI-12 plots for the 1961-2100 period and for the Tagus basin using monthly rainfall from the gridded observation dataset from the 15 downscaled and bias corrected climate models. The vertical dotted line separates the DSI-12 reference period (1961-1990) from the rest of the record, while the horizontal line defines extreme droughts.

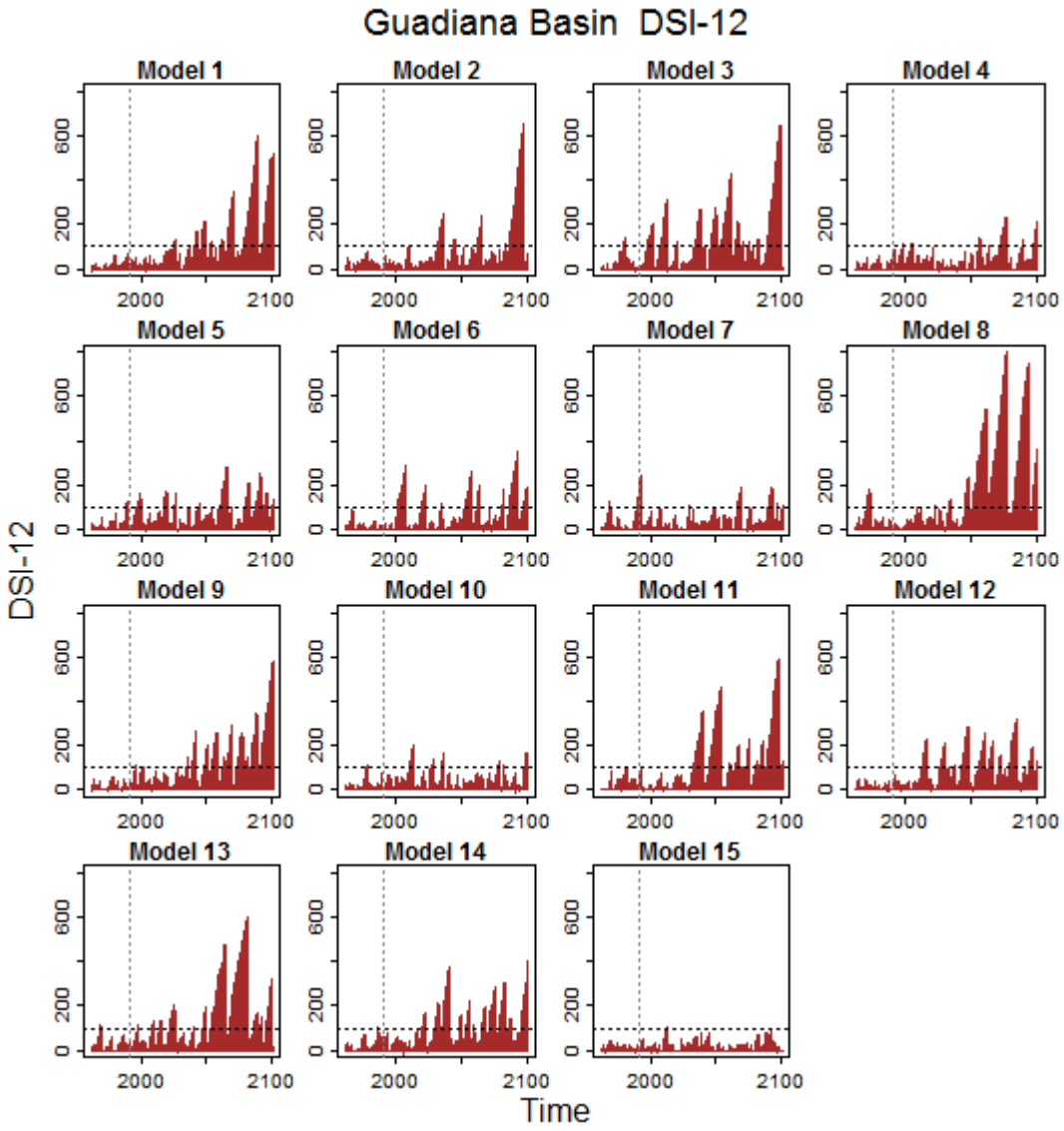

Figure 5.20 – DSI-12 plots for the 1961-2100 period and for the Guadiana basin using monthly rainfall from the gridded observation dataset from the 15 downscaled and bias corrected climate models. The vertical dotted line separates the DSI-12 reference period (1961-1990) from the rest of the record, while the horizontal line defines extreme droughts.

Similar patterns are observed in the SPI-12 projections where models show drier futures for the three basins (Figure 5.21, Figure 5.22 and Figure 5.23). For the Douro and the Tagus, models 1, 2, 3, 6, 8, 9, 11, 12 and 13 project a move towards drier conditions that result in decades of almost continuous extreme drought conditions. For the Guadiana the same also happens with model 14, while model 15 shows cycles of extreme drought and extremely wet periods.

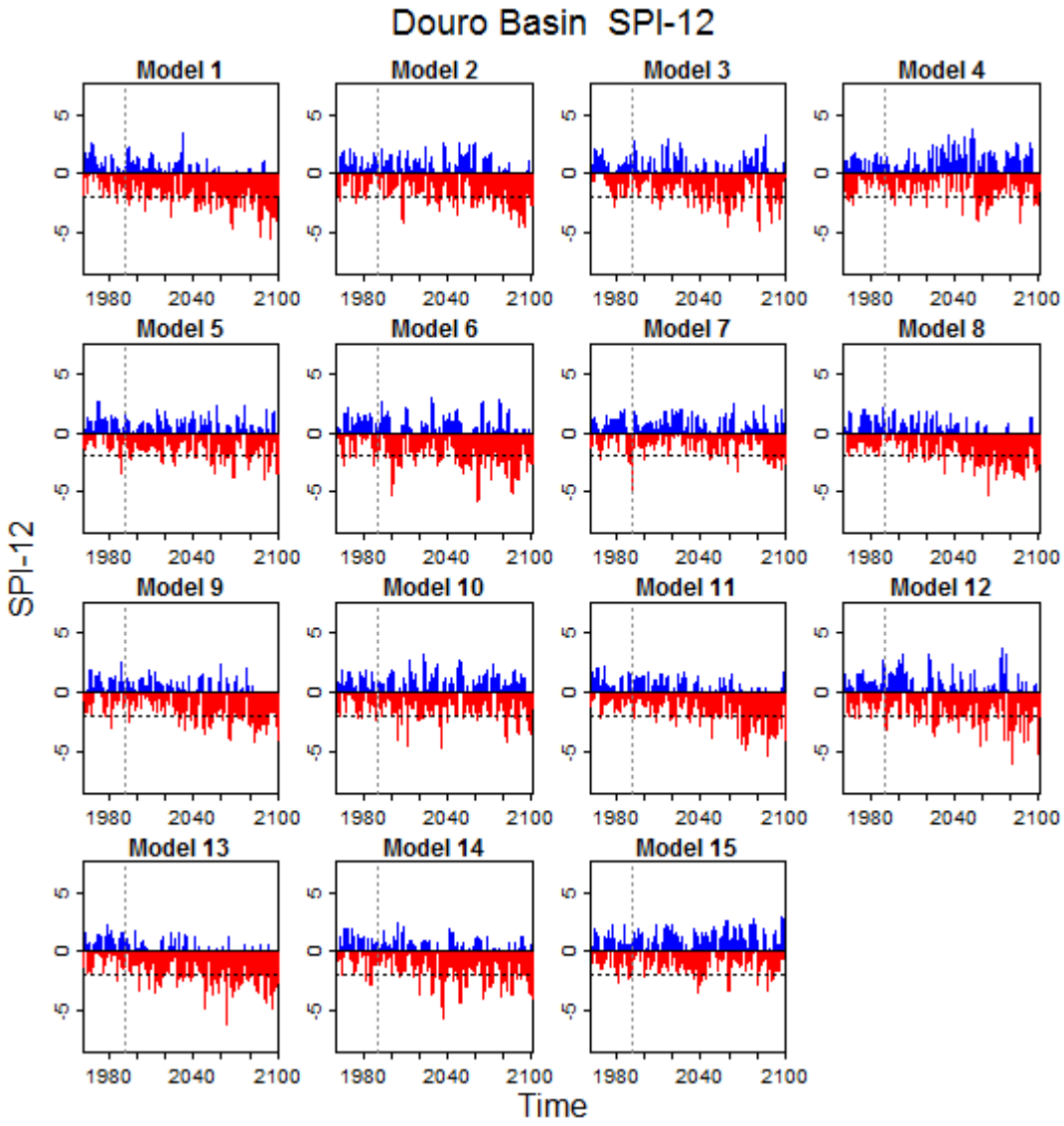

Figure 5.21 – SPI-12 plots for the 1961-2100 period and for the Douro basin using monthly rainfall from the gridded observation dataset from the 15 downscaled and bias corrected climate models. The vertical dotted line separates the SPI -12 reference period (1961-1990) from the rest of the record, while the horizontal line defines extreme droughts.

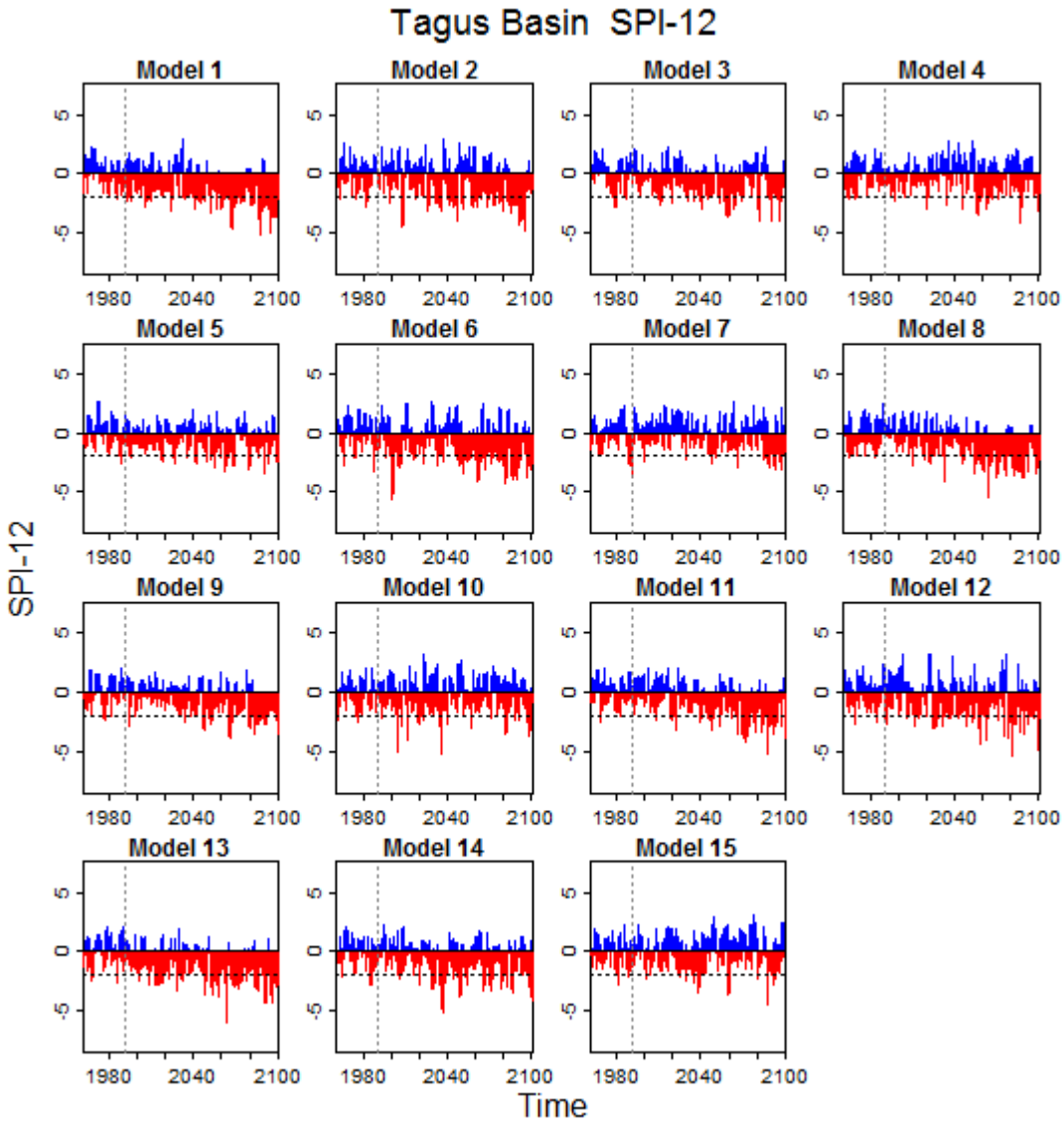

Figure 5.22 – SPI-12 plots for the 1961-2100 period and for the Tagus basin using monthly rainfall from the gridded observation dataset from the 15 downscaled and bias corrected climate models. The vertical dotted line separates the SPI -12 reference period (1961-1990) from the rest of the record, while the horizontal line defines extreme droughts.

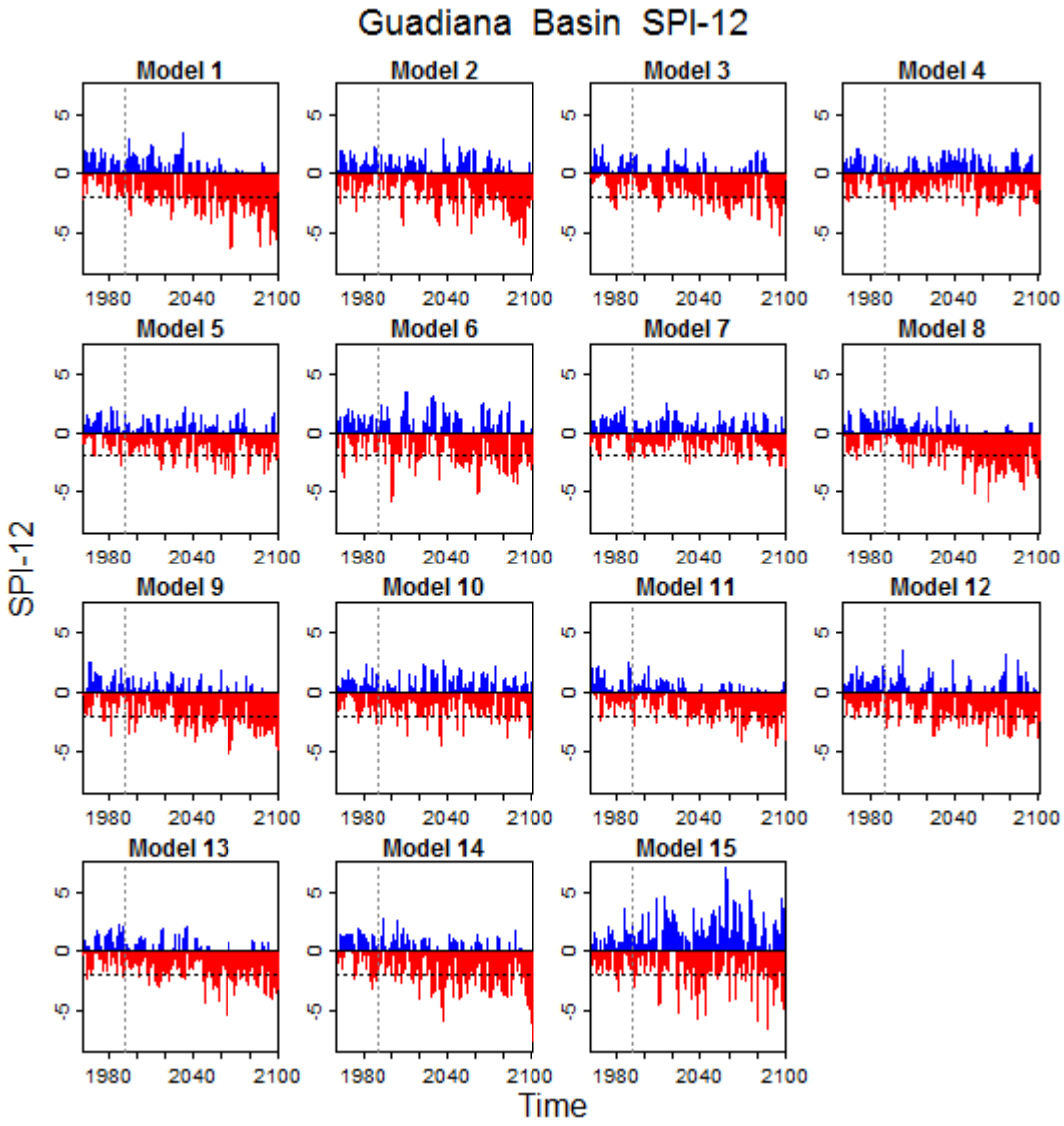

Figure 5.23 – SPI-12 plots for the 1961-2100 period and for the Guadiana basin using monthly rainfall from the gridded observation dataset from the 15 downscaled and bias corrected climate models. The vertical dotted line separates the SPI-12 reference period (1961-1990) from the rest of the record, while the horizontal line defines extreme droughts.

Plots of 30-year rolling means of the percentage of basin in severe and in extreme drought, using DSI-12, were produced for the three basins (see Figure 5.24, Figure 5.25 and Figure 5.26). Again, all models project increases but the range of projections is wide. Models 4, 7, 10 and 15 show a small increase in the mean area of the basin that will be in drought. By the end of the century, models 1, 2, 8, 9, 11, 13 and 14 project that, on average, more than half the basin will be experiencing severe or extreme drought. Model 8 projects the worse scenario where around 80% of each basin would experience extreme drought conditions.

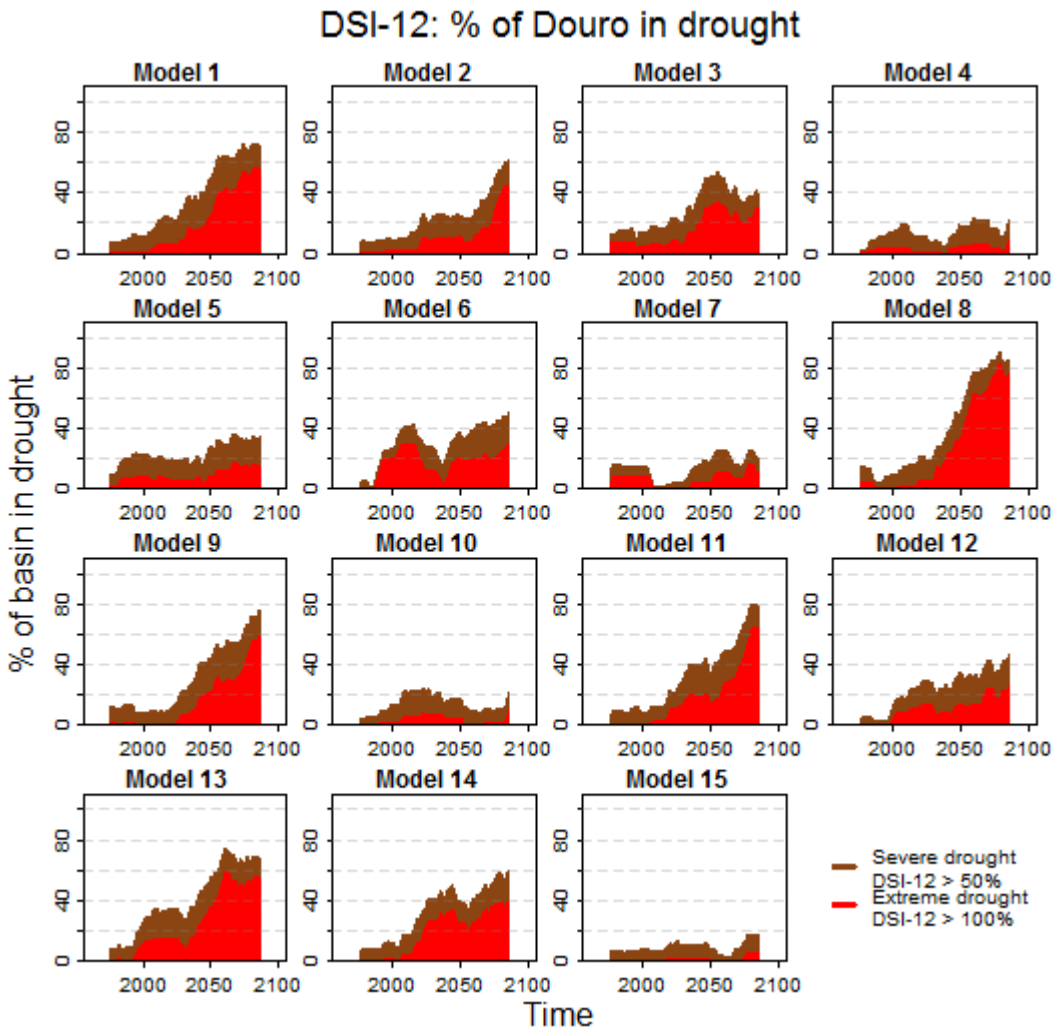

Figure 5.24 – 30-year rolling means of percentage of basin in severe (brown) and extreme (red) drought, using DSI-12, for the time period 1961-2100 for the Douro basin.

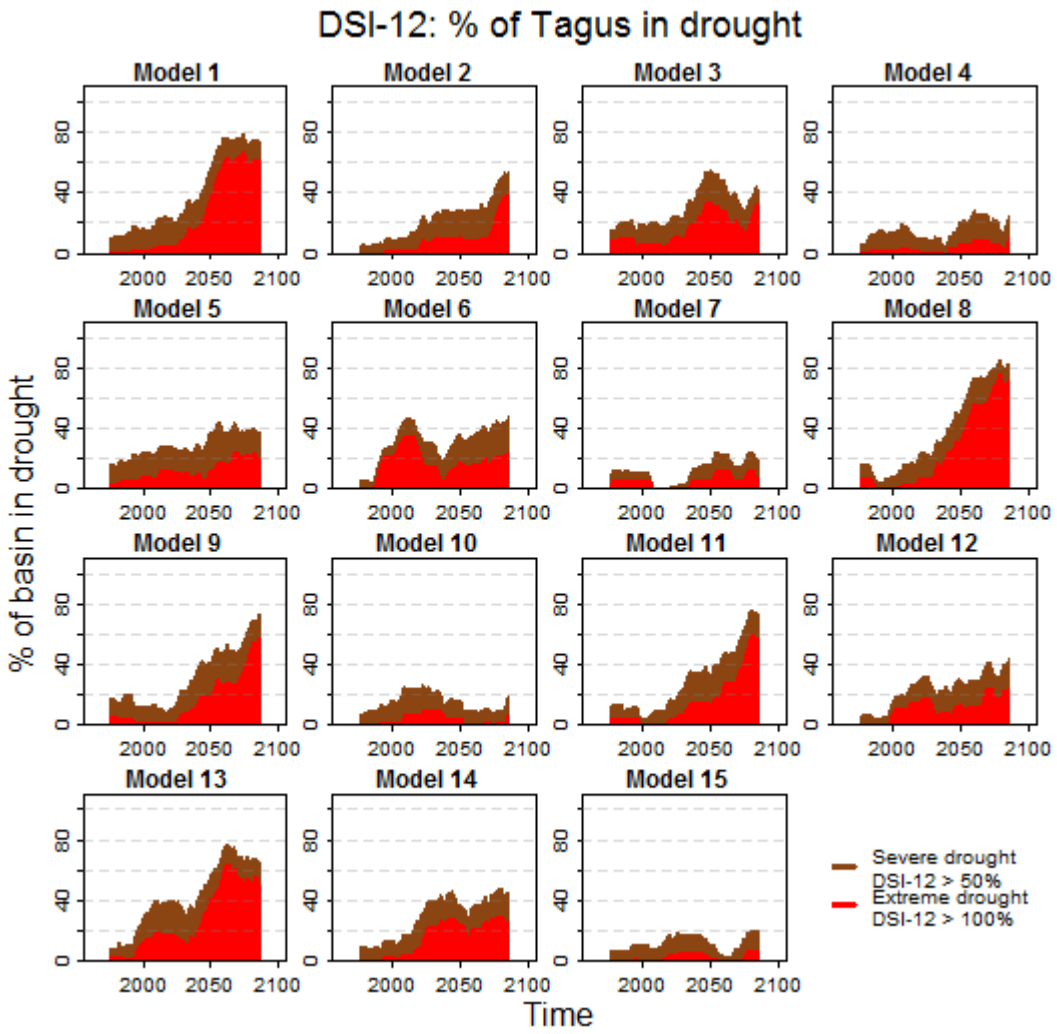

Figure 5.25 – 30-year rolling means of percentage of basin in severe (brown) and extreme (red) drought, using DSI-12, for the time period 1961-2100 for the Tagus basin.

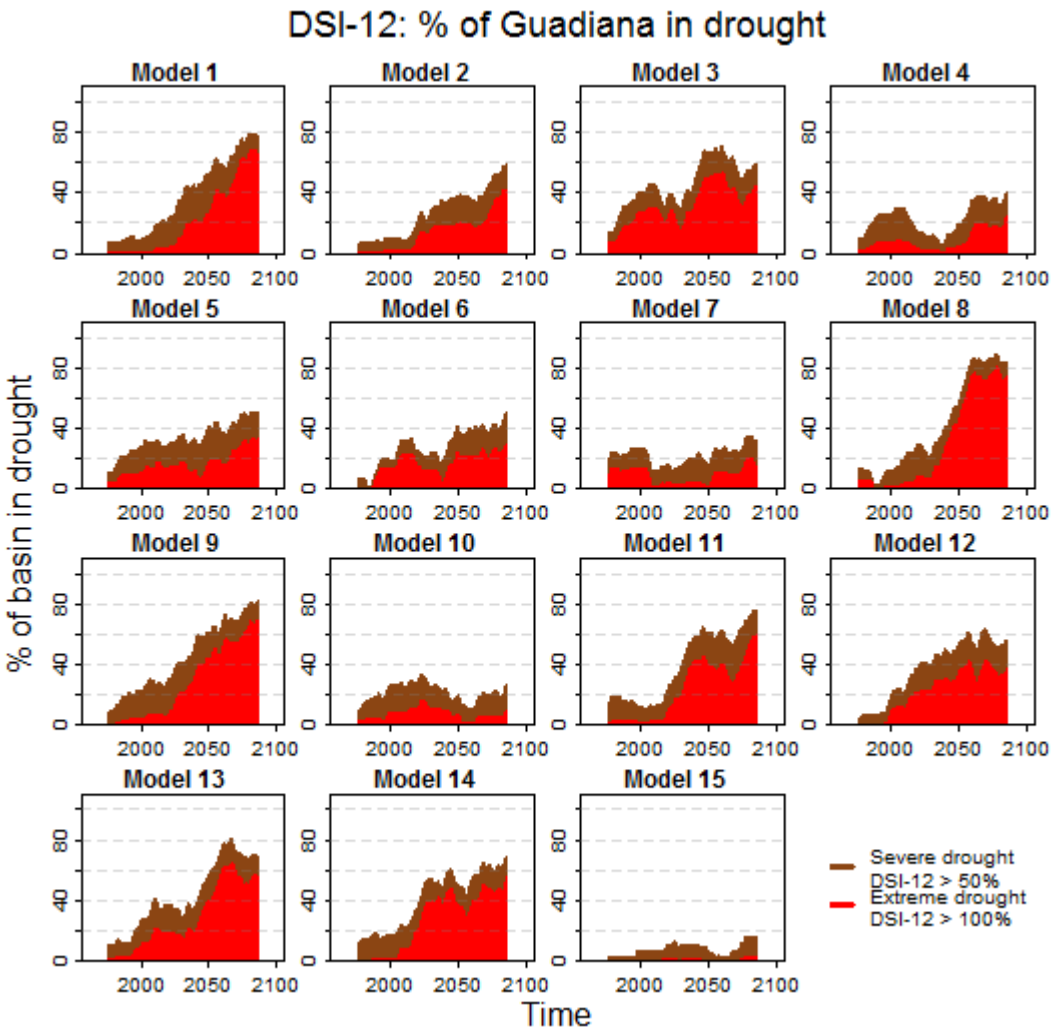

Figure 5.26 – 30-year rolling means of percentage of basin in severe (brown) and extreme (red) drought, using DSI-12, for the time period 1961-2100 for the Guadiana basin.

The percentages of basin in severe and extreme drought defined using SPI-12 do not increase as much as the ones defined by DSI-12 (see Figure 5.27, Figure 5.28 and Figure 5.29). However, similar patterns are seen with models 4, 7, 10 and 15 showing little or no change and models 1, 8 and 9 showing larger changes (around 40% of the Douro and the Tagus and 50% of the Guadiana in drought at the end of the century). The differences between the northern basins and the Guadiana are more evident when using SPI-12 than when using DSI-12.

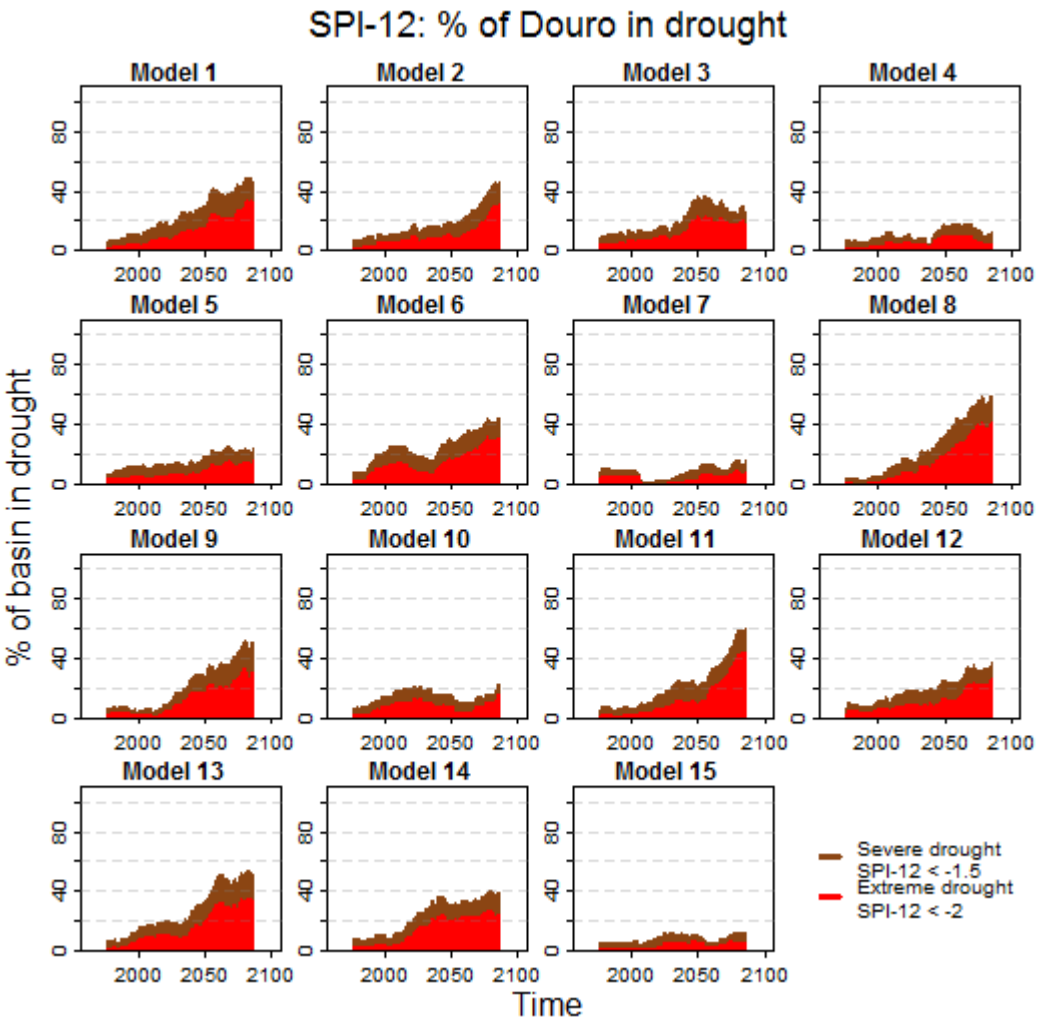

Figure 5.27 – 30-year rolling means of percentage of basin in severe (brown) and extreme (red) drought, using SPI-12, for the time period 1961-2100 for the Douro basin.

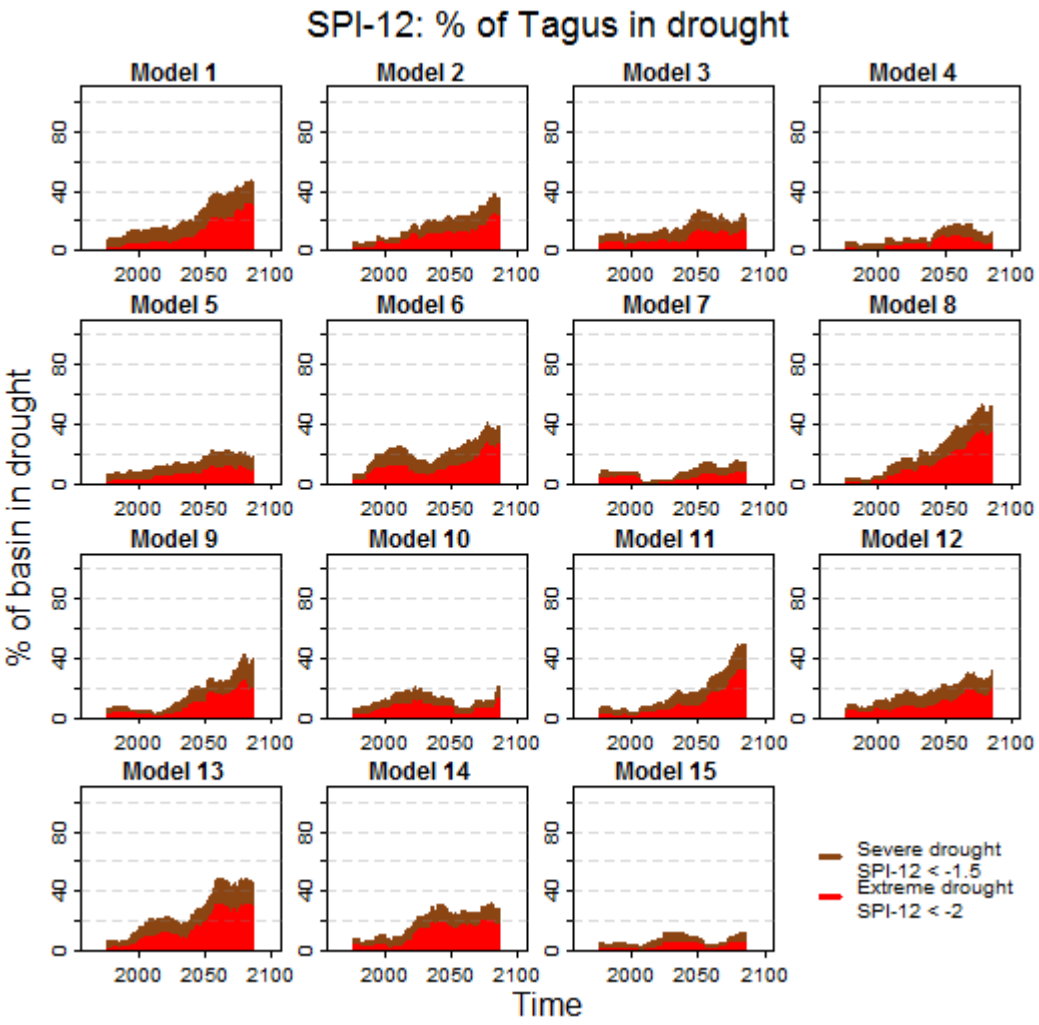

Figure 5.28 – 30-year rolling means of percentage of basin in severe (brown) and extreme (red) drought, using SPI-12, for the time period 1961-2100 for the Tagus basin.

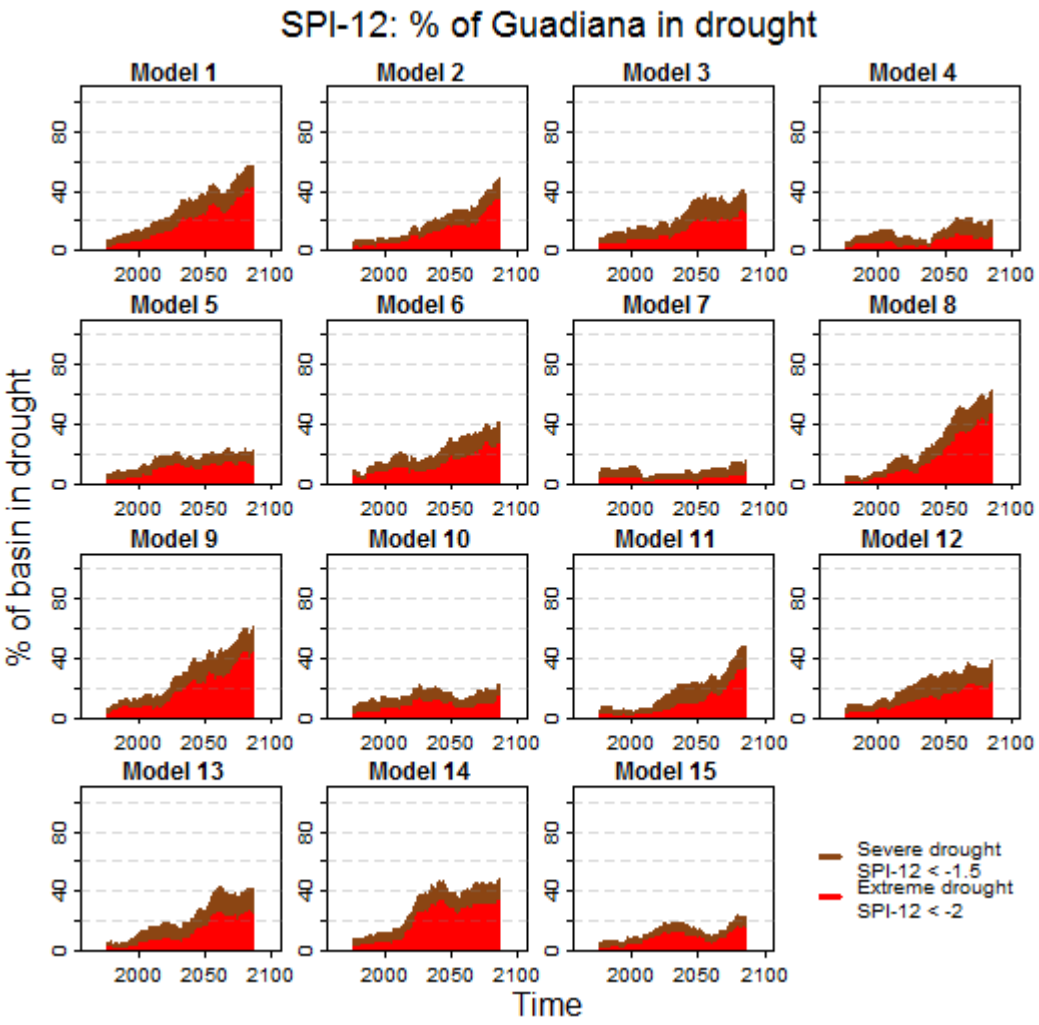

Figure 5.29 – 30-years rolling means of percentage of basin in severe (brown) and extreme (red) drought, using SPI-12, for the time period 1961-2100 for the Guadiana basin.

5.5 Discussion and conclusion

Despite the popularity of SPI as a drought index, it was shown that it is not an appropriate index to use with rainfall from the Douro, Tagus and Guadiana basins. The Pearson III distribution does not fit the 12 month aggregated rainfall well enough for several locations inside these basins, producing SPI-12 values of minus infinity even during the historical period. Therefore, the Gamma distribution had to be used in this study despite being a worse fit for most grid points inside the three basins.

Furthermore, even for the areas without minus infinity values, the differences in drought severity between $SPI\text{-}12_{Gamma}$ and $SPI\text{-}12_{Pearson\ III}$ can reach up to 70%. This is contrary to Guttman (1999) who found very little difference in the characteristics of SPI using different probability distributions for the US. However, it is similar to the differences of up to 54% in SPI-12 severity found by Soľáková et al. (2013) for Rome and differences between 20% and 50% found by Sienz *et al.* (2012) for different areas of the globe.

Even when aggregating the rainfall to the basin level, the inadequacy of the Gamma distribution is obvious in SPI-12 values that reach up to -3.8 in the reference period (1961-1990), which has an associated probability of occurrence of just 7.2×10^{-5}. The bad fit of the Gamma distribution results in the probability of low rainfall being too low, which in turn leads to very low SPI-12 values indicative of extremely intense droughts.

A comparison between DSI-12 time-series using the gridded observation dataset IB02 and the 15 downscaled and bias corrected climate models for the 1961-2003 period (all available data) was performed. Models 3, 5, 6, 7, and 8 showed droughts that were too long/too severe in all basins. Also, most models overestimated the length/severity of droughts in the Guadiana basin, with only models 1, 2, 12 and 15 showing a similar range to the observed. This overestimation of historical drought affects the confidence in these models' projections for future drought.

Table 5.4 shows the most extreme droughts projected by each model for each basin (maximum values of DSI-12) and the maximum 30 year rolling mean of percentage of basin in extreme drought (DSI-12 > 100%) per basin and per climate model. All for the period 1961-2100 and for the period 1961-2003.

Table 5.4 – Summary of DSI-12 results: maximum values of DSI-12 for the historical period (1961-2003) and for the period 1961-2100 (all), and maximum percentage of basin in extreme drought (DSI-12 > 100%) for the same periods.

Models	Maximum DSI-12						Maximum 30 yrs rolling mean of percentage of basin in extreme drought (DSI-12 > 100%)					
	Douro		Tagus		Guadiana		Douro		Tagus		Guadiana	
	hist	all	hist	all	hist	all	hist	all	hist	all	hist	all
1	60	437	79	728	72	602	0	56	1	67	0	68
2	61	522	52	534	74	657	1	45	0	39	0	42
3	166	233	229	488	208	649	7	33	10	34	17	54
4	97	166	99	198	114	232	3	8	2	11	6	25
5	140	173	129	203	162	282	8	17	5	25	10	33
6	186	313	219	363	177	347	8	30	10	35	7	30
7	206	206	178	186	242	242	8	16	6	13	14	21
8	124	772	178	703	181	805	5	83	8	76	6	81
9	90	783	139	790	110	582	1	59	5	58	3	69
10	74	189	98	177	107	197	0	10	1	10	4	16
11	81	499	122	417	102	591	1	65	4	60	2	60
12	67	254	68	258	68	318	0	25	1	25	1	43
13	82	430	116	500	110	603	1	59	3	64	3	64
14	99	268	108	325	107	405	0	40	1	29	1	55
15	76	108	79	185	50	101	0	5	0	7	0	3

The 15 models display a big range of future drought projections when using both DSI-12 and SPI-12 . Some show little change in drought conditions (or a possibly cyclic behaviour) while others project decades of extreme drought conditions reaching up to 800% accumulated precipitation deficit. However, all models are projecting an increase in drought conditions for the future with most models showing a substantial worsening of drought conditions.

The most extreme drought projections were from model 8, which showed droughts that were too severe in the historical period for all basins, and model 9 which showed droughts that were too severe in the historical period for the Tagus and the Guadiana. However, extreme future drought conditions are also projected by other models, including models 1 and 2 which were found to perform well in all basins during the historical period. These two models project extreme drought conditions reaching around 500% accumulated precipitation deficits using DSI-12 and decade long conditions with a SPI-12 at around -5.

In terms of the 30 year rolling means of percentage of basin in severe and extreme drought, using DSI-12, all models show increases. Models 4, 7, 10 and 15 showed small increases while all other models showed substantial increases in drought area.. By the end of the century, models 1, 2, 8, 9, 11, 13 and 14 project that, on average, more than half of the basins area will

be experiencing severe or extreme drought. Again, the percentages of basin in drought for the Guadiana are slightly higher than in the more northern basins.

Using SPI-12, the changes in the percentage of basin in severe and extreme drought show the same patterns but with smaller increases and bigger differences between the more northern basins and the Guadiana.

The 15 climate models used were chosen to sample the range of uncertainty for rainfall and temperature future projections for the Douro, Tagus and Guadiana basins for the four seasons. This drought indices analysis has shown a wide range of possible future drought conditions, with some models projecting future conditions that would be extremely hard, if at all possible, to adapt to.

As reviewed in Chapter 2, and referred to in section 4.5, the rainfall in Iberia and its inter-annual variability is driven largely by large scale circulation patterns like the NAO. Zappa et al. (2013) found that CMIP5 models' ability to simulate the North Atlantic stormtrack is very diverse, which makes their ability to project changes in circulation patterns questionable. However, an overall drying of regime is a component of most of the climate model projections and this may most obviously be associated with circulation pattern features such as the extension of the Azores High, a northward migration of the storm track or the weakening of the NAO. Whilst these changes may superficially explain (some of) the drying/change in rainfall regime, they are themselves only simple measures of the global/Atlantic circulation and not fundamental physical mechanisms. Nevertheless such attribution is beyond the scope of the present work.

Chapter 6. Hydrological Model Set Up

This chapter describes the setting up of SHETRAN, the hydrological model used in this study, for the basins of the Douro, Tagus and Guadiana, as well as their sub-basins. Four sub-basins with natural discharge regimes were used for the calibration and validation of the SHETRAN hydrological model since the three main rivers are highly impacted by human activities and only naturalized discharges are being simulated.

The chapter starts with a short introduction to hydrological models and a description of SHETRAN. It then describes all of the data used to run SHETRAN for the different basins and the methodology used.

The results of the calibration and validation procedure for the sub-basins are shown, followed by a sensitivity to parameterization analysis for the three larger river basins.

Chapter 7 then builds on from the work presented in this chapter with an analysis of the results of the historical and future SHETRAN runs for the basins of the Douro, Tagus and Guadiana.

6.1 Introduction

Hydrological models are simplified mathematical representations of the hydrological cycle and can be sub-divided in numerous ways. A common way is, on the one hand, lumped conceptual models and, on the other, physically-based distributed models. Conceptual models vary in complexity but tend to consider the basin as a single entity. Also, at least some of the parameters do not have a physical interpretation and therefore have to be derived through calibration (Pechlivanidis *et al.*, 2011). Physically based models use physical equations to represent the underlying hydrological processes (evapotranspiration, infiltration, overflow…). Model parameters are normally estimated using soil type and land cover spatial datasets and subsequent adjusted to improve discharge simulations. This final adjustment is necessary due to the inability to account for the heterogeneity in the basin, scaling effects, and the existence of input and output errors (Reed *et al.*, 2004). There can also be issues with the extrapolation of laboratory/small scale field experiments physics to catchment scale and with the simplification of processes (Pechlivanidis *et al.*, 2011).

In both model types problems of equifinality, where different parameter sets can produce equally good results, may arise (Pechlivanidis *et al.*, 2011). One of the conclusions of the distributed model intercomparison project – DMIP – was that model formulation, parameterization, and the skill of the modeller might be more important for simulation accuracy than the choice of a lumped or distributed model (Reed *et al.*, 2004)

There are four main sources of uncertainty in hydrological modelling (Renard *et al.*, 2010):

- Input uncertainty (e.g. sampling and measurement errors in rainfall data);
- Output uncertainty (e.g. rating curve errors and extrapolations affecting discharge data);
- Structural uncertainty (or model uncertainty) arising from lumping and/or simplifying the hydrological processes;
- Parametric uncertainty.

Ideally a quantitative measure of uncertainty, that includes these four sources, should accompany any result of simulations aimed for decision making. However, rigorous methods to do so still need to be developed and sampling-based methods such as Monte Carlo, GLUE and MARKOV CHAIN MONTE CARLO can be prohibitively computationally expensive (Pechlivanidis *et al.*, 2011).

Also, when hydrological modelling is used for assessing the impacts of climate change, the uncertainty associated with hydrological models is generally considered less important than

the uncertainties resulting from selecting emission scenarios, global circulation models and downscaling their output to a scale that can be used for hydrology (Wilby and Harris, 2006; Prudhomme and Davies, 2009; Kay et al., 2009; Arnell, 2011; Teng et al., 2011 *in (Coron et al., 2012).*

On the other hand, transferring the calibration of parameters under historical climatic conditions to futures with different climatic characteristics raises questions of validity. Especially so when using conceptual/lumped models where the values of parameters are just derived through calibration and there is no physical meaning and/or constraints to these values. Coron *et al.* (2012) applied three conceptual models to 216 water limited catchments in southeast Australia and assessed their extrapolation capacity in different climate conditions. They found a tendency in most catchments to overestimate mean runoff when the calibration period was wetter (wet to dry parameter transfer) and to underestimate mean runoff when the calibration period was drier (dry to wet parameter transfer). Despite this common tendency, the magnitude of the errors varied greatly between basins.

To minimize the problem of parameter transferability under climate change, a physically based, spatially distributed (PBSD) model will be used. The model is called SHETRAN (Ewen *et al.*, 2000; Birkinshaw *et al.*, 2010) and was developed based on the SHE (*Système Hydrologique Européen*) model. It models water flow, sediment and solute transport in river catchments (Ewen *et al.*, 2000), however, in this study only the water flow component is used.

SHETRAN is a 3D coupled surface/subsurface PBSD finite difference model. The channel and overland flow is modelled using the Saint-Venant equations with diffusion approximation (1D and 2D respectively). Subsurface flow is modelled using the variably saturated flow equation (3D). Evaporation uses either the Penman-Monteith equation or a fraction of potential evaporation rate.

The basin is modelled as a set of columns and the river networks are modelled as networks of stream links. Each column is made up of stacked finite difference cells. This column approach makes the coupling of the surface and subsurface strong and simple. The stream banks have narrow columns lying on each side of the river to capture the fast dynamics of these areas (Ewen *et al.*, 2000).

SHETRAN uses three computation elements: grid elements, channel links and bank elements. There are also three basic flow modules: variably saturated zone (VSS), evapotranspiration/interception (ET) and overland/channel (OC) that are automatically included in every simulation. Snowmelt (SM) is an optional module that will not be used in this

study because it is not relevant for the area. All of these components use the same time-step, which can be different throughout the simulation (smaller time-steps during storm events which is controlled by the rainfall amount in each time-step).

For the simulations of the Douro, Tagus and Guadiana, a 5km spatial resolution and a daily time-step were used (with the time-step being automatically reduced during rainfall events). The spatial resolution was a compromise between the resolution of the available data and the processing time of the model runs.

6.2 Data

6.2.1 *Spatially distributed data*

The following spatially distributed datasets were used as input to SHETRAN:

- DEM - "Hydro1K Europe": a 30 arc-second digital elevation map with rivers and catchment areas from the US Geological Survey (USGS, 2011) shown in Figure 6.1;

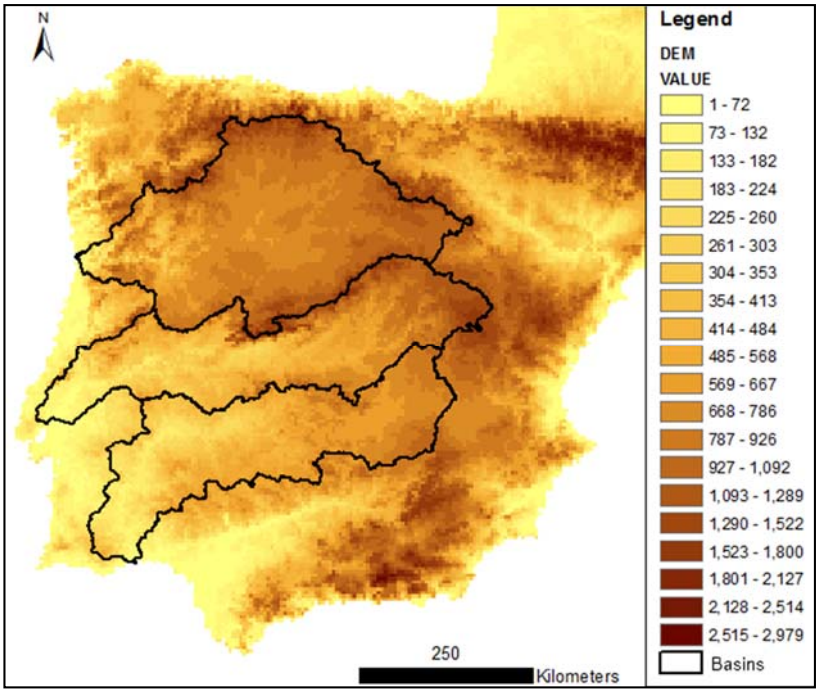

Figure 6.1 - Digital elevation map for Iberia from "Hydro1K Europe" with the three studied basins highlighted.

- Land use (100x100m) - provided by Dr Wiberg from IIASA (created for project “Refuel” by merging CLC2000, GLC2000 and the old Corine dataset). Initially there were 37 land use classes, these were aggregated (by similarity) to the 9 land use/vegetation classes shown in Figure 6.2, which is a more manageable number for calibration purposes.

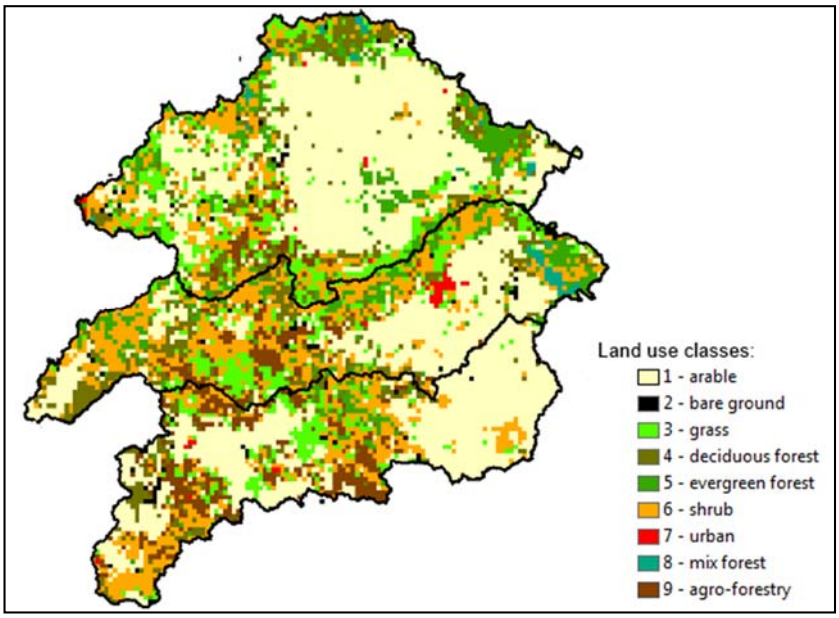

Figure 6.2 – Land use map of the three studied basins.

- Soil data (1000x1000m) – from the Joint Research Centre - European Soil Database v2.0 (JRC, 2013). The appropriate raster layers (dominant topsoil texture, depth to textural change, dominant subsoil texture and depth to rock) were selected and combined by Elizabeth Lewis using a python script. These described the Van Genuchten parameters (θs, θr, Ks, α, n) and the depth of each soil/rock layer that SHETRAN requires for each grid square. In the end 73 classes of soil types were obtained, consisting of different combinations of different soils types in layers at different depths (more information is provided in the methodology section and in Figure 6.5). The soil parameters used in SHETRAN were the ones from the original (JRC) dataset and only the aquifer layers were subjected to calibration (as described in the methodology).

6.2.2 *Meteorological data*

The meteorological datasets used to run SHETRAN were all previously introduced in Chapter 4:

- The observed gridded daily rainfall dataset IB02 with a resolution of 0.2° × 0.2°. It was constructed based on 2000 gauges in Spain and 400 in Portugal and is available for the period 1950 to 2003 (see Figure 6.3).
- Daily gridded rainfall obtained by downscaling 15 GCMs using empirical quantile mapping. Since IB02 was used to downscale and bias correct the GCMs the two datasets have the same resolution. This dataset has been produced for1961 to 2100.

- Daily gridded rainfall obtained by applying delta change factors (calculated from the 15 GCMs) to IB02 (see Chapter 4). These two datasets have therefore the same resolution and this dataset is available from 2045-2070.
- Potential evapotranspiration (PET) data – from the Climatic Research Unit (Jones and Harris, 2008). Monthly time-series spanning 1901-2009 with a resolution of 0.5° x 0.5° calculated using more than 4000 weather stations distributed around the world (see Figure 6.3). For the hydrological modelling, the PET is assumed to be constant throughout the month.
- Monthly gridded PET obtained by applying delta change factors (calculated from the 15 GCMs) to the CRU dataset (see Chapter 4). These two datasets have therefore the same resolution and this dataset is available from 2045-2070.

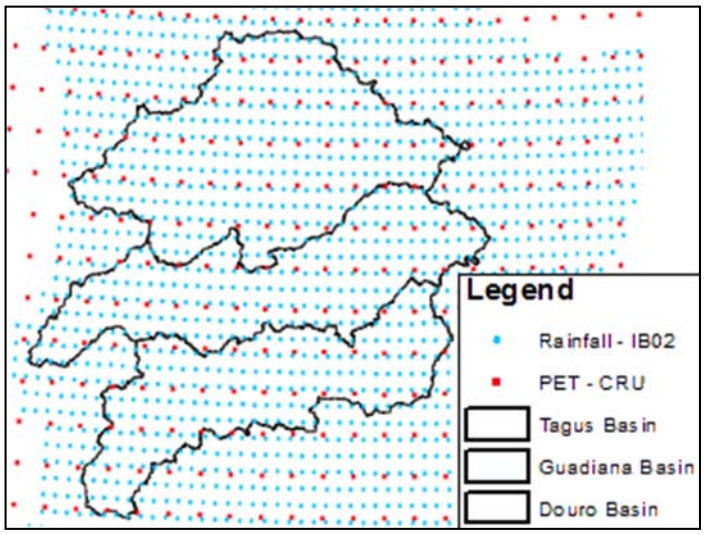

Figure 6.3 – Rainfall and PET grid points map with the three studied basins.

6.2.3 *Discharge data*

The discharge gauge data used in this thesis was compiled from various sources. For Portugal, the data from the water institute (INAG – Instituto da Água) were retrieved from http://snirh.pt/ during the month of February 2012. For Spain, data were provided by "Sistema integrado de información del Agua" which is an integrated information system from the Spanish government. However, these data finished in 2006. Complementary data was retrieved from the Spanish Ministry of development website: http://hercules.cedex.es/general/default.htm during the month of February 2012. This website has data until September 2009. Also, for the Douro basin, annual discharge books until the hydrological year 2009-2010 were retrieved from the following website: http://www.chduero.es/Inicio/ElaguaenlacuencaCantidad/Datosdecaudales/Anuariosdedatosf

oron%C3%B3micosydeembalses/tabid/486/Default.aspx. The location of the gauges used for this study is discussed in the methodology section.

6.3 Methodology

Measured discharges are necessary to calibrate and validate hydrological models. However flows in the Douro, Tagus and Guadiana basins are highly impacted by human activities that will not be taken into account in the model, since it would be impossible, in the time-frame available for this project, to do so. Since naturalized flows are being modelled, measured output discharges in the Douro, Tagus and Guadiana cannot be used for the purposes of calibration/validation.

A thorough search for sub-basins of the three main rivers with long records of discharge measurements and without upstream dams was conducted. Although we cannot exclude the existence of water abstractions or other human activities in these places, an assumption was made that without the presence of a dam the discharges could be considered "natural". Due to the presence of thousands of dams in these three basins, only nine sub-basins with long available discharge records that were not affected by dams were identified (see Figure 6.4).

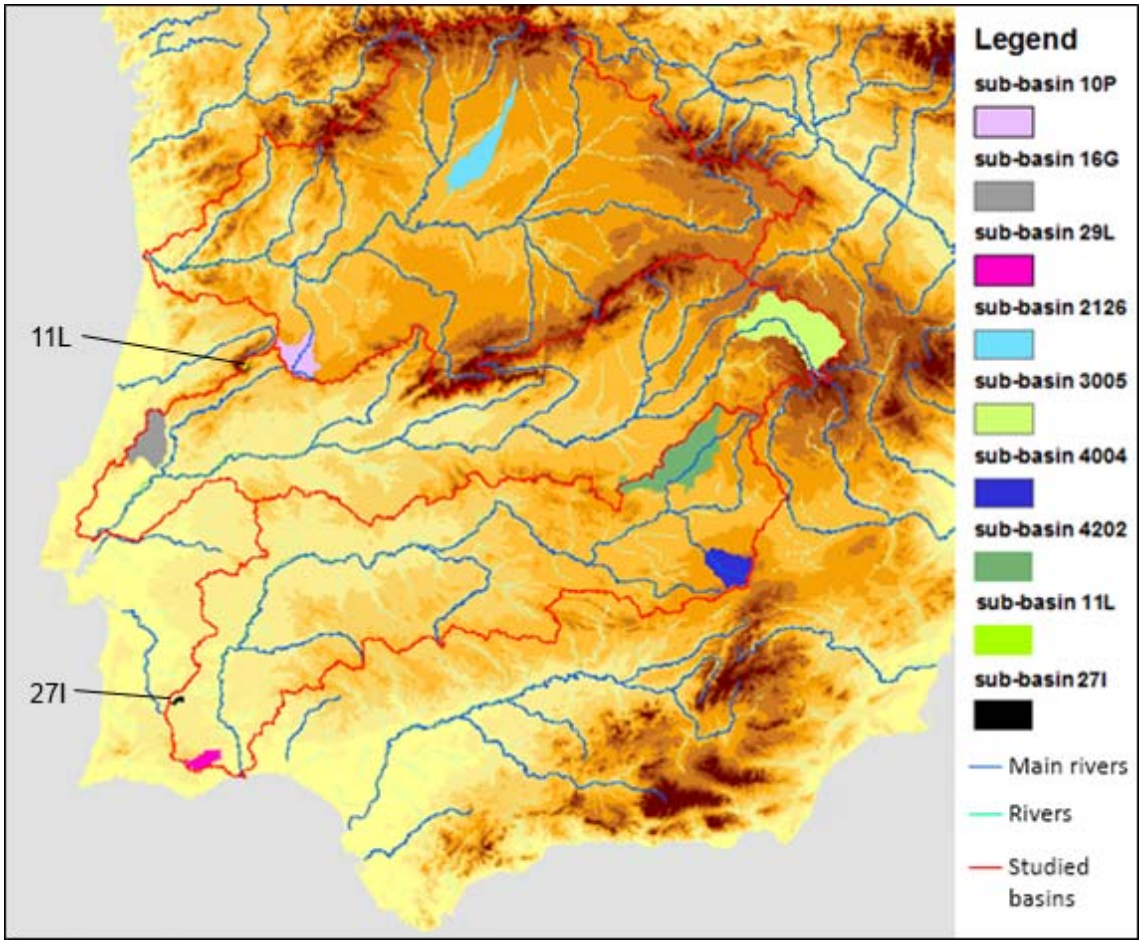

Figure 6.4 – Map of the study area with the nine sub-basins not affected by dams.

From these nine sub-basins, 11L and 27I were not considered because of their small area (43 and 48km^2, respectively). Also, as visible in the map above, the shape of sub-basin 4202 cannot

be properly calculated with the DEM used (1km resolution); therefore this basin could not be used.

Sub-basin 4004 is situated in the “high Guadiana” which is a complex hydrological system whose water drains to the “Mancha Occidental” aquifer and re-emerges downstream in a complex network of lagoons, the most important being the national park of “Tablas de Daimiel” and the single location called “Ojos del Guadiana”(CEDEX). The simulation of these complex interactions between the superficial flows and the underlying aquifer are beyond the scope of this project and therefore this sub-basin could not used.

The five sub-basins that remained are well distributed over the study area and SHETRAN simulations were run for all of them. A split-sample calibration-validation strategy was used, although restricted by the period of available measured discharge for each sub-basin. Since the main objective is to simulate monthly discharges, the widely used Nash–Sutcliffe Efficiency (NSE) was not used, because in basins with high discharge variability the NSE is not very susceptible to volume errors and favours simulations that underestimate variability (Gupta *et al.*, 2009). Instead the following monthly measures of goodness of fit were used in combination with daily and monthly discharge plots and annual water-balance plots:

- bias.total = sum of simulated discharge / sum of observed discharge
- bias.var = variance of simulated discharge / variance of observed discharge
- cor = Spearman's rank correlation coefficient (Spearman's rho)

The calibration of these sub-basins consisted of the adjustment of the following parameters:

- Ratio of actual/potential evapotranspiration for each vegetation/land use classes;
- Storage capacity of canopy for each vegetation/land use classes;
- Permeability and depth of aquifers associated with each soil type;
- Overland flow roughness parameter for the different land cover classes.

The initial values for these parameters were based on expert knowledge and supplied by Dr Stephen Birkinshaw who also helped with setting up the models.

The manual calibration was performed using the same values for these parameters in all the sub-basins so they could be extrapolated for the three main basins. This means the value for the parameters are not optimums for any sub-basin but the best values for all the sub-basins. It is important to note that the spatial resolution used in the simulation (5km) and the rainfall dataset used are appropriate for the simulation of the three big basins but not for the simulation of the small sub-basins. Unfortunately in order to extrapolate the results of the

calibration of the sub-basins to the bigger basins, the same datasets and the same spatial resolution must be used.

Initially no aquifers were introduced in the simulation but the results were very poor due to very small or absent base flow in the rivers. To identify areas with aquifers, maps from the Spanish Mineral and Geological Institute (IGME, 2012) and from the Portuguese Water Institute (INAG, 2012) were consulted (see Figure 6.6) and visually matched with different soil types present in the three basins (see Figure 6.5). Aquifer layers (detrital or karstic) were then added to the soil types identified; Karstic aquifers have higher saturated hydraulic conductivity than detrital aquifers and the parameters used in these aquifer layers are therefore different (and presented in Appendix H) This was a necessary simplification of the complex aquifer systems justified by the size of the study area and the type of outputs of interest: long-term changes of the monthly discharges of the three main rivers in their outlet and at the border.

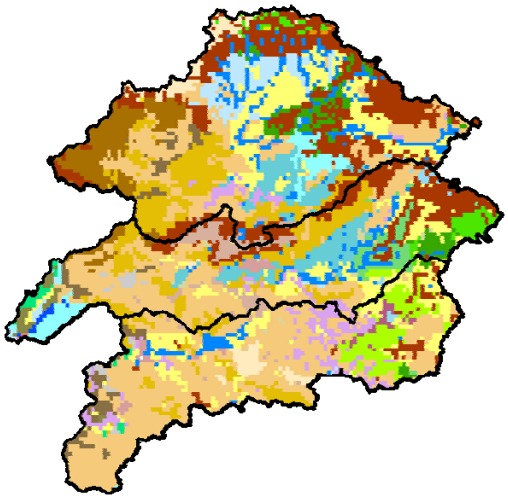

Figure 6.5 – Soil map of the three studied basins (with 73 classes). Soil types that have an added permeable detrital formation type of aquifer are presented in blues and soil types with added karst aquifers are presented in green

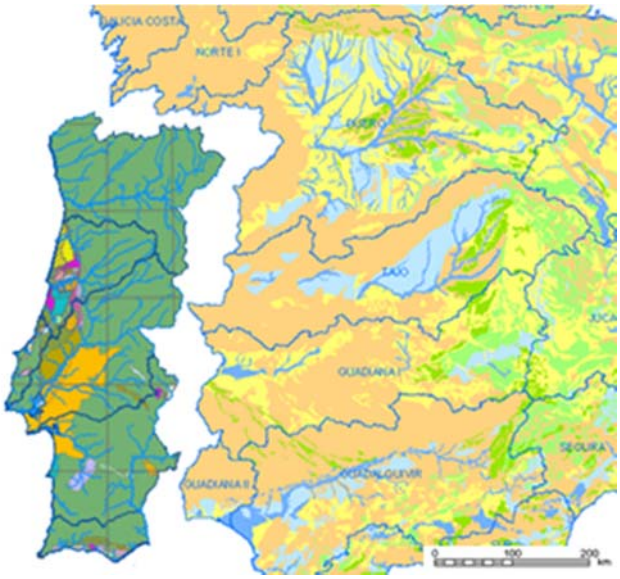

Figure 6.6 – Map of Portugal with areas without significant aquifers in green and single aquifers in different colours (INAG, 2012). Map of Spain with areas without important aquifers in beige and yellow, detrital type of aquifers in blues and karst type of aquifers in greens (IGME, 2012).

After the calibration and validation was performed in the sub-basins, the chosen parameters (see Appendix H) were used to run historical (1961-1990) and future (2041-2070) SHETRAN runs for the Douro, the Tagus and the Guadiana. Historical runs were also performed for the three basins without calibration (all vegetation/land use classes had the same parameters) and with different aquifer parameters to assess the impact of calibration on the simulated discharges.

The locations where discharge was analysed were, as much as possible, the locations used in the Albufeira convention (see Figure 6.7). However, there are no discharge gauges in the Douro near the border after the river enters Portugal. In the Albufeira Convention a mix of information was used for the reconstruction of discharges in this area (INAG, 1998):

- simulated discharges from the Spanish Douro Basin Plan;
- discharged and turbinated discharges at Saucelle dam;
- Águeda river levels at Spanish gauge of Castillejo Martin Viejo;
- discharges arriving at Pocinho dam.

All these locations are displayed as red circles in Figure 6.7 but were not used in this study. The Douro discharge was analysed using the other two points defined in the Convention: gauge 05T/01A (Miranda), thereafter called Douro-border, and gauge 07G/01A (Crestuma) thereafter called Douro-outlet.

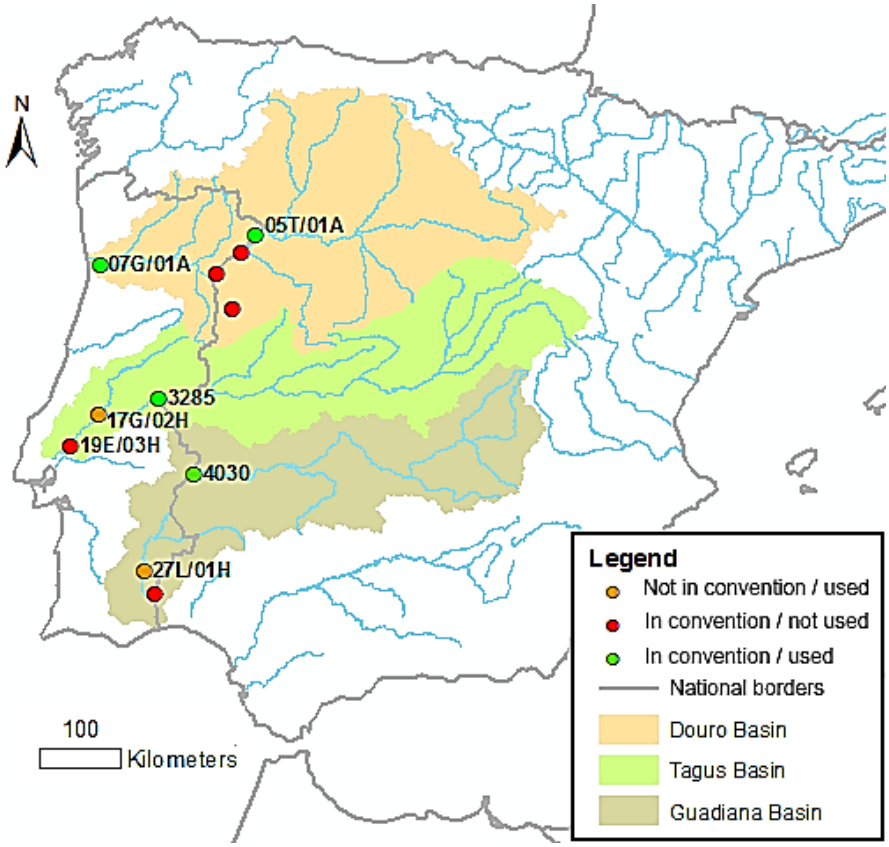

Figure 6.7 – Map of Iberia with the three studied basins, the locations where discharge was analysed and the locations of the Albufeira convention discharge points.

The Tagus outlet gauge used in the Convention (Ponte de Muge – 19E/03H) was a hydrometric gauge that only worked between 1945 and 1983 and that has no rating curve. The closest discharge gauge that could be found with long discharge records was Almourol - 17G/02H

thereafter called Tagus-outlet. The gauge used in the Convention for the Tagus-border (3285 – Cedillo) was also used in this study.

The only gauge that could be found in the Guadiana with the same name (Pomarão) and location as the one used in the Convention as the Guadiana-outlet, was a water quality station that worked from 2002 to 2003. The closest discharge gauge that could be found with long discharge records was Pulo do Lobo – 27L/01H which was used instead. The Convention gauge for the Guadiana-border (4030 – Badajoz) was used in this study.

6.4 Sub-basins: calibration and validation

6.4.1 *Sub-basin 10P*

Sub-basin 10P is situated in an area with mean rainfall of 890mm/yr and there are no aquifers present. It has five vegetation classes (see Figure 6.8); a majority of shrub cover, followed by arable, grass and deciduous forest and 3% of bare ground.

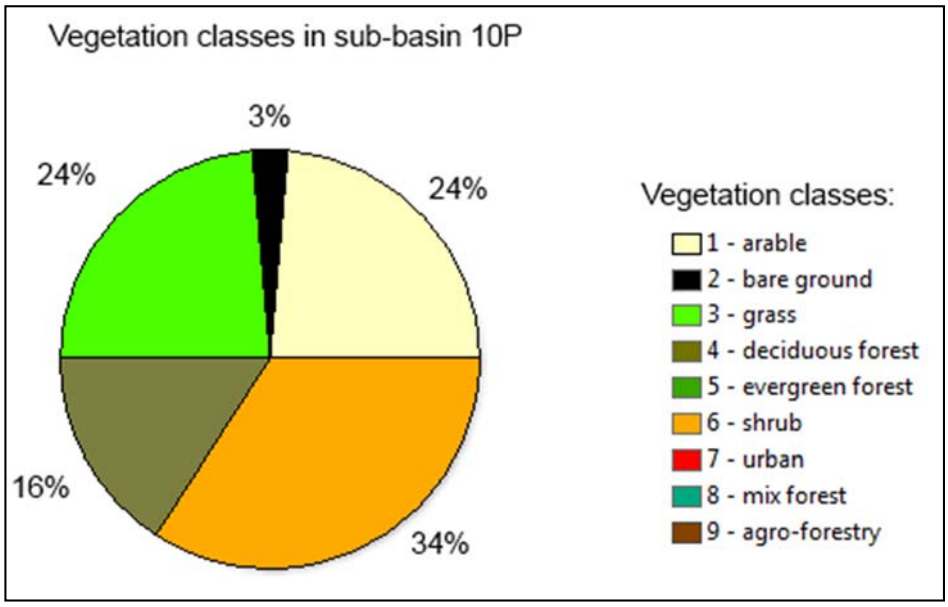

Figure 6.8 – Vegetation classes present in sub-basin 10P

The simulation results for basin 10P are shown in Figure 6.9, the calibration period was 1965 to 1980 and the validation period was 1981 to 1999. Although the monthly discharge is slightly overestimated, the base-flow is very well simulated and the correlation coefficient is high (0.88). The behaviour in the validation period is identical to the calibration period although there is an increase in the variability bias. This bias shows an overestimation of peak discharge in both periods.

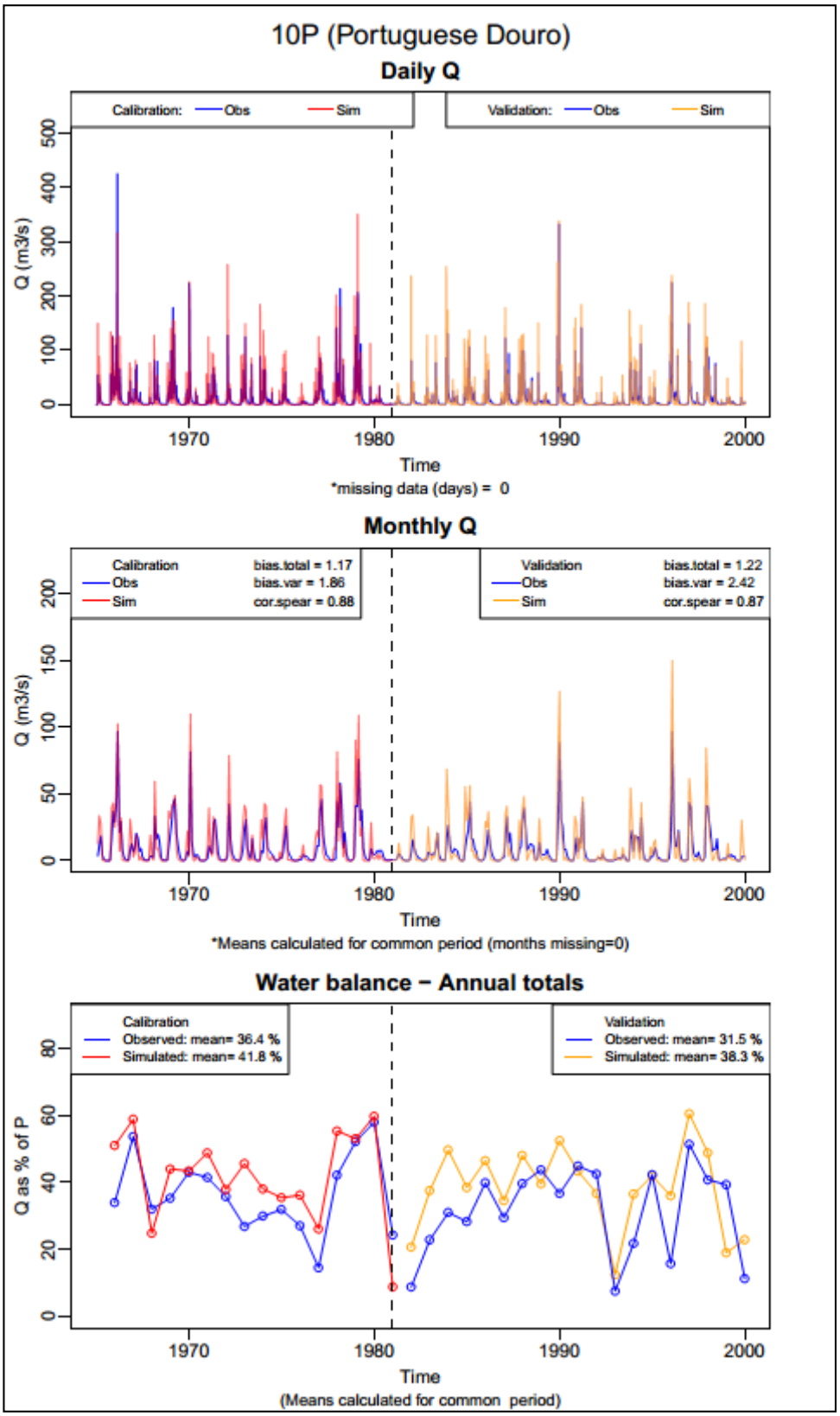

Figure 6.9 – Simulation results for sub-basin 10P, in the Portuguese side of the Douro basin. Observed (blue) and simulated (red for the calibration period and yellow for the validation period) daily discharge (top), monthly discharge (middle) and annual water balance discharge as percentage of rainfall (bottom).

6.4.2 *Sub-basin 2126*

Sub-basin 2126 is situated in an area with mean rainfall of 440mm/yr. Aquifers in this area consist of permeable detrital formations (especially alluvium near rivers). This sub-basin is covered mainly by agricultural land with only 2% of shrubs and 2% of deciduous forest (see Figure 6.10).

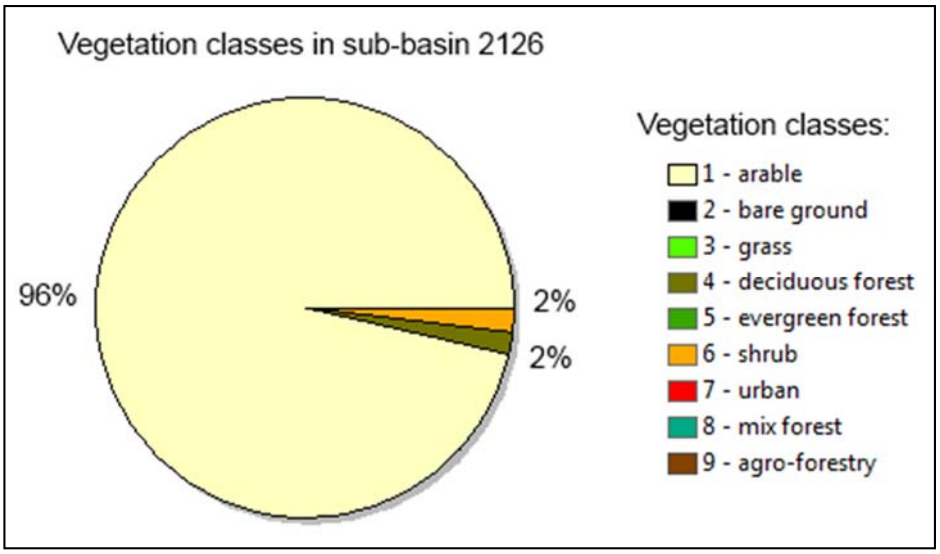

Figure 6.10 – Vegetation classes present in sub-basin 2126

There are two gaps in the observed discharge dataset for gauge 2126. The behaviour of the observed discharge before the first gap follows the behaviour of the rainfall, but after the gap it does not (see Figure 6.11). This change in behaviour cannot be explained by changes in PET, therefore it was considered that after the first gap in the dataset the assumption of a natural system did not hold and only the data before 1987 was used for calibration/validation.

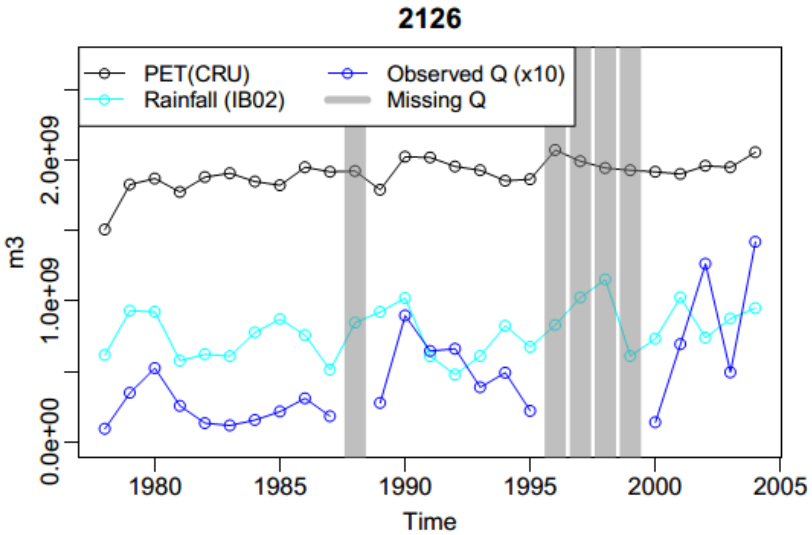

Figure 6.11 – Annual time-series of potential evapotranspiration, rainfall and observed discharged (multiplied by a factor of 10 so that the behaviour of the time-series can be perceptible) for the entire record of sub-basin 2126, with the data gaps in the record of observed discharged highlighted.

The simulation results for basin 2126 are shown in Figure 6.12, the calibration period was 1978 to 1983 and the validation period was 1984 to 1986. This is a very dry basin, where only around 3% of the rainfall is converted into discharge and it is therefore very difficult to simulate. Despite this, the results are satisfactory with the behaviour in the validation and calibration period being identical. In both periods there is a slight underestimation of the discharge and a slight overestimation of the variance that increases in the validation period. The very short validation period (three years) can affect the results and might explain the increase in variability.

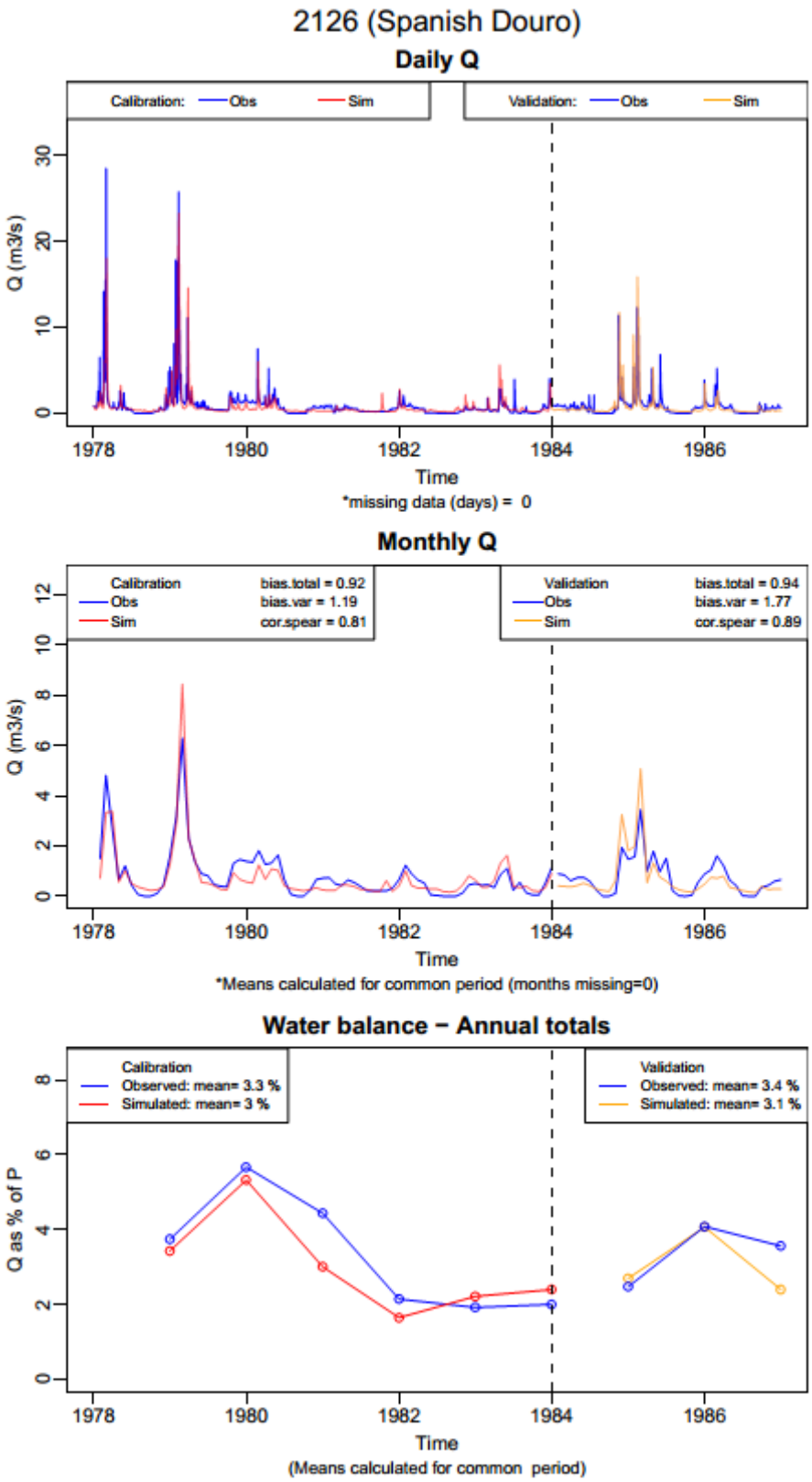

Figure 6.12 – Simulation results for sub-basin 2126, in the Spanish side of the Douro basin. Observed (blue) and simulated (red for the calibration period and yellow for the validation period) daily discharge (top), monthly discharge (middle) and annual water balance – discharge as percentage of rainfall (bottom).

6.4.3 *Sub-basin 16G*

The water balance results for basin 16G are presented in Figure 6.13. It is clear that the simulation is capturing the behaviour of the river but is producing too much discharge.

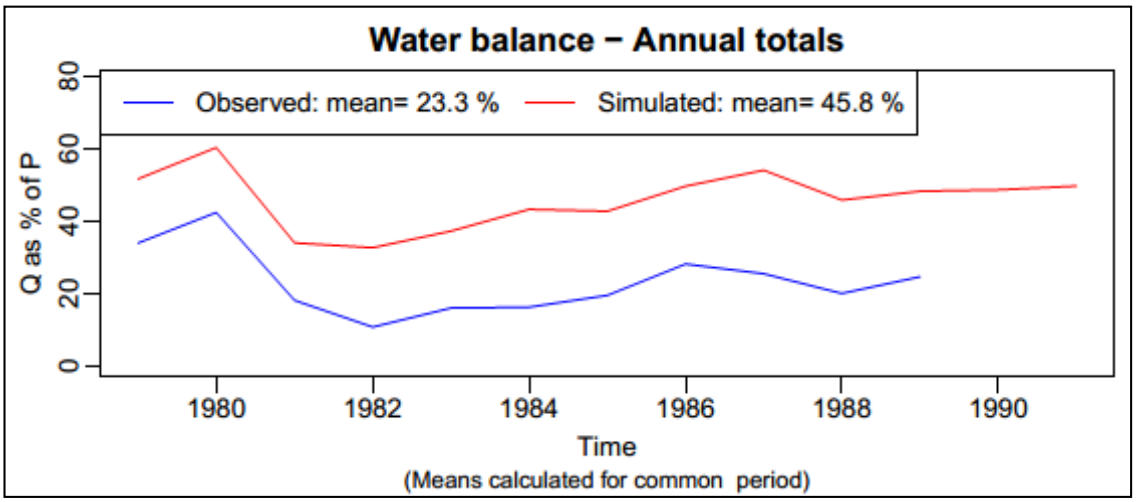

Figure 6.13 – Simulation results of sub-basin 16G – annual water balance (discharge as percentage of rainfall).

The west part of sub-basin 16G and the adjacent catchment to the west (Alviela catchment) are in a karstic area (Almeida *et al.*, 2000). The Alviela is one of the rivers that supplies water to Lisbon and the water abstraction is just downstream of its spring (see Figure 6.14).

Figure 6.14 – Alviela spring (photo from http://www.panoramio.com/photo/20838067)

A probable explanation for the differences between the observed and simulated discharges is that part of the rain falling on 16G sub-basin drains to the Alviela through the karst aquifers. Therefore this sub-basin was not used for the calibration/validation of the SHETRAN model.

6.4.4 *Sub-basin 3005*

Sub-basin 3005 is situated in an area with mean rainfall of 507 mm/yr. Roughly a third of this sub-basin is situated in a karstic area and there is also a small permeable detrital aquifer. This sub-basin has a very diverse land cover with 60% of it being forest (see Figure 6.15).

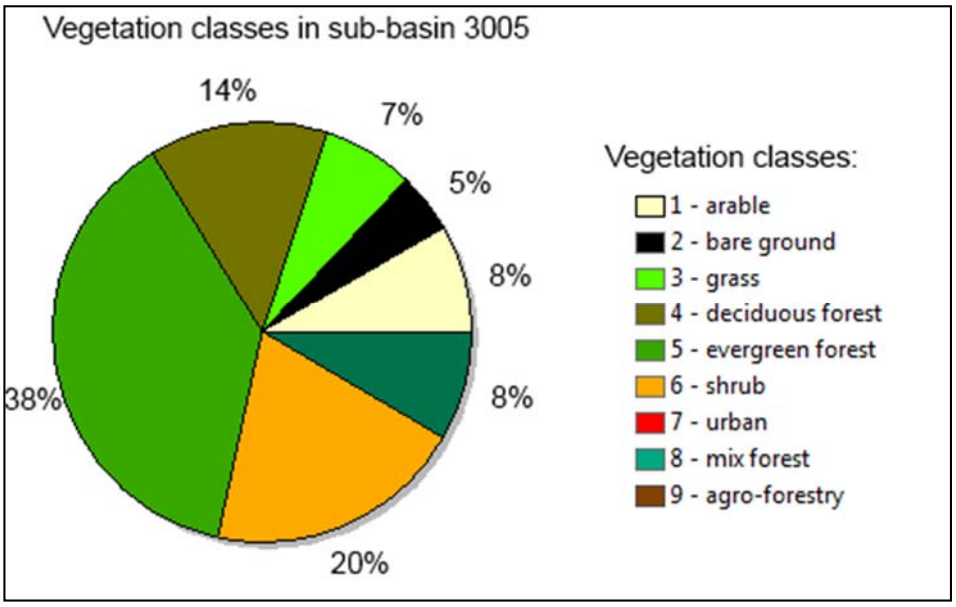

Figure 6.15 – Vegetation classes present in sub-basin 3005

Because a significant portion of sub-basin 3005 has karst aquifers, the behaviour of the river was not accurately simulated. However, as visible in Figure 6.16, the discharge amounts are very well simulated with bias of 0.99 in the calibration period and 0.94 in the validation period. The calibration period for this sub-basin was 1965 to 1981 and the validation period was 1982 to 2003.

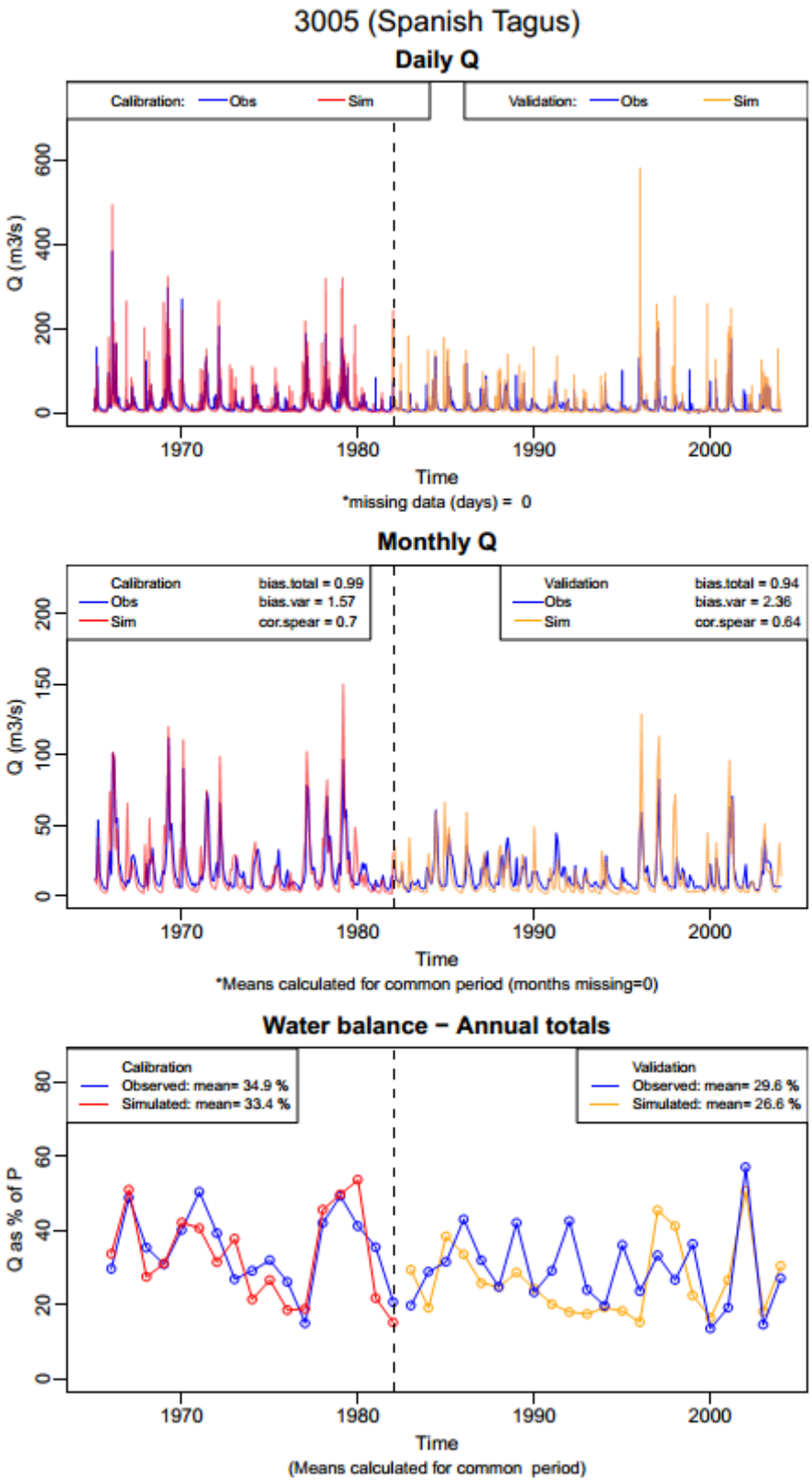

Figure 6.16 – Simulation results for sub-basin 3005, in the Spanish side of the Tagus basin. Observed (blue) and simulated (red for the calibration period and yellow for the validation period) daily discharge (top), monthly discharge (middle) and annual water balance – discharge as percentage of rainfall (bottom).

6.4.5 *Sub-basin 29L*

Sub-basin 29L is situated in an area with mean rainfall of 686mm/yr and there are no aquifers present. This sub-basin has mainly a shrub cover (73%) with small areas of deciduous forest, grass and arable land (see Figure 6.15).

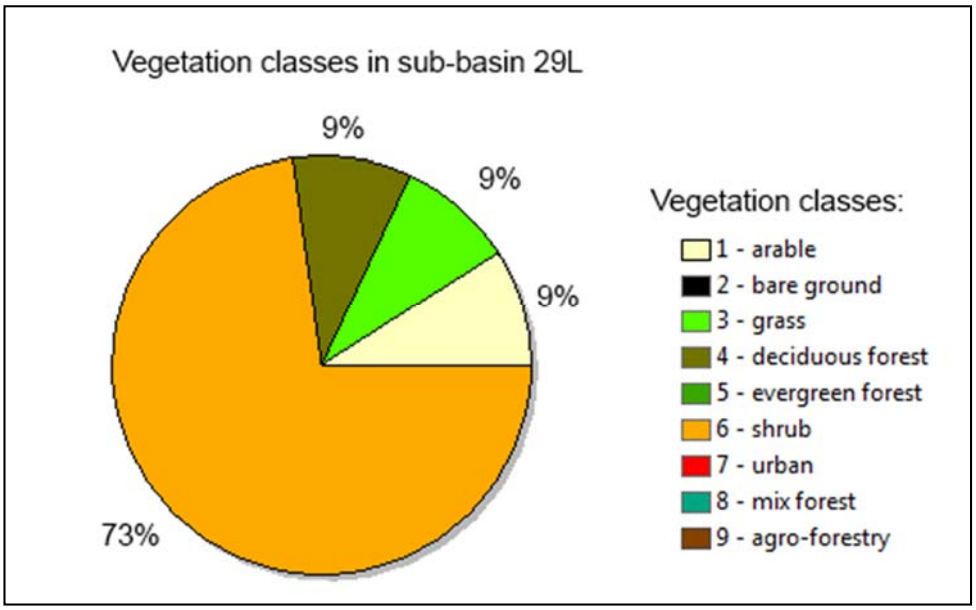

Figure 6.17 – Vegetation classes present in sub-basin 29L

The calibration period was 1961 to 1980 and the validation period was 1981 to 2000. It can be seen in Figure 6.18 that the simulated discharge for sub-basin 29L is considerably below the observed discharge.

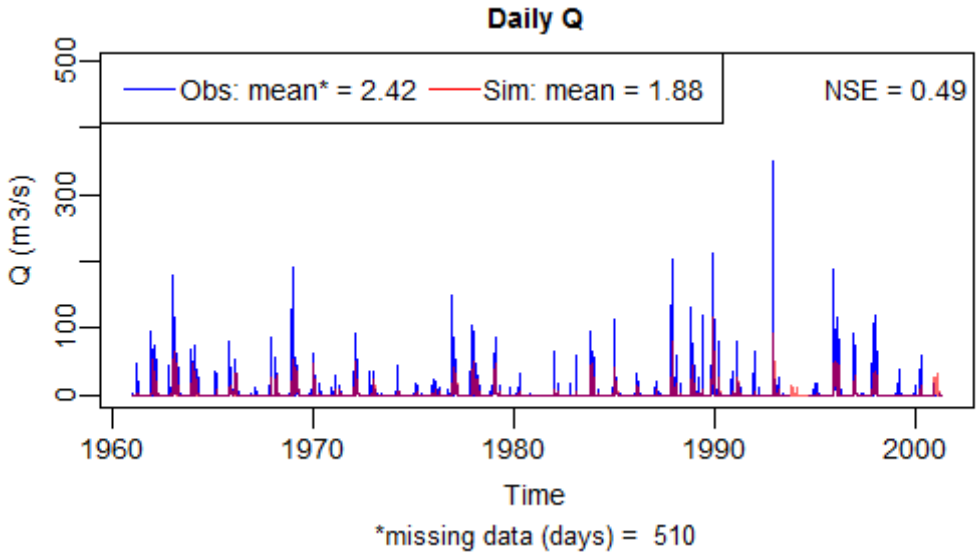

Figure 6.18 – Observed and simulated daily discharge (m3/s) for sub-basin 29L, with indication of the mean discharges and the Nash-Sutcliffe efficiency.

The water balance (Figure 6.19) calculated with gridded rainfall (IB02) and observed discharge shows the annual discharge going above 100% of the annual rainfall which is not possible. Therefore there is a problem with the input data (the rainfall, the discharge or both).

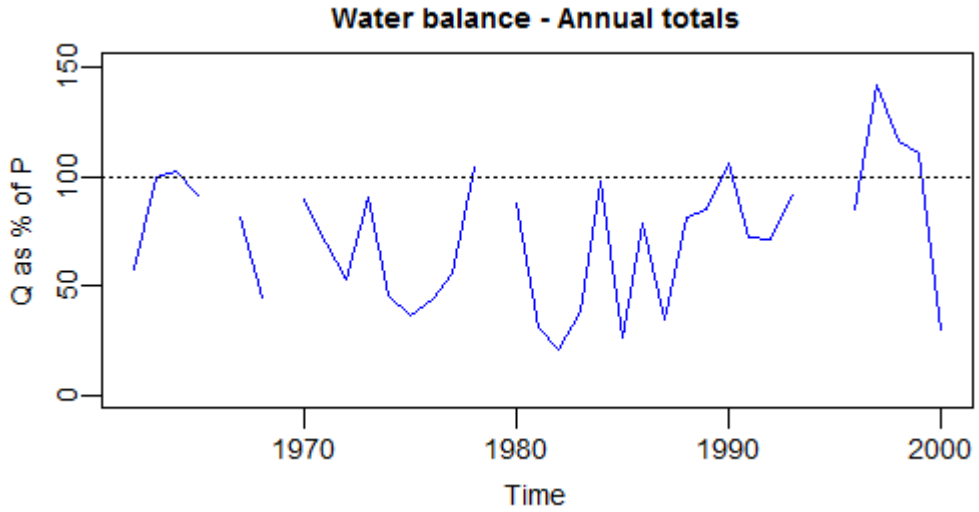

Figure 6.19 – Annual water balance (discharge as percentage of rainfall calculated for annual totals).

Sub-basin 29L is a small basin, with an area of 297km^2, situated in a mountainous area which has a steep rainfall gradient. Possibly this means that the gridded rainfall (IB02) does not capture the rainfall of this small sub-basin with enough detail. Five time-series of measured rainfall for this sub-basin were downloaded from INAG (http://snirh.pt) to compare with the gridded rainfall (see Figure 6.20 and Figure 6.21).

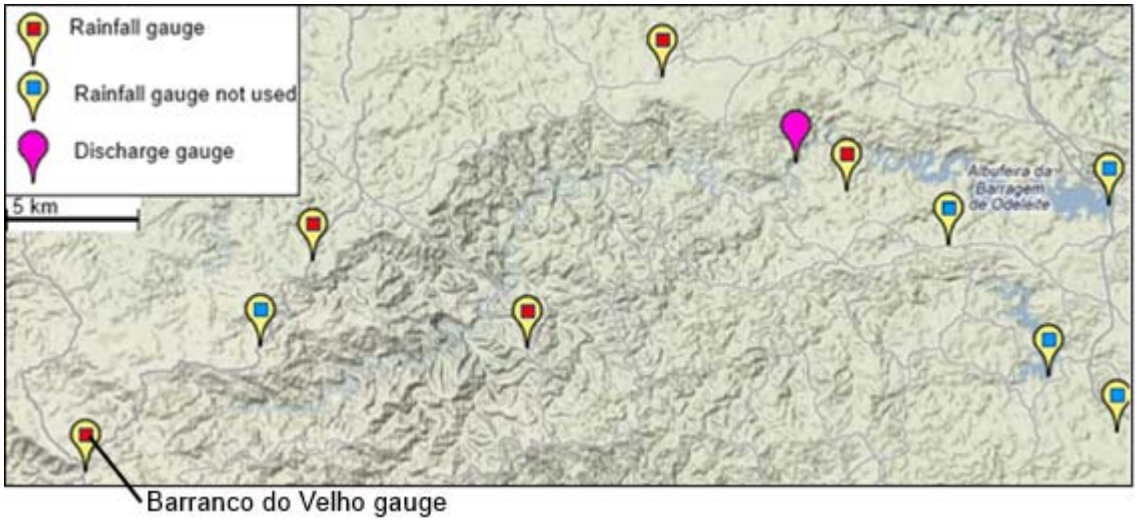

Figure 6.20 – Map of sub-basin 29L with rainfall and discharge gauges from INAG (adapted from http://snirh.pt). One of the gauges that is inside the basin was not used due to its very short record.

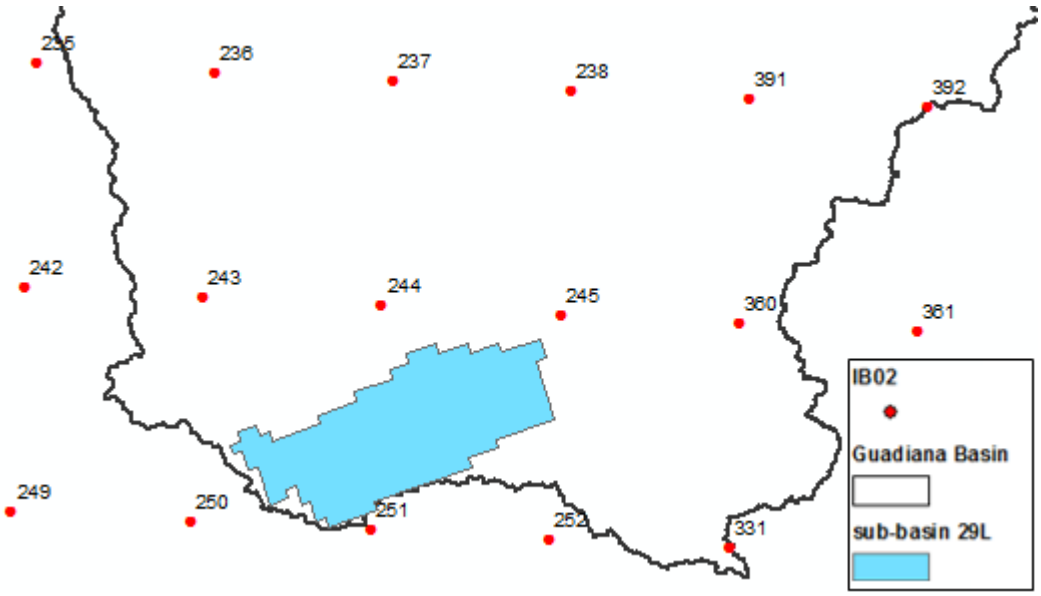

Figure 6.21 – Map of sub-basin 29L with the points from the gridded rainfall dataset IB02.

When comparing the rainfall from these two datasets (Figure 6.22) it is clear that the gridded rainfall does not reproduce the spatial variability of the observed data. INAG's gauge "Barranco do Velho" (gauge 4 in Figure 6.22 left) has a mean daily rainfall well above the other gauges and above all the IB02 rainfall grid points in the area. Rainfall IB02 grid point 250 (rainfall point 4 in Figure 6.22 right) is in the area of INAG's "Barranco do Velho" but its mean rainfall is 30% lower. Therefore, for the purpose of the SHETRAN simulation for this sub-basin, a 30% increase in rainfall for grid point 250 was used.

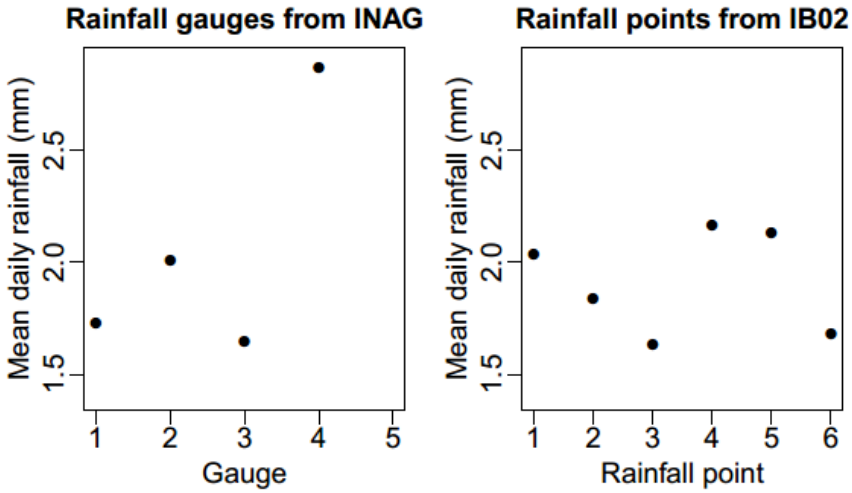

Figure 6.22 – Mean daily rainfall (mm) for the INAG rainfall gauges (observed rainfall) in the left and for gridded rainfall IB02 in the right for the period 1985 to 2000. The fifth gauge from INAG doesn't have data for this time interval, but when it does have data (1961-1975) its mean is very similar to gauge four (2.47mm and 2.49mm).

It is visible in Figure 6.23, that after the rainfall correction the daily peaks are still not correctly simulated. However, the monthly flows and the annual water balance, which are the focus of

this study, are well simulated (with only a slight overestimation of variability in the monthly data).

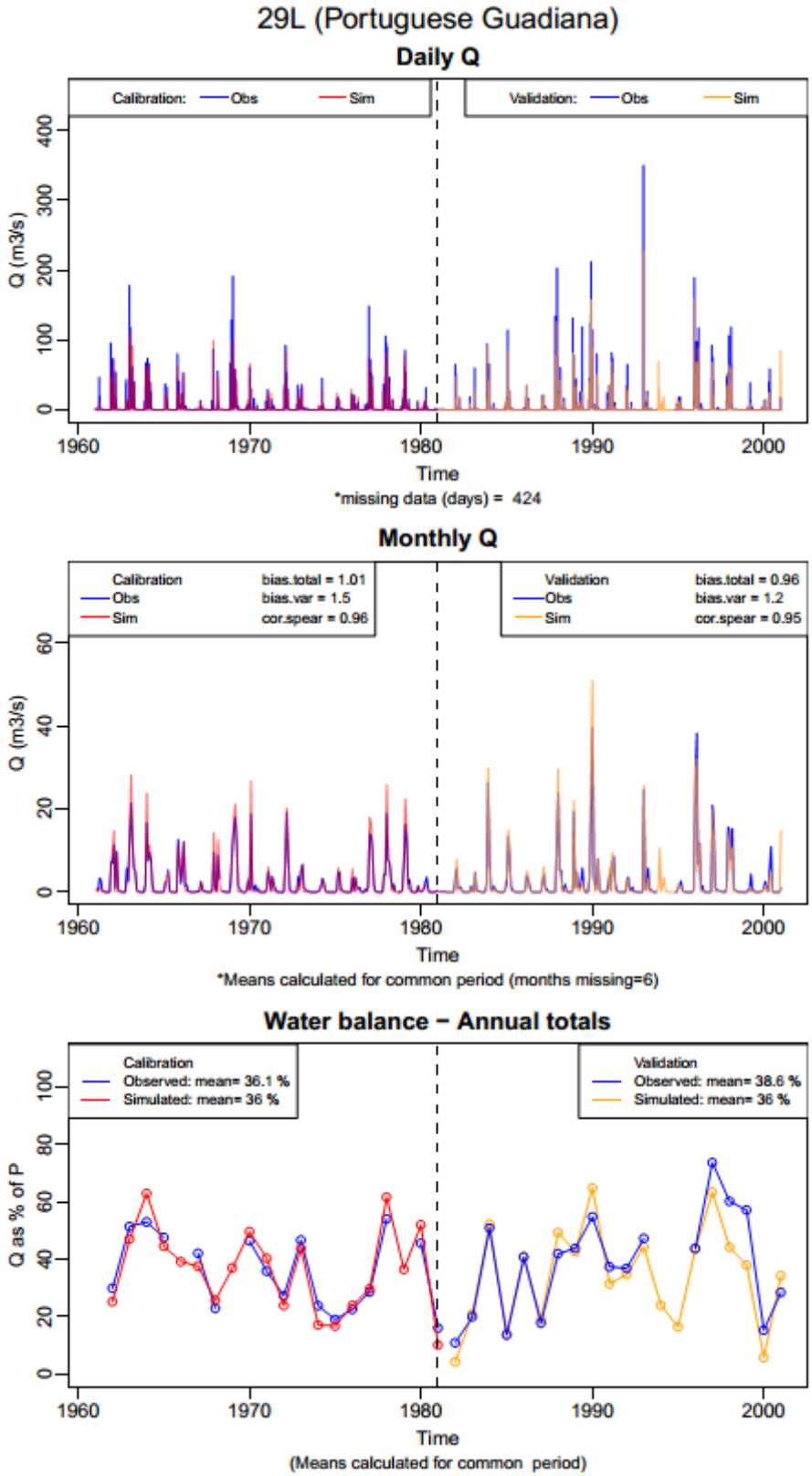

Figure 6.23 – Simulation results for sub-basin 2126, in the Portuguese side of the Guadiana basin. Observed (blue) and simulated (red for the calibration period and yellow for the validation period) daily discharge (up), monthly discharge (middle) and annual water balance – discharge as percentage of rainfall (bottom).

6.4.6 *Sensitivity to parameterization*

The parameters used to calibrate SHETRAN were the ones associated with each vegetation/land use class and the ones associated with aquifers. To assess the impacts of the SHETRAN calibration on the monthly discharge of the rivers Douro, Tagus and Guadiana (at their border gauges and outlets), SHETRAN runs using the same parameters for all land use/vegetation classes were performed. This means the simulations were done as if the entire study area (the three basins) had a uniform land use/vegetation class. As can be seen in Figure 6.24, Figure 6.25 and Figure 6.26 the effects of calibration on the monthly discharges at the border and outlet gauges of the three rivers are small, possibly due to the large size of the basins. Bias in the total discharge varies between 0.83 (Guadiana) to 0.94 (Douro-outlet). Bias in the variance ranges between 0.87 (Tagus and Guadiana border) to 0.97 (Douro-border). The Spearman correlation between calibrated and non-calibrated results is always very high (from 0.98 to 1) and the NSEs are also always very high (0.96 to 0.99).

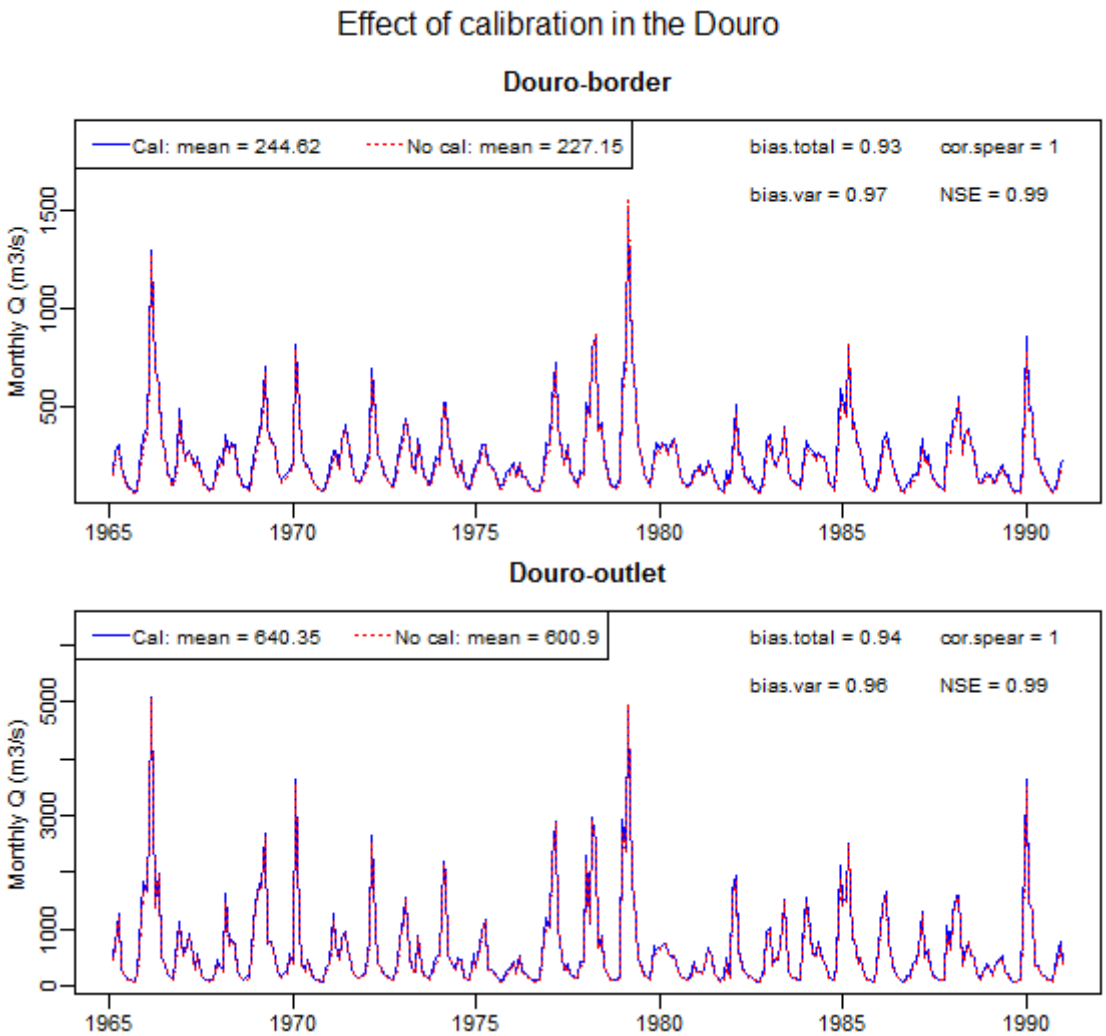

Figure 6.24 – Time-series of simulated monthly discharge with (blue) and without (red) calibration for Douro-border (top) and Douro-outlet (bottom). The no-calibration run was done using the same parameters for all land use/vegetation classes (i.e. assuming the entire study area had a uniform land use/vegetation class).

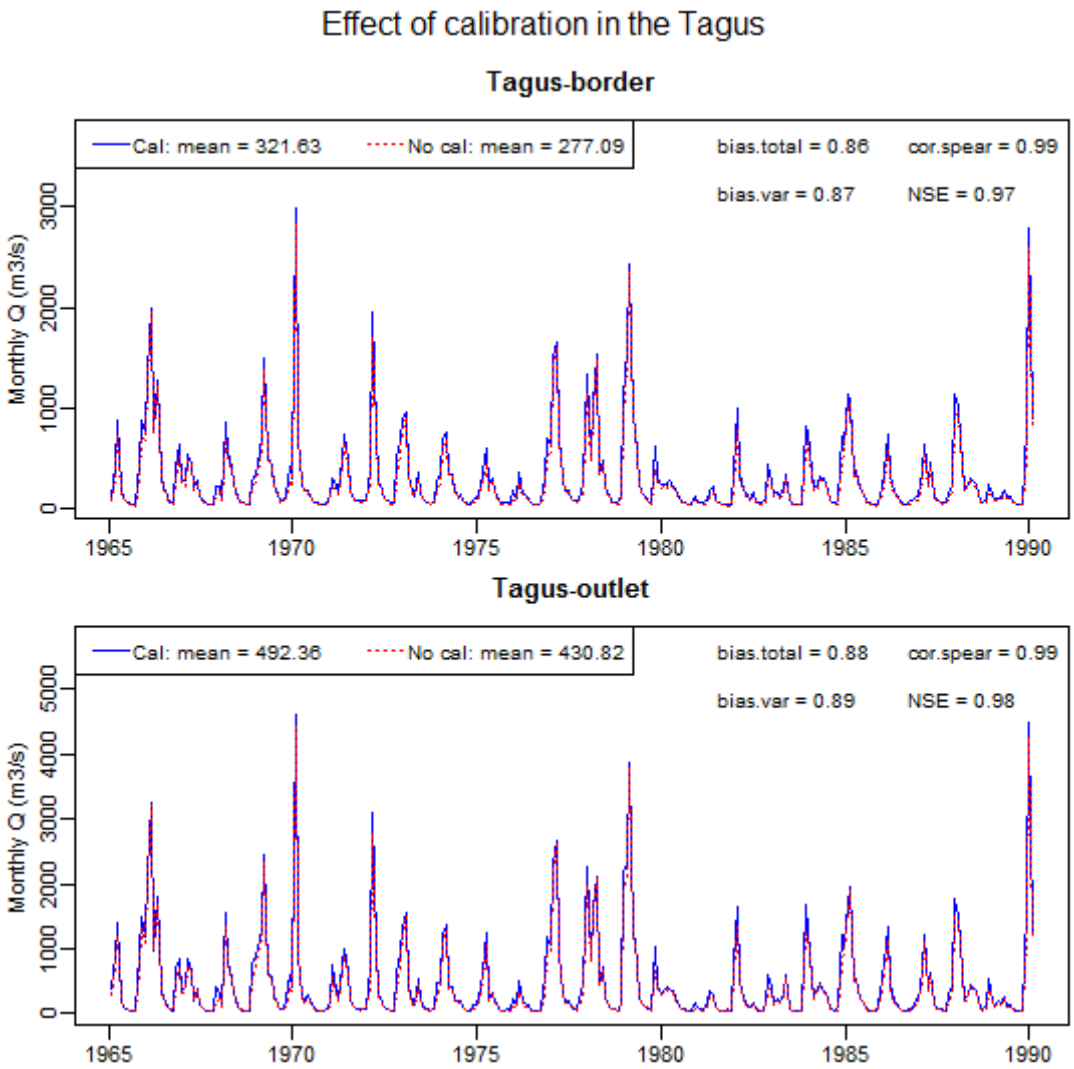

Figure 6.25 – Time-series of simulated monthly discharge with (blue) and without (red) calibration for Tagus-border (top) and Tagus-outlet (bottom). The no-calibration run was done using the same parameters for all land use/vegetation classes (i.e. assuming the entire study area had a uniform land use/vegetation class).

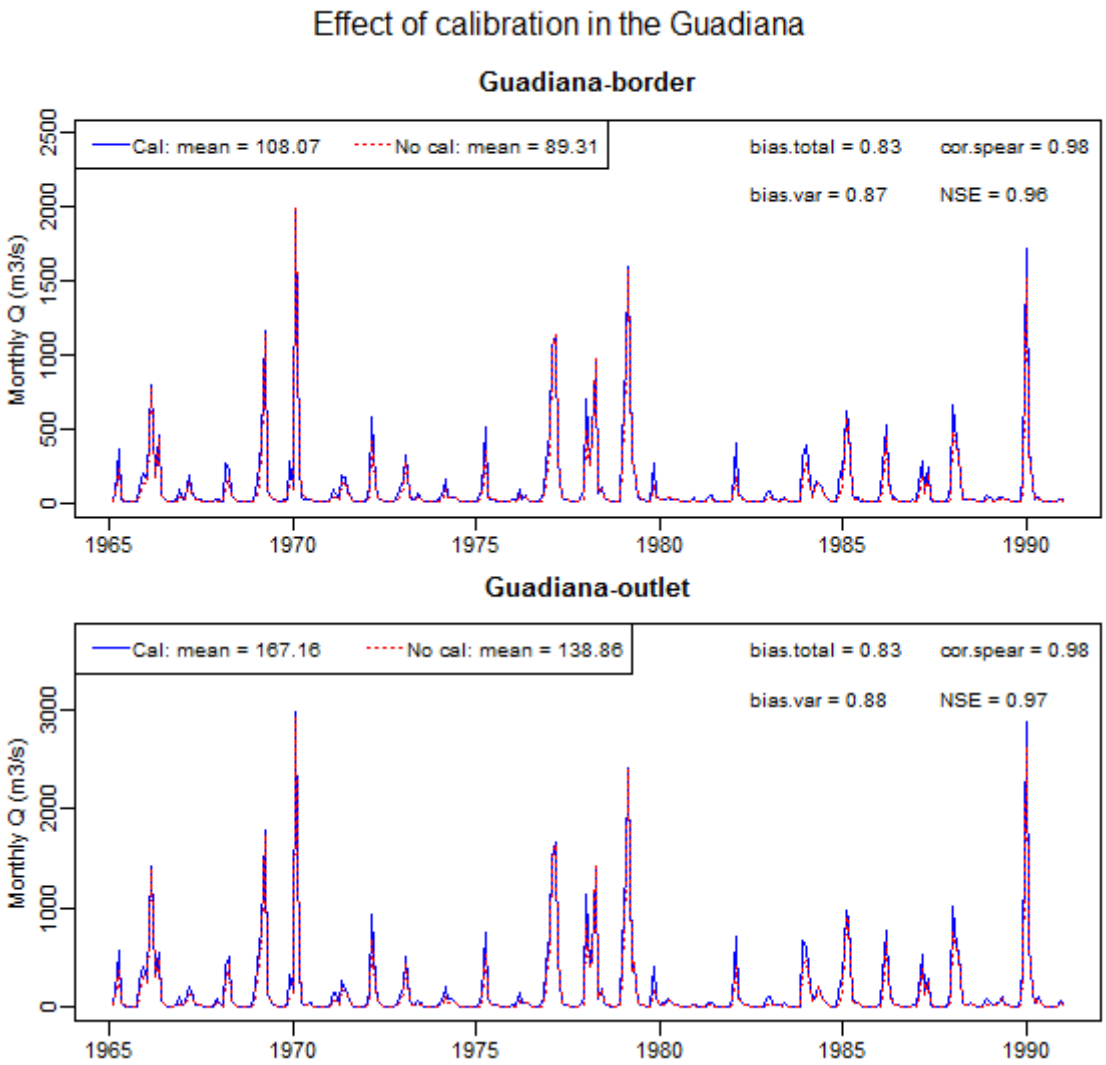

Figure 6.26 – Time-series of simulated monthly discharge with (blue) and without (red) calibration for Guadiana-border (top) and Guadiana-outlet (bottom). The no-calibration run was done using the same parameters for all land use/vegetation classes (i.e. assuming the entire study area had a uniform land use/vegetation class).

To assess the sensitivity to aquifer parameterization, SHETRAN runs were done, for the Tagus, with different aquifer saturated hydraulic conductivities (in the x, y and z direction). The original value was 2m/day and simulations were also done with 5m/day and 10m/day. Figure 6.26 shows the results for Tagus-outlet. The simulations are virtually indistinguishable in the time-series plot and differences are only noticeable for the low flows in the logarithmic scale of the flow duration plot.

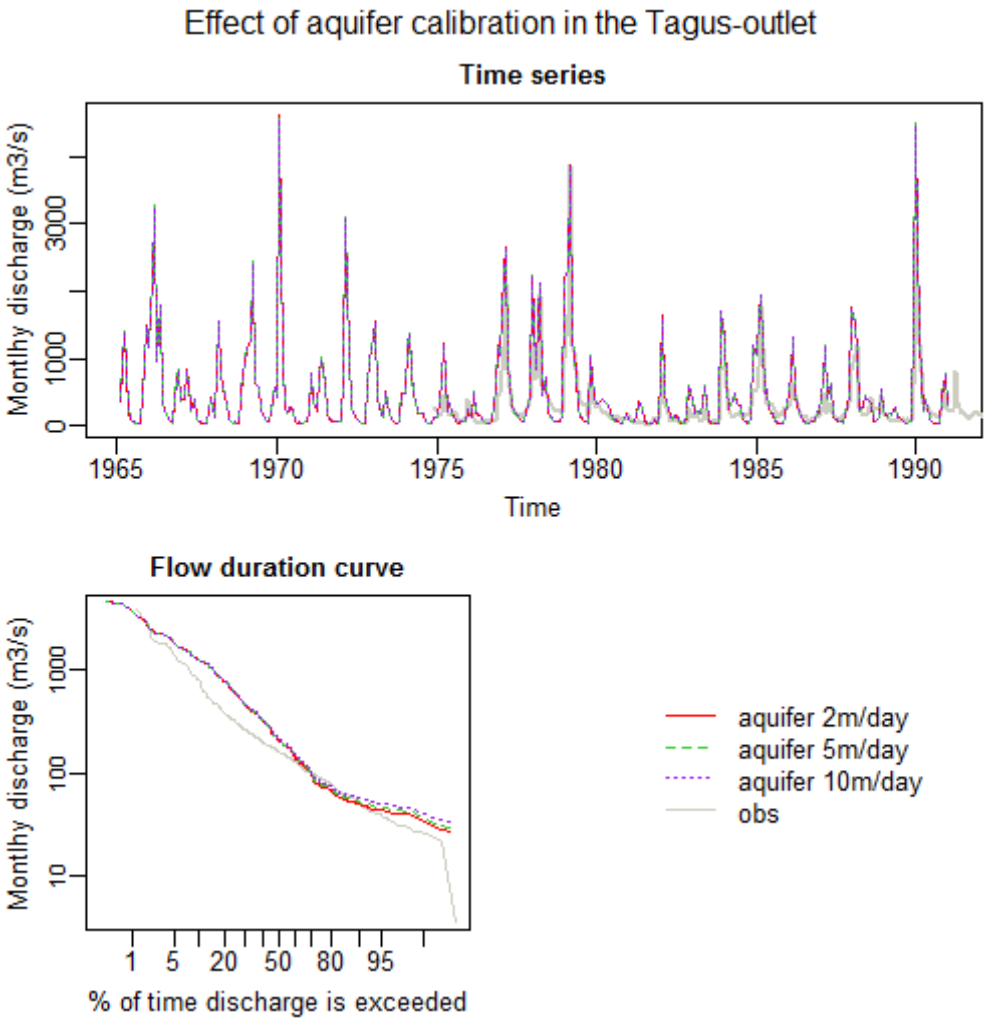

Figure 6.27 – Time-series (top) and flow duration curves (bottom-left) of monthly mean discharges for Tagus-border. Observations are plotted in grey and SHETRAN simulations with different aquifer saturated hydraulic conductivities (in metres per day) are plotted according to the legend.

6.5 Discussion and conclusions

Ideally the calibration and validation of a hydrological model would be performed using measured outputs of the simulated rivers, however in highly managed rivers like the Douro, the Tagus and the Guadiana that is not possible. Finding sub-basins with natural flows and using the same calibration parameters in all of them was the methodology adopted to circumvent this problem. Only four were available for the calibration and validation of the model but they represented different climatic zones, different soil types (some with and some without aquifers) and different land-uses classes.

Figure 6.28 shows the location of the sub-basins and a summary of the results of the calibration and validation. Despite problems of scale (the datasets used are appropriate to simulate the three big basins but not necessarily appropriate to simulate the small sub-basins) the results were considered good so the calibration parameters were used for the simulation of the big basins.

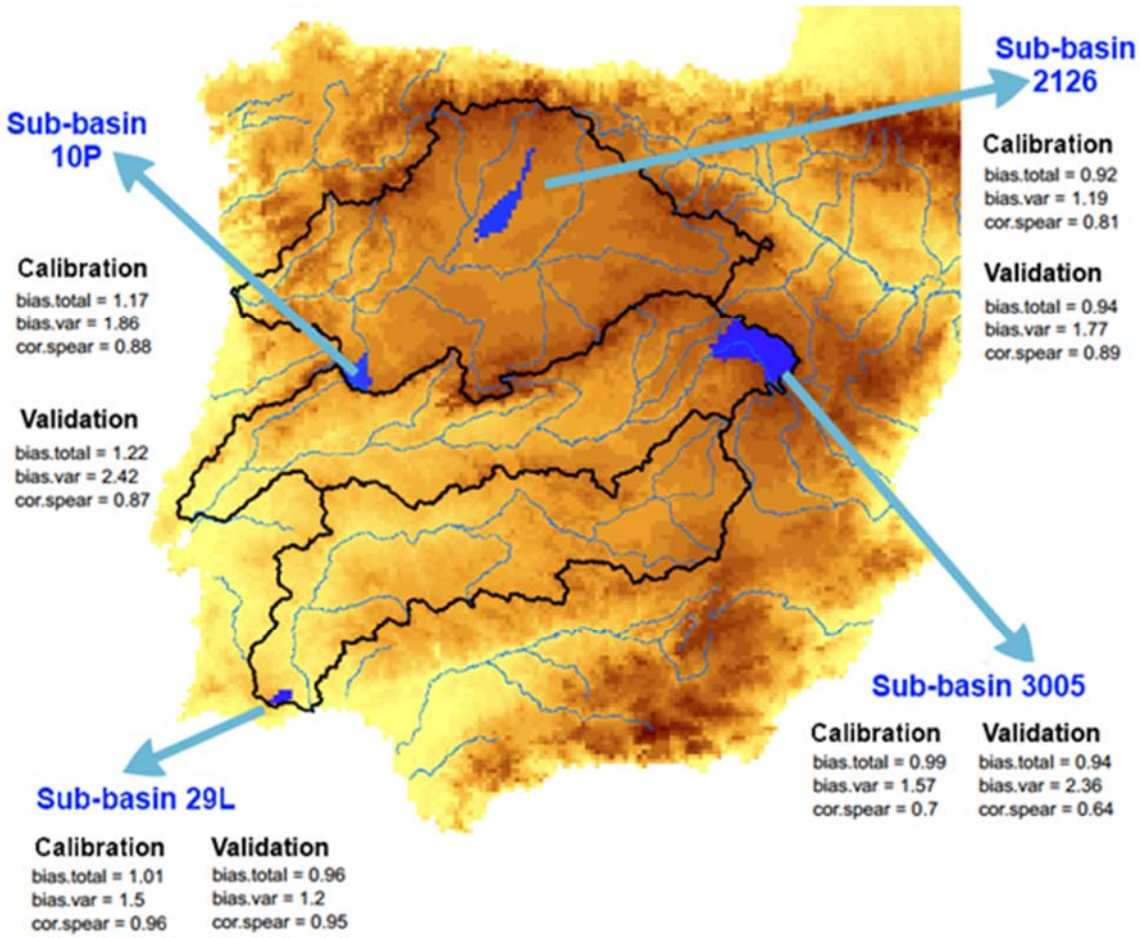

Figure 6.28 – Map of Iberia with the Douro, Tagus and Guadiana basins highlighted in black and the four sub-basins used for calibration and validation highlighted in blue. The calibration and validation goodness of fit results are also presented for each sub-basin.

It was shown that the impacts of land use/vegetation classes calibration on the monthly discharges of the Douro, Tagus and Guadiana at the border and outlet gauges were small. Also, the impact of aquifer parameterization (saturated hydraulic conductivities) was very small and restricted to the low discharges. Considering these were the main parameters used for the calibration of the model, this allows us to infer that the impact of SHETRAN's calibration on the historic and future river discharges is small and therefore it's contribution to future discharge uncertainty will also be small.

Chapter 7. Hydrological Model Results

This chapter presents the SHETRAN simulation results for historical (1965-1990) and future (2045-2070) periods and it compares the historical (naturalized) SHETRAN runs with observed discharges. Both annual and monthly simulated discharges compare well with observed ones and the order of magnitude of the differences between observed and simulated annual discharges were as expected.

Most models show decreases in daily, seasonal and annual discharges for all basins, especially for medium and low discharges. Some models project increases in high discharges, especially for winter. The magnitude of the decreases in discharge varies significantly for the different runs throughout the seasons and basins. However, autumn is the season showing the biggest decreases in discharge and the Guadiana is the basin consistently presenting the bigger discharge reductions and the higher future probabilities of being below the Convention limits.

This chapter is followed by the Conclusions chapter, where the results of the different methods are compared, overall conclusions are presented and future work is proposed.

7.1 Introduction

7.1.1 *Studies of hydrological impacts of climate change in Iberia*

Climate change studies that focus on hydrological impacts on the Douro, Tagus or Guadiana basins are virtually non-existent, although some studies can be found for small sub-basins inside these three international river basins. The exception is a study by Kilsby et al. (2007) that looked at the hydrological impacts of climate change on the Tagus and the Guadiana rivers for 2070-2100 under the SRES A2 scenario. They used one RCM (HadRM3H driven by HadCM3), two downscaling techniques (monthly bias correction and a circulation pattern based stochastic rainfall model) and a conceptual rainfall-runoff routing model. Reductions in flows for both basins were projected through the year due to increased PET and year-round rainfall decreases. The circulation pattern (CP) based method showed smaller reductions in flows (21% for Guadiana and 20% for Tagus) than the bias correction method (26% and 49%). This could be explained by the projected annual mean changes in rainfall: -30.5% for the bias correction method for the Guadiana but only -15.1% for the CP method and for the Tagus -24.3% versus -11.5%. The differences between methods were not surprising because the CP method only changes the frequency of existing weather types. Nevertheless the authors point out the need for "major improvements of the hydrological modelling" since observed and simulated flows showed great discrepancy. This improvement is a challenge since the hydrological modelling is hindered by the effect of dams and abstractions on the observed discharges. Also, the use of just one climate model did not allow an exploration of the range of uncertainty of future climate projections.

In terms of national projects, the Portuguese project SIAM (Santos *et al.*, 2002), introduced in section 4.1.3, assessed discharge changes using a lumped hydrological model (which makes their results heavily dependent on the calibration for the historical period) with a monthly time-step. Additionally, only small basins were simulated, not the Douro, the Tagus or the Guadiana. Nevertheless, annual and winter runoff for 2050 and 2100 varied depending on the climate model and emission scenario but spring, summer and autumn showed consistent reductions (up to 80%).

The Spanish national project "Generación de Escenarios Regionalizados de Cambio Climático para España" (Brunet *et al.*, 2009), also introduced in section 4.1.3, produced changes in water volumes in Spanish basins but without using a hydrological model.

7.1.2 *The Albufeira Convention*

The Albufeira Convention, the water treaty between Portugal and Spain introduced in section 1.3, establishes minimum annual discharges for the Iberian international rivers (except the Lima) at determined locations (see Figure 7.1, left). However, the discharge minima do not have to be complied with if the year is considered "exceptionally dry". This is defined by the rainfall in selected rainfall gauges (see Figure 7.1, right), and, for the Guadiana, it also takes into account the water levels in the basin's reservoirs.

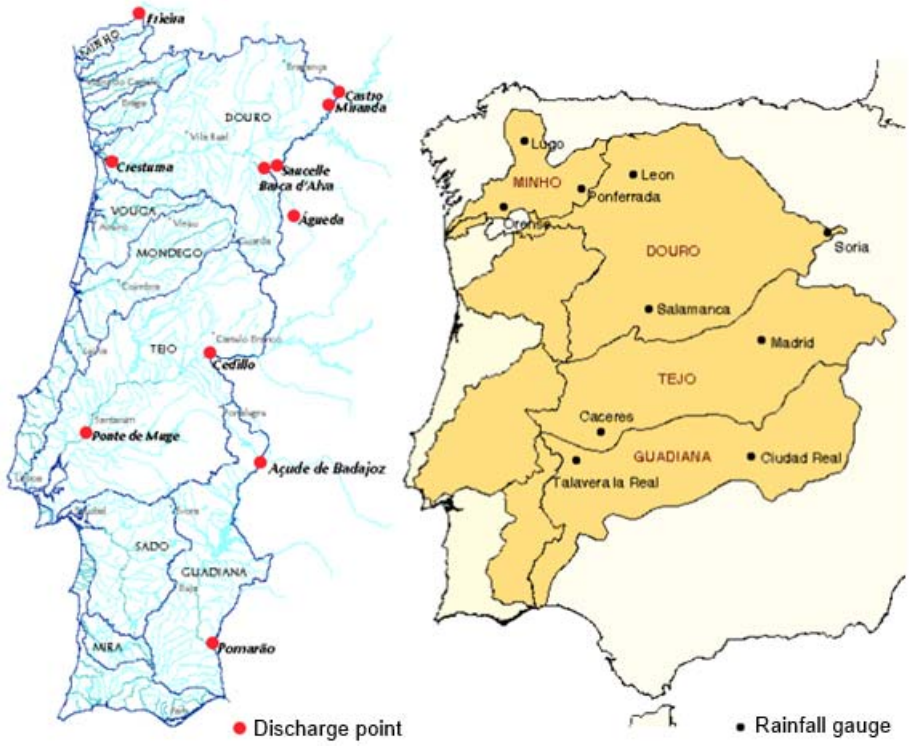

Figure 7.1 – Location of the reference discharge gauges on the left and of the reference rainfall gauges on the right (INAG, 1998).

In February 2008 a more detailed flow regime for the Douro, Tagus and Guadiana was defined (as a revision of the Convention), which included different minimum flows for different times of the year. For the Douro, these limits are presented in Table 7.1. However, if the rainfall between the 1st of October and the 1st of June is less than 65% of the mean rainfall for the same period, the annual discharge limits do not apply. The quarterly discharge limits do not apply if the rainfall for the six months up to the 1st day of the 3rd month of the trimester is below 65% of mean rainfall for the same period. Weekly discharge limits do not apply when quarterly discharge limits do not apply.

Table 7.1 – Discharge minima (in hm^3) for reference gauges in the Douro for different periods under the Albufeira Convention revision.

Period	Miranda / Bemposta	Saucelle + Águeda	Crestuma
Annual	3500	3800	5000
Oct-Dec	510	580	770
Jan-Mar	630	720	950
Apr-Jun	480	520	690
Jul-Sep	270	300	400
Weekly	10	15	20

For the Tagus, these limits are presented in Table 7.2. However, if the rainfall between the 1st of October and the 1st of April is less than 60% of the mean rainfall for the same period, or less than 70% and the previous year was less than 80% the annual discharge, limits do not apply. The quarterly discharge limits do not apply if the rainfall for the six months up to the 1st day of the 3rd month of the trimester is below 60% of mean rainfall for the same period. Weekly discharge limits do not apply when quarterly discharge limits do not apply.

Table 7.2– Discharge minima (hm^3) for reference gauges in the Tagus for different periods under the Albufeira Convention revision.

Period	Cedillo	Ponte Muge*
Annual	2700	1300
Oct-Dec	295	150
Jan-Mar	350	180
Apr-Jun	220	110
Jul-Sep	130	60
Weekly	7	3

*Discharges for the Portuguese sub-basin between Cedillo and Ponte de Muge

The Guadiana River is drier and the inter-annual variability is higher than the other international rivers in Iberia, with zero or very low annual discharge sometimes occurring under natural conditions. The water usage is also more intense and several dams have been built throughout the river resulting in an average discharge, at the border, that is around half of what it would be under natural conditions. Therefore the definition of discharge minima for the Guadiana River is more complex and takes into account the water level in six Spanish dams: Cijara, Garcia de Sola, Orellana, La Serena, Zújar and Alanje which have a combined capacity of 7 247hm^3.

The annual minimum discharges and exception periods for Badajoz gauge (Portuguese-Spanish border) are presented in Table 7.3 and the quarterly ones are presented in Table 7.4. The daily discharge minima is 2m^3/s for both Badajoz and Pomarão (the two reference gauges in the Guadiana).

Table 7.3 – Annual discharge minima (hm^3) for Badajoz gauge according to rainfall and reservoir volume (hm^3). Exception years, where discharge limits do not apply, are also indicated.

Total volume in the reservoirs on the 1st of March	Rainfall (Oct-Mar) > 65% of the mean	Rainfall (Oct-Mar) < 65% of the mean
>4000	600	400
3150-400	500	300
2650-3150	400	Exception
<2650	Exception	Exception

Table 7.4 – Quarterly discharge minima (hm^3) for Badajoz gauge according to season, rainfall and reservoir volume (hm^3). Exception years, where discharge limits do not apply, are also indicated.

Total volume in the reservoirs in Oct-Dec	Rainfall >65% of the mean	Rainfall < 65% of the mean
>3700	63	42
2850 – 3700	53	32
2350 – 2850	42	Exception
<2350	Exception	Exception
Total volume in the reservoirs in Jan-Mar	**Rainfall >65% of the mean**	**Rainfall < 65% of the mean**
4000	74	49
3150 – 4000	61	37
2650 – 3150	49	Exception
<2650	Exception	Exception
Total volume in the reservoirs in Apr-Jun	**Rainfall >65% of the mean**	**Rainfall < 65% of the mean**
>3700	42	28
2850 – 3700	35	21
2350 – 2850	28	Exception
<2350	Exception	Exception
Total volume in the reservoirs in Jul-Sep	**Rainfall >65% of the mean**	**Rainfall < 65% of the mean**
>3400	32	21
2550 – 3400	26	16
2050 – 2550	21	Exception
<2050	Exception	Exception

7.2 Data and Methodology

The data and the methodology used for setting up the SHETRAN models of the Douro, the Tagus and the Guadiana rivers are described in Chapter 6. SHETRAN runs were performed using different climatological input data (introduced in Chapter 4):

- observed rainfall and PET (control run);
- downscaled rainfall and PET using the change factor method (change factor runs);
- downscaled rainfall and PET using the bias correction method (bias corrected runs).

The periods used for the above simulations were: historical (1961-1990) and future or 2050s (2041-2070). The first years of each simulation were not used because the model was stabilizing and results will be presented for the periods 1965-1990 and 2045-2070. For the interpretation of the simulation results, flow duration curves (FDC) of daily discharges were plotted for both periods. Boxplots of change (2045-2070 in relation to 1965-1990) for mean seasonal and mean annual discharges were also plotted for all gauges and both downscaling methods.

The analysis regarding the Convention was performed by plotting annual and seasonal flow duration curves together with the Convention discharge limits and boxplots with the probability of being below those limits. For this analysis the rainfall associated with the discharges below the set limits was not taken into consideration; therefore there is no distinction between breaches of the Convention and exception periods. This assumption was made because, from a water resources perspective, it is the future available discharge that is important. The discharge limits set in the Albufeira Convention are merely used as an indication of what is an “insufficient discharge”. A different approach is considered in the “Future Developments Section” of the final chapter. Also, since the SHETRAN runs are naturalized runs, the water level in the Guadiana dams could not be taken into consideration. Therefore the highest discharge limits for the Guadiana were used.

7.3 Results for the historical period

7.3.1 *Annual discharges*

As explained in Chapter 6, the simulated discharges are naturalized discharges and cannot be expected to behave in the same way as the observed discharges when considering the level of human influence in the Douro, Tagus and Guadiana. Nevertheless, annual and monthly observed and simulated discharge time-series (for the available periods) were plotted for the border and outlet gauges of the three rivers and are shown in Figure 7.2, Figure 7.3 and Figure 7.4.

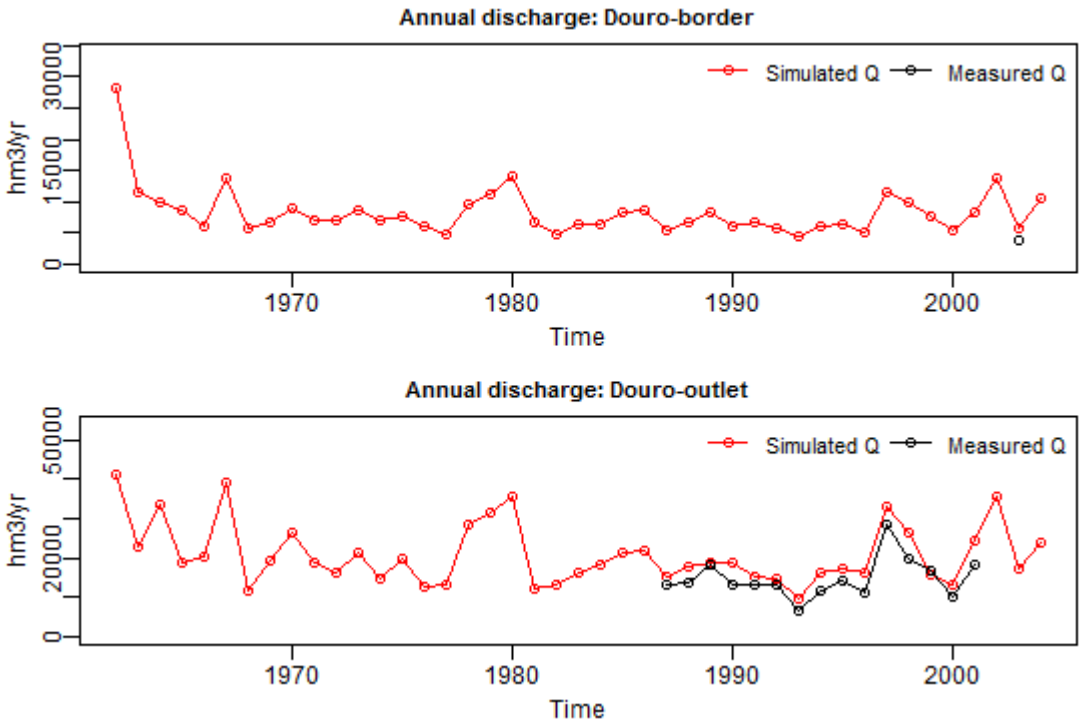

Figure 7.2 – Simulated (in red) and measured (in black) annual discharge for the Douro-border (top) and Douro-outlet (bottom) for the period 1965-2003.

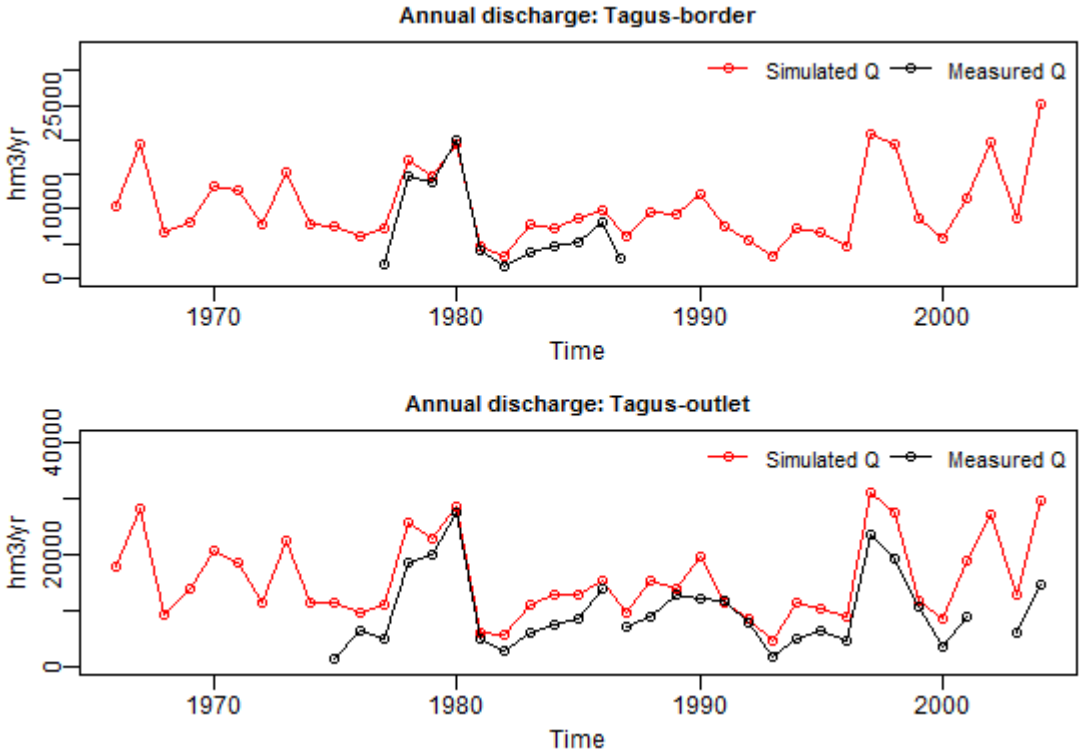

Figure 7.3 – Simulated (in red) and measured (in black) annual discharge for the Tagus-border (top) and Tagus - outlet (bottom) for the period 1965-2003.

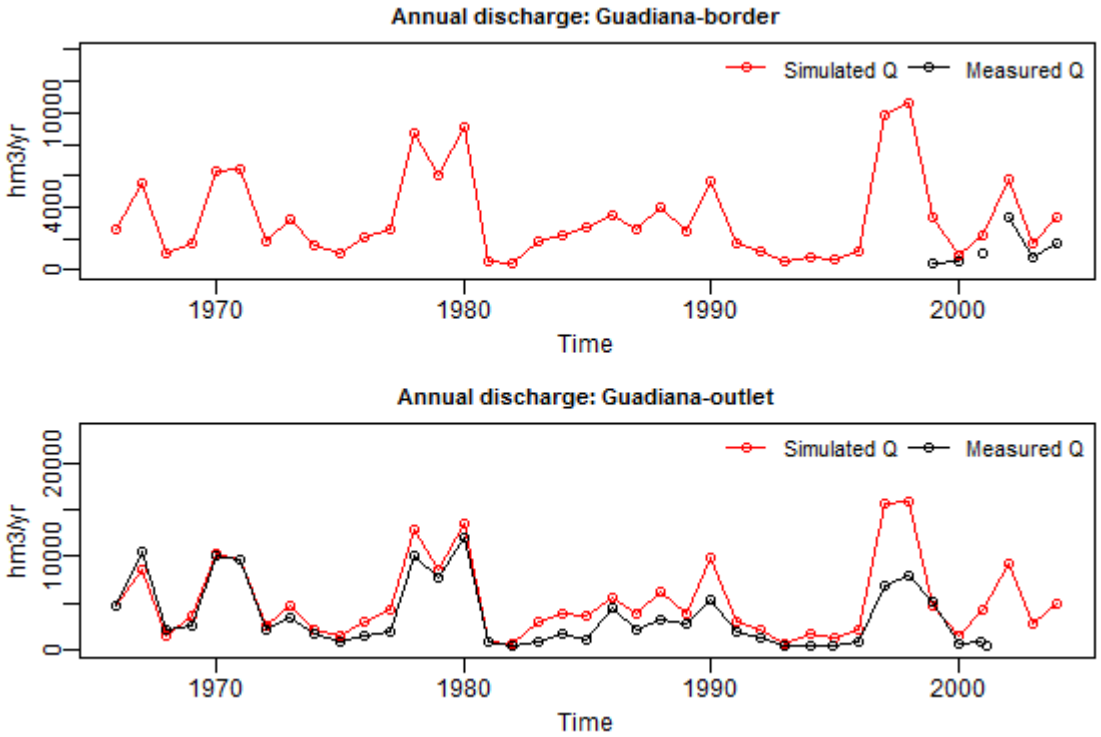

Figure 7.4 – Simulated (in red) and measured (in black) annual discharge for the Guadiana-border (top) and Guadiana-outlet (bottom) for the period 1965-2003.

The available records for the border gauges are too short to be analysed but the outlet gauges have longer records. The mean annual differences between simulated and observed discharges (for the period when both are available) for the Douro-outlet gauge is 3 407hm^3/yr, for the Tagus-outlet gauge is 4 410hm^3/yr and for the Guadiana-outlet gauge is 1 516hm^3/yr.

These are the same order of magnitude as the water uses in the Spanish section of the three basins shown in Table 7.5 and suggest that the model is adequately simulating the water balance in the three catchments. However, these water uses are met not only by surface water but also by aquifer exploration. For example, in the Douro, a more up to date estimate of annual irrigation needs is 3 250hm^3/year, 25% of which comes from aquifers (CHD, 2007). Nevertheless a more in depth analysis of the system will not be performed because of the highly complex network of aquifers, the thousands of exploration points and the unavailability of data.

Table 7.5 – Water uses (in hm^3/yr) in the Spanish Douro, Tagus and Guadiana (CHD, 1999; CHG, 1999; CHT, 1999). Followed by differences between simulated and measured discharge (hm^3/yr) at the outlet gauges calculated in this study and reservoir storage capacity in Portugal and Spain from Almeida *et al.* (2009).

	Douro			**Tagus**			**Guadiana**	
Water uses in Spain	urban	214		urban + industrial (includes irrigation)	2 643		urban	119
	irrigation	3 603					irrigation	2 157
	industrial	43					livestock	18
							industrial	36
				power stations cooling	1 397		others	2
	environment	1658		environment	765		environment	79
Total consumptive use in Spain	**3 860**			**4 041**			**2 331**	
Difference between simulated and measured annual Q at the outlet gauges (hm^3/yr)	**3 407**			**4 410**			**1 516**	
Storage capacity in Spain (hm^3)	1 670			11 140			9 222	
Storage capacity in Portugal (hm^3)	1 080			2 750			3 610	

Not considered in this simple comparison are the inter-basin water transfers which have long been used in Spain, with some examples dating from the sixteenth century (MIMAN, 1998). The most important water-transfer nowadays in Spain is the "Tajo-Segura" aqueduct which brings water from the high Tagus to the Guadiana, Sur, Segura and Júcar basins (MIMAN, 1998). The volume of water transferred annually from the Tagus varies significantly (see Figure 2.21) and has a maximum of 650hm^3/yr, which can only be transferred when a number of conditions are met (CHT, 1999). Also not considered are the evaporative losses from the hundreds of dams in the area. For example, for the Spanish area of the Tagus, the *Confederación Hidrográfica del Tajo* (C.H.TAJO, 2014) lists 83 dams with a combined area of 47 564hm^2. Assuming an annual mean PET of 1000mm in the Spanish part of the basin (see Figure 4.3) around 500hm^3/yr are lost through evaporation from Spanish dams in the Tagus.

Nevertheless, the temporal evolution of simulated and observed annual discharges for the three basins are as expected. Also, the differences between the two are of the same order as the magnitude of the Spanish water uses. Furthermore the biggest difference was in the Tagus and the smallest in the Guadiana, as would be expected considering the water uses and the Tagus-Segura transfer. Although these results cannot be used to validate the SHETRAN simulations, they do increase the confidence in them.

7.3.2 *Monthly discharges*

The comparison of monthly simulated and measured discharges is harder to make since monthly measured discharges are strongly affected by regulation. Nevertheless, Figure 7.5, Figure 7.6 and Figure 7.7 show monthly time-series for the border gauges of the three rivers and respective flow duration curves and boxplots. The time period used for each gauge was different because it corresponds to the period where measured discharge data is available.

As expected, all gauges show higher peaks in the simulated series than in the measured series. However, low flows might be too low in the simulated series. This can be seen in the time-series of the Tagus and in the flow duration curves of the three gauges where simulated discharges in the area of 80% of time exceeded are slightly lower than observed ones.

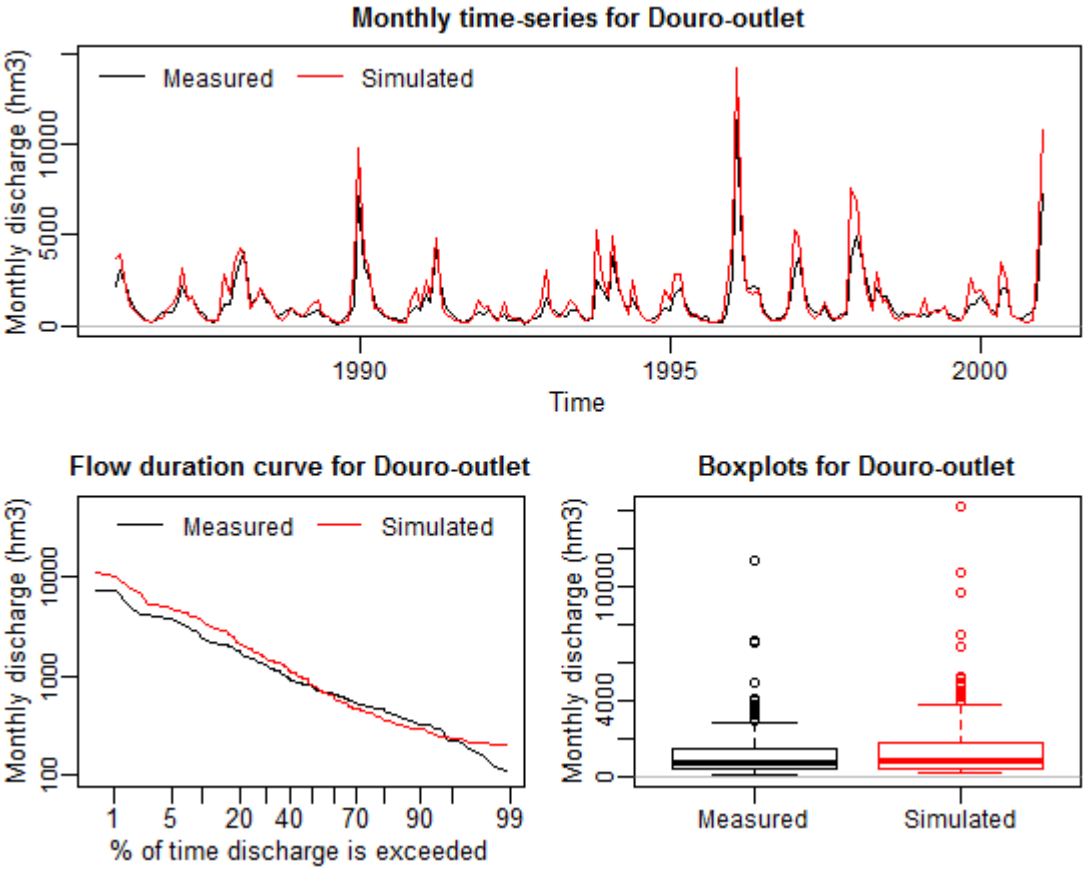

Figure 7.5 – Douro-outlet simulated (in red) and measured (in black) monthly discharge for the period 1986-2000 (top). Respective flow duration curves (bottom-left) and boxplots (bottom-right).

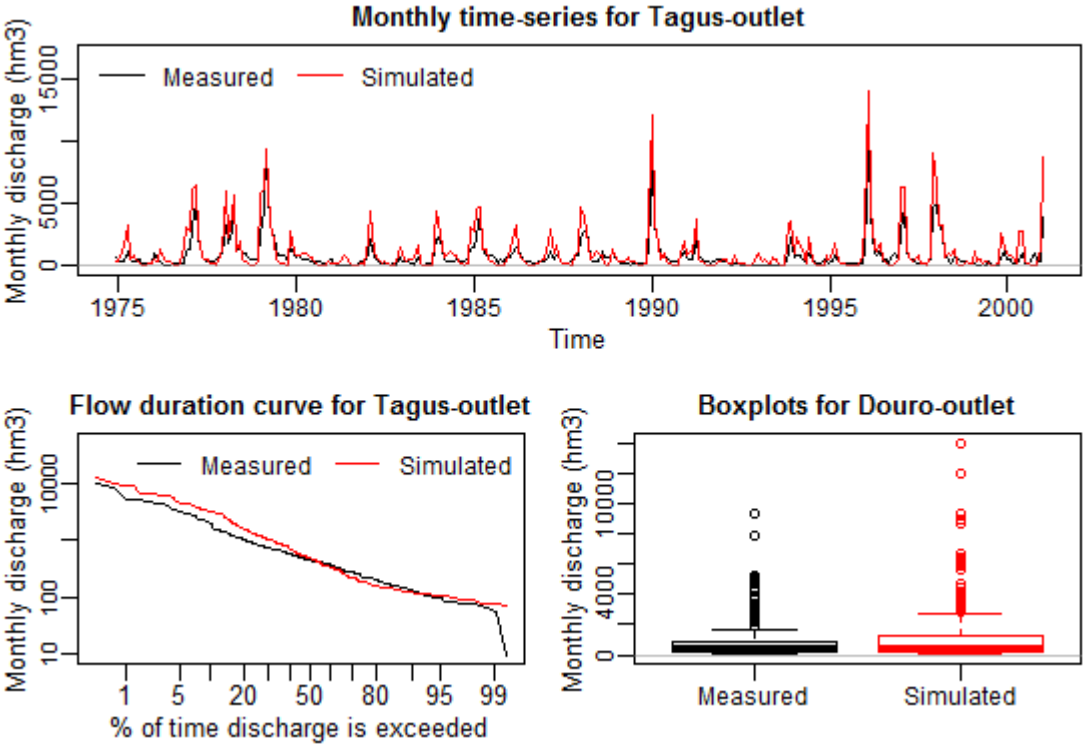

Figure 7.6 – Tagus-outlet simulated (in red) and measured (in black) monthly discharge for the period 1974-2000 (top). Respective flow duration curves (bottom-left) and boxplots (bottom-right).

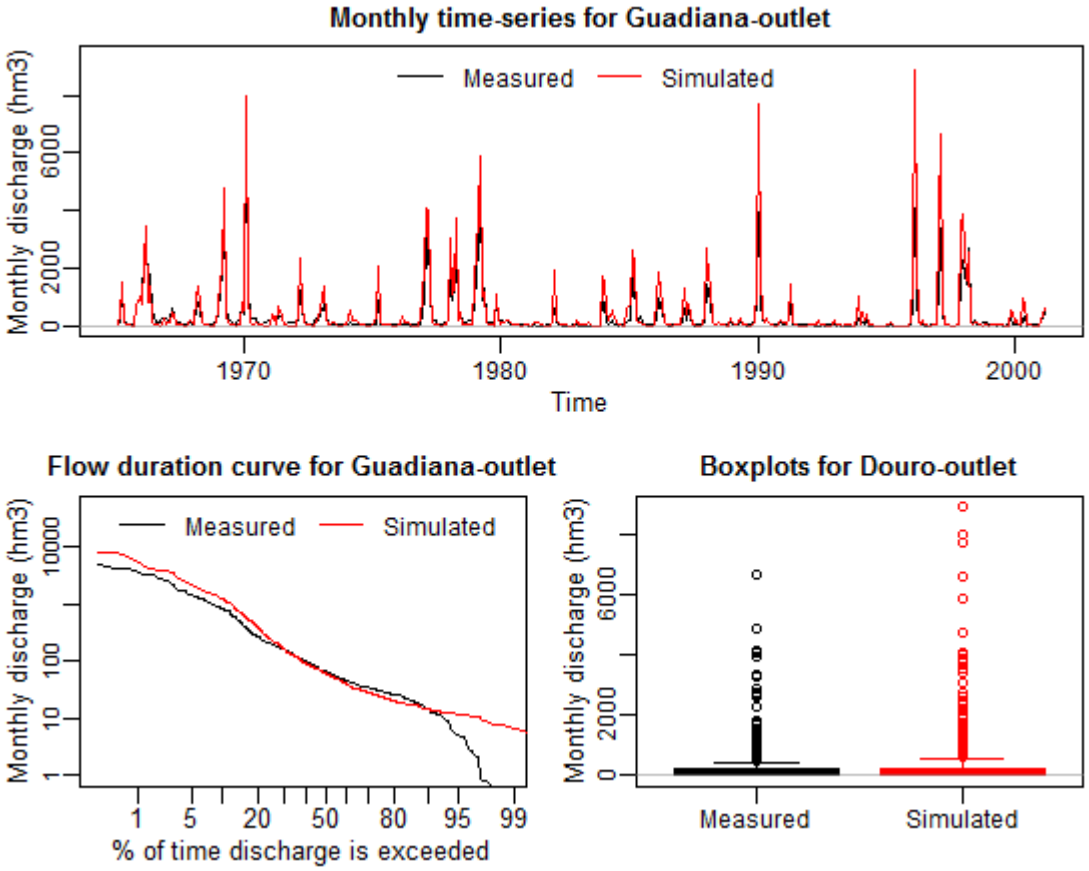

Figure 7.7 – Guadiana-outlet simulated (in red) and measured (in black) monthly discharge for the period 1965-2000 (top). Respective flow duration curves (bottom-left) and boxplots (bottom-right). Please notice the existence of zeros in the monthly measured discharge (the monthly simulated discharge minimum is 3.8hm^3/month).

7.4 Results for the future period

Historical and future SHETRAN simulations were performed using observed rainfall and PET (control run), downscaled rainfall and PET using the change factor method (change factor runs) and downscaled rainfall and PET using the bias correction method (bias corrected runs).

The Kolmogorov-Smirnov test (at 0.05 significance) was used to assess the statistical significance of seasonal and annual changes in discharge for the outlet of the three rivers (between 1965-1990 and 2045-2070). The results are presented in Table 7.6.

Table 7.6 – Number of models showing positive (pos) and negative (neg) significant changes in rainfall between 1965-1990 and 2045-2070using the Kolmogorov-Smirnov test at 0.05 significance level for each basins' outlet and for each season (annual values also included).

Season	Douro - outlet				Tagus - outlet				Guadiana - outlet			
	Change Factor		Bias Correction		Change Factor		Bias Correction		Change Factor		Bias Correction	
	pos	neg	pos	neg	pos	neg	pos	neg	pos	neg	pos	neg
OND	0	9	0	8	0	6	0	7	0	9	0	9
JFM	0	0	2	4	0	1	1	6	0	1	0	8
AMJ	0	6	0	11	0	11	0	10	0	14	0	14
JAS	0	12	0	14	0	12	0	13	0	13	0	14
Annual	0	8	0	8	0	5	0	7	0	3	0	10

Despite the range of results presented in the next sections, the only positive significant changes in discharge are in winter (two runs in the Douro and one in the Tagus), all other seasons and annual discharge either show negative or no significant changes. The bias corrected runs show more significant changes than the change factor runs and the seasons with more runs showing significant changes are spring and summer. The Guadiana River shows the higher number of runs with significant changes, and in spring and summer almost all runs showed significant reductions in this basin.

The next sections show all the results for the three basins, including the ones that are not statistically significant using the Kolmogorov-Smirnov test (at 0.05 significance). This is done because in noisy series, like the discharges of these three basins, is hard to assess change using just 25 years of data.

7.4.1 *Douro*

Figure 7.8 shows the flow duration curve (FDC) of daily discharge for the Douro-border and Douro-outlet. At both locations, the simulation for the control run is encompassed by the historical bias corrected runs, which increases the confidence in the SHETRAN bias corrected

runs. All models show a decrease in medium and low daily future discharges, which is more accentuated in the bias corrected runs. While the behaviour of high flow is model dependent.

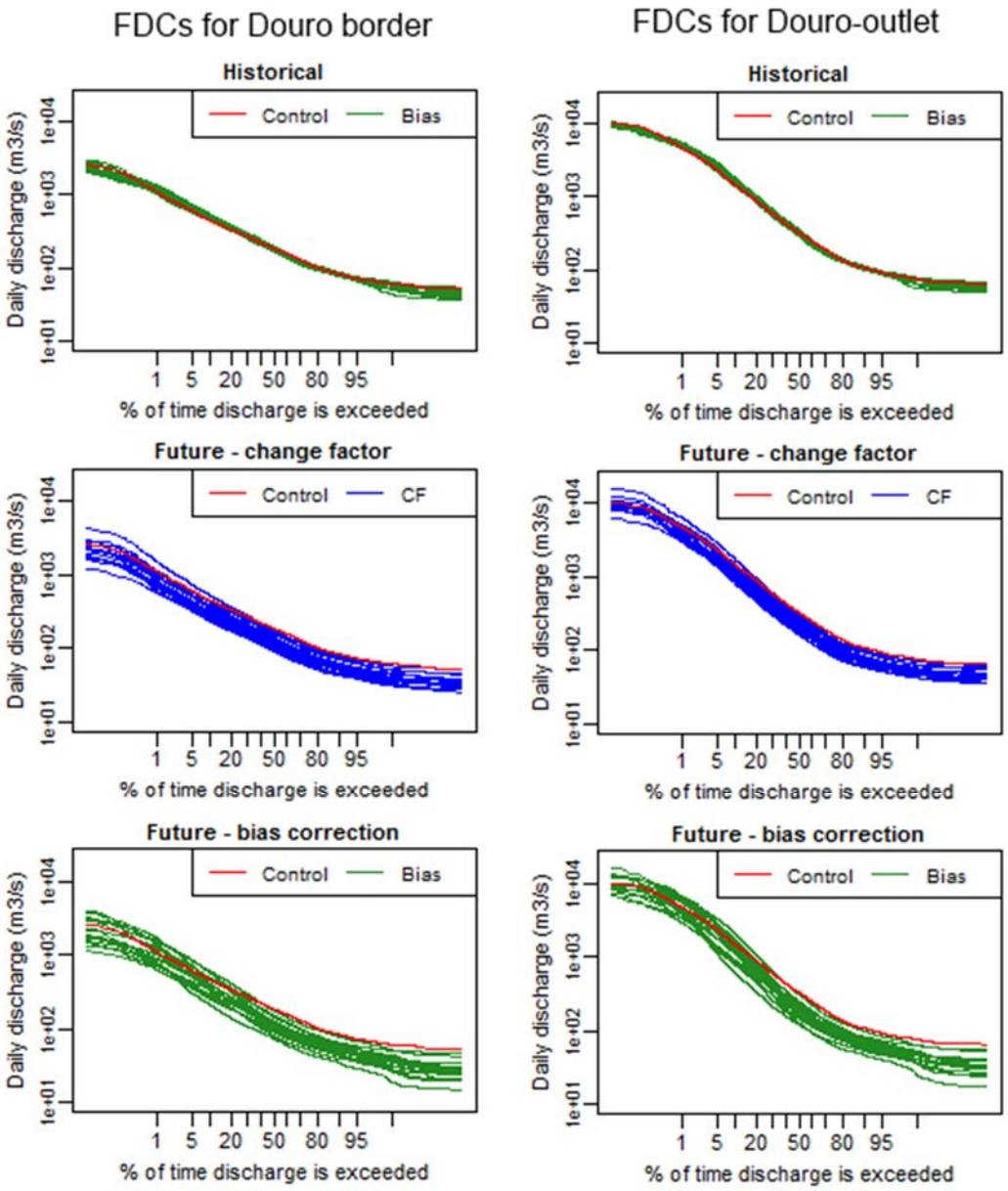

Figure 7.8 – Flow duration curves for Douro-border (left) and Douro-outlet (right) for historical (1965-1990) daily discharge (top), future (2045-2070) daily discharge obtained using the change factor method (middle) and future (2045-2070) daily discharge obtained using the bias correction method (bottom). The flow duration curve of daily discharge for the control run (SHETRAN simulation using observed meteorology) was added to the three plots (red line).

Figure 7.9 shows the projected changes in mean seasonal and mean annual discharges for the Douro, at both the border and outlet gauges and for both change factor and bias corrected model runs for the 2050 (2045-2070 in relation to 1965-1990). The spread of results is high but most models show a decrease in mean discharge for all seasons. The most pronounced decreases are in autumn (October-November-December) which can reach around 60% decrease in discharge at both the border and the outlet gauges. In winter some models show an increase in discharge (with a maximum of 51%), but most still show a decrease in discharge

that can reach -50%. In spring most models show a decrease that can reach -58% and in summer all runs show decreases ranging from -53% to -4%. Annual projected changes are between +19% and -54% for Douro-border and between +13% and -51% for Douro-outlet.

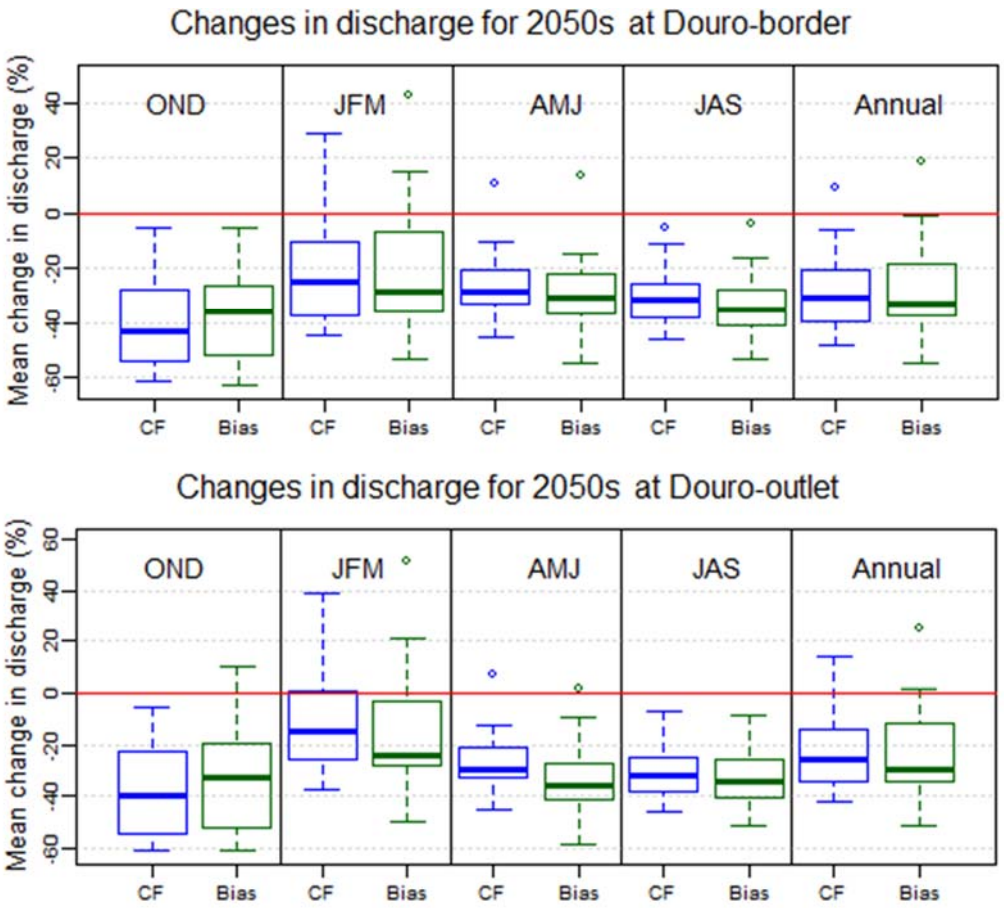

Figure 7.9 – Boxplots of mean changes (2045-2070 in relation to 1965-1990) at Douro-border (top) and Douro-outlet (bottom) for seasonal and annual discharges. Results using the change factor method are shown in blue, while bias-correction results are shown in green. Red line shows zero change.

Figure 7.10 and Figure 7.11 show the FDC of annual discharge for the Douro-border and Douro-outlet for historical and future periods and boxplots with the probability of being below the Albufeira Convention discharge limits. As with the historical daily discharge FDC, for both locations, the control run is encompassed by the historical bias corrected model runs. Most models project a decrease in annual future discharges which is more pronounced for the bias corrected runs.

The probability of being below the annual discharge limit set in the Convention (calculated based on the number of years when discharge was below the convention limit during the 26 year period for each model run) is zero for the control run in the Douro-border gauge and ranges between 0% and 12% for the historical bias corrected model runs. A marked increase is projected for the future, and the probability of being below the annual discharge limit for the change factor model runs ranges between 0% and 40% and for the bias corrected runs is

between 0% and 68%. For the Douro-outlet gauge (Figure 7.11) the control run also has zero probability of being below the Convention limit, but so do all historical bias corrected runs. An increase is also projected for the future, but this is not as marked as for Douro-border. The probability of the change factor runs being below the convention limit ranges between 0% and 12% and for the bias corrected runs it ranges between 0% and 24%.

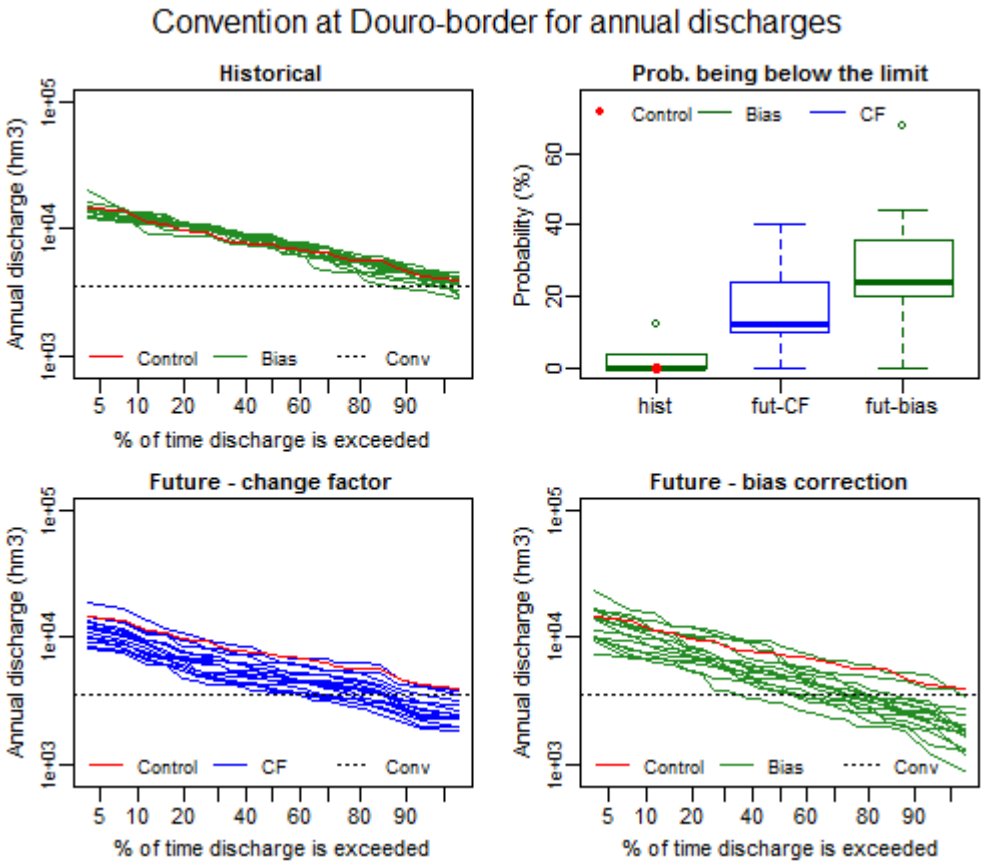

Figure 7.10 – Flow duration curves for Douro-border for historical (1965-1990) annual discharge (top-left). Probability of annual discharge being below the annual Convention limit for bias-corrected historical discharge, control discharge, future discharge using the change factor method and using the bias correction method (top-right). Flow duration curves of annual future discharge (2045-2070) using the change factor method (bottom-left) and using the bias correction method (bottom-right).

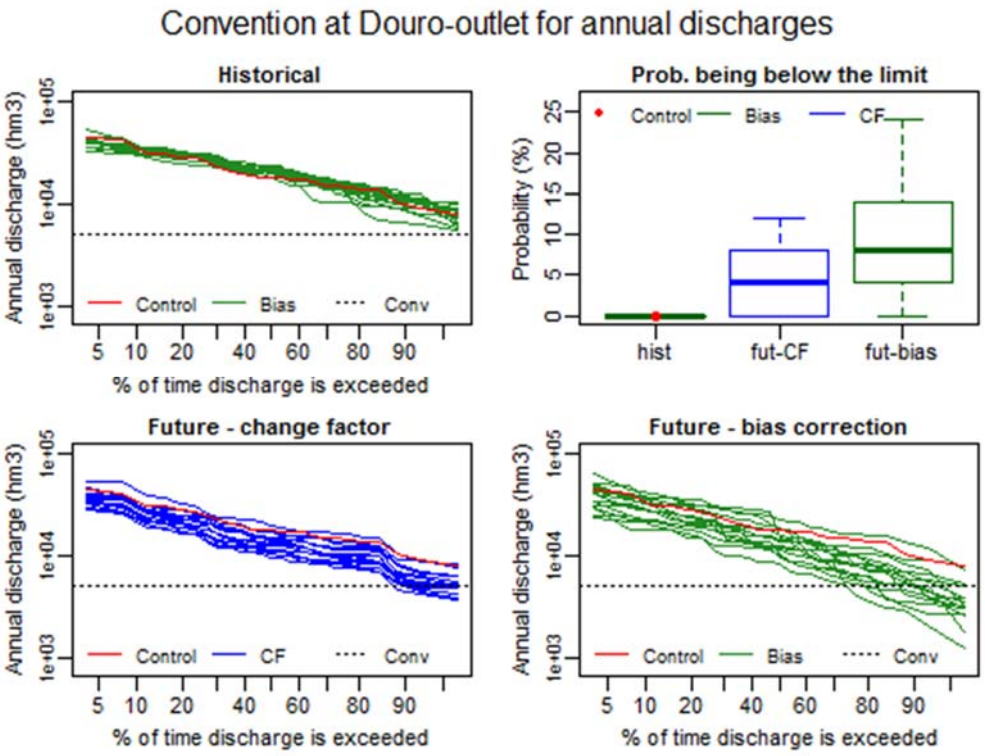

Figure 7.11 – Flow duration curves for Douro-outlet for historical (1965-1990) annual discharge (top-left). Probability of annual discharge being below the annual Convention limit for bias-corrected historical discharge, control discharge, future discharge using the change factor method and using the bias correction method (top-right). Flow duration curves of annual future discharge (2045-2070) using the change factor method (bottom-left) and using the bias correction method (bottom-right).

Next we analyse the seasonal distribution of changes. Figure 7.12 shows the FDCs of autumn and winter discharge for the Douro-border for historical and future periods and boxplots with the probability of being below the discharge limit. In both seasons, the control run is encompassed by the historical bias corrected runs and never goes below the Convention limit. In winter, neither do the bias corrected historical runs. For autumn, the probability of being below the limit is very low, ranging from 0% to 4%.

For autumn, all the future change factor runs show a decrease in discharge with the probability of being below the Convention limit ranging from 0% to 31%. For the future bias corrected model runs, some simulations show an increase in high discharges. However, most model runs show a decrease of medium discharges and all models show a decrease of low discharges with the probability of being below the convention limit ranging from 0% to 42%.

For winter, some model runs show an increase in discharges but most still show a decrease. The probability of being below the Convention limit is low for the change factor runs, ranging between 0% and 4%, but is significantly higher for the bias corrected runs, between 0% and 15% .

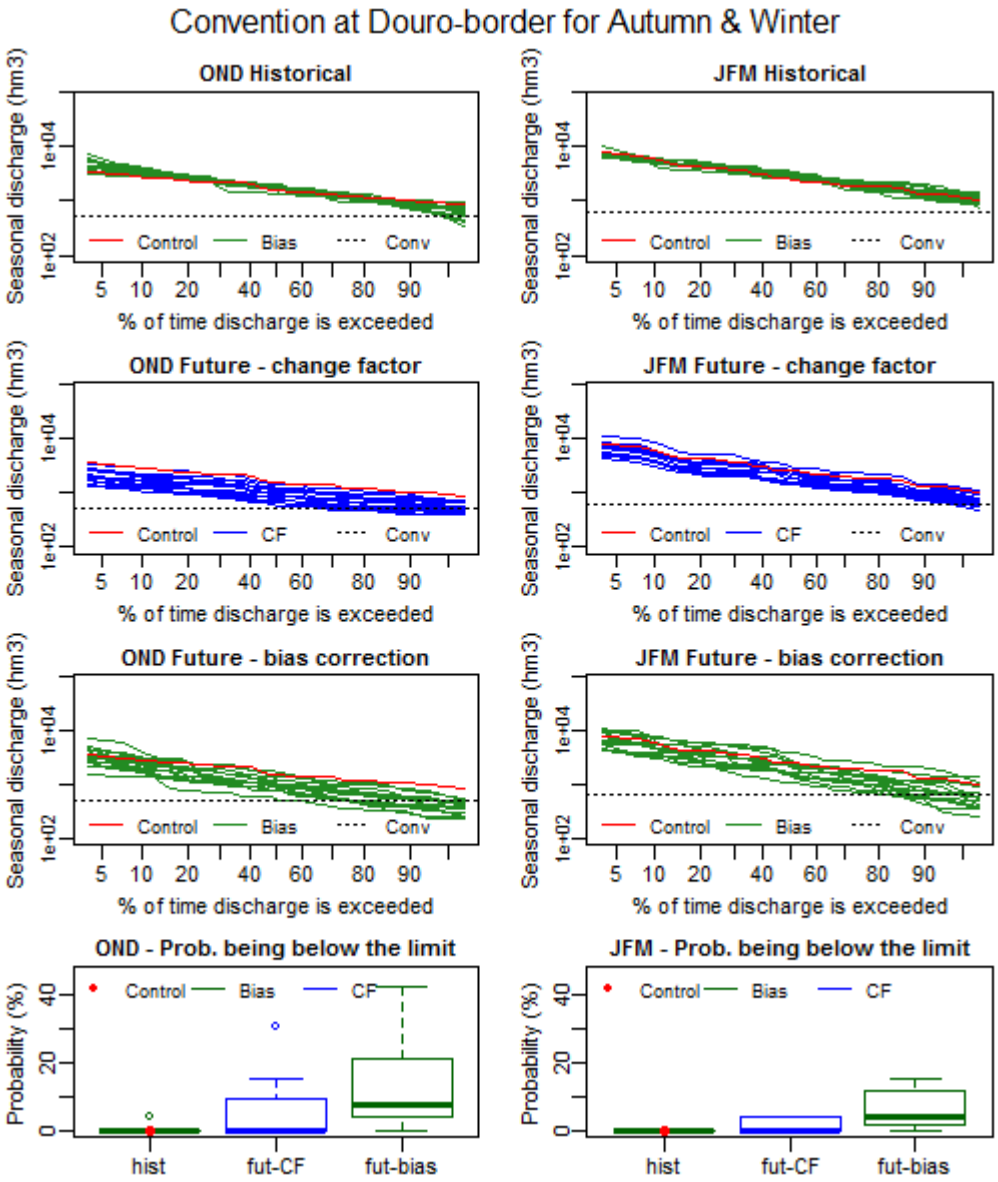

Figure 7.12 – Flow duration curves for Douro-border for historical (1965-1990) seasonal discharge (top) and future seasonal discharge using change factor method (second row) and using the bias correction method (third row). Boxplots of probability of seasonal discharge being below the seasonal Convention limit (bottom). Plots on the left are for autumn (October, November, December) and plots on the right are for winter (January, February and March).

Figure 7.13 shows the FDCs of spring and summer discharge for the Douro-border for historical and future periods and boxplots with the probability of being below the discharge limit. In both seasons, the control run is encompassed by the historical bias corrected runs and never goes below the Convention limit and neither do the bias corrected historical runs.

For spring, some model runs project a small increase in discharges but most models show a decrease. Like in winter, the probability of being below the Convention limit ranges between 0% and 4% for the change factor runs and 0% and 15% for the bias corrected runs.

For summer, all model runs show a decrease in discharge with the probability of being below the Convention limit ranging between 0% and 19% (with most models showing zero

probability) for the bias corrected runs and being always zero for the change factor runs. The seasonal results for the Douro-outlet are similar to the Douro-border results and are presented in Appendix I.

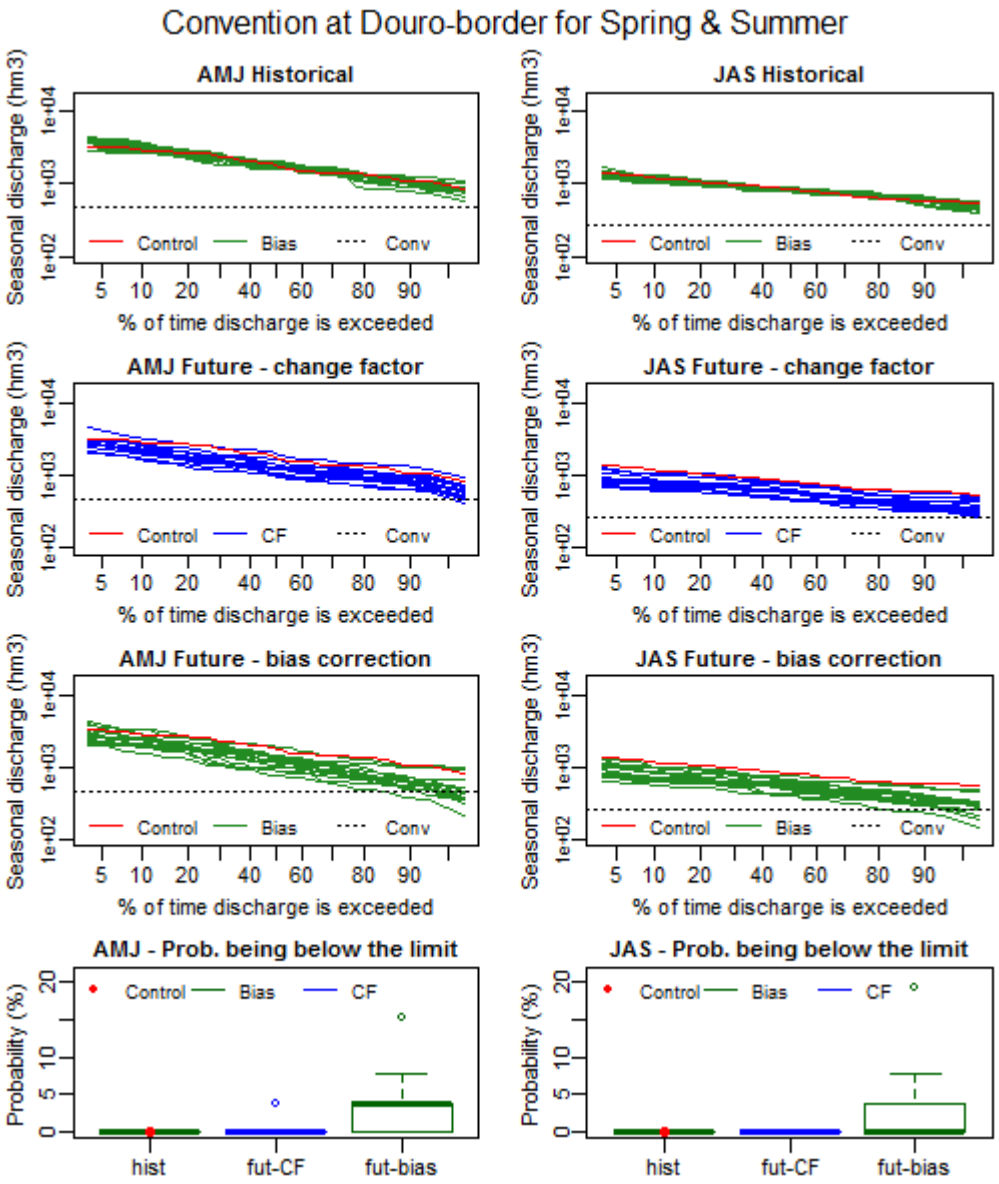

Figure 7.13 – Flow duration curves for Douro-border for historical (1965-1990) seasonal discharge (top) and future seasonal discharge using change factor method (second row) and using the bias correction method (third row). Boxplots of probability of seasonal discharge being below the seasonal Convention limit (bottom). Plots on the left are for spring (April, May, June) and plots on the right are for summer (July, August, September).

7.4.2 *Tagus*

Figure 7.14 shows the FDCs of daily discharge for the Tagus-border and Tagus-outlet. In both gauges, the control run is encompassed by the historical bias corrected runs, which increases the confidence in the SHETRAN bias corrected runs. All but one bias-corrected run show a decrease in medium and low daily future discharges, which is more accentuated in the bias corrected runs.

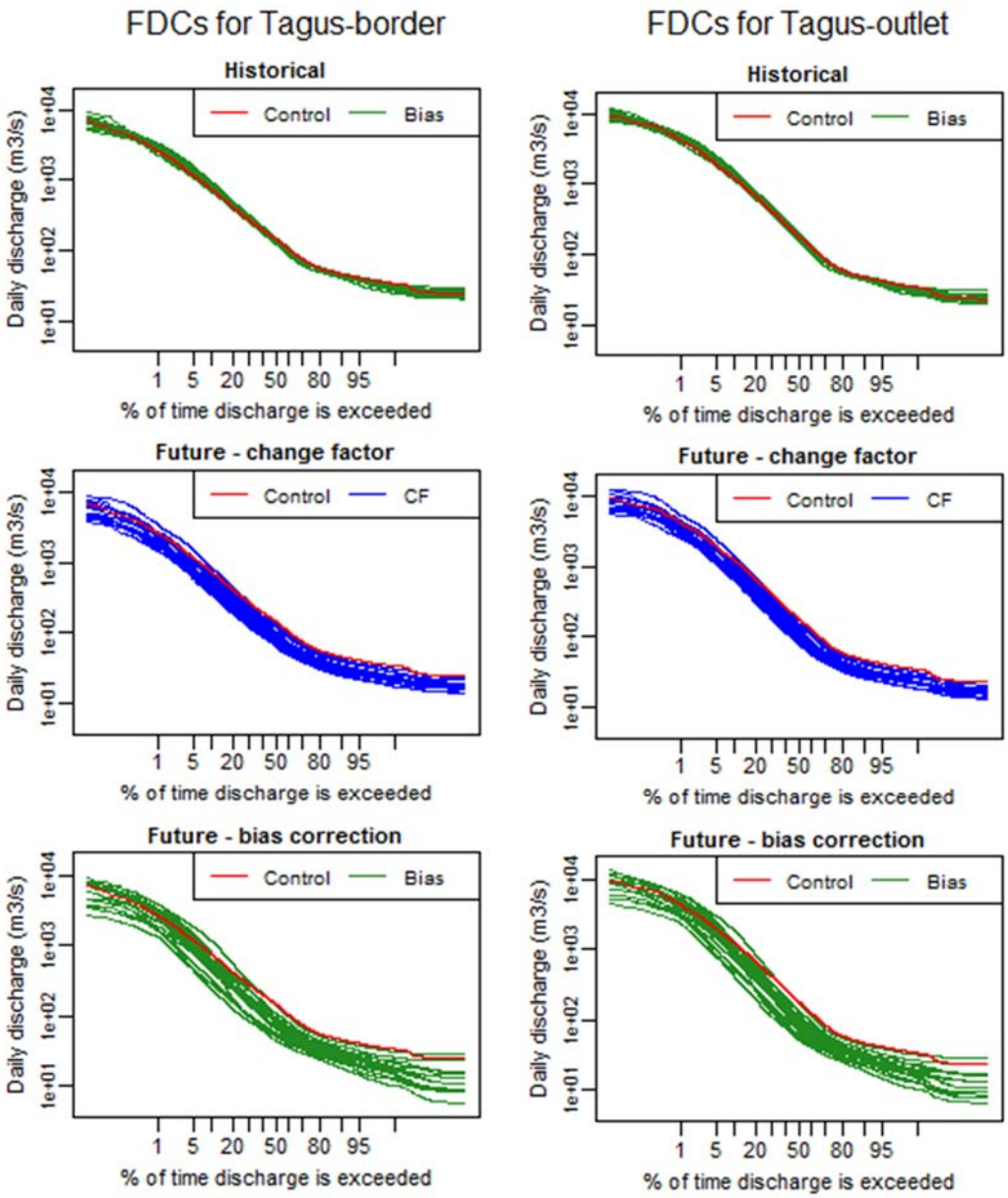

Figure 7.14 – Flow duration curves for Tagus-border (left) and Tagus-outlet (right) for historical (1965-1990) daily discharge (top), future (2045-2070) daily discharge obtained using the change factor method (middle) and future (2045-2070) daily discharge obtained using the bias correction method (bottom). The flow duration curve of daily discharge for the control run (SHETRAN simulation using observed meteorology) was added to the three plots (red line).

Figure 7.15 shows the projected changes in mean seasonal and mean annual discharges for the Tagus, at both the border and outlet gauges and for both change factor and bias corrected

model runs. The spread of results is high but most model runs project a decrease in discharge for all seasons. The most pronounced decreases are in autumn (October-November-December), reaching decreases of around 60%, both at the border and at the outlet gauges. In winter some models show an increase in discharge that can reach up to 65%, but most show a decrease in discharge that can reach -56%. In spring most models show a decrease that can reach -65% and in summer all models show decreases ranging from -50% to -4%. Annual changes range between +32% and -62% for the Tagus-border and between +32% and -60% for the Tagus-outlet.

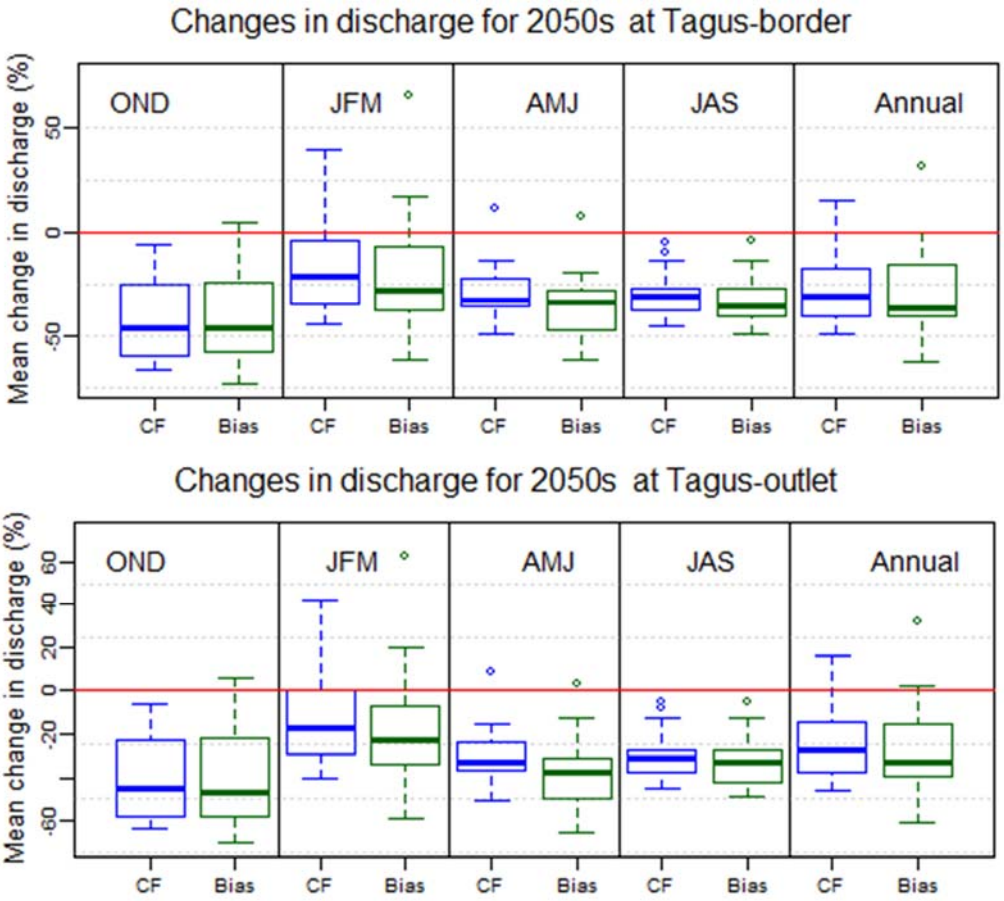

Figure 7.15 – Boxplots of mean change (2045-2070 in relation to 1965-1990) for seasonal and annual discharges for Tagus-border (top) and Tagus-outlet (bottom). Results using the change factor method are shown in blue, while bias-correction results are shown in green.

Figure 7.16 and Figure 7.17 show the FDCs of annual discharge for the Tagus-border and Tagus-outlet for historical and future periods and boxplots with the probability of being below the Albufeira Convention discharge limits. As with the historical daily discharge FDC, in both gauges, the control run is encompassed by the historical bias corrected models runs. Also, most model runs project a decrease in annual future discharges which is more pronounced for the bias corrected runs.

The probability of being below the annual discharge limit set in the convention is zero for the control run in the Tagus-border gauge and ranges between 0% and 16% for the bias historical runs. A marked increase is seen for the future and the probability for the change factor runs ranges between 4% and 28% and for the bias corrected runs ranges between 0% and 48%. For the Tagus-outlet gauge the control run has 4% probability of being below the convention limit, and ranges between 0% and 16% for the bias historical runs. An increase is also seen for the future with the probability of the change factor runs being below the convention limit ranging between 4% and 20% and for the bias corrected runs ranging between 0% and 44%.

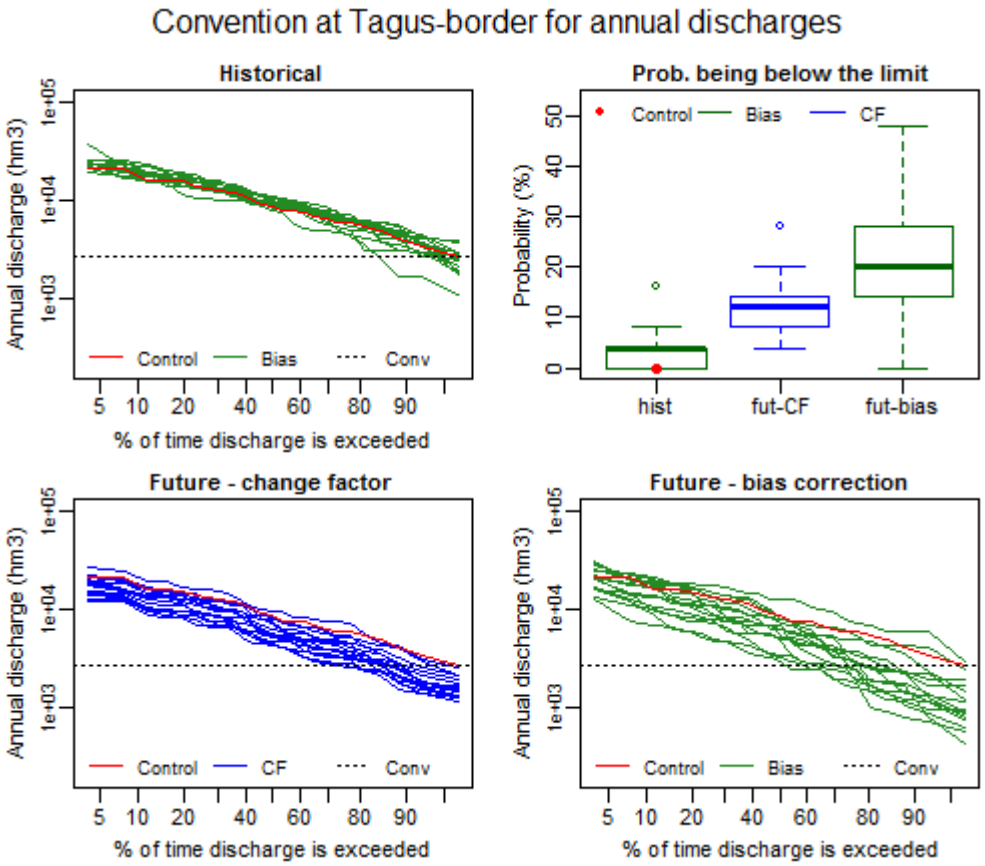

Figure 7.16 – Flow duration curves for Tagus-border for historical (1965-1990) annual discharge (top-left). Probability of annual discharge being below the annual convention limit for bias-corrected historical discharge, control discharge, future discharge using the change factor method and using the bias correction method (top-right). Flow duration curves of annual future discharge (2045-2070) using the change factor method (bottom-left) and using the bias correction method (bottom-right).

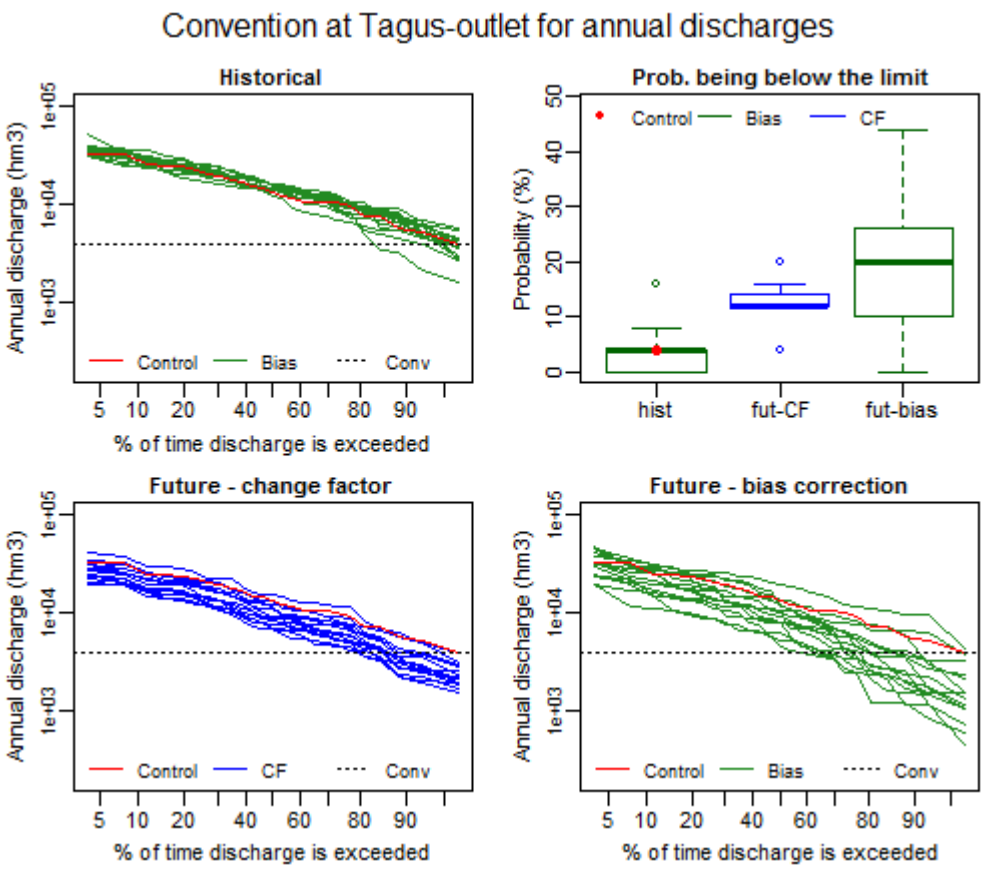

Figure 7.17 – Flow duration curves for Tagus-outlet for historical (1965-1990) annual discharge (top-left). Probability of annual discharge being below the annual convention limit for bias-corrected historical discharge, control discharge, future discharge using the change factor method and using the bias correction method (top-right). Flow duration curves of annual future discharge (2045-2070) using the change factor method (bottom-left) and using the bias correction method (bottom-right).

Figure 7.18 shows the FDCs of autumn and winter discharge for the Tagus-border for the historical and future periods and boxplots with the probability of being below the discharge limit. In both seasons, the control run is encompassed by the historical bias corrected runs and never goes below the convention limit. Also for both seasons, the probability of the historical bias corrected runs being below the limit ranges from 0% to 4%.

For autumn, all the future change factor runs show a decrease in discharge, with the probability of being below the convention limit ranging between 0% and 31% (despite one run showing an increase in some high discharges). For the future bias corrected runs, some simulations show an increase in high discharges. However, most runs show a decrease of medium discharges and all runs show a decrease of low discharges with the probability of being below the convention limit ranging between 0% and 42%.

For winter, some runs show an increase in discharges but most runs still show a decrease. The probability of being below the convention limit in the future ranges between 0% and 8% for the change factor runs and 0% and 15% for the bias corrected runs.

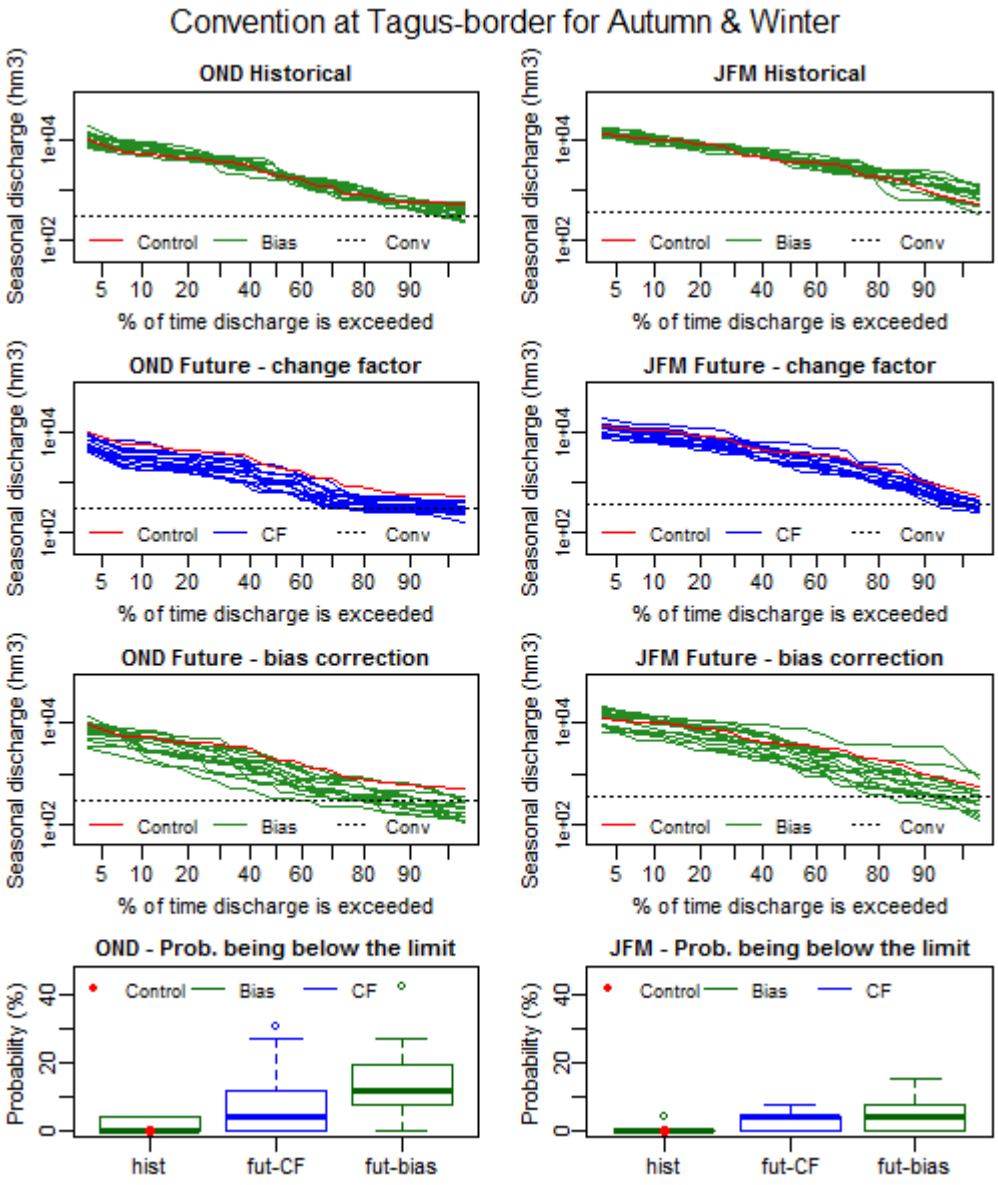

Figure 7.18 – Flow duration curves for Tagus-border for historical (1965-1990) seasonal discharge (top) and future seasonal discharge using change factor method (second row) and using the bias correction method (third row). Boxplots of probability of seasonal discharge being below the seasonal convention limit (bottom). Plots on the left are for autumn (October, November, December) and plots on the right are for winter (January, February and March).

Figure 7.19 shows the FDCs of spring and summer discharge for the Tagus-border for historical and future periods and boxplots with the probability of being below the discharge limit. In both seasons, the control run is broadly encompassed by the historical bias corrected runs. However, in spring, for the lowest discharges the control run has discharges slightly higher than the historical bias corrected runs. Both control and bias historical runs never go below the convention limits for spring or summer.

For spring, all but one change factor run show a decrease in discharge. The probability of being below the convention limit ranges between 0% and 8% for the bias corrected runs and is always zero for the change factor runs.

For summer, all runs show a decrease in discharge. The probability of being below the convention limit ranges between 0% and 12% for the bias corrected runs and is always zero for the change factor runs. The seasonal results for the Tagus-outlet are similar to the Tagus-border results (although the future probabilities of being below the convention discharge limit are higher) and are presented in Appendix I.

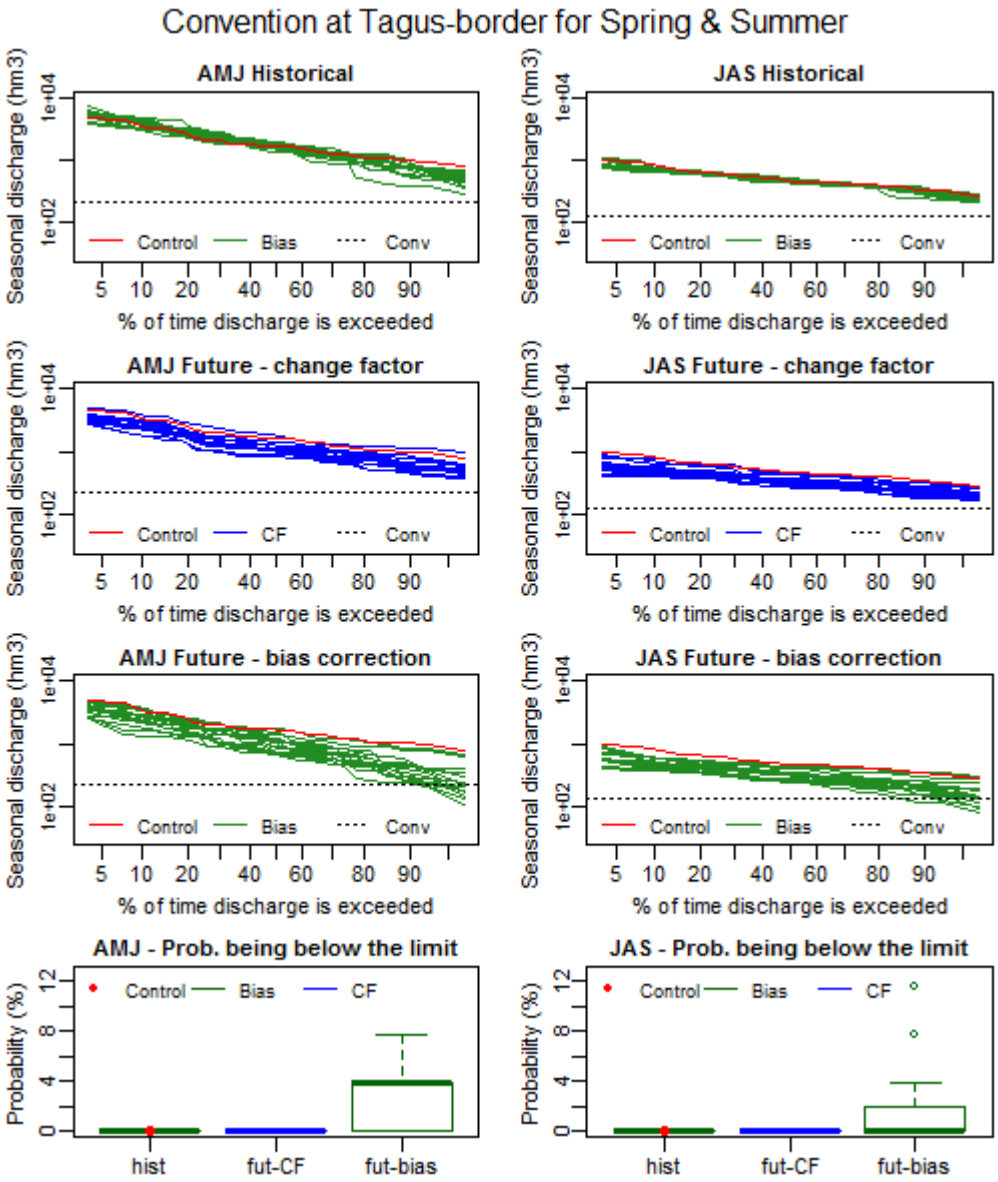

Figure 7.19 – Flow duration curves for Tagus-border for historical (1965-1990) seasonal discharge (top) and future seasonal discharge using change factor method (second row) and using the bias correction method (third row). Boxplots of probability of seasonal discharge being below the seasonal convention limit (bottom). Plots on the left are for spring (April, May, June) and plots on the right are for summer (July, August, September).

7.4.3 *Guadiana*

Figure 7.20 shows the FDCs of daily discharge for the Tagus-border and the Tagus-outlet. In both gauges, the control run is encompassed by the historical bias corrected runs, which increases the confidence in the SHETRAN bias corrected runs. All but one run show a decrease in medium and low daily future discharges, which is more accentuated in the bias corrected runs.

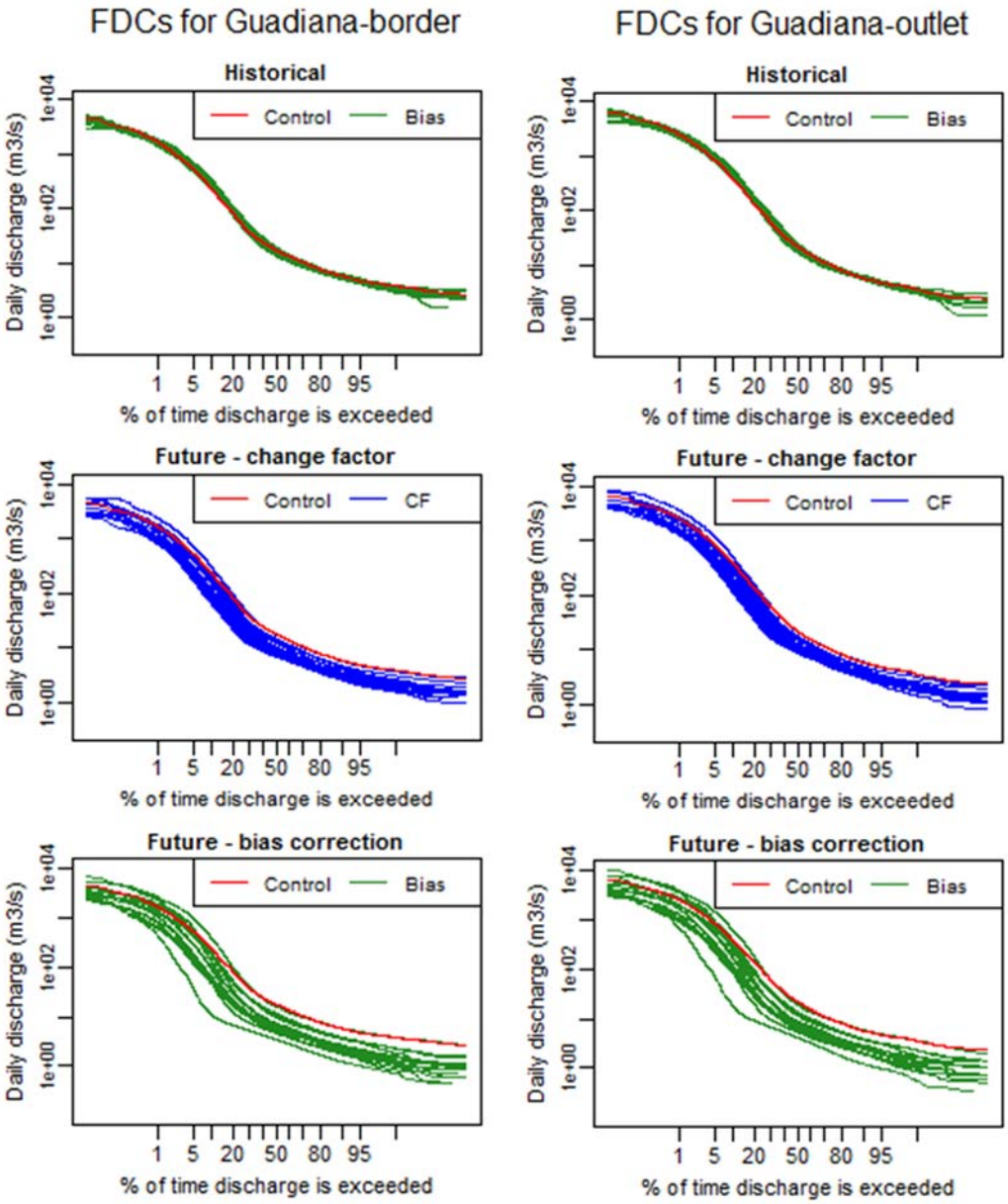

Figure 7.20 – Flow duration curves for Guadiana-border (left) and Guadiana -outlet (right) for historical (1965-1990) daily discharge (top), future (2045-2070) daily discharge obtained using the change factor method (middle) and future (2045-2070) daily discharge obtained using the bias correction method (bottom). The flow duration curve of daily discharge for the control run (historical SHETRAN simulation using observed meteorology) was added to the three plots (red line).

Figure 7.21 shows the changes in mean seasonal and mean annual discharges for the Guadiana, at both the border and outlet gauges and for both change factor and bias corrected

runs. The spread of results is high but most runs project a decrease in discharge for all seasons. The most pronounced decreases are in autumn (October-November-December), reaching a 92% (93%) decrease in discharge at the border (outlet) gauge.

Model 15 is the only one that projects increases in spring, summer and annual discharge for both Guadiana gauges. It also projects winter increases that are significantly higher than all the other models. This can be explained by a significantly higher projected increase in winter rainfall and perhaps also by the small temperature increase projected for all seasons (see Figure 4.8). This model also shows a possibly cyclic rainfall pattern and projects a few decades of high rainfall around 2050 for winter (see Figure G.13 in Appendix G).

In winter a few runs show an increase in discharge that can reach up to 91% (8% without model 15), but most show a decrease in discharge that can reach -78%. In spring (summer) all runs except model 15 show a decrease in discharge that can reach up to -88% (-70%). Annual discharge changes range between +33% (-2% without model 15) and -82% for Guadiana-border and between +66% (-2% without model 15) and -82% for Guadiana-outlet.

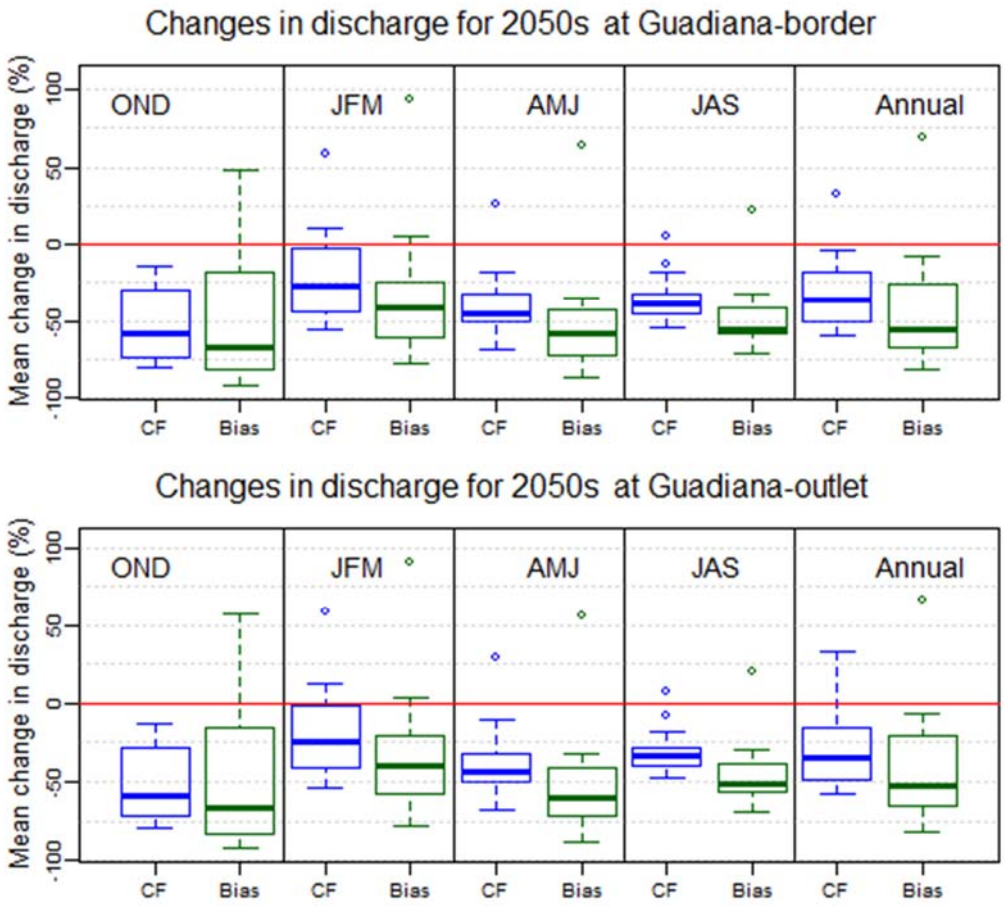

Figure 7.21 – Boxplots of mean change (2045-2070 in relation to 1965-1990) for seasonal and annual discharges for Guadiana-border (top) and Guadiana-outlet (bottom). Results using the change factor method are shown in blue, while bias-correction results are shown in green.

Figure 7.22 show the FDCs of annual discharge for the Guadiana-border for historical and future periods and boxplots with the probability of being below the discharge limit. Guadiana-outlet does not have annual discharge limits defined in the Albufeira convention so it was not analysed. As with the historical daily discharge FDCs, the control run of Guadiana-border is encompassed by the historical bias corrected runs. Most runs show a decrease in annual future discharges which is more pronounced for the bias corrected runs.

The probability of being below the annual discharge limit set in the convention is 4% for the control run and ranges between 0% and 20% for the bias historical runs. A marked increase is seen for the future with the probability for the change factor runs ranging between 8% and 48% and for the bias corrected runs between 4% and 76%.

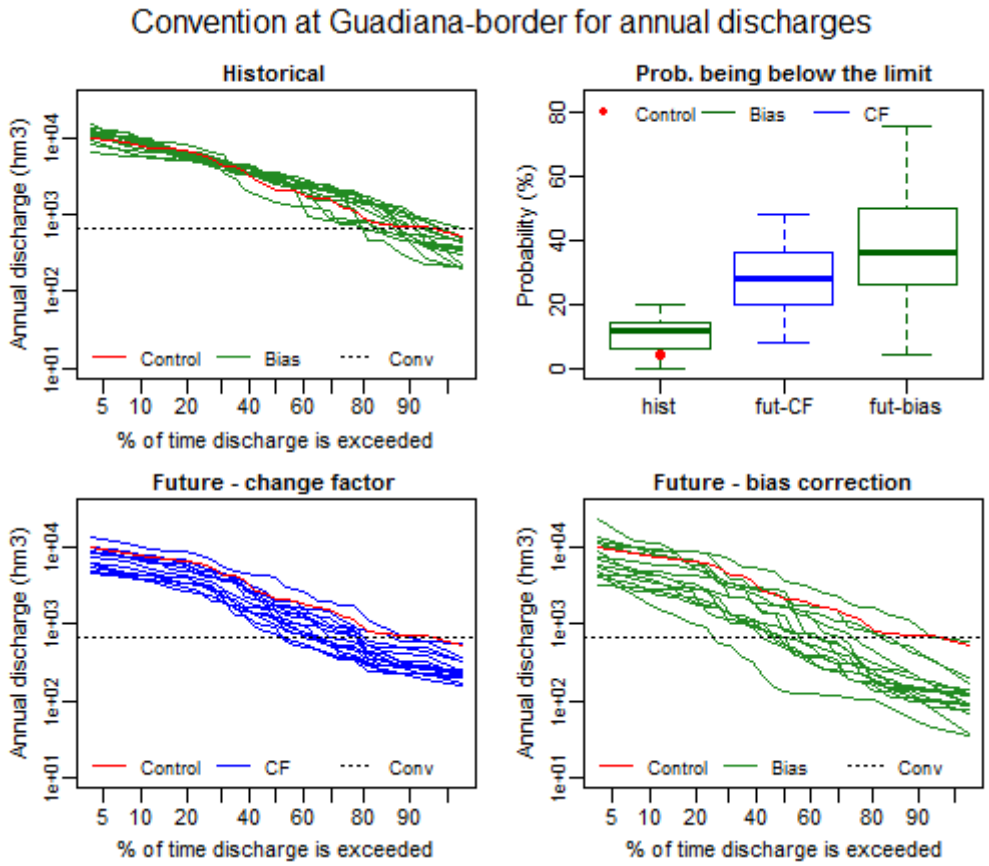

Figure 7.22 – Flow duration curves for Guadiana-border for historical (1965-1990) annual discharge (top-left). Probability of annual discharge being below the annual convention limit for bias-corrected historical discharge, control discharge, future discharge using the change factor method and using the bias correction method (top-right). Flow duration curves of annual future discharge (2045-2070) using the change factor method (bottom-left) and using the bias correction method (bottom-right).

Figure 7.23 shows the FDCs of autumn and winter discharge for the Guadiana-border for the historical and future periods and boxplots with the probability of being below the discharge limit. In both seasons, the control run is encompassed by the historical bias corrected runs.

For autumn, the probability of being below the convention limit is 12% for the control run and ranges between 0% and 27% for the historical bias corrected runs. All the future change factor runs show a decrease in discharge with the probability of being below the convention limit ranging between 19% and 58% (despite one run showing an increase of some high discharges). For the future bias corrected, some runs show an increase in high discharges. However, most runs show a decrease of medium discharges and all runs show a decrease of low discharges with the probability of being below the convention limit ranging between 8% and 81%.

For winter, the probability of being below the convention limit is zero for the control run and ranges between 0% and 12% for the historical bias corrected runs. Some runs show an increase in discharges but most runs show a decrease. The probability of being below the convention limit ranges between 0% and 15% for the change factor runs and 0% and 58% for the bias corrected runs.

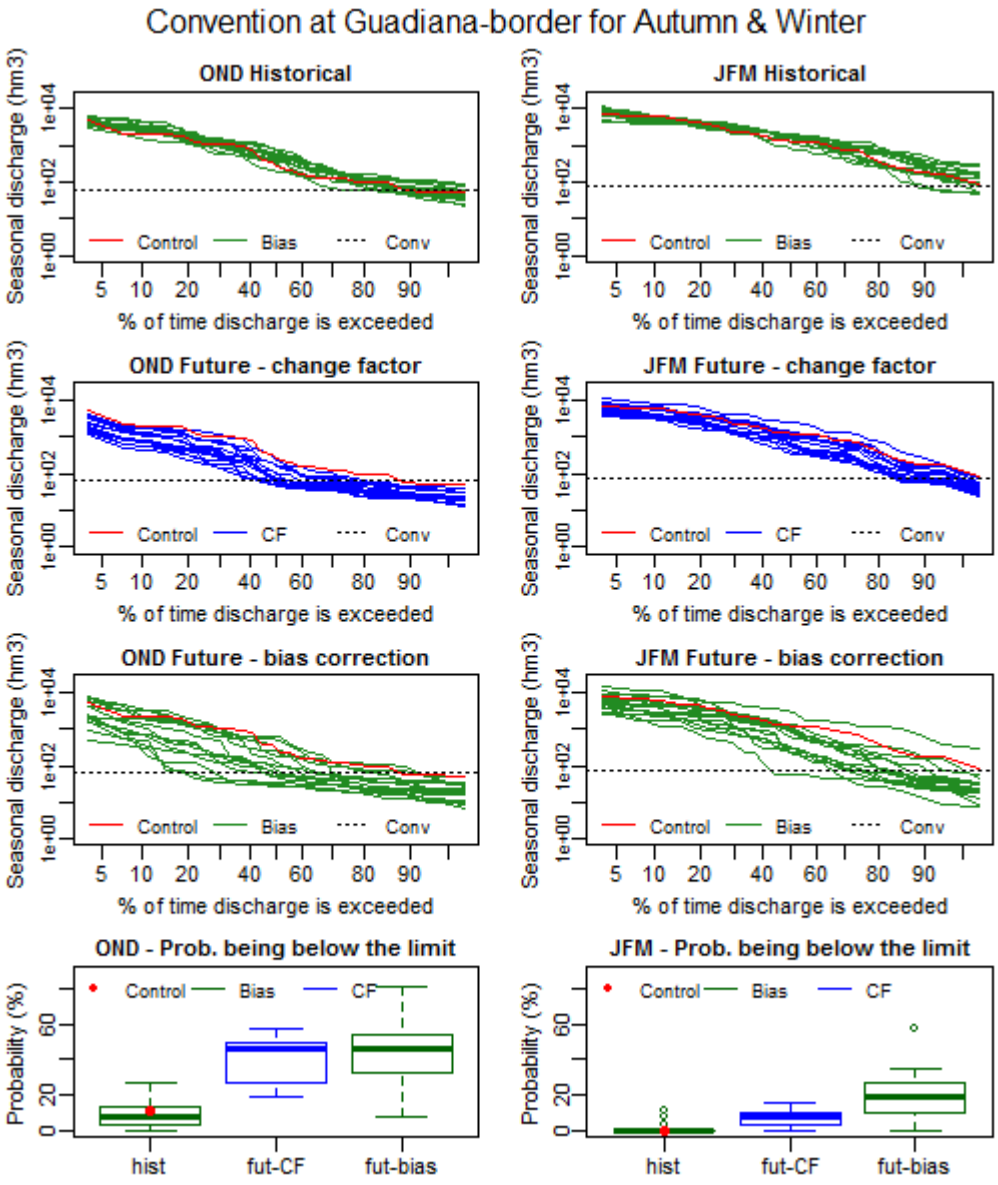

Figure 7.23 – Flow duration curves for Guadiana-border for historical (1965-1990) seasonal discharge (top) and future seasonal discharge using change factor method (second row) and using the bias correction method (third row). Boxplots of probability of seasonal discharge being below the seasonal convention limit (bottom). Plots on the left are for autumn (October, November, December) and plots on the right are for winter (January, February and March).

Figure 7.24 shows the FDCs of spring and summer discharge for the Guadiana-border for historical and future periods and boxplots with the probability of being below the discharge limit. In both seasons, the control run is broadly encompassed by the historical bias corrected runs. However, in spring, for the lowest discharges the control run has discharges slightly higher than the historical bias corrected runs. Both control and bias historical runs never go below the convention limits for spring while in summer the probability ranges between 0% and 4%.

For spring, all but one change factor run (model 15) project a decrease in discharge. The probability of being below the convention limit ranges between 0% and 58% for the bias corrected runs and is always zero for the change factor runs.

For summer, all runs except model 15 show a decrease in discharge. The probability of being below the convention limit ranges between 0% and 54% for the change factor runs and ranges between 0% and 100% for the bias corrected runs. Summer discharge simulated using bias corrected rainfall and PET from model 8 are always below the convention limit.

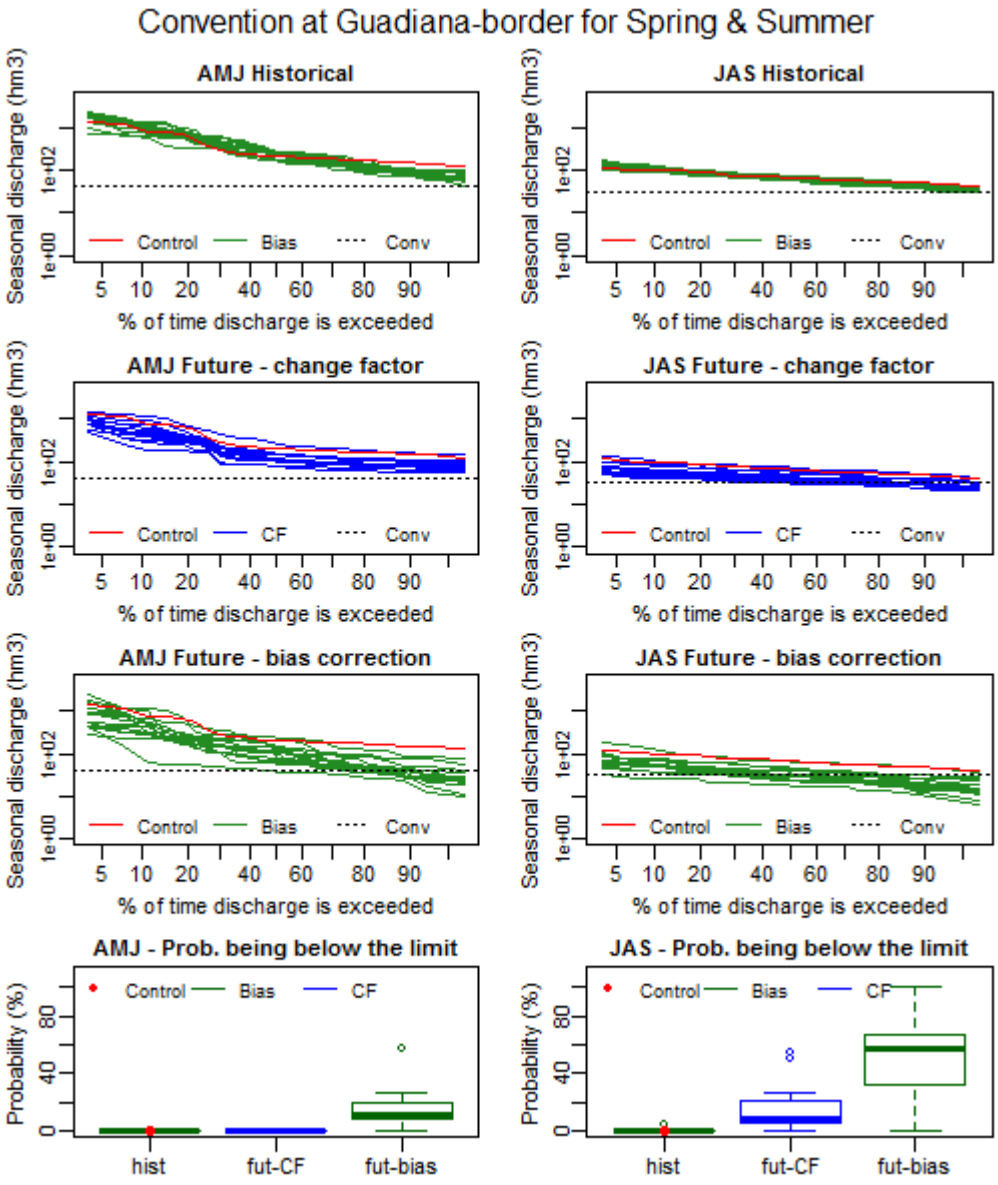

Figure 7.24 – Flow duration curves for Guadiana-border for historical (1965-1990) seasonal discharge (top) and future seasonal discharge using change factor method (second row) and using the bias correction method (third row). Boxplots of probability of seasonal discharge being bellow the seasonal convention limit (bottom). Plots on the left are for spring (April, May, June) and plots on the right are for summer (July, August, September).

7.5 Discussion and conclusions

In this chapter, the SHETRAN simulation results for historical (1965-1990) and future (2045-2070) periods were analysed. The historical (naturalized) SHETRAN runs were compared with observed discharges. In terms of annual discharges, the temporal evolution of simulated and observed discharges for the three basins were as expected. As were the order of magnitude of the differences between observed and simulated discharges. In terms of monthly flows, the performance of the simulations was also good. However, some low flows might perhaps be too low in the SHETRAN simulations, especially in the Tagus.

Looking at the evolution between historical and 2050s daily discharges, all models show a decrease in the medium and low discharges (except model 15 for the Tagus and the Guadiana). Most models also show a decrease of high daily discharges, but others show increases. Comparing rainfall downscaling methods, the spread of results is wider with bias corrected runs than with the change factor runs.

Climate model 15 is the only one that projects substantial increases in mean annual discharge (in all basins and for both downscaling methods). It is also the model projecting the highest discharges for winter, spring and summer in all basins. This model has a possibly cyclic rainfall behaviour and does not show significant long term trends (1961-2100) for annual rainfall in any of the basins (see section 4.4.3). However, in all basins, the 30 year period of the 2050s just happens to coincide with a period of high annual rainfall within its possibly cyclic behaviour (see figures G.1, G.6 and G.11 in Appendices). The same is also seen in winter rainfall (Figure G.3, Figure G.8 and G.13) but not in other seasons. This explains the distinct behaviour of model 15 in terms of winter discharges and the impact of very high winter rainfall is also felt in spring and summer discharges but not in autumn discharges, where model 15 does not have a distinct behaviour.

The range of results for mean change in seasonal and annual discharge is high (see Table 7.7) but most runs show a decrease for all seasons in all basins. Most models also showed decreases in the mean annual discharge, which ranged between -52% to +25% for Douro-outlet, -60% to +32% for Tagus-outlet and -82% to +68% for Guadiana-outlet (-82% to -3% without model 15). The most pronounced seasonal discharge decreases are in autumn (October-November-December) when almost all models project decreases for all basins. These can reach -61% for the Douro, -71% in the Tagus, and -92% for the Guadiana.

In winter some runs show an increase in discharge and model 15 shows particularly high discharge increases using the bias corrected method: 51% in the Douro, 65% in the Tagus and

91% in the Guadiana. Nonetheless most models still project mean winter discharge decreases, which can reach -50% in the Douro, -56% in the Tagus and -78% in the Guadiana.

In spring, all runs except model 15 show decreases in mean seasonal discharge that can reach -59% in the Douro, -65% in the Tagus and -86% in the Guadiana. In summer all runs show decreases in discharge (except model 15 for the Guadiana) reaching -51% in the Douro, -49% in the Tagus and -71% in the Guadiana. The range of all changes in mean discharge is presented in Table 7.7.

Table 7.7 – Range of seasonal and annual changes (%) in mean discharge (2045-2070 in relation to 1965-1990) at Douro-outlet, Tagus-outlet and Guadiana-outlet. Results are shown for both the change factor (CF) method and the bias-correction (bias) method. When model 15 shows outlier behaviour the range is shown for the other 14 models and the projected change for model 15 is shown in brackets.

		Douro		Tagus		Guadiana	
		max	min	max	min	max	min
Annual	CF	-42	-3 (14)	-46	-4 (16)	-60	-3 (33)
	Bias	-52	2 (25)	-60	2 (32)	-82	-7 (68)
OND	CF	-60	-5	-64	-6	-80	-14
	Bias	-61	10	-71	6	-92	48
JFM	CF	-37	9 (39)	-41	10 (42)	-56	10 (59)
	Bias	-50	21 (51)	-59	20 (63)	-78	5 (93)
AMJ	CF	-45	-12 (7)	-51	-15 (9)	-68	-18 (26)
	Bias	-59	-9 (2)	-65	-13 (4)	-86	-34 (64)
JAS	CF	-46	-7	-45	-5	-54	6
	Bias	-51	-8	-49	-6	-71	23

Results were also analysed for the annual and seasonal convention discharge limits for the border gauges of the three rivers (see Table 7.8). Starting with the limits for annual discharge, for the border gauges of the Douro and the Tagus the control run never goes beneath the annual discharge set in the convention. For the Guadiana-border gauge there is a 4% chance of being below the annual discharge limit for the control run. The historical bias corrected runs for the three basins are all between 0% and 20% chance of being bellow their respective limit. The future probability ranges of being below the annual convention discharge limits are substantially higher for the three basins, being higher for the bias corrected runs and for the Guadiana where they range from 4% to 76% (between 0% and 68% for the Douro and 0% and 48% for the Tagus).

Table 7.8 – Historical and future probability (%) of being below the Albufeira Convention discharge limits for annual and seasonal discharges at the border gauges of the Douro, Tagus and Guadiana rivers. Results are shown for both the change factor (CF) method and the bias-correction (bias) method.

		Douro		Tagus		Guadiana	
		historical	2050s	historical	2050s	historical	2050s
Annual	CF		0-40		4-28		4-48
	Bias	0-12	0-68	0-16	0-48	0-20	4-76
OND	CF		0-31		0-31		19-58
	Bias	0-4	0-42	0-4	0-42	0-27	8-81
JFM	CF		0-4		0-8		0-15
	Bias	0	0-15	0-4	0-15	0-12	0-58
AMJ	CF		0-4		0		0
	Bias	0	0-15	0	0-8	0	0-58
JAS	CF		0		0		0-54
	Bias	0	0-19	0	0-8	0-4	0-100

In terms of seasonal discharges, the bias corrected runs produce lower discharges than the change factor runs. Most change factor runs show decreases in seasonal discharges for all basins (in many cases all runs show decreases). In the bias corrected runs some models show increases in the high discharges but generally all models show decreases in medium and low discharges. However, in summer all bias corrected runs (except model 15 in the Tagus and Guadiana) show decreases in all discharges.

For the historical bias corrected runs and for the control runs, the probability of being below the convention limit for seasonal discharge varies between 0% and 4%, except for the Guadiana in autumn (0-27%) and in winter (0-12%). For future autumn discharges this probability ranges from 0% to 42% for the Douro and the Tagus and 8% to 81% for the Guadiana. For other seasons the probability of being below the convention limits are relatively low for the Douro and the Tagus (always below 19%) but for the Guadiana they range between 0% and 58% for the winter and spring and 0% and 100% for the summer. The 100% corresponds to model 8, whose summer discharges range between 6.5 hm^3 and 30.9hm^3 (with the convention limit being 32hm^3).

Most models project decreases in daily, seasonal and annual discharges for all basins, especially for medium and low discharges. Some models project increases in high discharges, especially for winter. However the model showing the highest increases does so because of a possibly cyclic rainfall behaviour, not a significant increasing rainfall trend. The magnitude of the decreases in discharge varies significantly throughout the seasons and basins, partly due to the high natural inter-annual variability of the region and partly due to the spread in rainfall and temperature future projections of the different climate models. However autumn is the

season showing the biggest decreases in discharge throughout the models and the Guadiana is the basin consistently presenting the biggest discharge reductions and the higher future probabilities of being below the convention limit.

Chapter 8. Conclusions

Throughout the previous chapters the possible impacts of climate change on the water resources of the international rivers Douro, Tagus and Guadiana were studied. The earlier chapters set the context of the problem and have shown the impact of high inter-annual rainfall variability when analysing long-term changes.

In view of the wide range of future changes projected by different climate models, the uncertainty associated with each climate model and the lack of an agreed method for selecting models, an attempt was made to select a few models that convey the entire range of future climate projections available from CMIP5 RCP8.5.

Possible ways of presenting the results were discussed in Chapter 4. Averaging the results of climate models showing significantly different future projections can lead to physically implausible results due to smoothing of spatially heterogeneous patterns (Knutti, 2010). Also, the use of probability density functions (PDF) is based on assumptions that are not met in a multi-model ensemble (like the CMIP5), where models share process representations and/or calibrations on particular datasets (Knutti *et al.*, 2010a), the sampling of models is not random or systematic (Knutti, 2010) and it is hard to verify (or falsify) that the ensemble spans the full uncertainty range (Masson and Knutti, 2011). Therefore, the results in this thesis were not presented as means or as PDFs, but as ranges in order to present a range of plausible outcomes that can be used to test different adaptation strategies.

In an ideal world, climate model outputs could be used directly to analyse future changes in rainfall or temperature or to run hydrological models. However, due to their spatial scale and their intrinsic biases, downscaling and bias-correction must be performed. The different methods available to do so have advantages and disadvantages, and in this study two methods (change factor and bias correction through empirical quantile mapping) were used in order to assess the impact of the choice of method on the final results.

Future projections for rainfall, drought and discharge were analysed. For future rainfall, a 30 year time-slice approach was compared with a transient approach. Two drought indices (DSI-12 and SPI-12) were used to assess drought evolution from 1961 to 2100. A spatially distributed, physically-based, hydrological modelling system (SHETRAN) was used to provide historical (1965-1990) and future (2045-2070) discharges. The main conclusions for future rainfall, drought and discharge are presented in the next three sub-sections. Then, the main conclusions of the thesis are discussed and lastly, possible future research directions are presented.

8.1 Future rainfall

There was considerable spread within model projections for mean future rainfall changes, in agreement with what was found in both the Portuguese and the Spanish national climate change impact studies (Santos *et al*., 2002; Brunet *et al*., 2009). However, the two downscaling methods used in this thesis to assess projected mean monthly changes produced similar results, although the bias correction method showed a larger inter-model range than the change factor method.

The majority of models projected a reduction in rainfall in the three basins for the 2050s for annual rainfall (for both downscaling methods). The range of projected changes to annual rainfall was between -33% and +7% in the Douro, -33% and +10% in the Tagus and -41% and +10% in the Guadiana. The majority of models also projected a reduction in rainfall for all months in the three basins (except December in the Douro and the Tagus when using the bias correction method). And almost all models projected rainfall decreases for the spring (up to -43% for the Douro, -40% for the Tagus and -36% for the Guadiana) and autumn months (-56% for the Douro, -54% for the Tagus and -51% for the Guadiana).

In terms of long-term trends (1961-2100) there were no significant positive projected trends in annual rainfall or in any season except winter (DJF) where most models projected no significant trend. In spring (MAM) and autumn (SON) the majority of models showed negative projected trends that reach -6% per decade in the Douro and -7% per decade in the Tagus and the Guadiana. Annual projected changes ranged between -5% (-6%) and no significant change for the Douro and the Tagus (Guadiana).

The transient approach (linear trends between 1961-2100) showed that a considerable part of the climate model disagreement in the projection of future rainfall changes when using the time-slice approach (changes between 1961-1990 and 2041-2070) was due to the choice of 30-year intervals within natural cyclic patterns of rainfall.

8.2 Future drought

It was shown that SPI-12 is not an appropriate index to use in the Douro, Tagus and Guadiana basins. This is due to problems in choosing and fitting distributions to aggregated monthly rainfall which lead to a very low probability of low rainfall amounts, which in term leads to very low SPI-12 values indicative of extremely intense droughts.

Using DSI-12, most models overestimate the duration /severity of droughts for the historical period (1961-2003).The 15 models display a big range of future drought projections when using both DSI-12 and SPI-12 . Some show small increases in drought conditions while others project decades of extreme drought conditions reaching up to 800% accumulated precipitation deficit. However, all models are projecting an increase in drought conditions for the future with most models showing a substantial worsening of drought conditions.The most extreme drought projections were from models that had simulated droughts that were too severe in the historical period (models 8 and 9). However extreme future drought conditions (reaching up to 500% accumulated precipitation deficits) were also projected by models that performed well in all basins during the historical period (models 1 and 2).

In terms of the percentage of the basin in severe and extreme drought, using DSI-12, all models show increases. Models 4, 7, 10 and 15 showed small increases while all other models showed substantial increases in drought area. By the end of the century, models 1, 2, 8, 9, 11, 13 and 14 projected that, on average, more than half of the each basin's area will be experiencing severe or extreme drought. The percentages of the basin in drought for the Guadiana are slightly higher than for the more northern basins.

8.3 Future discharge

For annual discharge, the temporal evolution of the simulated (control run) and observed/measured discharges for the three basins was as expected (similar behaviour despite the differences in magnitude), as were the order of magnitude of the differences between observed and simulated discharges. The performance of the simulations in terms of monthly flows was also good; however, some simulated low flows might perhaps be too low, especially in the Tagus.

The range of future projections (2050s) for the mean change in seasonal and annual discharge is high but most runs showed a decrease for all seasons in all basins. In the three basins, climate model 15 is the only one which showed substantial increases in mean annual discharge and is also the model which projected higher discharges for winter, spring and summer.

Most runs showed decreases in annual future discharges which are more pronounced for low discharges and for the bias corrected runs in all basins. Most runs also showed decreases in the mean annual discharge, which ranged between -52% to +25% for Douro-outlet, -60% to +32% for Tagus-outlet and -82% to +68% for Guadiana-outlet (-82% to -3% without model 15). As mentioned before, Kilsby *et al.* (2007) was the only study found that assessed the impacts of climate change in the discharges of the Tagus and Guadiana (although using just one climate model and a conceptual rainfall-runoff routing model) and no studies were found for the Douro. Nevertheless, Kilsby *et al.* (2007) found reductions in discharge (-21% to -26% for the Guadiana and -49% to -20% for the Tagus) that are within the range of changes found in this study. Nevertheless, the present study showed the substantial increase in the range of future discharge projections that arises from using several climate models and downscaling techniques.

The probability of flow being below the annual discharge limit set in the Albufeira Convention for the historical bias corrected runs of the three basins is simulated as between 0% and 20%. The simulated future probabilities are substantially higher for the three basins, being higher for the bias corrected runs and for the Guadiana where they range from 4% to 76% (between 0% and 68% for the Douro and 0% and 48% for the Tagus).

The most pronounced decreases in seasonal discharge are in autumn (October-November-December) when almost all models projected decreases for all basins. These can reach up to -61% for the Douro, -71% in the Tagus, and -92% for the Guadiana.

In winter, some models showed an increase in mean seasonal discharge but most models still projected decreases in mean winter discharge. In spring, all models except model 15 showed

decreases in mean seasonal discharge and in summer all models showed decreases in discharge (except for model 15 for the Guadiana).

For the historical bias corrected runs and for the control runs, the probability of flows being below the convention limit for seasonal discharge was found to vary between 0% and 4%, except for the Guadiana in autumn (0-27%) and in winter (0-12%). For future autumn discharges this probability increased and ranged from 0% to 42% for the Douro and the Tagus and 8% to 81% for the Guadiana. For other seasons the probability of discharges being below the convention limits were found to be relatively low for the Douro and the Tagus (always below 19%) but for the Guadiana they ranged between 0% and 58% for the winter and spring and 0% and 100% for the summer.

The substantial increases of the probability of flows being below the convention limit for annual discharges and autumn discharges in the three basins (and in the Guadiana for all seasonal discharge) has strong implications for the validity of the convention for the future. These results should lead to a discussion of future water use and allocations between the two countries and subsequently to a revision of the convention.

8.4 Discussion and general conclusions

The universal issue affecting all the different methods of assessing future changes in water resources used in this study was the spread of the GCM projections for the region. Different GCMs project different possible futures; for example, climate model 15 shows a possibly cyclical rainfall behaviour (where the 30-year period of the 2050s happens to coincide with a period of high annual rainfall), while model 8 projects severe rainfall reductions in all seasons and all basins (around 6% rainfall reduction per decade). This spread in rainfall behaviour leads to different results in terms of projections of changes to future drought and future discharge.

The issue of the "cascade of uncertainties" in climate change impacts studies and identification of the main contributors to the overall uncertainty is frequently discussed (Wilby and Harris, 2006; Prudhomme and Davies, 2009; Kay et al., 2009; Arnell, 2011; Teng et al., 2011 *in (Coron et al., 2012)*. However, in Iberia, the spread of climate model projections dwarfs the uncertainties arising from the use of two different downscaling methods, or even the method chosen to analyse the future (different drought indices or a hydrological model).

It could be argued that, detailed hydrological modelling is not justified due to the wide range of GCM rainfall projections for the area. However, the use of simple drought indices like the DSI and the SPI do not provide information about future changes in discharge, so when this information is necessary a more complex methodology must be used. Another possible method for assessing changes in discharge would be to calculate a regression between observed rainfall and discharge, but physical changes in the future might make these relations invalid. A "hybrid" method, where this regression is underpinned by hydrological modelling is discussed in section 8.5 and will be pursued in the future. This would allow other rainfall projections for the area to be taken into account without re-running the hydrological model.

To further complicate the issue, the high inter-annual rainfall variability of the region means that the selection of a specific 30-year time-period can be a crucial factor in influencing the results. This was shown in the analysis of trends in the observed rainfall where the start and end date of the analysis is critical, and is also responsible for the outlier behaviour of model 15 in terms of rainfall and discharge projections for the 2050s. However, if the disagreement between projections for the 2050s is interpreted as a superimposition of model errors, long-term change and the cyclical patterns of rainfall due to natural variability, it then provides an estimate of the minimum range of future changes that should be considered for adaptation studies.

No model projects significant long term increases in rainfall or annual discharge and all of them project increases in drought conditions. There is therefore a general agreement, between the different methods used, in the sign of change, i.e., a move to drier conditions. However, future projections range from small or non-significant changes, to large reductions in rainfall, droughts unlike any recorded in the area and discharge reductions that would be incompatible with present land use, especially in the Guadiana.

Only in winter is there a disagreement between climate model projections in terms of the signal of rainfall trends (1961-2100). Furthermore, most models project drier springs, summers and autumns which result in greater discharge reductions being felt in autumn. Even assuming an increase in winter rainfall (which is projected by models 10 and 15 for the Douro and by model 10 for the Tagus), this lengthening of the dry season could have serious implications for agriculture, water supply and forest fires in the region. If, however, winter rainfall does not change or decreases (or its inter-annual variability increases as projected by model 15) the hundreds of dams in the region may no longer be the pivotal water resources management asset they are at present and serious water scarcity problems will arise.

If the uncertainties in future projections were small it would be easier to plan adaptation measures. However the large uncertainties in climate projections cannot lead to inaction for the enormity of the possible impacts in the middle and worst-case scenarios, and the fact that probabilities cannot be associated with any of the models' projections, means that adaptation to drier futures must be considered a priority. This would, in any case, improve the resilience of the region to present day drought, which would be an important positive outcome even if the best case scenario materializes.

Therefore, possible measures to adapt to drier futures need to be researched. Better solutions, especially for source/supply measures and for water transfer, could be achieved through Integrated River Basin Management involving both Portugal and Spain, and the Albufeira Convention could be seen as a starting point. Demand side approaches would be more robust to a possible regime shift to a drier climate. Since irrigation is the largest water use in these basins (above 90% of water consumption in the Spanish Douro and Guadiana – see Table 7.5), more efficient irrigation techniques like drip irrigation should be incentivise. According to Baldock *et al.* (2000) drip irrigation accounts for only 17% of irrigation in Spain, the rest being gravity irrigation (furrows and flooding - 60%) and sprinklers (24%), while in Portugal the irrigation is still mainly by gravity with both sprinklers and drip systems increasing. Efficiency in domestic consumption could also be pursued and, at least in Portugal, water losses in the water supply network should be improved. The Portuguese water regulator points out that

water loses in the system are one of the main sources of inefficiency (Baptista, 2014), despite an improvement in the last few years from 40% losses to 25% (Magalhães and Bessa, 2012).

Previous climate change studies that focus on hydrological impacts on the transnational basins of the Douro, Tagus or Guadiana basins are virtually non-existent, therefore all the results of this thesis can be considered "new findings". The exception is the Kilsby et al. (2007) paper on the hydrological impacts of climate change on the Tagus and the Guadiana rivers. However, this study was done with just one climate model and a conceptual rainfall-runoff routing model. At national level, Portugal has a climate impact study using change factors from five climate model runs, but only very small national hydrological basins were modelled and only a lumped hydrological model with a monthly step was used. Spain has a national climate impact study using several climate models and different downscaling techniques but no hydrological modelling. Therefore, this thesis has extended previous work in several important aspects:

- by using more up-to-date climate model outputs;
- by selecting climate model outputs that sampled the entire range of future climate projections available from CMIP5 RCP8.5;
- by being the first study to analyse projections of future drought in the Douro, Tagus and Guadiana basins;
- and by modelling these three basins using a spatially distributed, physically-based, hydrological model for the first time.

8.5 Basin water balance relationships

A powerful way to synthesise the work performed for this thesis, which was not pursued in detail due to time constraints, is to analyse basin water balance by presenting the relationship between basin-average annual discharge and annual rainfall, and its variation between the historical regime and different climate projections. The averaging incorporated in such an analysis of course hides several critical heterogeneities, in spatial variation in rainfall and runoff, as well as in seasonal variation of rainfall and discharge. This renders the analysis unsafe for use with historical data for the purpose of prediction of discharge given an estimate of future rainfall. However, if such an analysis is carried out using the model outputs from this thesis, it is underpinned by the space and time distributed modelling and provides a powerful means of assessing natural and model variability and potentially a very simple and fast means of estimating future resource. Plotting data in this way (see Fig 8.1) accounts for the climate model uncertainties and for natural variability and could be a very useful tool for testing the adequacy of possible adaptation strategies since they allow the analysis of historical and future ranges of rainfall and discharge in a simple way without focusing on the projections of individual models.

This could also be used to assess the form and future validity of the Albufeira Convention. Each plot in Figure 8.1 comprises 375 points (25 years for each of the 15 models) and the discharge limits of the Albufeira Convention can be added to the plots (red lines) and the percentage of years below the discharge limits can be calculated (values in red). The percentage of years below any rainfall threshold can also be calculated (value in brown for a 60% of annual rainfall threshold). Likewise, the percentage of years below both a rainfall and a discharge threshold can also be calculated, giving, for example, the percentage of years where the discharges are below the convention limits but there is no breach of the convention because they are considered exception years (values in black). These plots could be used in discussions between Portugal and Spain regarding the adequacy of the Albufeira convention discharge limits and the definition of “exception years” for present and future climate.

Also, regression relations can be calculated (see Figure 8.2) to assess if the response of the basin to climate change is fixed (i.e. lower rainfall and discharges but the same regression line) and therefore a hydrological model might not be essential, or whether they are varied (i.e. not only lower rainfall and discharges but also different regression lines) and therefore the use of a reliable hydrological model is crucial in order to understand the future behaviour of the basins. In the last case, the use of different physically based, spatially distributed hydrological models would be advisable to understand the impact of the choice of hydrological model in the basin’s

behaviour. The regression lines could also be used to compare the results from the different downscaling methods used.

Here only plots for annual (October to September) rainfall and discharge are shown, but seasonal plots would also need to be considered due to the seasonality in the region. Also, if these plots were to be used to assess the Albufeira convention the relationship between the reference rainfall gauges used in the convention and the gridded rainfall used in these plots would have to be investigated. Nevertheless, this approach allows a simple and rapid evaluation of many future climates and convention formulations while being underpinned by detailed spatially distributed modelling accounting for a range of non-linear processes.

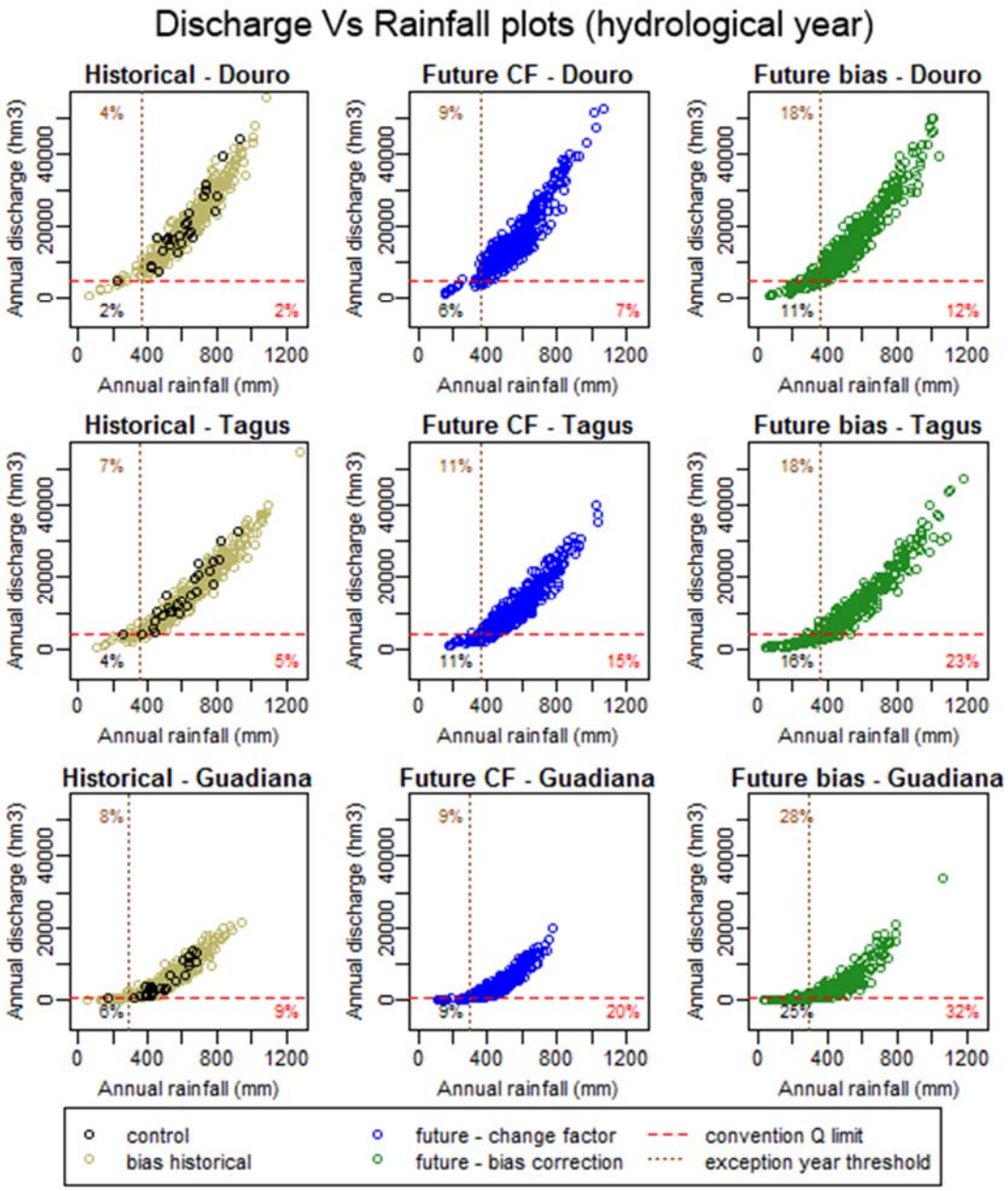

Figure 8.1 – Annual (October to September) discharge vs annual (October to September) precipitation plots for historical rainfall (left) and future annual rainfall (centre for the change factor rainfall downscaling method and right for the bias correction/empirical mapping method) for the basins of the rivers Douro (top), Tagus (middle) and Guadiana (bottom) using the annual values of the 15 climate models. The annual Albufeira convention discharge limits for the outlets of the rivers are plotted in red. The Guadiana River does not have a discharge limit for the outlet, so the limit for the border was used for illustration purposes. The 60% of mean annual (October to September) rainfall is plotted as a proxy for the exception years defined in the Albufeira convention.

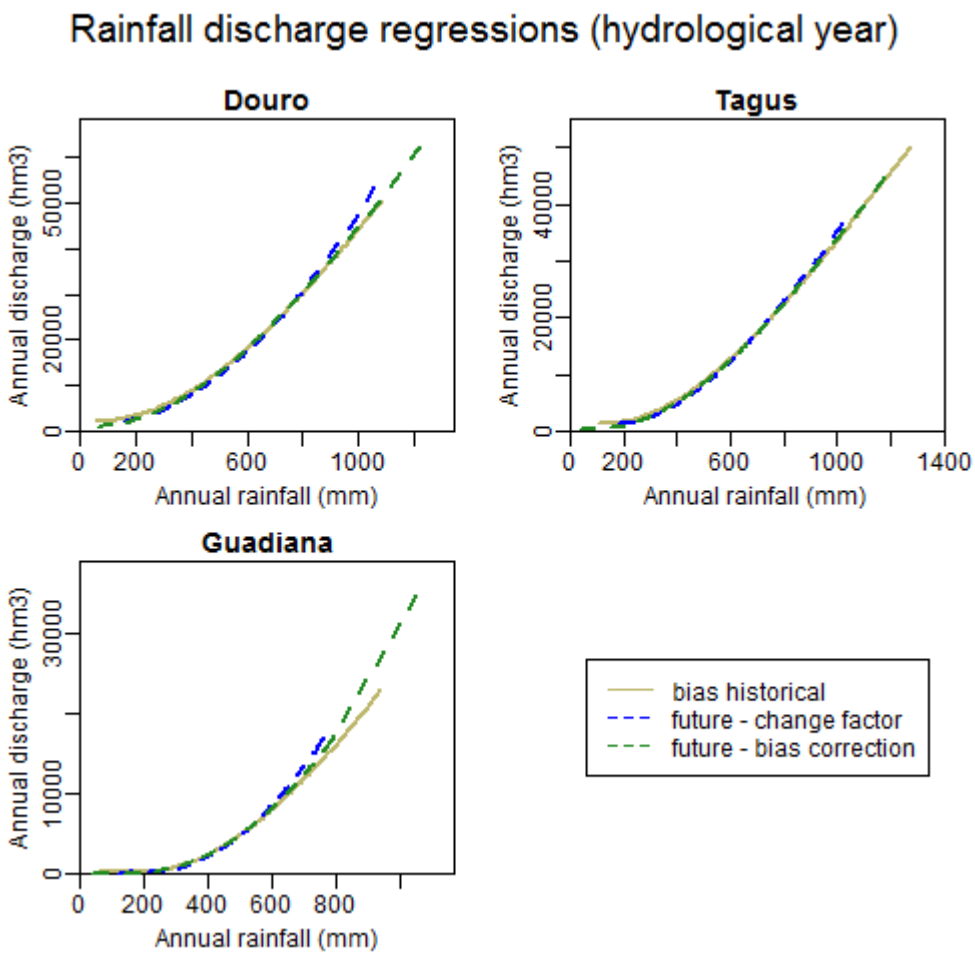

Figure 8.2 – Third order polynomial regressions of the annual (October to September) discharge vs annual (October to September) precipitation presented in Figure 8.1. The r-squared of all the regressions is between 0.89 and 0.94.

8.6 Other future work

Considering the wide ranging nature of work presented in this thesis, there are several ways it could be improved, given the time and the data. A better understanding of climate model projections for large scale atmospheric circulation patterns, and in particular the North Atlantic storm track, may improve the understanding of discrepancies in the rainfall projections. More complex downscaling methods could also be used, although the usefulness of such an exercise is not obvious when considering the scale of climate model disagreement in future rainfall projections for Iberia.

The three basins studied have an extremely complex multi-layered network of aquifers, both detrital and karstic. Therefore the aquifer representation in the hydrological model was extremely simplified and could be improved. Also, these basins have been highly impacted by human activities for several centuries and there are thousands of dams and groundwater extraction points in the region that were not modelled. The main dams, water abstractions and inter-basin transfers could be added to the model. However, both these improvements are dependent on data availability and they would be very time-consuming.

The obvious next steps in a future water resources study for the area would be to research the future demands of water by looking at projections for population changes and, for example, future agricultural consumption. This would be an important step before developing possible adaptation measures. Considering the uncertainty in the climate projections (and possibly the demand side projections too), the focus should be on robust adaptation measures, perhaps with an emphasis on win-win measures tackling the demand side. For example, more efficient irrigation methods might make a significant contribution to the reduction of water consumption considering the high potential evapotranspiration of the region.

Appendices

Appendix A. R code for the Pettitt test

```
#code developed by Dr Francesco Serinaldi
pettitt.test <- function(x, time, alternative="two.sided"){
#           Pettitt test based on Kendall's U statistic (Pettitt 1979)
#           input
#                       x: vector of data
#                       time: auxiliary vector: it can be simply 1:N (where N is the sample size)
#                             or the dates e.g. 1950:2000 (for annual values)
#         alternative: first "two-sided"; if the test result is significant
#         (p-value<0.05) then perform alternative=="greater" (decreasing change)
#         and "less" (incresing change) output
#                                   K: test statistics
#                                   p.value: p-value
#          c.time: change point time (a date if "time" is in the form 1950:2000
#          or the position of the change point if "time" is on the form 1:N
                        n <- length(x)
                        U.t <- numeric()
                        V.t <- numeric()
                        u.t <- 0
                        for (i in 1:n) {
                                    V.t[i] <- sum(sign(x[i]-x))
                                    U.t[i] <- V.t[i] + u.t
                                    u.t <- U.t[i]
                        }
                        if (alternative=="two.sided"){
                                    K <- max(abs(U.t))
                                    c.time <- time[which(abs(U.t)==K)]
                        }
                        else if (alternative=="greater"){
                                    K <- max(U.t)
                                    c.time <- time[which(U.t==K)]
                        }
                        else if (alternative=="less"){
                                    K <- -min(U.t)
                                    c.time <- time[which(U.t== -K)]
                        }
                        if (alternative=="two.sided")
                                    p.value <- 2*exp(-6*K^2/(n^3+n^2))
                        else
                                    p.value <- exp(-6*K^2/(n^3+n^2))
                        if (p.value > 0.5) p.value <- 0.5  # limit of validity of the Pettitt approximation: when
the p-value is larger than 0.5, the code return 0.5 (not significant)

   res <- list()
   res$K <- K
   res$p.value <- p.value
   res$c.time <- c.time[1]
#                       windows()
            #plot(time,abs(U.t),type="l", xlab="t", ylab="U(t,T)", lwd=1, main="Serie U(t,T)",panel.first =
grid(lty=1),ylim=c(0,K)  )
                        return(res)    # the code returns a list with K, p-value, and c.time
}
```

Appendix B. R codes for the cusum test

```
#code developed by Dr Francesco Serinaldi
#for:
            # the application of the cusum test to the data
            # the calculation of the null distribution (used for calculating field significance with "cusum
test_b")

cusum.test <- function(x, time, N=10000){
#           CUSUM test based on Smadi and Zghoul (2006): p-value by bootstrap
#           input
#                       x: vector of data
#                       time: auxiliary vector: it can be simply 1:N (where N is the sample size)
#                       or the dates e.g. 1950:2000 (for annual values)
#           output
#                                   S.diff: test statistics
#                                   p.value: p-value
#          c.time: change point time (a date if "time" is in the form 1950:2000
#          or the position of the change point if "time" is on the form 1:N

set.seed(666)  #to make the generator reproduce the same sequence of random numbers each time the
code runs
n <- length(x)
CS.t <- numeric()
mea <- mean(x)
for (i in 1:n)
            {
                        CS.t[i] <- sum(x[1:i]-mea)
            }
S.diff <- max(CS.t)-min(CS.t)
c.time <- time[which(abs(CS.t)==max(abs(CS.t)))][1]
 S.diff.j <- numeric()
 x.sample <- sapply(seq(1,N), function(i,xx) sample(xx,replace=T), xx=x)
  loop <- function(x.aux)
            {
                        n <- length(x.aux)
                        S.j <- numeric()
                        mea.j <- mean(x.aux)
                        for (i in 1:n)
                                    {
                                    S.j[i] <- sum(x.aux[1:i]-mea.j)
                                    }
                        S.di.j <-  max(S.j[1:n])-min(S.j[1:n])
#       cat("loop","\n")
                        S.di.j
            }

S.diff.j <- apply(x.sample, 2, loop)

p.value <- length(which(S.diff.j > S.diff))/N

   res <- list()
   res$S.diff <- S.diff
   res$p.value <- p.value
   res$c.time <- c.time[1]
   res$null.distr <- S.diff.j
                        return(res)
}
```

```
#code developed by Dr Francesco Serinaldi

#for the calculation of field significance, it builds on cusum_a (which calculates the null.distr)

cusum.test.2 <- function(x, time, null.distr){

#  input
 #                    x: vector of data
 #                    time: auxiliary vector: it can be simply 1:N (where N is the sample size)
 #         or the dates e.g. 1950:2000 (for annual values)
 #    null.distr: vector of S.diff from a previous ran of cusum.test.
 #   output
 #                                S.diff: test statistics
 #                                p.value: p-value
 #    c.time: change point time (a date if "time" is in the form 1950:2000
 #          or the position of the change point if "time" is on the form 1:N


                    n <- length(x)
                    CS.t <- numeric()

                    mea <- mean(x)

                    for (i in 1:n) {
                              CS.t[i] <- sum(x[1:i]-mea)
                    }
                    S.diff <- max(CS.t)-min(CS.t)
                    c.time <- time[which(abs(CS.t)==max(abs(CS.t)))][1]

                    p.value <- length(which(null.distr > S.diff))/length(null.distr)

   res <- list()
   res$S.diff <- S.diff
   res$p.value <- p.value
   res$c.time <- c.time[1]
                    return(res)
}
```

Appendix C. CMIP5 models

Table C.1 – List of GCMs used in this study

Model number (used in this study)	Model name	Modelling center
1	CanESM2	Canadian Centre for Climate Modelling and Analysis
2	CanESM2	Canadian Centre for Climate Modelling and Analysis
3	IPSL-CM5A-LR	Institut Pierre-Simon Laplace
4	CNRM-CM5	Centre National de Recherches Météorologiques / Centre Européen de Recherche et Formation Avancée en Calcul Scientifique
5	CNRM-CM5	Centre National de Recherches Météorologiques / Centre Européen de Recherche et Formation Avancée en Calcul Scientifique
6	CSIRO-Mk3-6-0	Commonwealth Scientific and Industrial Research Organization (CSIRO) and Bureau of Meteorology (BOM), Australia
7	EC-EARTH	EC-EARTH consortium
8	GFDL-CM3	NOAA Geophysical Fluid Dynamics Laboratory
9	GFDL-ESM2M	NOAA Geophysical Fluid Dynamics Laboratory
10	GISS-E2-R	NASA Goddard Institute for Space Studies
11	HadGEM2-ES	Met Office Hadley Centre (additional HadGEM2-ES realizations contributed by Instituto Nacional de Pesquisas Espaciais)
12	HadGEM2-ES	Met Office Hadley Centre (additional HadGEM2-ES realizations contributed by Instituto Nacional de Pesquisas Espaciais)
13	inmcm4	Institute for Numerical Mathematics
14	MPI-ESM-LR	Max-Planck-Institut für Meteorologie (Max Planck Institute for Meteorology)
15	MRI-CGCM3	Meteorological Research Institute

Table C.2 – List of GCMs available from CMIP5.

Modeling Center	Model	Institution
BCC	BCC-CSM1.1 BCC-CSM1.1(m)	Beijing Climate Center, China Meteorological Administration
CCCma	CanAM4 CanCM4 CanESM2	Canadian Centre for Climate Modelling and Analysis
CMCC	CMCC-CESM CMCC-CM CMCC-CMS	Centro Euro-Mediterraneo per I Cambiamenti Climatici
CNRM-CERFACS	CNRM-CM5	Centre National de Recherches Meteorologiques / Centre Europeen de Recherche et Formation Avancees en Calcul Scientifique
CNRM-CERFACS	CNRM-CM5-2	Centre National de Recherches Meteorologiques / Centre Europeen de Recherche et Formation Avancees en Calcul Scientifique
COLA and NCEP	CFSv2-2011	Center for Ocean-Land-Atmosphere Studies and National Centers for Environmental Prediction
CSIRO-BOM	ACCESS1.0 ACCESS1.3	CSIRO (Commonwealth Scientific and Industrial Research Organisation, Australia), and BOM (Bureau of Meteorology, Australia)
CSIRO-QCCCE	CSIRO-Mk3.6.0	Commonwealth Scientific and Industrial Research Organisation in collaboration with the Queensland Climate Change Centre of Excellence
EC-EARTH	EC-EARTH	EC-EARTH consortium
FIO	FIO-ESM	The First Institute of Oceanography, SOA, China
GCESS	BNU-ESM	College of Global Change and Earth System Science, Beijing Normal University
INM	INM-CM4	Institute for Numerical Mathematics
IPSL	IPSL-CM5A-LR IPSL-CM5A-MR IPSL-CM5B-LR	Institut Pierre-Simon Laplace
LASG-CESS	FGOALS-g2	LASG, Institute of Atmospheric Physics, Chinese Academy of Sciences; and CESS, Tsinghua University
LASG-IAP	FGOALS-gl FGOALS-s2	LASG, Institute of Atmospheric Physics, Chinese Academy of Sciences
MIROC	MIROC4h MIROC5	Atmosphere and Ocean Research Institute (The University of Tokyo), National Institute for Environmental Studies, and Japan Agency for Marine-Earth Science and Technology
MIROC	MIROC-ESM MIROC-ESM-CHEM	Japan Agency for Marine-Earth Science and Technology, Atmosphere and Ocean Research Institute (The University of Tokyo), and National Institute for Environmental Studies
MOHC (additional realizations by INPE)	HadCM3 HadCM3Q HadGEM2-A HadGEM2-CC HadGEM2-ES	Met Office Hadley Centre (additional HadGEM2-ES realizations contributed by Instituto Nacional de Pesquisas Espaciais)
MPI-M	MPI-ESM-LR MPI-ESM-MR MPI-ESM-P	Max Planck Institute for Meteorology (MPI-M)
MRI	MRI-AGCM3.2H MRI-AGCM3.2S MRI-CGCM3 MRI-ESM1	Meteorological Research Institute

Modeling Center	Model	Institution
NASA GISS	GISS-E2-H GISS-E2-H-CC GISS-E2-R GISS-E2-R-CC	NASA Goddard Institute for Space Studies
NASA GMAO	GEOS-5	NASA Global Modeling and Assimilation Office
NCAR	CCSM4	National Center for Atmospheric Research
NCC	NorESM1-M NorESM1-ME	Norwegian Climate Centre
NICAM	NICAM.09	Nonhydrostatic Icosahedral Atmospheric Model Group
NIMR/KMA	HadGEM2-AO	National Institute of Meteorological Research/Korea Meteorological Administration
NOAA GFDL	GFDL-CM2.1 GFDL-CM3 GFDL-ESM2G GFDL-ESM2M GFDL-HIRAM-C180 GFDL-HIRAM-C360	Geophysical Fluid Dynamics Laboratory
NSF-DOE-NCAR	CESM1(BGC) CESM1(CAM5) CESM1(CAM5.1, FV2) CESM1(FASTCHEM) CESM1(WACCM)	National Science Foundation, Department of Energy, National Center for Atmospheric Research

Appendix D. Rainfall boxplots

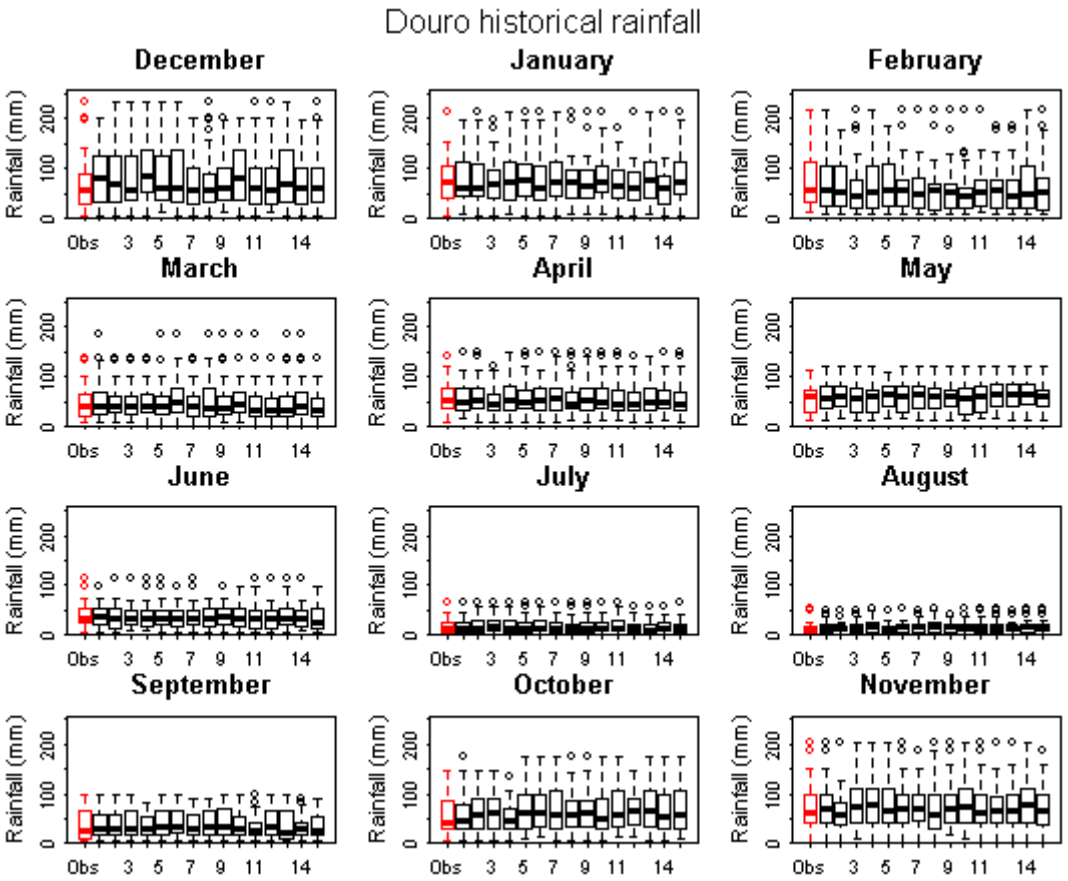

Figure D.1 – Boxplots of Douro basin rainfall for the period 1961 to 1990 for observed rainfall (in red) and the 15 bias corrected GCM rainfall (in black).

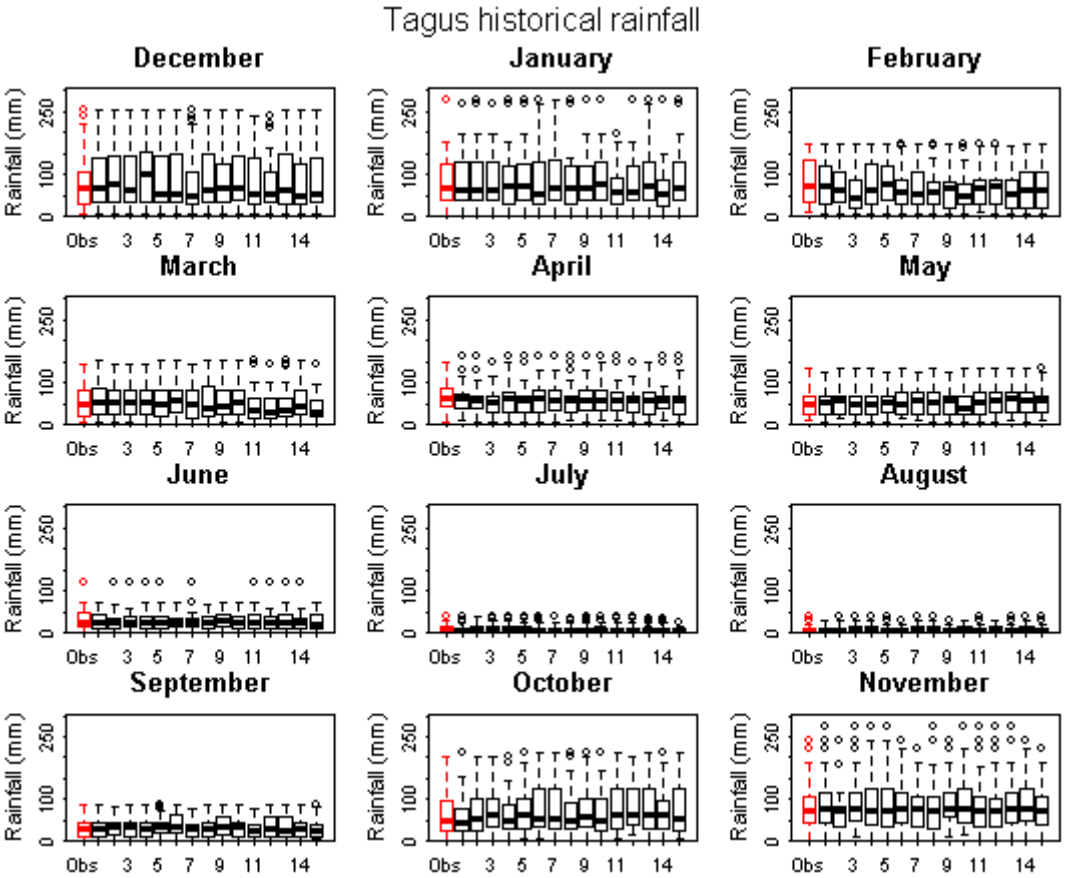

Figure D.2 – Boxplots of Tagus basin rainfall for the period 1961 to 1990 for observed rainfall (in red) and the 15 bias corrected GCM rainfall (in black).

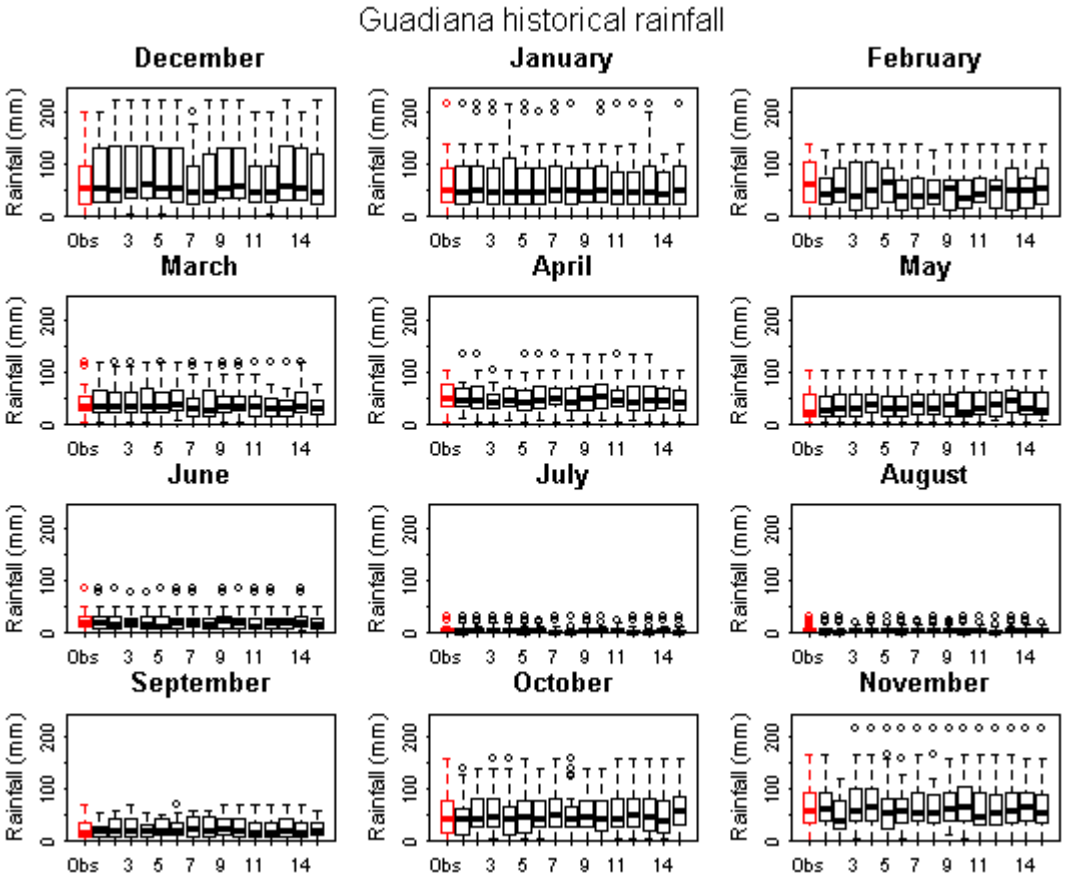

Figure D.3 – Boxplots of Guadiana basin rainfall for the period 1961 to 1990 for observed rainfall (in red) and the 15 bias corrected GCM rainfall (in black).

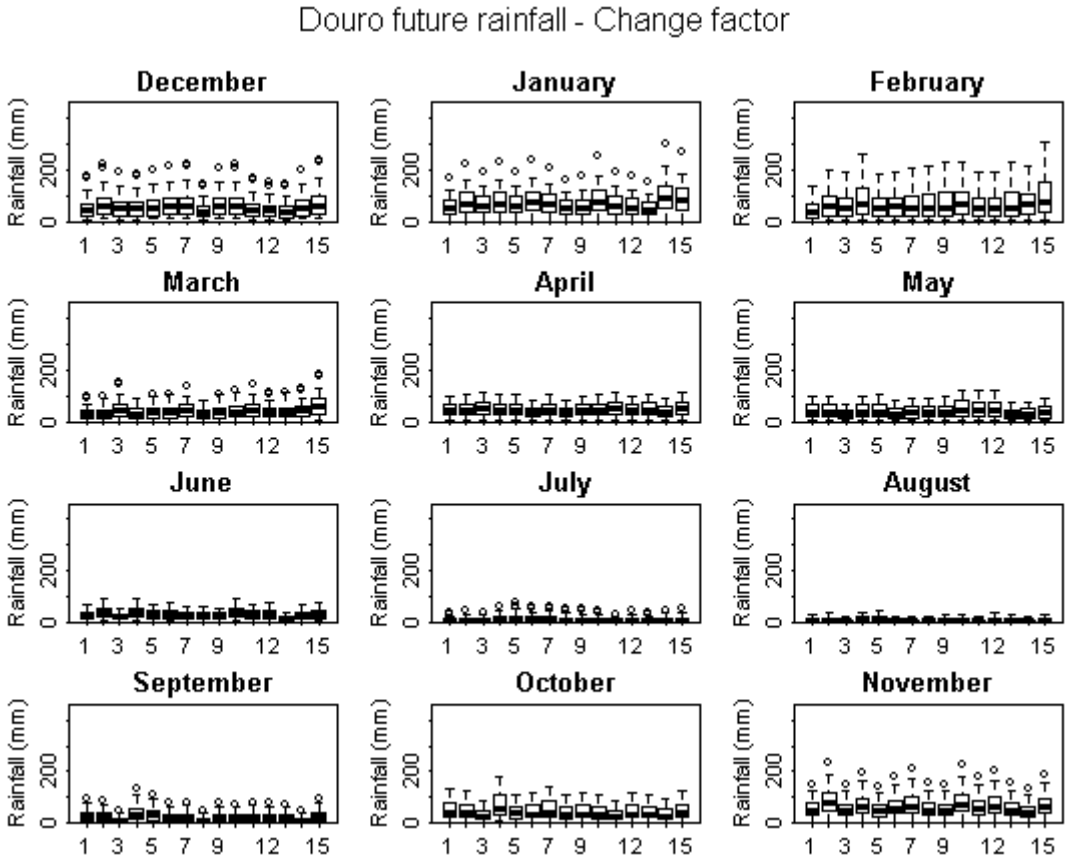

Figure D.4 – Boxplots of Douro's basin future rainfall, per month, for the 15 GCMs using the change factor method.

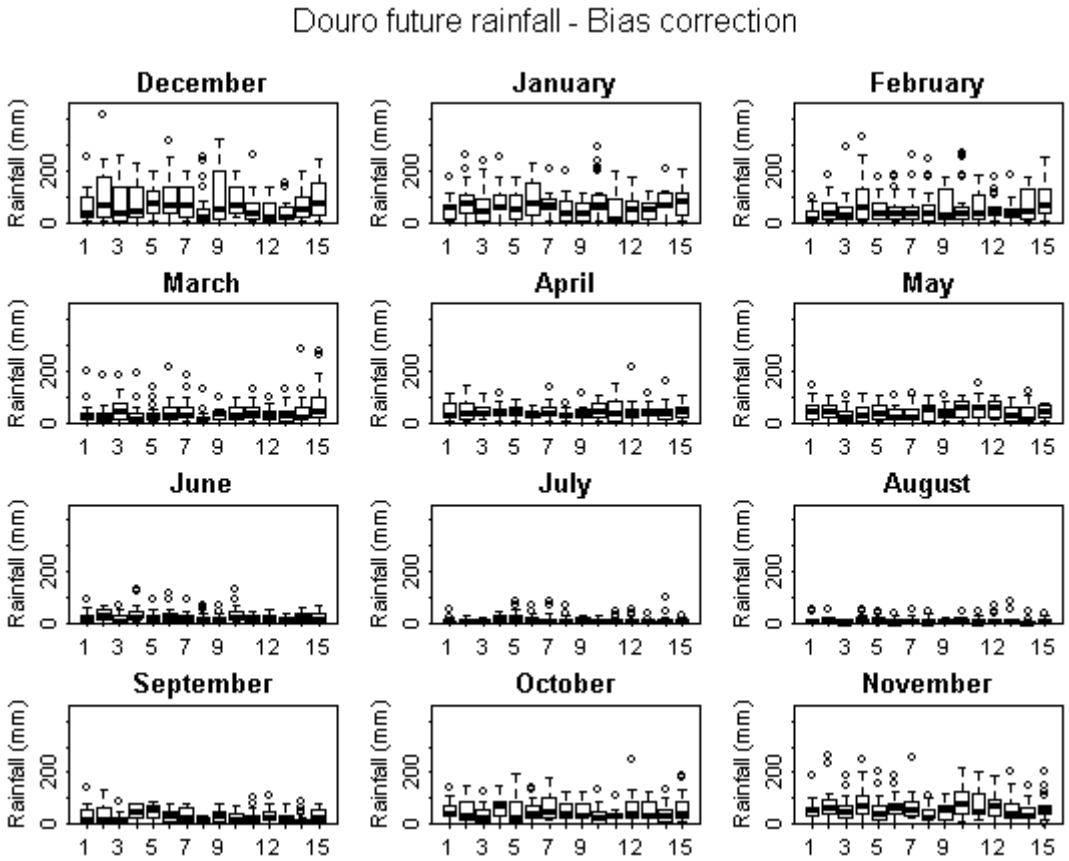

Figure D.5 – Boxplots of Douro's basin future rainfall, per month, for the 15 GCMs using the bias correction method.

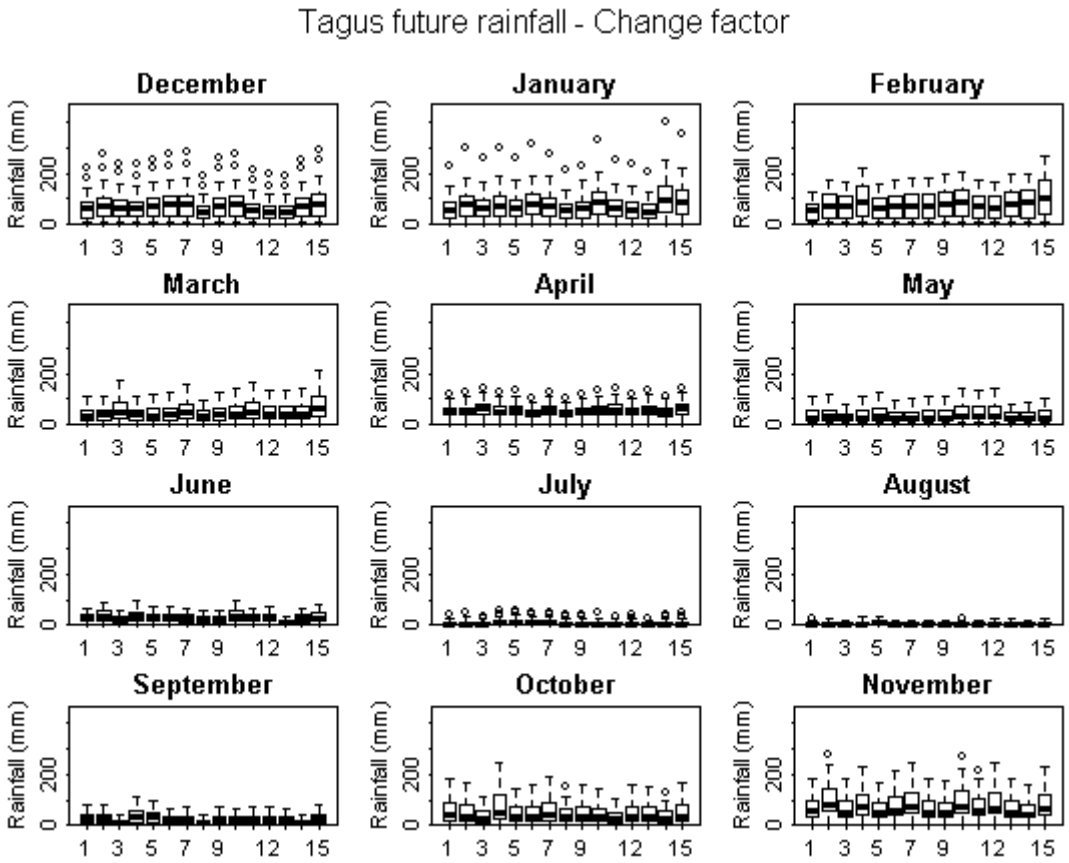

Figure D.6 – Boxplots of Tagus's basin future rainfall, per month, for the 15 GCMs using the change factor method.

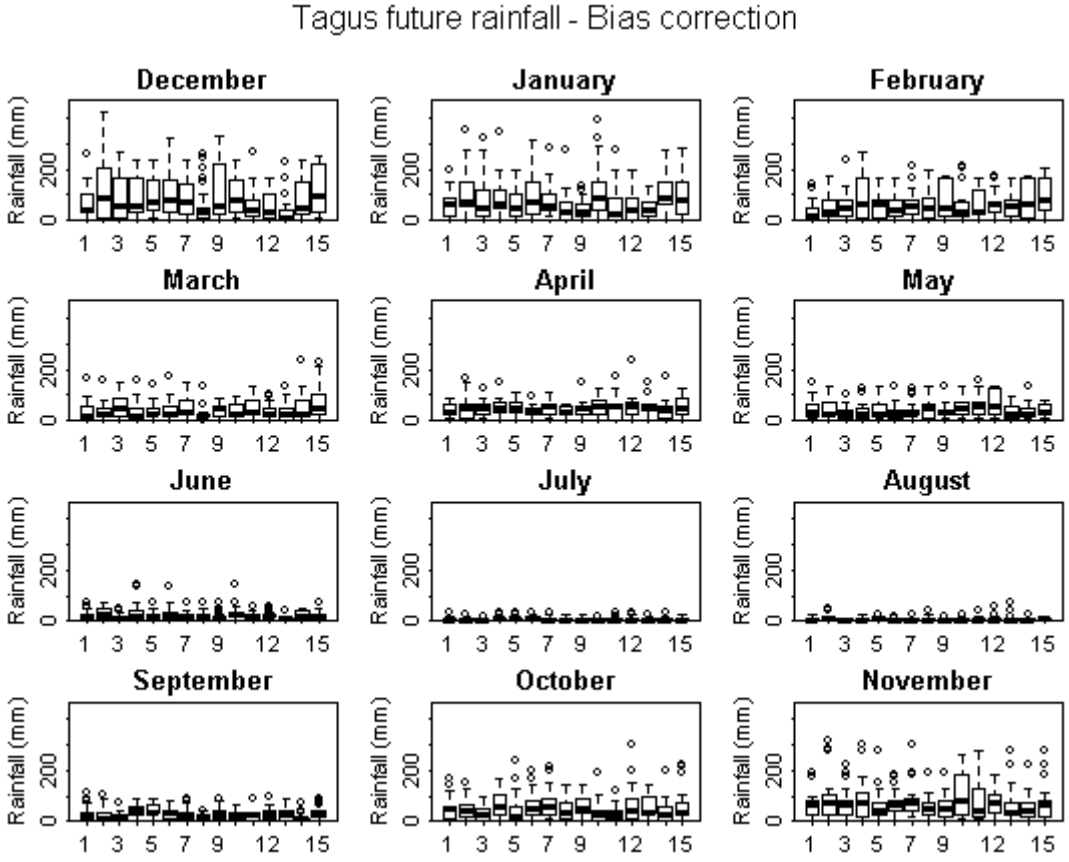

Figure D.7 – Boxplots of Tagus's basin future rainfall, per month, for the 15 GCMs using the bias correction method.

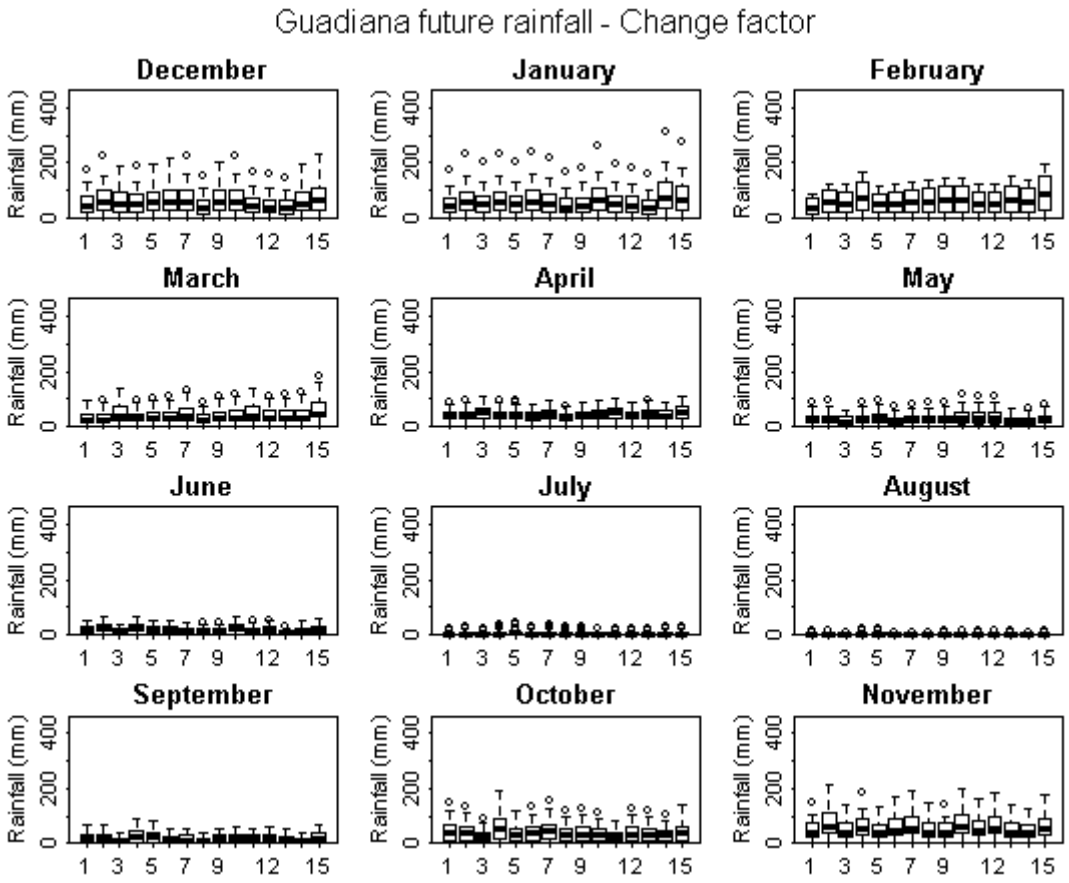

Figure D.8 – Boxplots of Guadiana's basin future rainfall, per month, for the 15 GCMs using the change factor method.

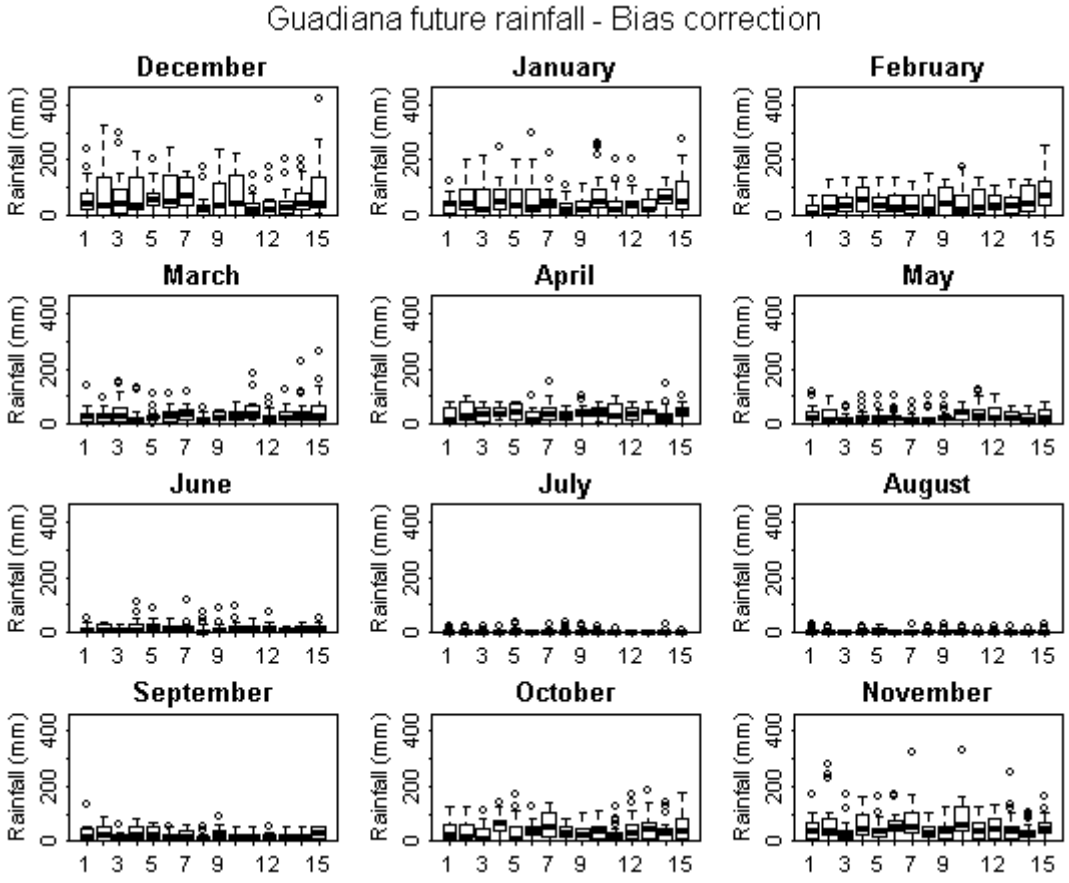

Figure D.9 – Boxplots of Guadiana's basin future rainfall, per month, for the 15 GCMs using the bias correction method.

Appendix E. R code for the calculation of SPI

```
#SPI calculation for transient data with choice of distribution: "gamma" or "pearson3"
#x = monthly rainfall time-series class=zoo
#also includes function to plot spi: "plot.spi"
#WARNING: using Pearson III aggregated rainfall might be
#outside the distribution fitted and SPI will be -inf

#^^^^^^^^^^^^^^^^^^^^^^^^^^^^^^^^^^^^^^^^^^^^^^^^^^^^^^^^^^^^^^^^^^^^^^^^^^^^^^^^^^^^^^^
library(lmomco) #L-moments
library(zoo)
library(xts)

"SPI" <- function(x,k,distribution = "gamma",ref = 1961:1990)
{
  x = cbind( year = as.numeric(format(time(x), "%Y")),
          month = as.numeric(format(time(x), "%m")),
          as.matrix(x))

 hist = x[which(as.numeric(x[,1]) %in% ref),]

 yrs = x[1,1]:x[length(x[,1]),1] #years of time-series
 leng = length(yrs)
 mat = cbind(rep(yrs,12),rep(1:12,each=leng),NA) #create matrix with the years, months and a columm
for SPI (filled with NAs)
 colnames(mat) = c("year","month","SPI")

 for (m in 1:12) #loop through the months
 {
  x.hist = vector()
  for (i in k: dim(hist)[1])
  {
   if (hist[i,2] == m) x.hist[i] = sum(hist[i:(i-(k-1)),3])
  }
  agg.hist = x.hist[which( !is.na(x.hist))] #vector with aggregated rainfall for the month m

  x.all = vector()
  for (i in k: dim(x)[1])
  {
   if (x[i,2] == m) x.all[i] = sum(x[i:(i-(k-1)),3])
  }
   agg.all = x.all[which( !is.na(x.all))]  #vector with aggregated rainfall for the month m

  #fit a distribution to the aggregated rainfall using L-moments:
  lmom = lmom.ub(as.numeric(agg.hist))
  if (distribution == "gamma")para = pargam(lmom)
  if (distribution == "pearson3")para = parpe3(lmom)

  prob = plmomco(agg.all,para)
  Z = qnorm(prob)

  if (m < k) Z=c(NA,Z) # add NA in beggining of series when necessary

  mat[which (mat[,2]==m),3] = Z
 }

 spi = mat[order(mat[,1]),]
```

```
  rownames(spi)=rownames(x)
  if (length(which(spi[,3]==-Inf))>0)print("WARNING: SPI= -inf")

  return(spi)
}

"plot.spi" = function(spi,x,k,ref = 1961:1990,tit=paste0("SPI-",k),lim=range(spi[,3],na.rm=T))
{
  plot(as.yearmon(time(x)),spi[,3],type="h",xaxs="i",
       col="blue",main=tit,ylim=lim,
       ylab="SPI",xlab="Date")
  neg.spi = ifelse(spi[,3]<0,spi[,3],0)
  lines(as.yearmon(time(x)),neg.spi,type="h",col="red")
  if(length(x)> (length(ref)*12))
    {
    abline(v=ref[length(ref)]+1,lty=3,col=rgb(0.5,0.5,0.5,0.9))
    }
  abline(h=0)
}
```

Appendix F. R code for the calculation of DSI

```
#DSI calculation
#x = monthly rainfall time-series class=zoo
#also includes function to plot DSI: "plot.dsi"
#^^^^^^^^^^^^^^^^^^^^^^^^^^^^^^^^^^^^^^^^^^^^^^^^^^^^^^^^^^^^^^^^^^^^^^^^^^^^^^^^^^^^^^^^^^
"DSI" <- function(x,k,ref= 1961:1990)
{
    x = cbind( year = as.numeric(format(time(x), "%Y")),
            month = as.numeric(format(time(x), "%m")),
            as.matrix(x))

  hist = x[which(as.numeric(x[,1]) %in% ref),]

  yrs = x[1,1]:x[length(x[,1]),1] #years of time-series
  leng = length(yrs)

   y = cbind(x,NA)
   colnames(y)[3:4] = c("rainfall","anomaly")
   dsi=rep(0,dim(y)[1])

   media= vector()
   for (m in 1:12)
     {
     media[m] = mean(hist[hist[,2]==m,3])
     y[y[,2]== m,4] = y[y[,2]== m,3]-media[m]
     }

   z = cbind(y,media)
   for (i in k: dim(y)[1])
   {
     #initiation rule
    if (z[i,4]<0 & sum(z[i:(i-(k-1)),3])<sum(z[i:(i-(k-1)),5]) & dsi[i-1]==0)
     {dsi[i] = -z[i,4]}

    #continuation rule
    if(sum(z[i:(i-(k-1)),3]) < sum(z[i:(i-(k-1)),5])& dsi[i-1]>0)
      { dsi [i] = -z[i,4]+dsi[i-1] }
    }

#standardizing the index
   dsi = dsi/sum(media)*100

   mat = cbind(x[,1:2], dsi)
   mat[1:(k-1),3] = NA
   colnames(mat) = c("year","month","DSI")
   return(mat)
}

"plot.dsi" = function(dsi,x,k,ref = 1961:1990,tit=paste0("DSI-",k),lim=c(0,max(dsi[,3],na.rm=T)))
{
  plot(as.yearmon(time(x)),dsi[,3],type="h", main=tit,
      ylab="DSI",xlab="Date",ylim=lim,
      col="Brown")
  if(length(x)> (length(ref)*12))
  {
    abline(v=ref[length(ref)]+1,lty=3,col=rgb(0.5,0.5,0.5,0.9))
  } }
```

Appendix G. Transient rainfall time-series

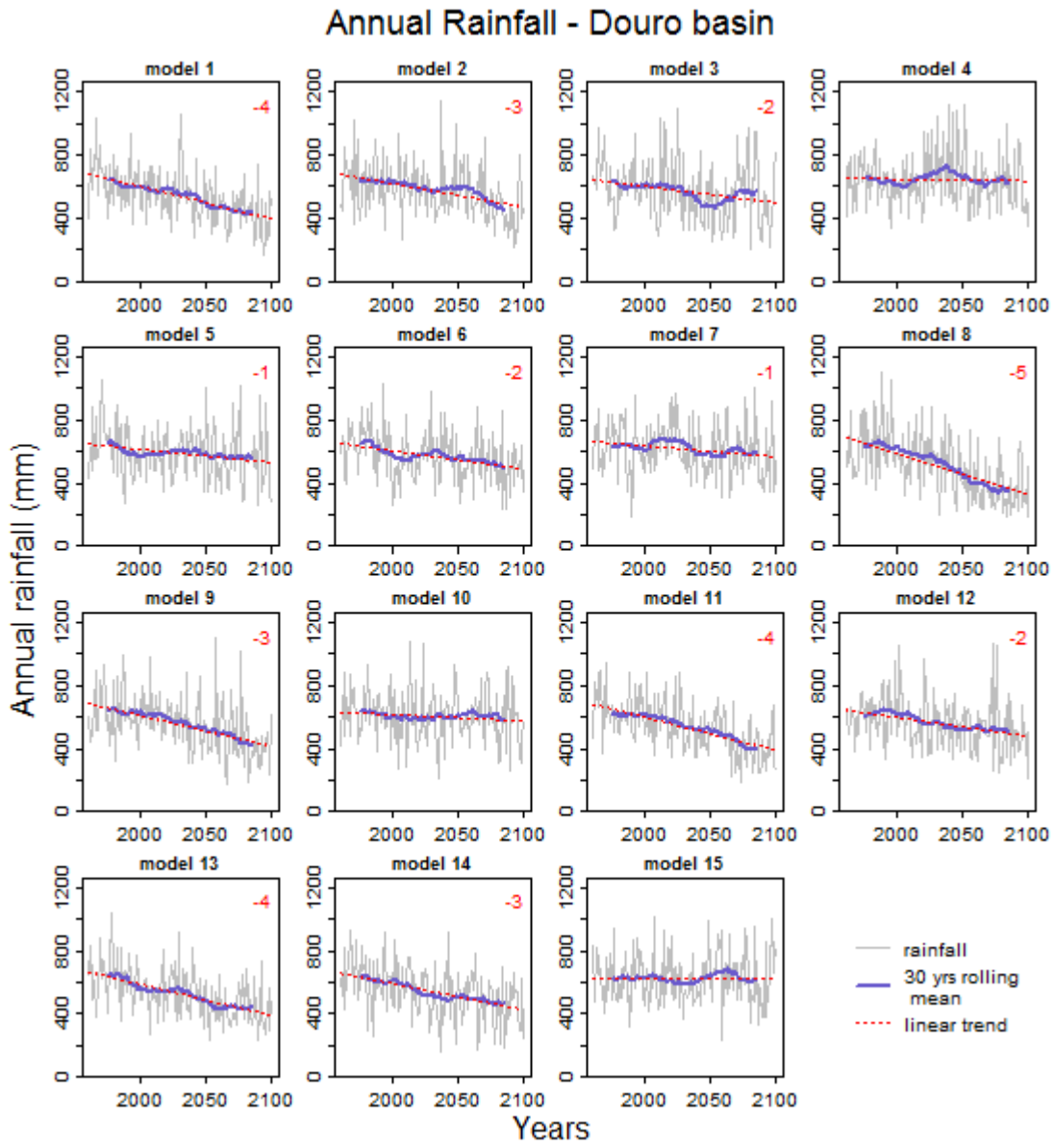

Figure G.1 – Annual transient bias corrected rainfall for the Douro basin and for the 15 GCMs. 30 year rolling means are plotted in purple and linear trends in red. When the monotonic trend was significant at a 5% level (using Mann-Kendall test) its magnitude, assuming a linear trend, is presented in the upper right corner of the plot in percentage of change per decade (relative to the 1961-2100 mean rainfall).

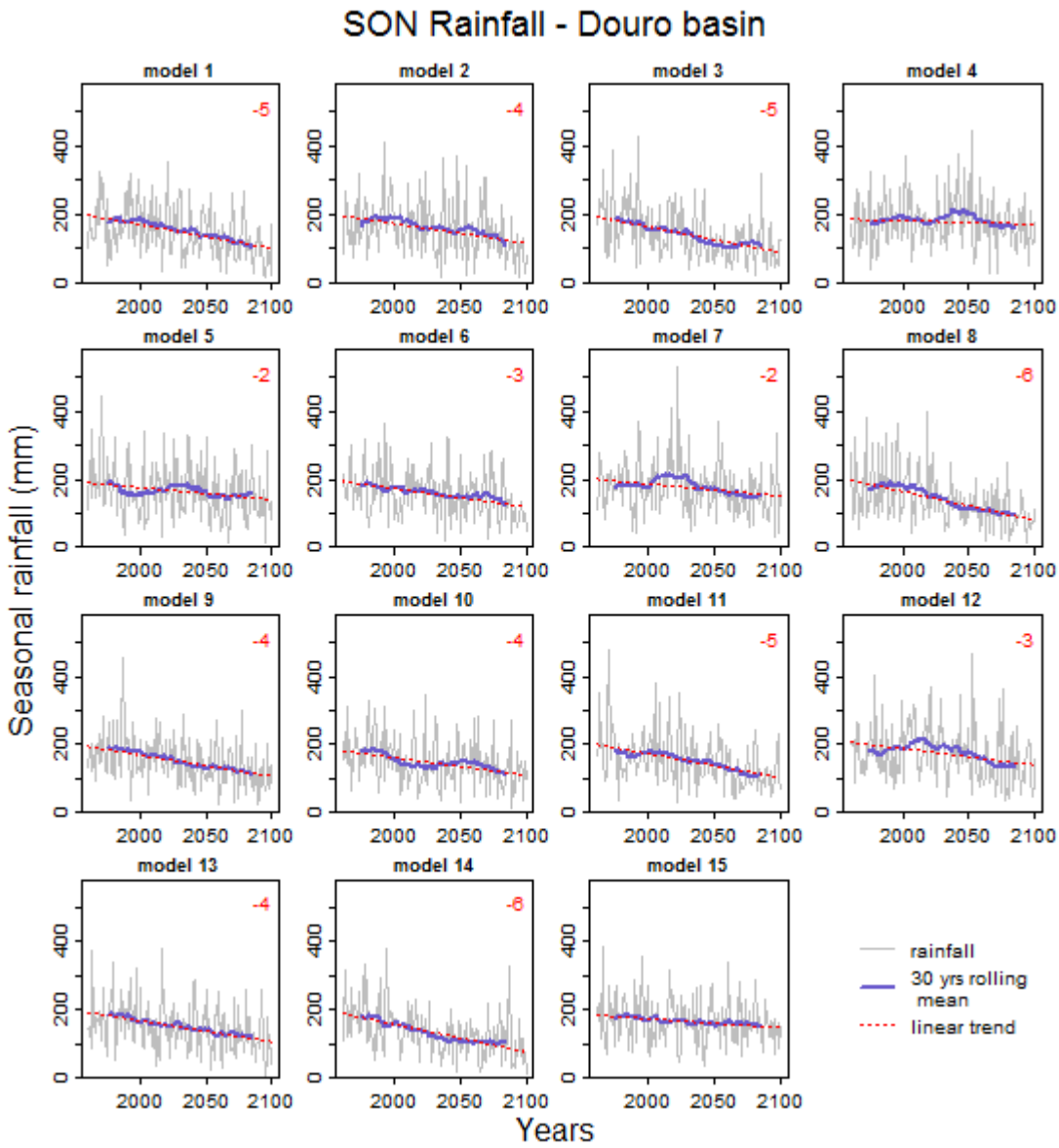

Figure G.2 – Autumn transient bias corrected rainfall for the Douro basin and for the 15 GCMs. 30 year rolling means are plotted in purple and linear trends in red. When the monotonic trend was significant at a 5% level (using Mann-Kendall test) its magnitude, assuming a linear trend, is presented in the upper right corner of the plot in percentage of change per decade (relative to the 1961-2100 mean rainfall).

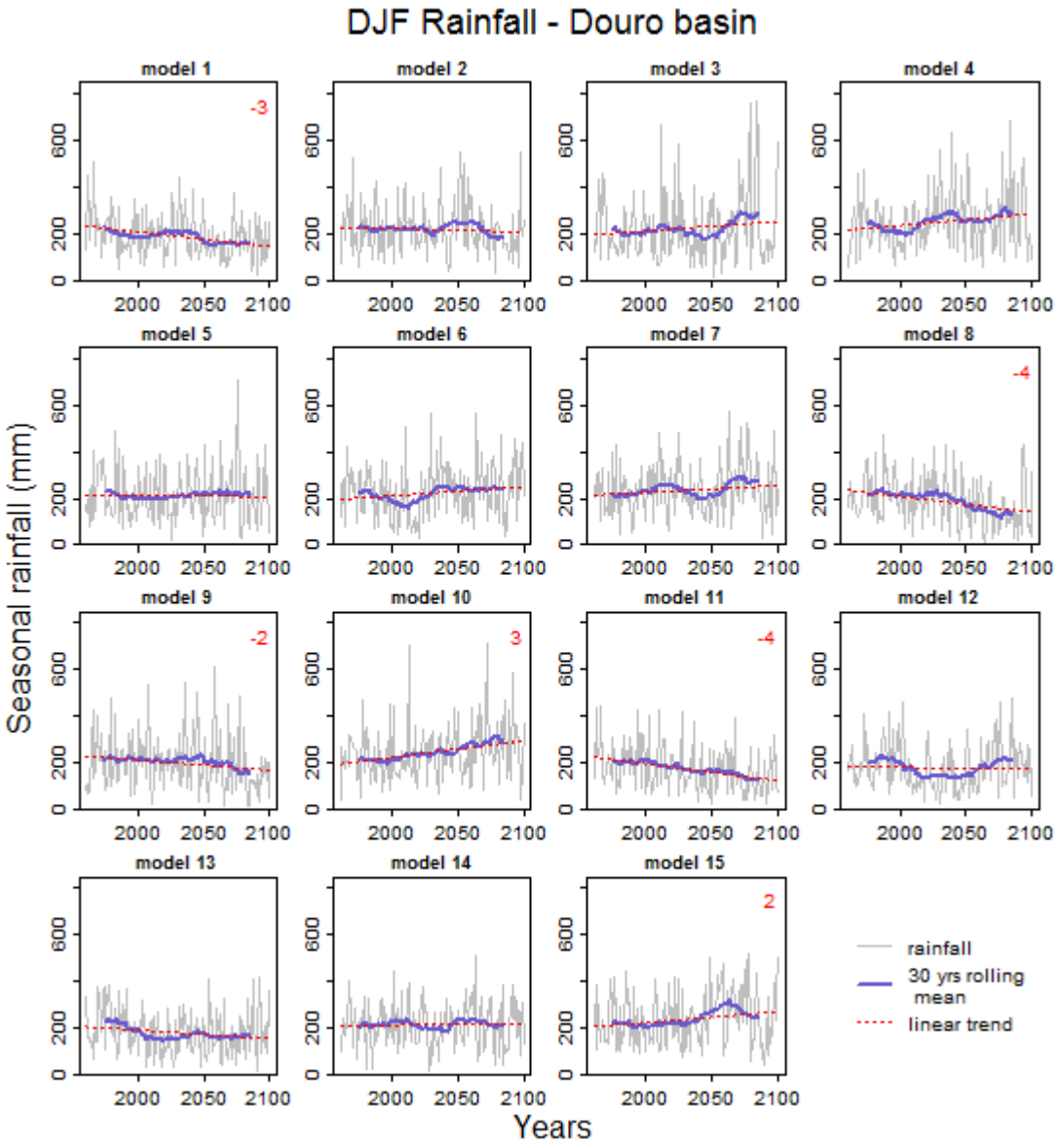

Figure G.3 – Winter transient bias corrected rainfall for the Douro basin and for the 15 GCMs. 30 year rolling means are plotted in purple and linear trends in red. When the monotonic trend was significant at a 5% level (using Mann-Kendall test) its magnitude, assuming a linear trend, is presented in the upper right corner of the plot in percentage of change per decade (relative to the 1961-2100 mean rainfall).

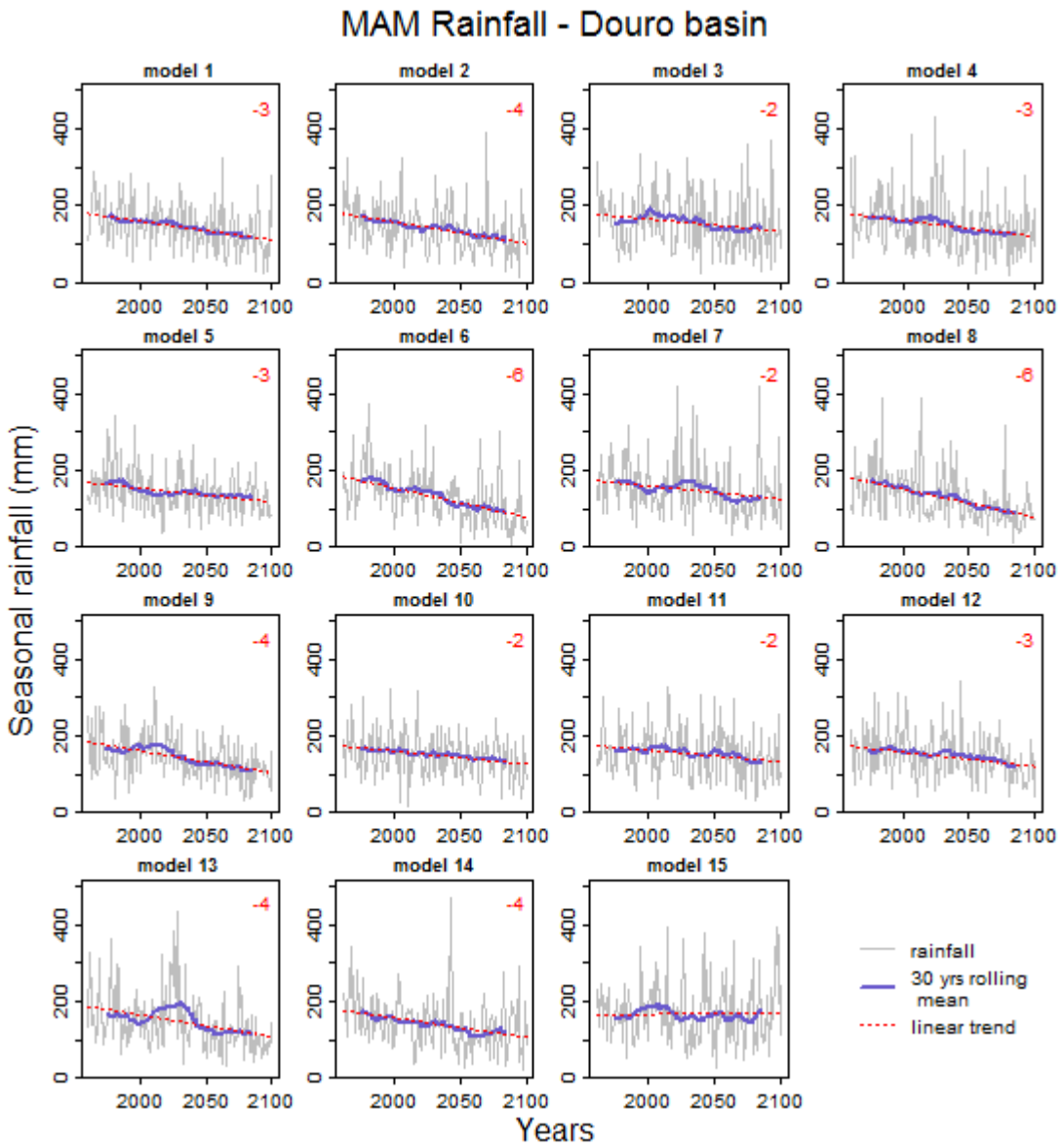

Figure G.4 – Spring transient bias corrected rainfall for the Douro basin and for the 15 GCMs. 30 year rolling means are plotted in purple and linear trends in red. When the monotonic trend was significant at a 5% level (using Mann-Kendall test) its magnitude, assuming a linear trend, is presented in the upper right corner of the plot in percentage of change per decade (relative to the 1961-2100 mean rainfall).

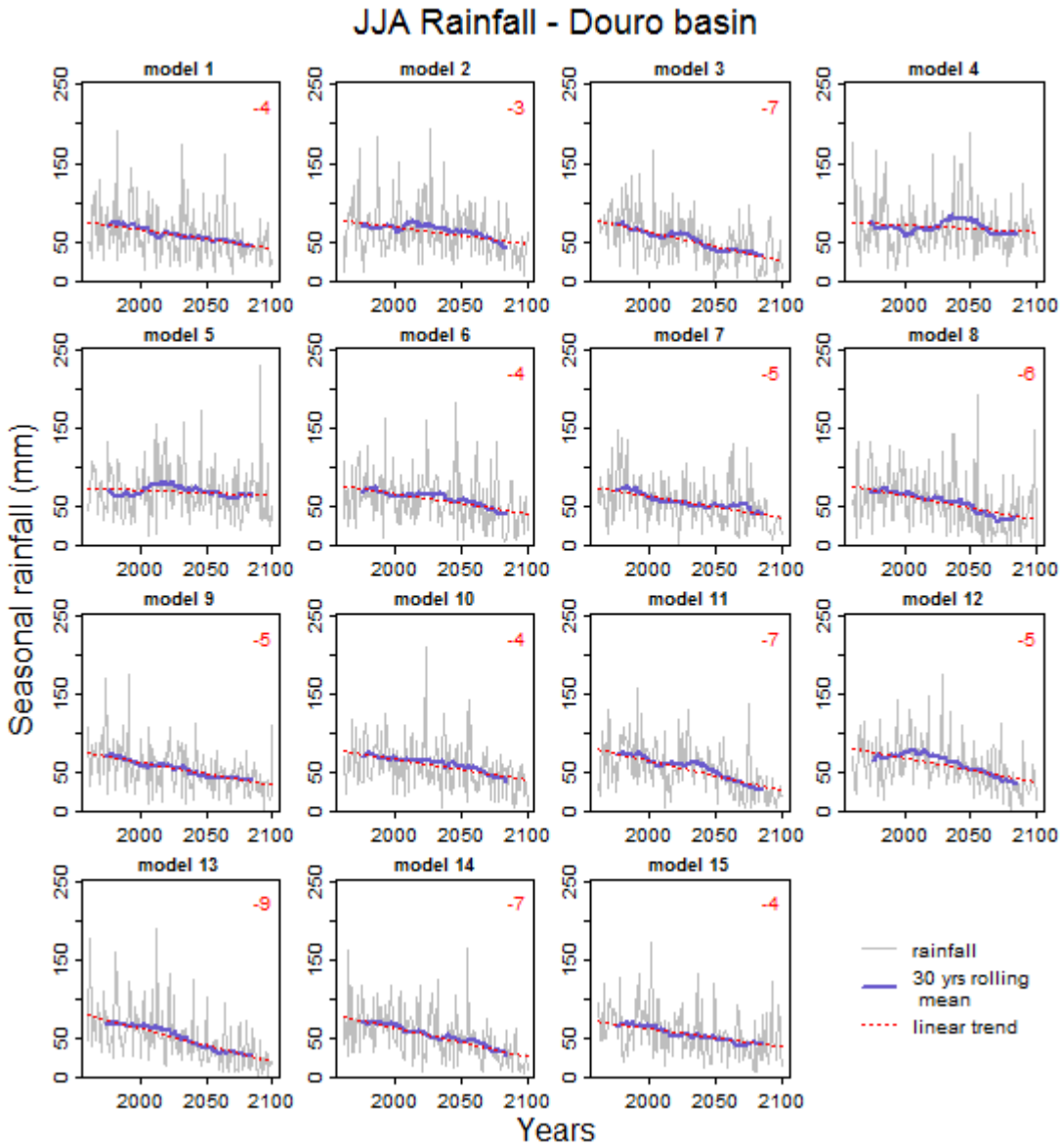

Figure G.5 – Summer transient bias corrected rainfall for the Douro basin and for the 15 GCMs. 30 year rolling means are plotted in purple and linear trends in red. When the monotonic trend was significant at a 5% level (using Mann-Kendall test) its magnitude, assuming a linear trend, is presented in the upper right corner of the plot in percentage of change per decade (relative to the 1961-2100 mean rainfall).

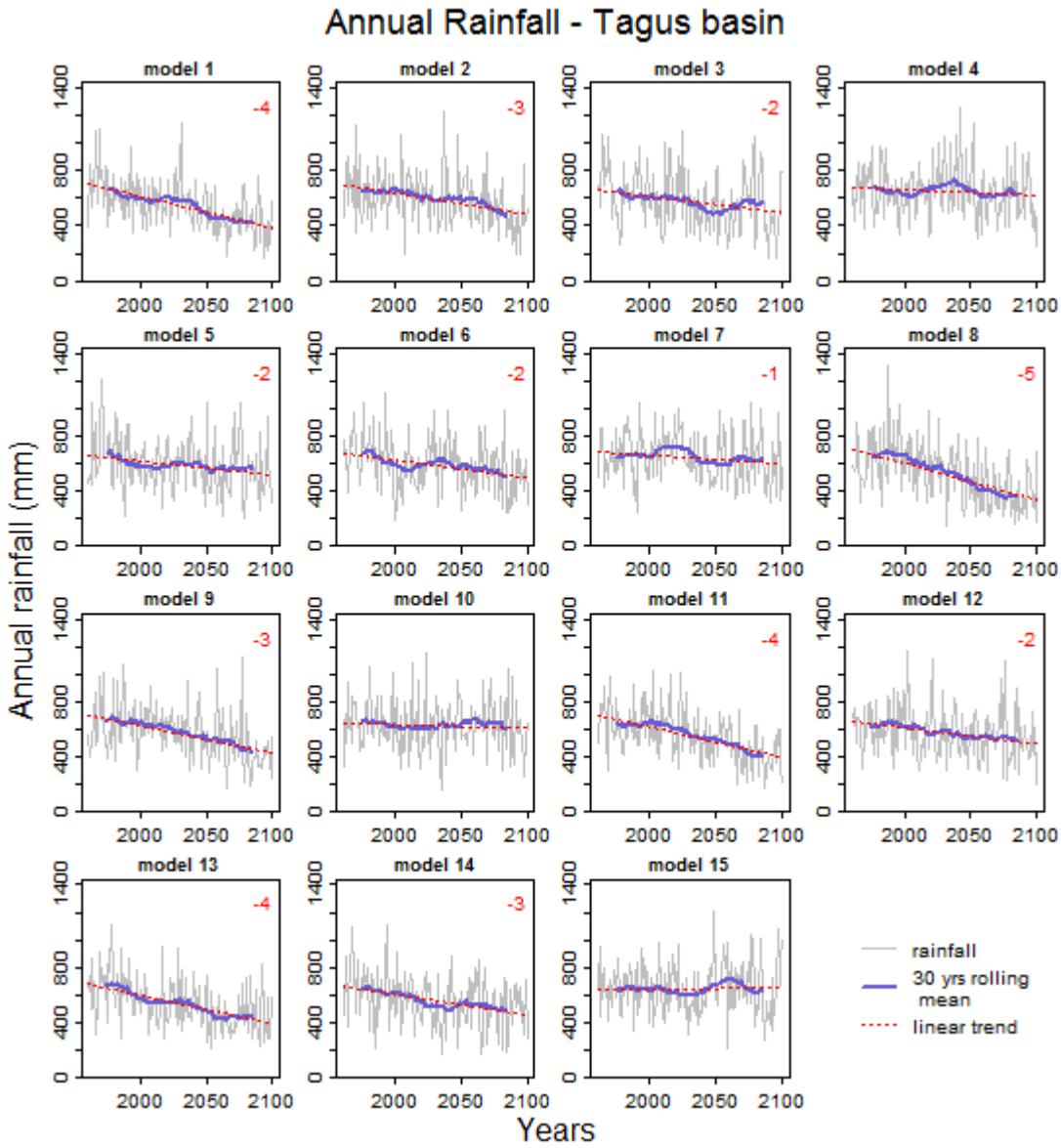

Figure G.6 – Annual transient bias corrected rainfall for the Tagus basin and for the 15 GCMs. 30 year rolling means are plotted in purple and linear trends in red. When the monotonic trend was significant at a 5% level (using Mann-Kendall test) its magnitude, assuming a linear trend, is presented in the upper right corner of the plot in percentage of change per decade (relative to the 1961-2100 mean rainfall).

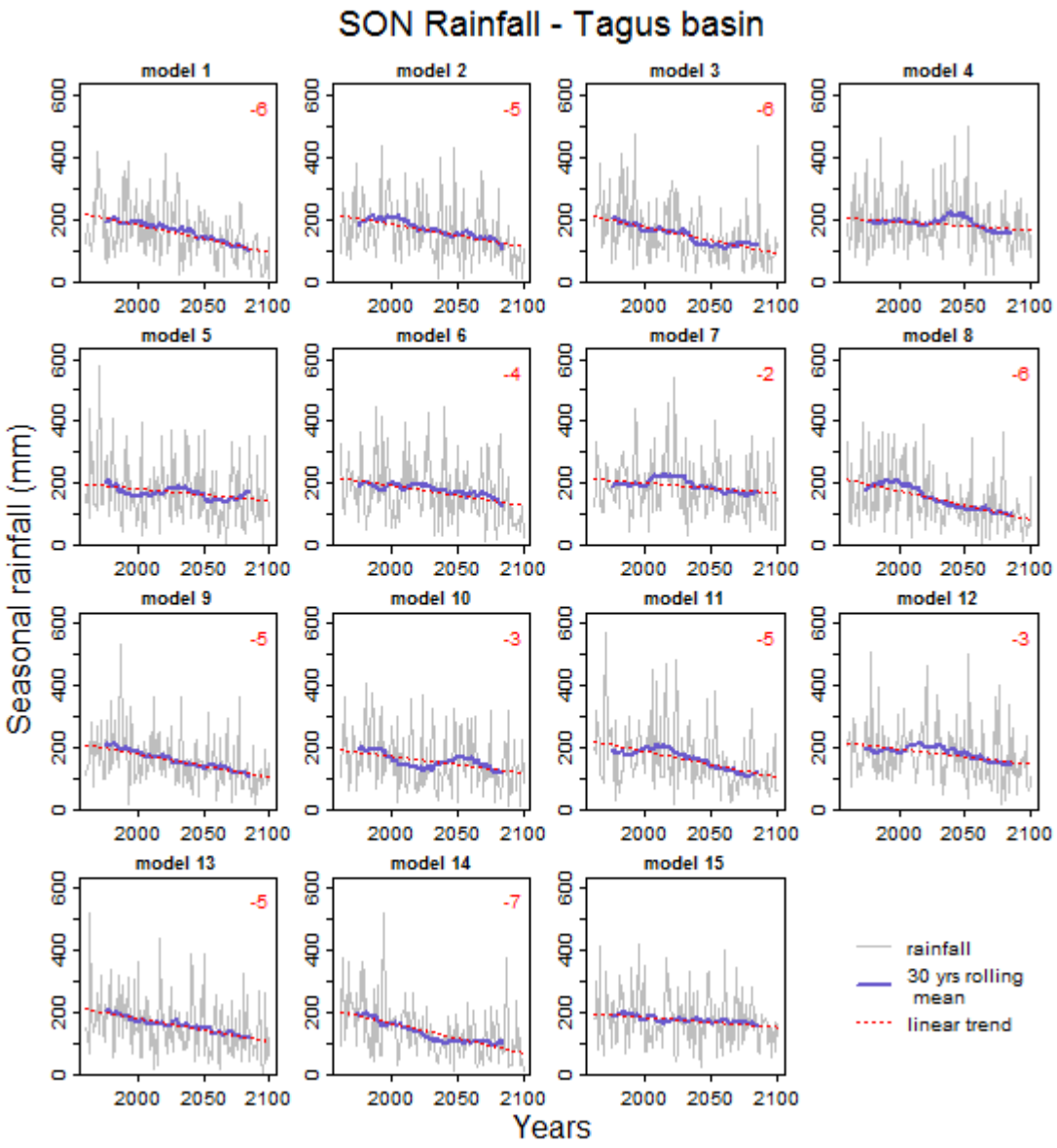

Figure G.7 – Autumn transient bias corrected rainfall for the Tagus basin and for the 15 GCMs. 30 year rolling means are plotted in purple and linear trends in red. When the monotonic trend was significant at a 5% level (using Mann-Kendall test) its magnitude, assuming a linear trend, is presented in the upper right corner of the plot in percentage of change per decade (relative to the 1961-2100 mean rainfall).

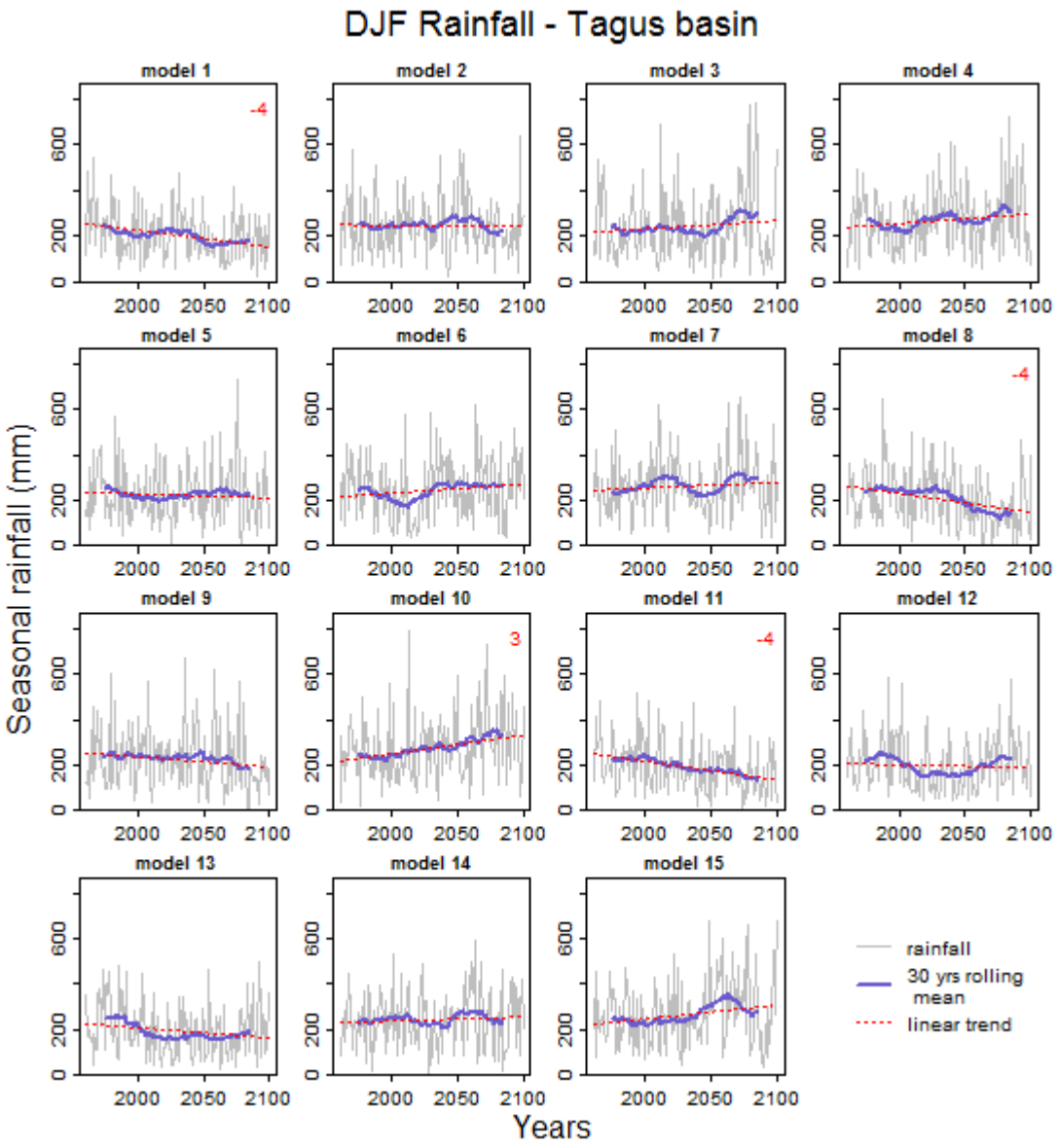

Figure G.8 – Winter transient bias corrected rainfall for the Tagus basin and for the 15 GCMs. 30 year rolling means are plotted in purple and linear trends in red. When the monotonic trend was significant at a 5% level (using Mann-Kendall test) its magnitude, assuming a linear trend, is presented in the upper right corner of the plot in percentage of change per decade (relative to the 1961-2100 mean rainfall).

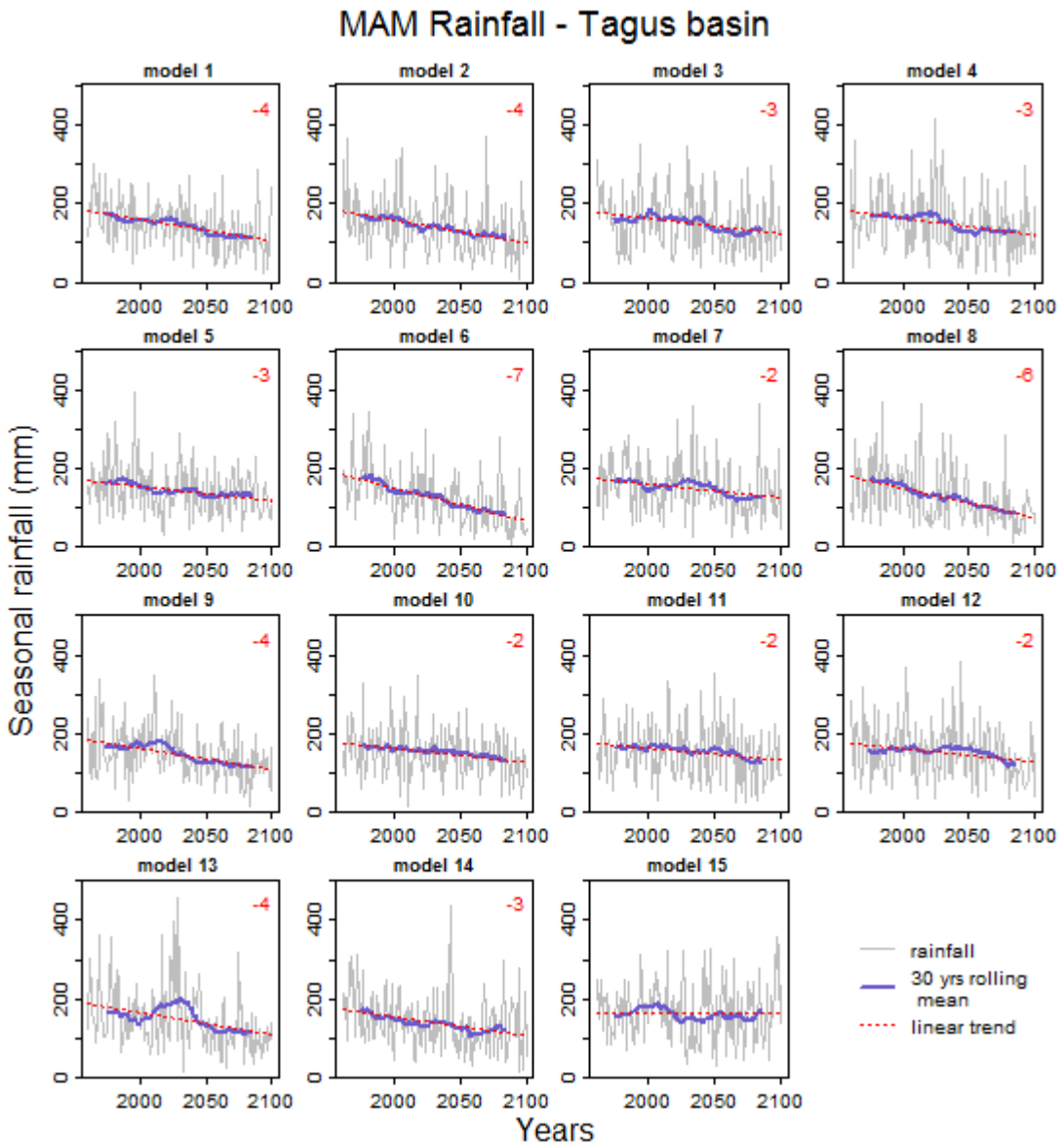

Figure G.9 – Spring transient bias corrected rainfall for the Tagus basin and for the 15 GCMs. 30 year rolling means are plotted in purple and linear trends in red. When the monotonic trend was significant at a 5% level (using Mann-Kendall test) its magnitude, assuming a linear trend, is presented in the upper right corner of the plot in percentage of change per decade (relative to the 1961-2100 mean rainfall).

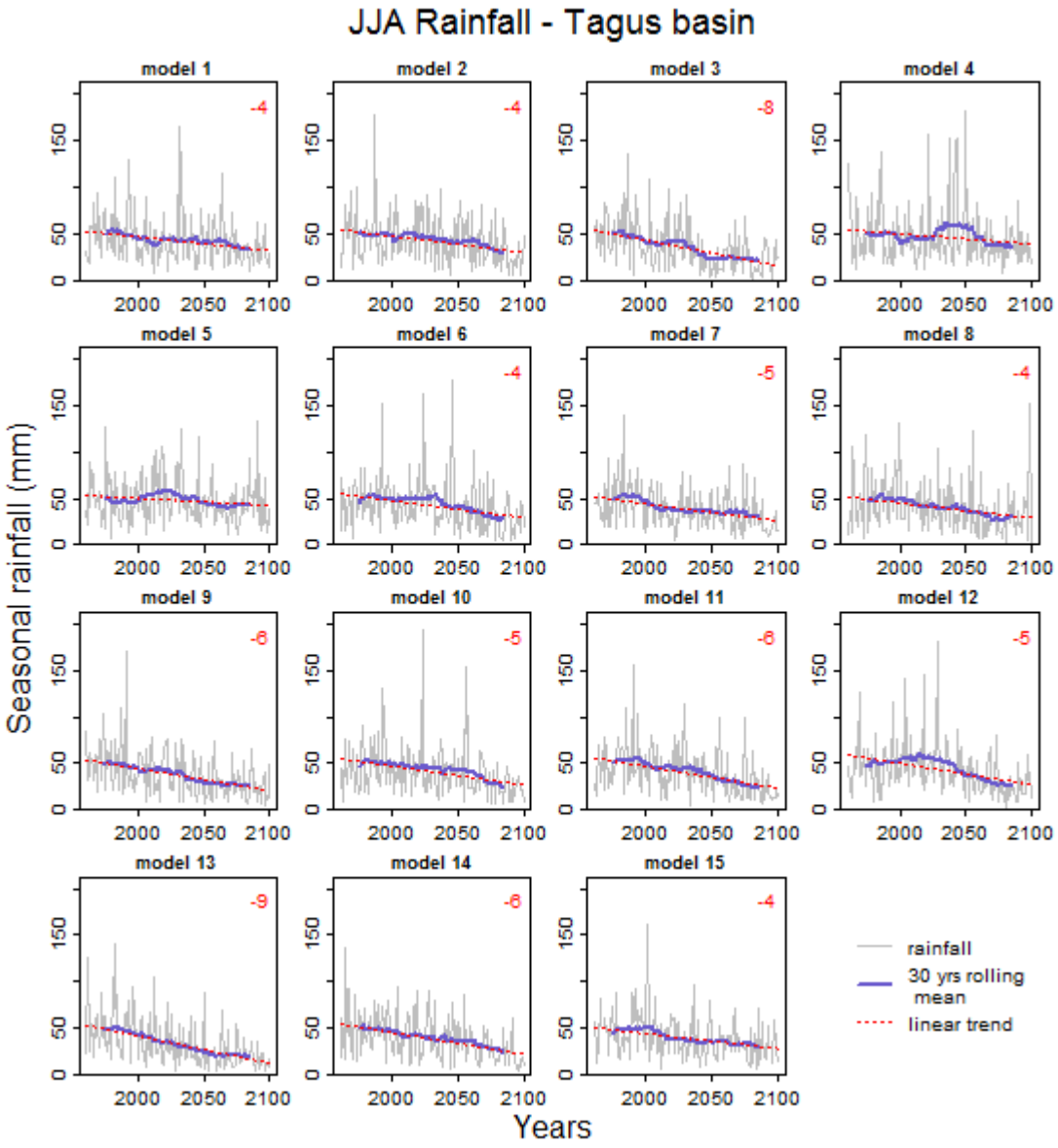

Figure G.10 – Summer transient bias corrected rainfall for the Tagus basin and for the 15 GCMs. 30 year rolling means are plotted in purple and linear trends in red. When the monotonic trend was significant at a 5% level (using Mann-Kendall test) its magnitude, assuming a linear trend, is presented in the upper right corner of the plot in percentage of change per decade (relative to the 1961-2100 mean rainfall).

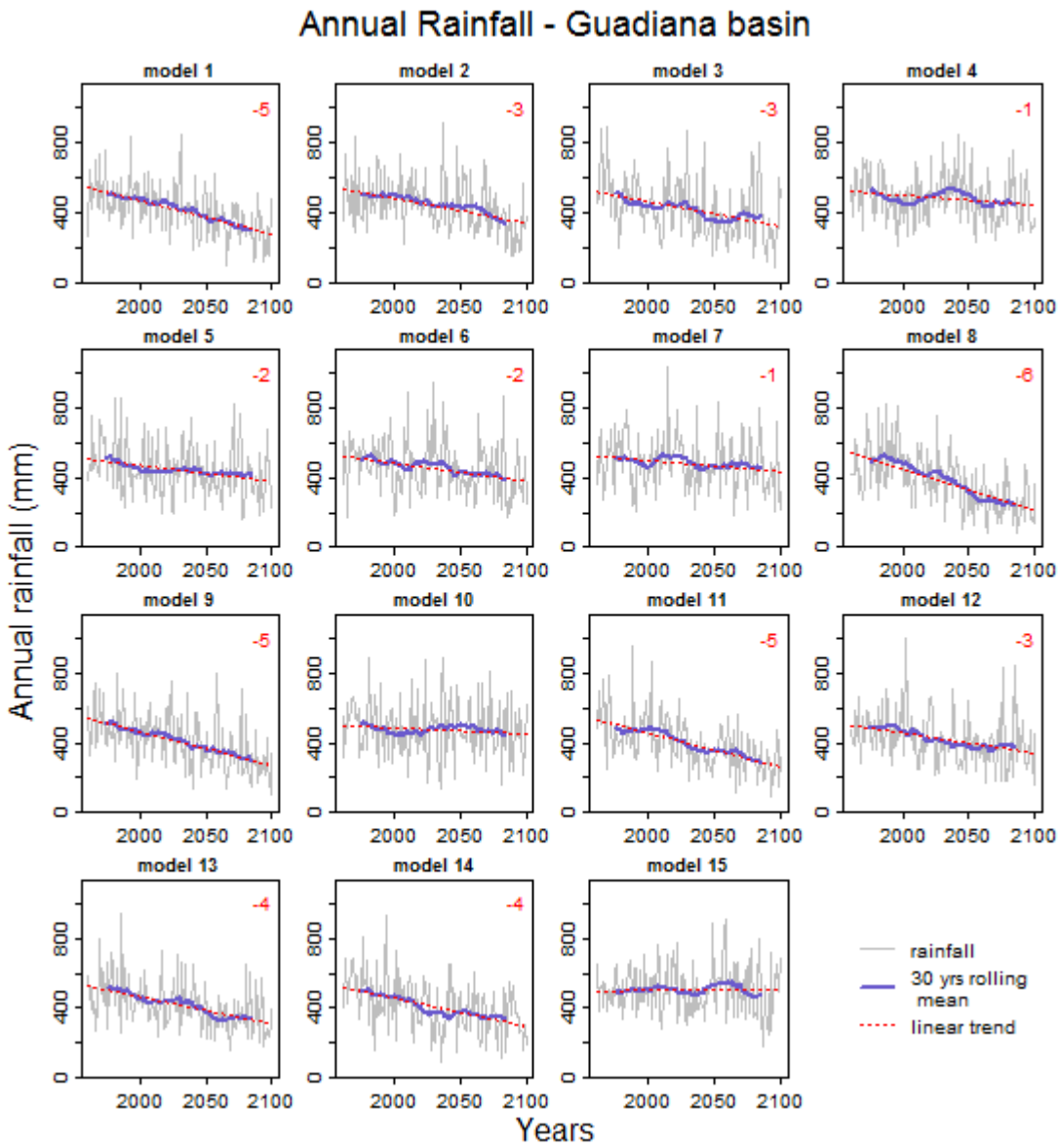

Figure G.11 – Annual transient bias corrected rainfall for the Guadiana basin and for the 15 GCMs. 30 year rolling means are plotted in purple and linear trends in red. When the monotonic trend was significant at a 5% level (using Mann-Kendall test) its magnitude, assuming a linear trend, is presented in the upper right corner of the plot in percentage of change per decade (relative to the 1961-2100 mean rainfall).

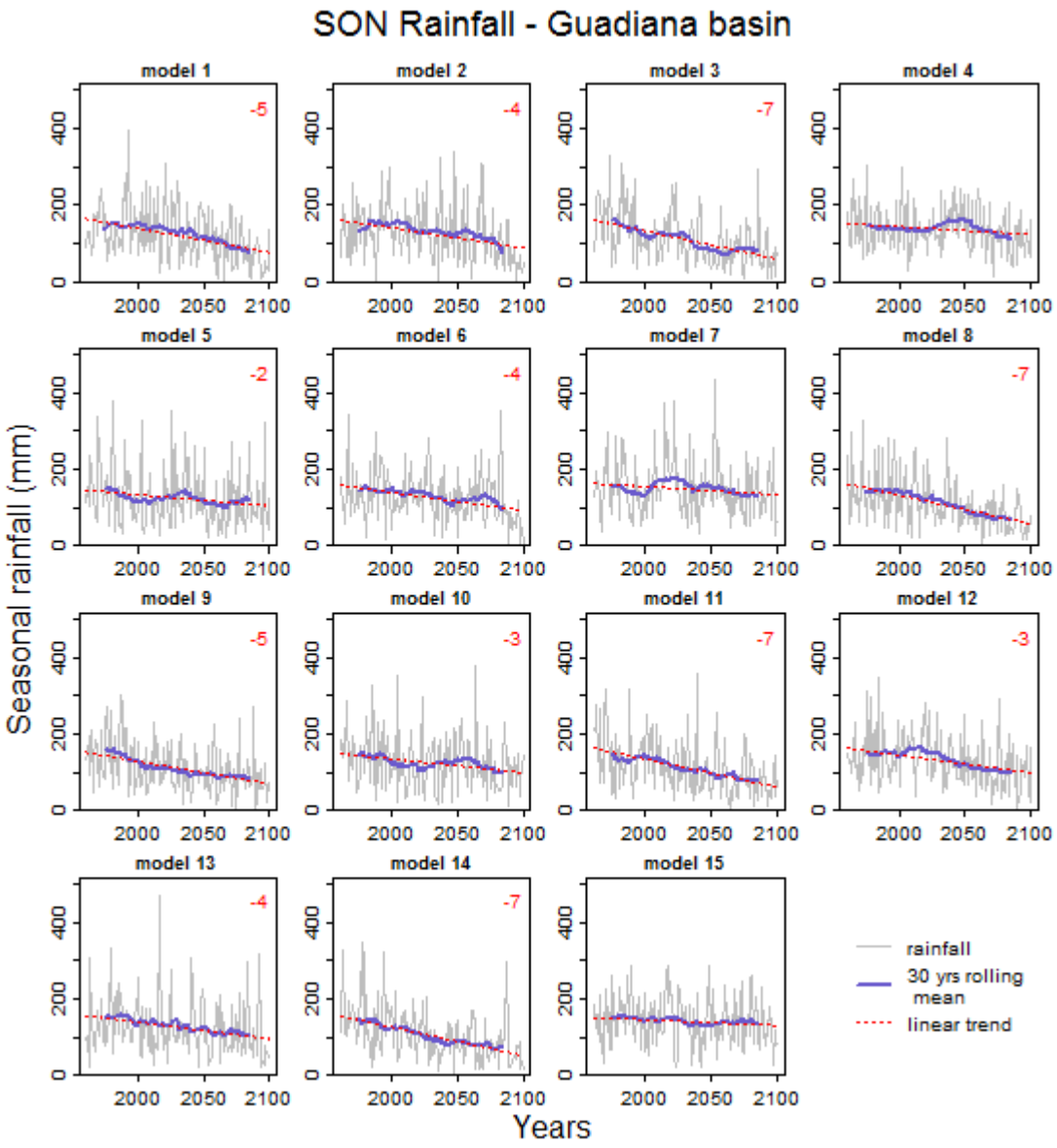

Figure G.12 – Autumn transient bias corrected rainfall for the Guadiana basin and for the 15 GCMs. 30 year rolling means are plotted in purple and linear trends in red. When the monotonic trend was significant at a 5% level (using Mann-Kendall test) its magnitude, assuming a linear trend, is presented in the upper right corner of the plot in percentage of change per decade (relative to the 1961-2100 mean rainfall).

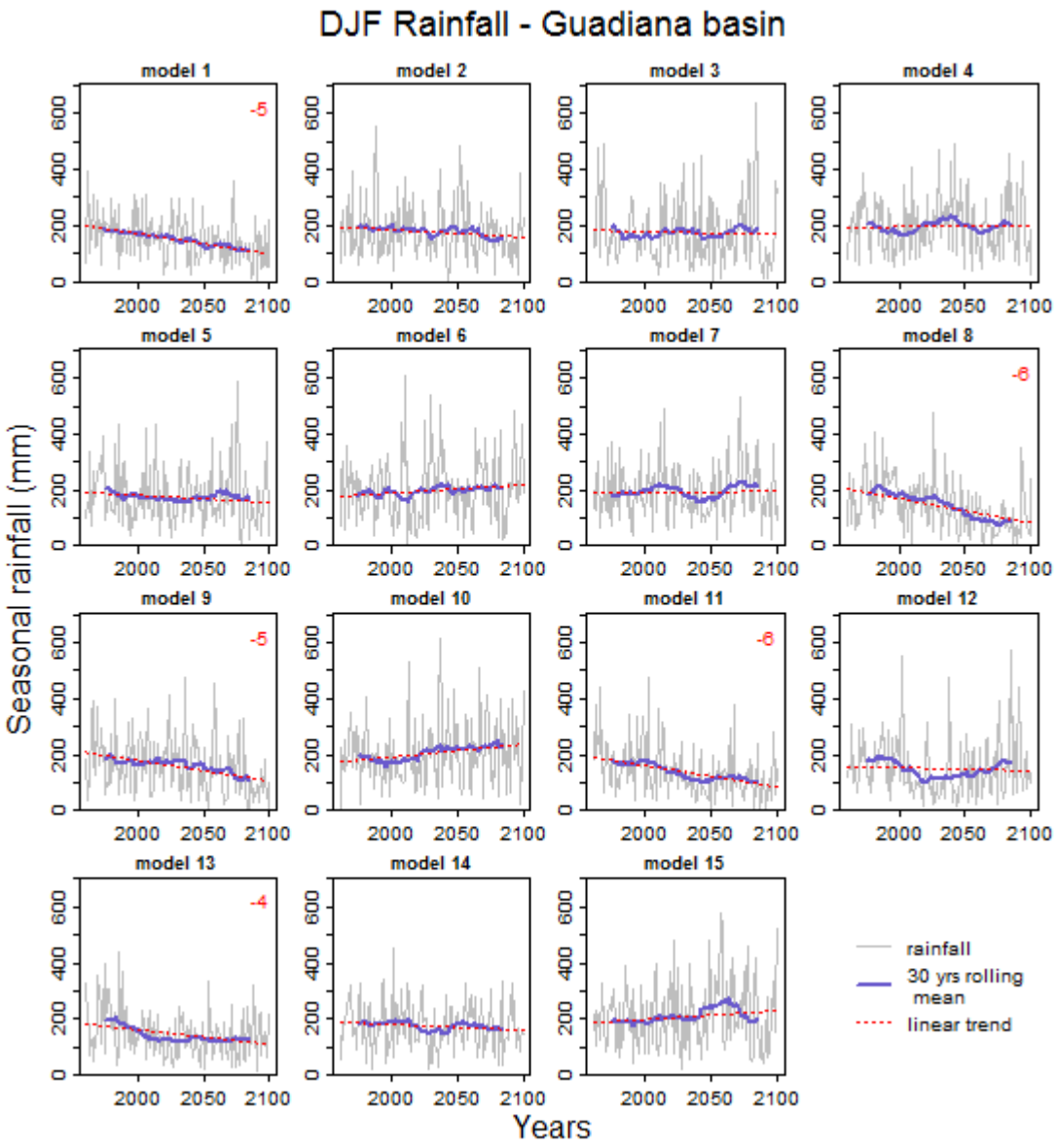

Figure G.13 – Winter transient bias corrected rainfall for the Guadiana basin and for the 15 GCMs. 30 year rolling means are plotted in purple and linear trends in red. When the monotonic trend was significant at a 5% level (using Mann-Kendall test) its magnitude, assuming a linear trend, is presented in the upper right corner of the plot in percentage of change per decade (relative to the 1961-2100 mean rainfall).

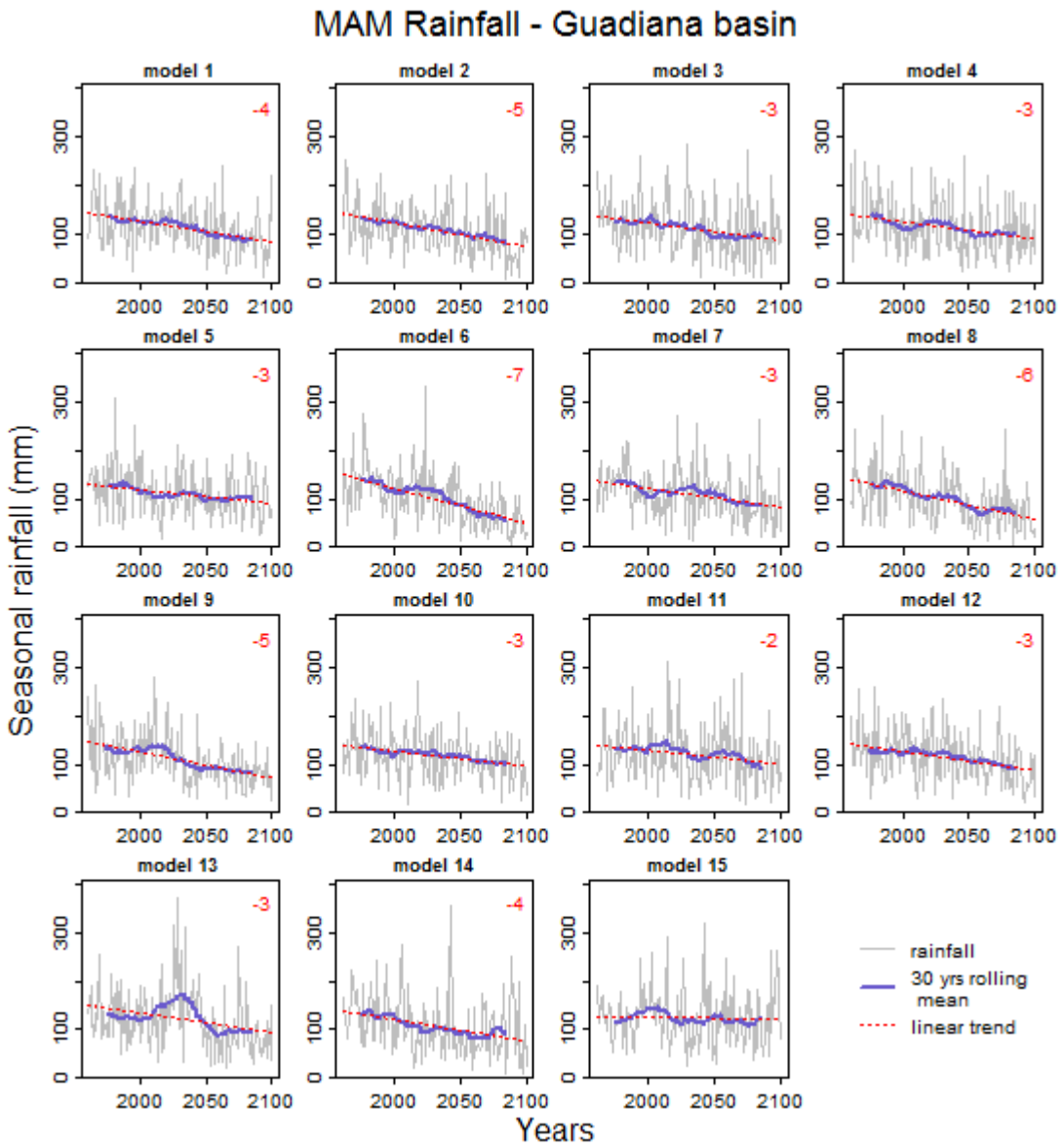

Figure G.14 – Spring transient bias corrected rainfall for the Guadiana basin and for the 15 GCMs. 30 year rolling means are plotted in purple and linear trends in red. When the monotonic trend was significant at a 5% level (using Mann-Kendall test) its magnitude, assuming a linear trend, is presented in the upper right corner of the plot in percentage of change per decade (relative to the 1961-2100 mean rainfall).

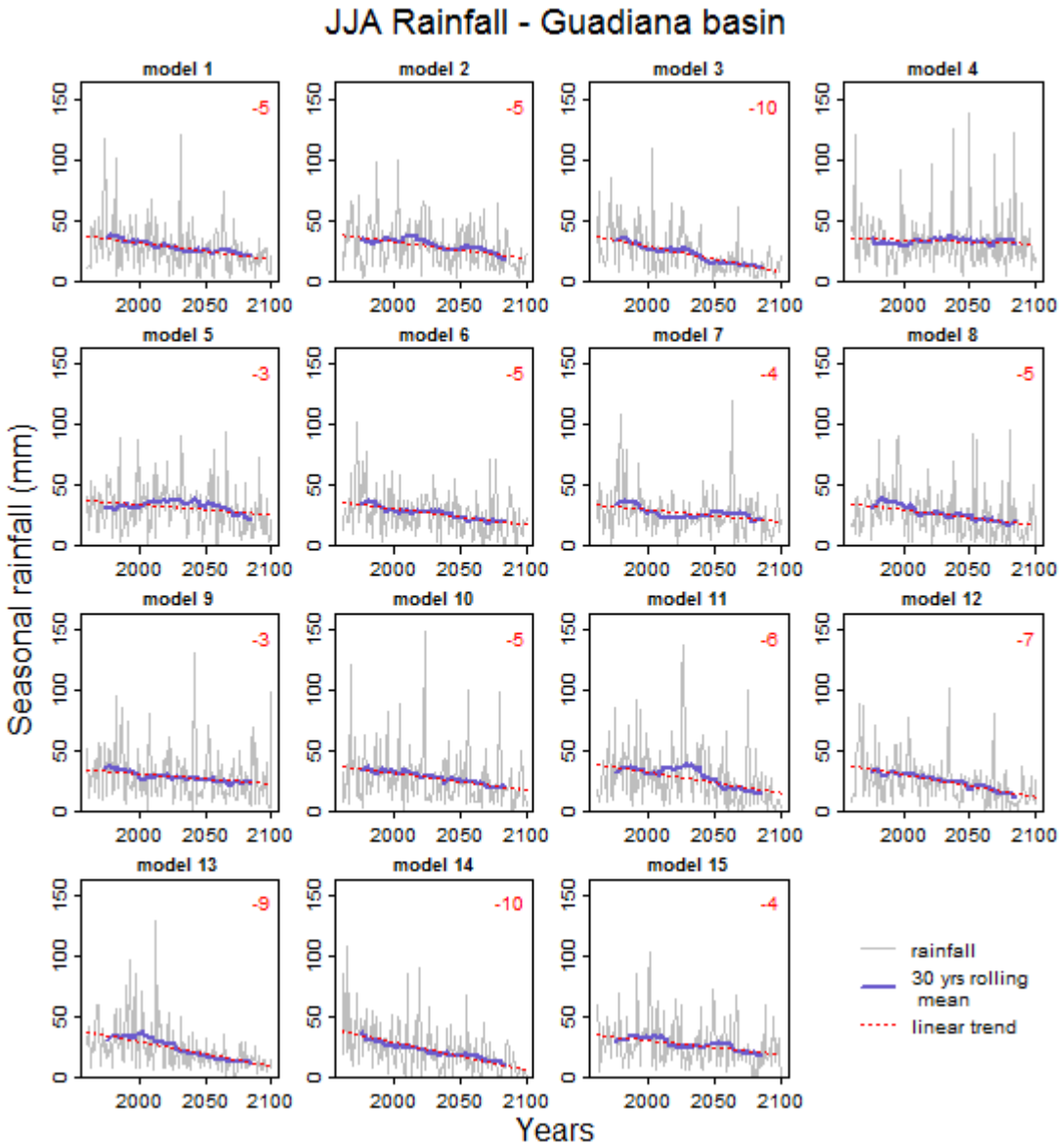

Figure G.15 – Summer transient bias corrected rainfall for the Guadiana basin and for the 15 GCMs. 30 year rolling means are plotted in purple and linear trends in red. When the monotonic trend was significant at a 5% level (using Mann-Kendall test) its magnitude, assuming a linear trend, is presented in the upper right corner of the plot in percentage of change per decade (relative to the 1961-2100 mean rainfall).

Appendix H. Main SHETRAN parameters used in calibration

H.1 – Evapotranspiration/interception module

:ET7 - VEGETATION TYPE 1.Arable
F 0. 0. 0. 0. 0. 3
7 1.0000 1.15001.40E-5 5.1000 8 4.0000 0 0
:ET15 - PSI/RCF/FET FUNCTION FOR VEGETATION TYPE
-1000. 0. 0.0
-150.0 0. 0.0060
-50.00 0. 0.0300
-20.00 0. 0.0700
-10.00 0. 0.1900
-1.000 0. 0.5000
-0.100 0. 0.5500

→Storage capacity of canopy (mm)

→ Soil moisture tension (m)

→ Ratio of actual and potential evapotranspiration

:ET7 - VEGETATION TYPE 2.BareGround
F 0. 0. 0. 0. 0. 3
7 0.0 0.01.40E-5 5.1000 1 1.0000 0 0
:ET15 - PSI/RCF/FET FUNCTION FOR VEGETATION TYPE
-1000. 0. 0.0
-150.0 0. 0.0060
-50.00 0. 0.0100
-20.00 0. 0.0150
-10.00 0. 0.0300
-1.000 0. 0.0800
-0.100 0. 0.0900

:ET7 - VEGETATION TYPE 3. Grass
F 0. 0. 0. 0. 0. 3
7 1.0000 1.15001.40E-5 5.1000 10 6.0000 0 0
:ET15 - PSI/RCF/FET FUNCTION FOR VEGETATION TYPE
-1000. 0. 0.0
-150.0 0. 0.0060
-50.00 0. 0.0150
-20.00 0. 0.0300
-10.00 0. 0.1000
-1.000 0. 0.5000
-0.100 0. 0.5100

:ET7 - VEGETATION TYPE DeciduousForest
F 0. 0. 0. 0. 0. 3
7 1.0000 2.00001.40E-5 5.1000 13 6.0000 0 0
:ET15 - PSI/RCF/FET FUNCTION FOR VEGETATION TYPE
-1000. 0. 0.0
-150.0 0. 0.0060
-50.00 0. 0.0150
-20.00 0. 0.0200
-10.00 0. 0.0350
-1.000 0. 0.1300
-0.100 0. 0.1350

```
:ET7 - VEGETATION TYPE EvergreenForest
    F    0.    0.    0.    0.    0.     3
    7 1.0000 1.15001.40E-5 5.1000    15 6.0000     0     0
:ET15 - PSI/RCF/FET FUNCTION FOR VEGETATION TYPE
-1000.    0.   0.0
 -150.0    0. 0.0060
 -50.00    0. 0.0150
 -20.00    0. 0.0200
 -10.00    0. 0.0350
 -1.000    0. 0.1300
 -0.100    0. 0.1350

:ET7 - VEGETATION TYPE Shrub
    F    0.    0.    0.    0.    0.     3
    7 1.0000 1.15001.40E-5 5.1000    10 3.0000     0     0
:ET15 - PSI/RCF/FET FUNCTION FOR VEGETATION TYPE
-1000.    0.   0.0
 -150.0    0. 0.0060
 -50.00    0. 0.0100
 -20.00    0. 0.0150
 -10.00    0. 0.0300
 -1.000    0. 0.1300
 -0.100    0. 0.1350

:ET7 - VEGETATION TYPE    Urban
    F    0.    0.    0.    0.    0.     3
    7   0.0   0.01.40E-5 5.1000     1 1.0000     0     0
:ET15 - PSI/RCF/FET FUNCTION FOR VEGETATION TYPE
 -1000.    0.   0.0
 -150.0    0.   0.0
 -50.00    0.   0.0
 -20.00    0.   0.0
 -10.00    0.   0.0
 -1.000    0.   0.0
 -0.100    0.   0.0

:ET7 - VEGETATION TYPE Mix Forest
    F    0.    0.    0.    0.    0.     3
    7 1.0000 1.60001.40E-5 5.1000    13 6.0000     0     0
:ET15 - PSI/RCF/FET FUNCTION FOR VEGETATION TYPE
-1000.    0.   0.0
 -150.0    0. 0.0060
 -50.00    0. 0.0150
 -20.00    0. 0.0200
 -10.00    0. 0.0350
 -1.000    0. 0.1300
 -0.100    0. 0.1350
```

```
:ET7 - VEGETATION TYPE AgroForestry
    F    0.    0.    0.    0.    0.     3
    7 1.0000 1.30001.40E-5 5.1000    15 3.0000     0     0
:ET15 - PSI/RCF/FET FUNCTION FOR VEGETATION TYPE
-1000.    0.   0.0
 -150.0    0. 0.0060
 -50.00    0. 0.0225
 -20.00    0. 0.0450
 -10.00    0. 0.1125
 -1.000    0. 0.3150
 -0.100    0. 0.3425
```

H.2 – Variably saturated subsurface module

```
:VS05 physical property data (IS,IVSFLG,IVSNTB / KX,KY,KZ,THSAT,THRES,SS,N,ALF)

  405     1     0        aquifer- karst (type 6, 76,87,191,224)
1100.0 1100.0 1100.0  0.30 0.200 0.0010 2.00 0.02

  406     1     0       aquifer - permeable detrital formations (type 240,280 - alluvium near rivers
 10.0  10.0  10.0  0.500  0.1000  0.0010  1.900  0.03

  407     1     0        permeable detrital formations (type 12,73,78,83)
 2.0  2.0  2.0  0.500  0.1000  0.0010  1.900  0.03
```

→ Saturated hydraulic conductivity in the x, y and z directions (m/day)

NOTE: Strickler coefficients were not changed for calibration proposes since their impact on monthly flows were negligible.

Appendix I. Convention plots

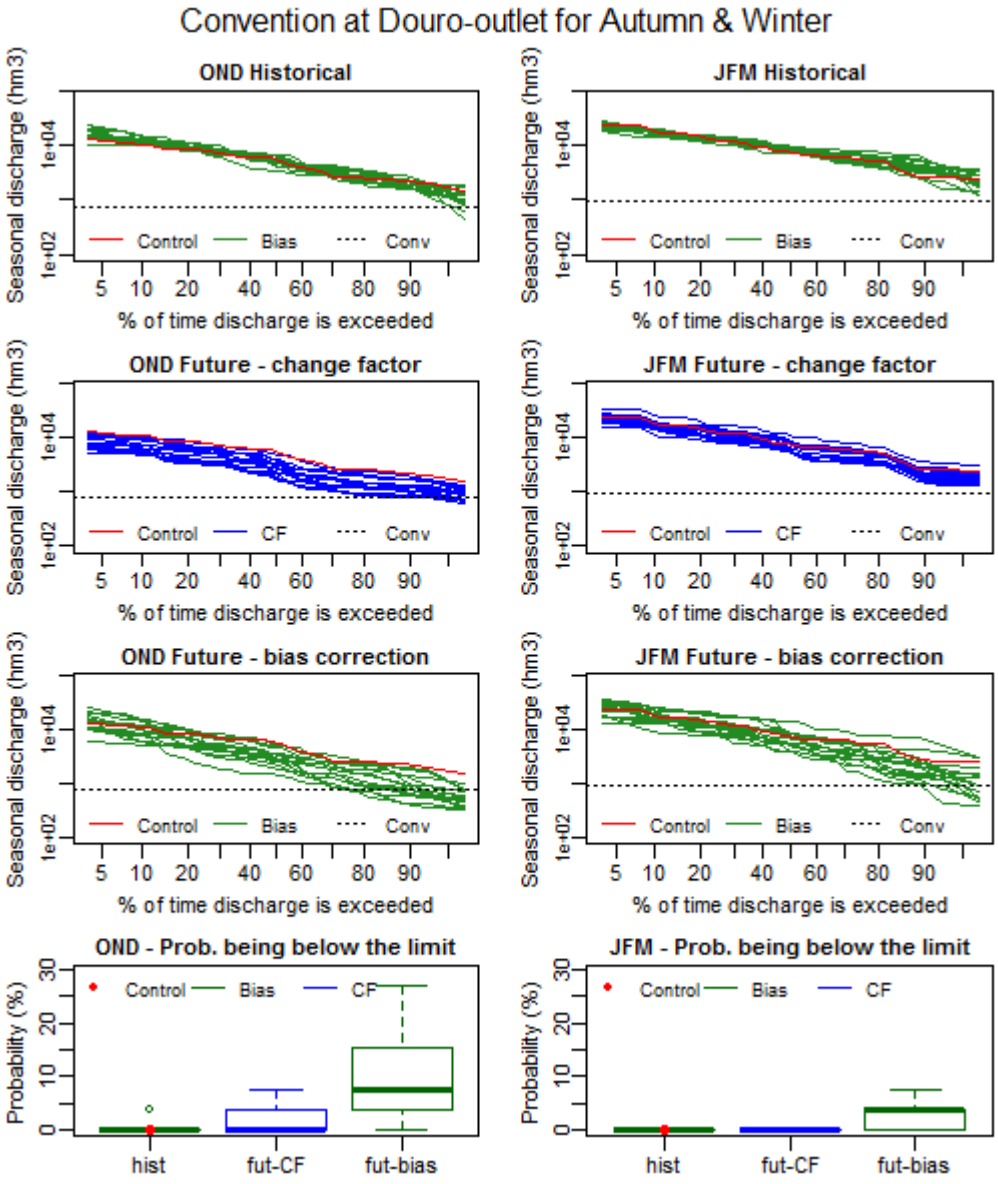

Figure I.1 – Flow duration curves for Douro-outlet for historical (1965-1990) seasonal discharge (top) and future seasonal discharge using change factor method (second row) and using the bias correction method (third row). Boxplots of probability of seasonal discharge being bellow the seasonal convention limit (bottom). Plots on the left are for autumn (October, November, December) and plots on the right are for winter (January, February and March).

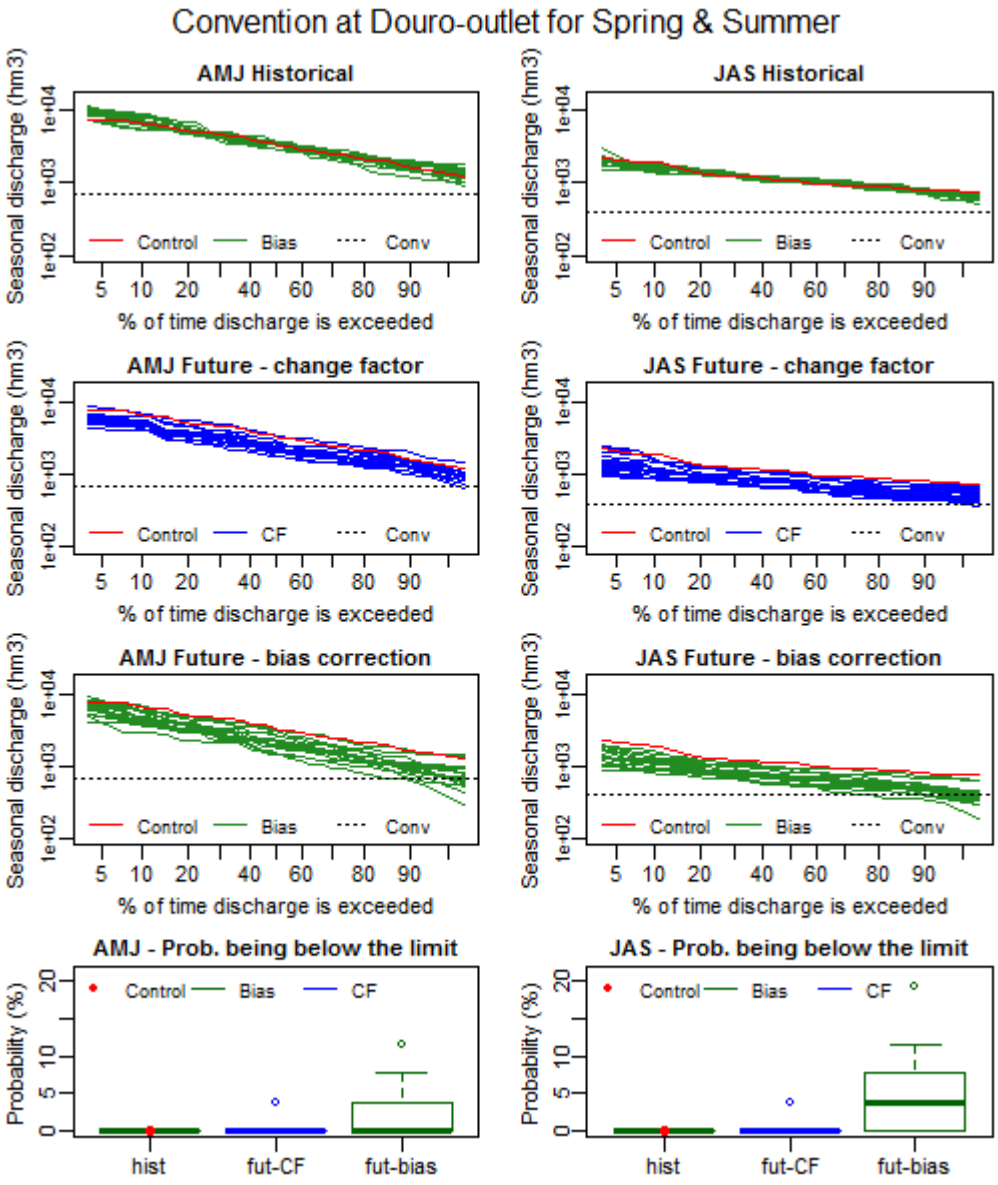

Figure I.2 – Flow duration curves for Douro-outlet for historical (1965-1990) seasonal discharge (top) and future seasonal discharge using change factor method (second row) and using the bias correction method (third row). Boxplots of probability of seasonal discharge being bellow the seasonal convention limit (bottom). Plots on the left are for spring (April, May, June) and plots on the right are for summer (July, August, September).

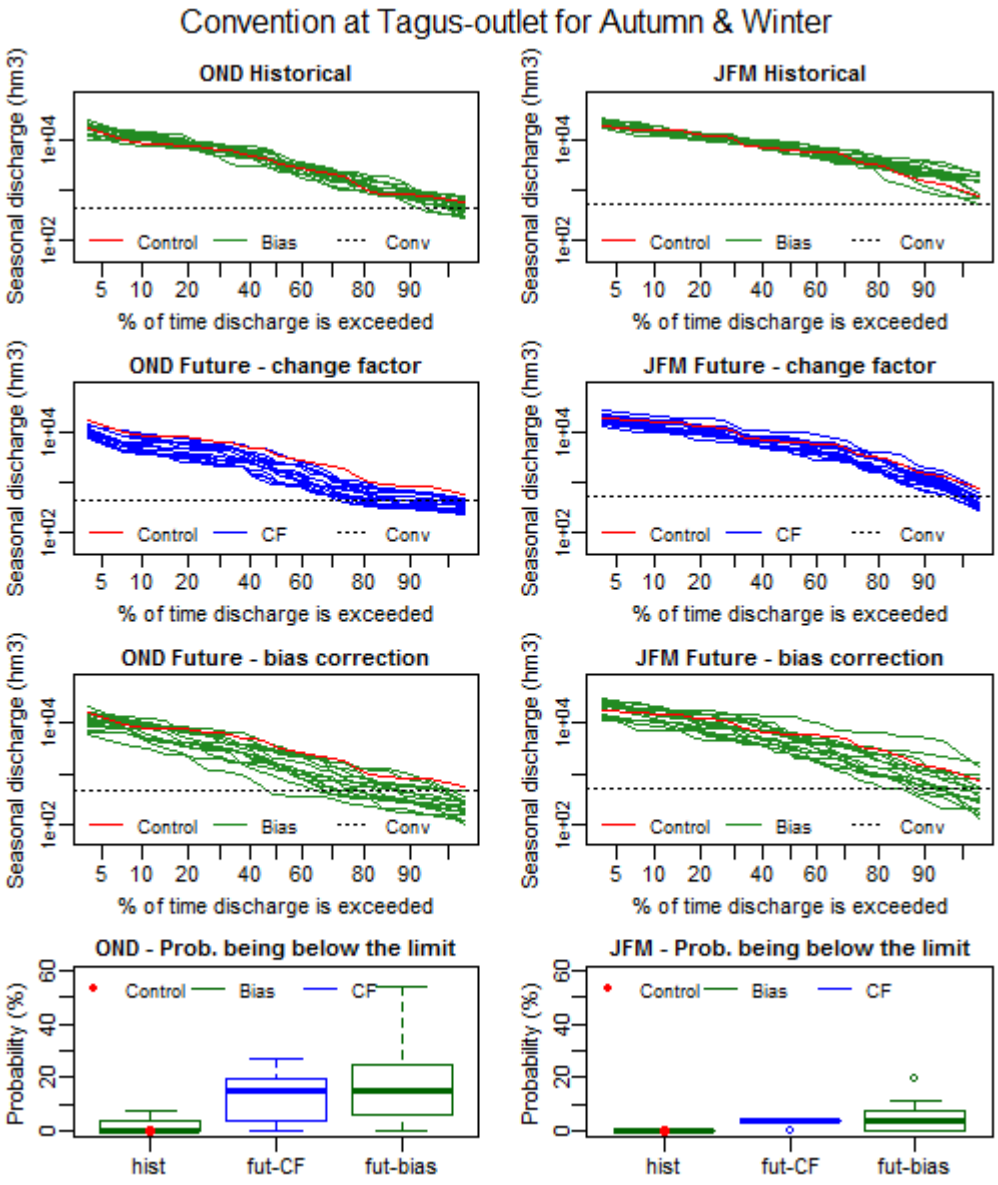

Figure I.3 – Flow duration curves for Tagus-outlet for historical (1965-1990) seasonal discharge (top) and future seasonal discharge using change factor method (second row) and using the bias correction method (third row). Boxplots of probability of seasonal discharge being bellow the seasonal convention limit (bottom). Plots on the left are for autumn (October, November, December) and plots on the right are for winter (January, February and March).

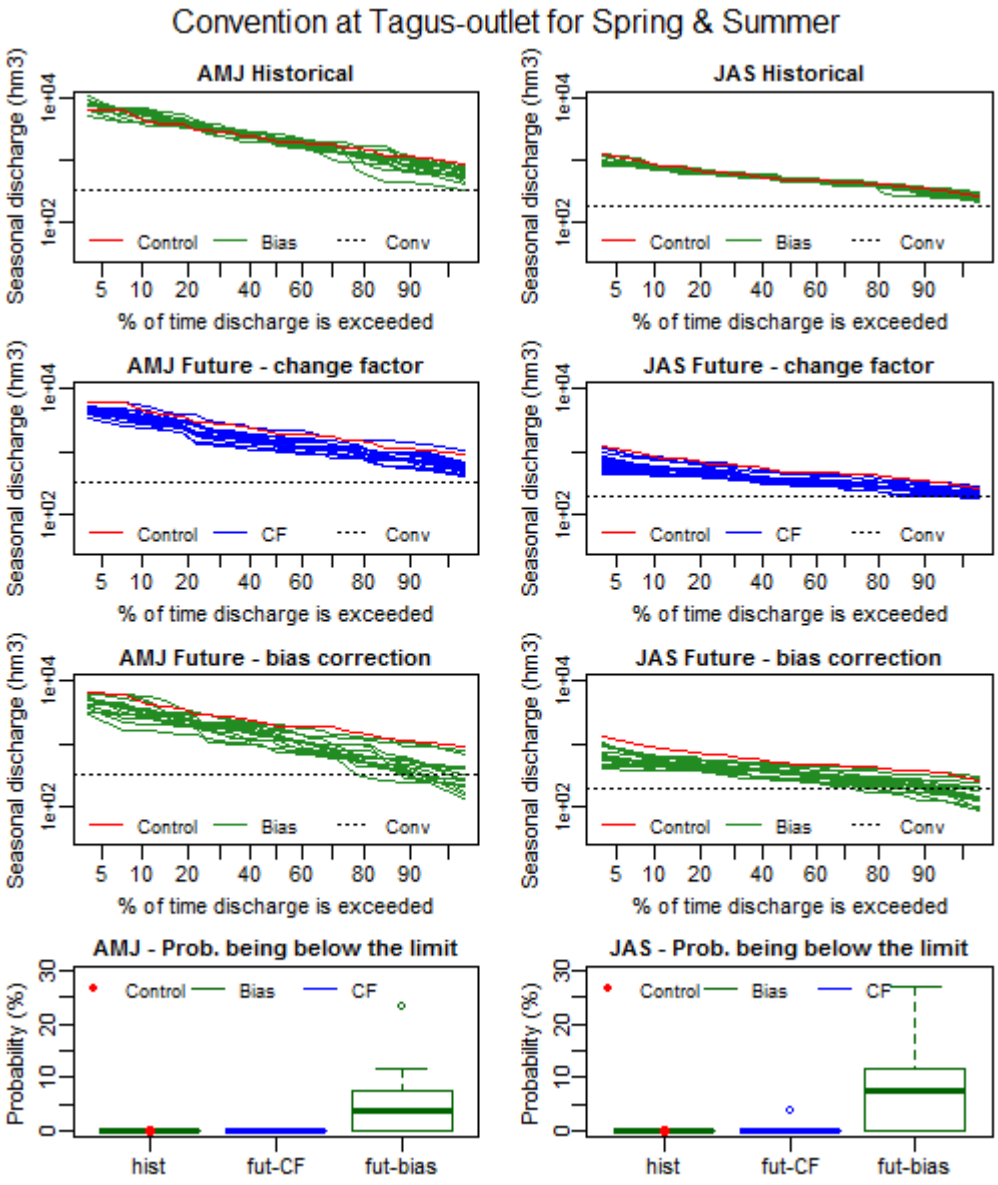

Figure I.4 – Flow duration curves for Tagus-outlet for historical (1965-1990) seasonal discharge (top) and future seasonal discharge using change factor method (second row) and using the bias correction method (third row). Boxplots of probability of seasonal discharge being bellow the seasonal convention limit (bottom). Plots on the left are for spring (April, May, June) and plots on the right are for summer (July, August, September).

References

- AEMET - Agencia Estatal de Meteorologia. Available at: http://www.meteo.pt/pt/media/noticias/newsdetail.html?f=/pt/media/noticias/textos/atlas_na_net.html (Accessed: 03-05-2011).
- AEMET (2013) Vigilancia de la sequía. Available at: http://www.aemet.es/es/serviciosclimaticos/vigilancia_clima/vigilancia_sequia?w=0 (Accessed: 04/07/2013).
- Almeida, A.B.d., Portela, M.M. and Machado, M. (2009) A case of transboundary water agreement - the Albufeira Convention in Strategy and methodology for improved IWRM - An integrated interdisciplinary assessment in four twinning river basins (STRIVER).
- Almeida, C., Mendonça, J.J.L., Jesus, M.R. and Gomes, A.J. (2000) Sistemas aquiferos de Portugal Continental - Aquifer systems of mainland Portugal. [Online]. Available at: http://snirh.pt/snirh/download/aquiferos_PortugalCont/Introducao_Orla_Ocidental.pdf.
- Andrade, C., Santos, J.A., Pinto, J.G. and Corte-Real, J. (2011) 'Large-scale atmospheric dynamics of the wet winter 2009–2010 and its impact on hydrology in Portugal', Climate Research, 46, pp. 29-41.
- Baldock, D., Caraveli, H., Dwyer, J., Einschütz, S., Petersen, J.E., Sumpsi-Vinas, J. and Varela-Ortega, C. (2000) The environmental Impacts of Irrigation in the European Union.Environment Directorate of the European Commision.
- Baptista, J.M. (2014) Uma abordagem regulatória integrada (ARIT-ERSAR) para os serviços de águas e resíduos. Lisbon: Entidade Reguladora dos Serviços de Águas e Resíduos (ERSAR).
- Beguería, S., Vicente-Serrano, S.M., López-Moreno, J.I., Lana-Renault, N., García-Ruiz., J.M., Almeida, A.B.d., Portela, M.M. and Machado, M. (2009) IWRM status in the Tagus basin, Spain in Strategy and methodology for improved IWRM - An integrated interdisciplinary assessment in four twinning river basins (STRIVER).
- Belo-Pereira, M., Dutra, E. and Viterbo, P. (2011) 'Evaluation of global precipitation data sets over the Iberian Peninsula', Journa of Geophysical Research, 116(D20101), p. 16.
- Birkinshaw, S.J., James, P. and Ewen, J. (2010) 'Graphical User Interface for Rapid Set-up of SHETRAN Physically-Based River Catchment Model', Environmental Modelling and Software, 25(4), pp. 609-610.
- Blenkinsop, S. and Fowler, H.J. (2007) 'Changes in European drought characteristics projected by the PRUDENCE regional climate models', International Journal of Climatology, 27, pp. 1595–1610.
- Boé, J., Terray, L., Habets, F. and Martin, E. (2007) 'Statistical and dynamical downscaling of the Seine basin climate for hydro-meteorological studies', International Journal of Climatology, 27, pp. 1643–1655.
- Boé, J., Terray, L., Martin, E. and Habets, F. (2009) 'Projected changes in components of the hydrological cycle in French river basins during the 21st century', Water Resources Research, 45.
- Bordi, I., Fraedrich, K. and sutera, A. (2009) 'Observed drought and wetness trends in Europe: an update', Hydrology and Earth System Sciences 13(1519-1530).

- Brandão, C. and Rodrigues, R. (2000) 'Hydrological Simulation of the International Catchment of Guadiana River ', Phys. Chem. Earth 25(3), pp. 329-339.
- Brunet, M., Casado, M.J., Castro, M.d., Galán, P., López, J.A., Martín, J.M., Pastor, A., Petisco, E., Ramos, P., Ribalaygua, J., Rodríguez, E., Sanz, I. and Torres, L. (2009) Generación de Escenarios Regionalizados de Cambio Climático para España.
- Bryant, S.J., Arnell, N.W. and Law, F.M. (1992) 'The long-term context for the current hydrological drought.', IWEM Conference on the Management of Scarce Water Resources.
- C.H.TAJO (2014). Available at: http://web.archive.org/web/20110704021300/http://www.chtajo.es/ventanas/f_ifpresaemb.htm (Accessed: 03-03-2014).
- Casou, C., Terray, L., Hurrell, J. and Deser, C. (2004) 'North Atlantic Winter Climate Regimes: Spatial Asymmetry, Stationarity with Time', Journal of Climate, 17, pp. 1055-1068.
- CEDEX GRAPES project. Available at: http://hercules.cedex.es/hidrologia/pub/proyectos/grapes.htm (Accessed: 30/05/2012).
- CHD (1999) Plan hidrologico Duero 1999.
- CHD (2007) Plan hidrológico de la parte española de la demarcación hidrográfica del Duero - Estudio general de la demarcación. Tomo 2. Anexo de actualización.
- CHG (1999) Plan hidrologico Guadiana 1999.
- CHT (1999) Plan hidrologico Tagus 1999.
- Climate Prediction Center, N. (2011). Available at: http://www.cpc.noaa.gov/data/teledoc/nao.shtml (Accessed: 17/10/2011).
- Conan, C., Marsily, G.d., Bouraoui, F. and Bidoglio, G. (2003) 'A long-term hydrological modelling of the Upper Guadiana river basin (Spain)', Physics and Chemestry of the Earth, 28, pp. 193-200.
- Coron, L., Andréassian, V., Perrin, C., Lerat, J., Vaze, J., Bourqui, M. and Hendrickx, F. (2012) 'Crash testing hydrological models in contrasted climate conditions: An experiment on 216 Australian catchments', Water Resources Research, 48(5).
- Costa, A.C. and Soares, A. (2009) 'Trends in extreme precipitation indices derived from a daily rainfall database for the South of Portugal', International Journal of Climatology, 29, pp. 1956-1975.
- Da Cunha, L.V., De Oliveira, R.P., Nascimento, J. and Ribeiro, L. (2007) 'Impacts of climate change on water resources: A case-study for Portugal', IAHS-AISH Publication, (310), pp. 37-48.
- Daniel, J.S., Portmann, R.W., Solomon, S. and Murphy, D.M. (2012) 'Identifying weekly cycles in meteorological variables: The importance of an appropriate statistical analysis', Journal of Geophysical Research 117(D13203).
- Deser, C., Phillips, A., Bourdette, V. and Teng, H. (2012) 'Uncertainty in climate change projections: the role of internal variability', Climate Dynamics, 38(3-4), pp. 527-546.
- Diaz-Nieto, J. and Wilby, R.L. (2005) 'A comparison of statistical downscaling and climate change factor methods: impacts on low flows in the River Thames, United Kingdom', Climatic Change (69), pp. 245-268.
- Dickson, B. (2010) The North Atlantic Sector during Positive and Negative Extrema of the NAO. Available at: http://www.ices.dk/globec/data/bf4/naomap.htm (Accessed: 13 December 2010).

- Douglas, E.M., Vogel, R.M. and Kroll, C.N. (2000) 'Trends in floods and low flows in the United States: impact of spatial correlation', Journal of hydrology, 240, pp. 90-105.
- EDIA (2010). Available at: http://www.edia.pt/portal/page?_pageid=53,39721&_dad=portal&_schema=PORTAL&actualmenu=4481468&p_agua_d=2201439&cboui=2201439 (Accessed: April 2010).
- Ehret, U., Zehe, E., Wulfmeyer, V., Warrach-Sagi, K. and Liebert, J. (2012) 'Should we apply bias correction to global and regional climate model data?', Hydrol. Earth Syst. Sci., 16, pp. 3391-3404.
- Ekström, M., Jones, P.D., Fowler, H.J., Lenderink, G., Buishand, T.A. and Conway, D. (2007) 'Regional climate model data used within the SWURVE project projected changes in seasonal patterns and estimation of PET', Hydrology and Earth System Sciences, 11(3), pp. 1069-1083.
- Ewen, J., Parkin, G. and O'Connell, P.E. (2000) 'SHETRAN: distributed river basin flow and transport modeling system ', Journal of Hydrologic Engineering, 5(3), pp. 250-258.
- Fatichi, S., Barbosa, S.M., Caporali, E. and Silva, M.E. (2009) 'Deterministic versus stochastic trends: Detection and challenges', Journal of Geophysical Research: Atmospheres 114(18).
- Fowler, H.J., Blenkinsop, S. and Tebaldi, C. (2007) 'Linking climate change modelling to impacts studies: recent advances in downscaling techniques for hydrological modelling', International Journal of Climatology, 27, pp. 1547-1578.
- Gámiz-Fortis, S., Pozo-Vázquez, D., Trigo, R.M. and Castro-Díez, Y. (2008) 'Quantifying the Predictability of Winter River Flow in Iberia. Part I: Interannual Predictability', Journal of Climate, 21, pp. 2484-2501.
- García-Herrera, R., Paredes, D., Trigo, R.M., Trigo, I.F., Hernández, E., Barriopedro, D. and Mendes, M.A. (2007) 'The Outstanding 2004/05 Drought in the Iberian Peninsula: Associated Atmospheric Circulation', Journal of Hydrometeorology, 8.
- González-Hidalgo, J.C., Brunetti, M. and Luis, M.d. (2010a) 'A new tool for monthly precipitation analysis in Spain: MOPREDAS database (monthly precipitation trends December 1945–November 2005)', International Journal of Climatology, 31(5), pp. 715-731.
- Gonzalez-Hidalgo, J.C., Brunetti, M. and Luis, M.d. (2010b) 'Precipitation trends in Spanish hydrological divisions, 1946–2005', Climate Research, 43, pp. 215-228.
- Gudmundsson, L., Bremnes, J.B., Haugen, J.E. and Engen-Skaugen, T. (2012) 'Technical Note: Downscaling RCM precipitation to the station scale using statistical transformations – A comparison of methods', Hydrology and Earth System Sciences, 16(9), pp. 3383-3390.
- Gupta, H.V., Kling, H., Yilmaz, K.K. and Martinez, G.F. (2009) 'Decomposition of the mean squared error and NSE performance criteria: Implications for improving hydrological modelling', Journal of Hydrology, 377(1-2), pp. 80-91.
- Guttman, N.B. (1999) 'Accepting the standardized precipitation index: a calculation algorithm', Journal of the American Water Resources Association, 35(2), pp. 311-322.
- Haerter, J.O., Hagemann, S., Moseley, C. and Piani, C. (2010) 'Climate model bias correction and the role of timescales', Hydrol. Earth Syst. Sci., 15, pp. 1064-1079.

- Harris, I., Jones, P.D., Osborn, T.J. and Lister, D.H. (2013) 'Updated high-resolution grids of monthly climatic observations – the CRU TS3.10 Dataset', international Journal of Climatology, in press.
- Heinrich, G. and Gobiet, A. (2012) 'The future of dry and wet spells in Europe: A comprehensive study based on the ENSEMBLES regional climate models', International Journal of Climatology, 32(13), pp. 1951-1970.
- Herrera, S., Gutiérrez, J.M., Ancell, R., Pons, M.R., Frías, M.D. and Fernández, J. (2012) 'Development and analysis of a 50-year high-resolution daily gridded precipitation dataset over Spain (Spain02)', International Journal of Climatology, 32, pp. 74-85.
- Hispagua (2013) La sequía en España. [Online]. Available at: http://hispagua.cedex.es/sites/default/files/especiales/sequia/historia.htm (Accessed: 04/07/2013).
- Hurrell, J.W. and Deser, C. (2009) 'North Atlantic climate variability: The role of the North Atlantic Oscillation', Journal of Marine Systems, (78), pp. 28-41.
- IGME (2012). Available at: http://www.igme.es/scripts/esrimap.dll?name=siasesi&cmd=map&too=3&cox=365428.9971430838&coy=4416692.074209869&niv=11&scw=1280&sch=1024&tem=punacu2&tem=cuenca&tem=permea&tem=per200 (Accessed: 13/12/20012).
- IM and AEMET (2011) Iberian Climate Atlas - Air Temperature and Precipitation (1971-2000). IM - Instituto de Meteorologia
- INAG (1998) Convenção sobre a cooperação para a protecção e o aproveitamento sustentável das águas das bacias hidrográficas Luso-Espanholas - Comprovação do regime de caudais do protocolo adicional.
- INAG (1999a) "Plano de bacia do Douro" (Douro Basin Management Plan). [Online]. Available at: http://www.inag.pt/inag2004/port/a_intervencao/planeamento/pbh/pbh02.html (Accessed: June 2011).
- INAG (1999b) "Plano de bacia do Tejo" (Tagus Basin Management Plan). [Online]. Available at: http://www.inag.pt/inag2004/port/a_intervencao/planeamento/pbh/pbh03.html (Accessed: June 2011).
- INAG (2001) "Plano de bacia do Guadiana" (Guadiana Basin Management Plan). [Online]. Available at: http://www.inag.pt/inag2004/port/a_intervencao/planeamento/pbh/pbh04.html (Accessed: June 2011).
- INAG (2002) Plano Nacional da Água
- INAG (2012). Available at: http://snirh.pt/snirh/_atlasagua/galeria/mapasweb/pt/aa1022.pdf (Accessed: 13/12/2012).
- IPCC (2007) Fourth Assessment Report: Climate Change 2007, Working Group I: The Physical Science Basis.
- IPMA (2013a) Monitorização da Seca - Índice PDSI - Evolução Histórica. Available at: http://www.ipma.pt/pt/oclima/observatorio.secas/pdsi/apresentacao/evolu.historica/ (Accessed: 04/07/2013).
- IPMA (2013b) Monitorização da Seca - Índice SPI - Definição. Available at: http://www.ipma.pt/pt/oclima/observatorio.secas/spi/apresentacao/definicao/index.jsp?page=spi_periods.xml (Accessed: 04/07/2013).

- IPMA (2013c) Monitorização da Seca - Índice SPI - Definição. Available at: http://www.ipma.pt/pt/oclima/observatorio.secas/spi/apresentacao/definicao/ (Accessed: 04/07/2013).
- Jenkins, K. and Warren, R. (2014) 'Quantifying the impact of climate change on drought regimes using the Standardised Precipitation Index', Theoretical and Applied Climatology.
- Jones, P. and Harris, I. (2008) 'CRU Time Series (TS) high resolution gridded datasets'. 30-03-2012. Internet: University of East Anglia Climatic Research Unit (CRU) - NCAS British Atmospheric Data Centre. Available at: http://badc.nerc.ac.uk/view/badc.nerc.ac.uk__ATOM__dataent_1256223773328276
- JRC (2013) Soil data and information systems. Available at: http://eusoils.jrc.ec.europa.eu/esdb_archive/ESDB_data_1k_raster_intro/ESDB_1k_raster_data_intro.html.
- JuntaDeAndalucia (2013) La sequía, un fenómeno complejo. Available at: http://www.juntadeandalucia.es/medioambiente/site/portalweb/menuitem.7e1cf46ddf59bb227a9ebe205510e1ca/?vgnextoid=52b43f05548e5310VgnVCM1000001325e50aRCRD&vgnextchannel=2e0fe3dbc95f4310VgnVCM2000000624e50aRCRD&lr=lang_es (Accessed: 04/07/2013).
- Kenawy, A.E., López-Moreno, J.I. and Vicente-Serrano, S.M. (2011) 'Recent trends in daily temperature extremes over northeastern Spain (1960–2006)', Natural Hazards and Earth System Sciences, 11, pp. 2583-2603.
- Kendall, M.G. (1948) Rank Correlation Methods. Oxford, England: Griffin.
- Kendon, E.J., Roberts, N.M., Senior, C.A. and Roberts, M.J. (2012) 'Realism of rainfall in a very high-resolution regional climate model', Journal of Climate, 25(17), pp. 5791-5806.
- Kilsby, C.G., Tellier, S.S., Fowler, H.J. and Howels, T.R. (2007) 'Hydrological impacts of climate change on the Tejo and Guadiana Rivers', Hydrol. Earth Syst. Sci., 11(3), pp. 1175-1189.
- Kingston, D.G., Todd, M.C., Taylor, R.G., Thompson, J.R. and Arnell, N.W. (2009) 'Uncertainty in the estimation of potential evapotranspiration under climate change', Geophysical Research Letters, 36.
- Knutti, R. (2008) 'Should we believe model predictions of future climate change?', Philosophical Transactions of the Royal Society A: Mathematical, Physical and Engineering Sciences, 366(1885), pp. 4647-4664.
- Knutti, R. (2010) 'The end of model democracy?', Climatic Change, 102(3), pp. 395-404.
- Knutti, R., Abramowitz, G., Collins, M., Eyring, V., Gleckler, P.J., Hewitson, B. and Mearns, L. (2010a) IPCC Expert Meeting on Assessing and Combining Multi Model Climate Projections - Good Practice Guidance Paper on Assessing and Combining Multi Model Climate Projections.
- Knutti, R., Furrer, R., Tebaldi, C., Cermak, J. and Meehl, G.A. (2010b) 'Challenges in combining projections from multiple climate models', Journal of Climate, 23(10), pp. 2739-2758.
- Lafon, T., Dadson, S., Buys, G. and Prudhomme, C. (2013) 'Bias correction of daily precipitation simulated by a regional climate model: a comparison of methods', International Journal of Climatology, 33, pp. 1367-1381.
- Lloyd-Hughes, B. and Saunders, M.A. (2002) 'A drought climatology for Europe', International Journal of Climatology, 22(13), pp. 1571-1592.

- López-Moreno, J.I., Beguería, S., Vicente-Serrano, S.M. and García-Ruiz, J.M. (2007) 'Influence of the North Atlantic Oscillation on water resources in central Iberia: Precipitation, streamflow anomalies, and reservoir management strategies', Water Resources Research, 43(9).
- Lorenzo-Lacruz, J., Vicente-Serrano, S.M., López-Moreno, J.I., Morán-Tejeda, E. and Zabalza, J. (2012) 'Recent trends in Iberian streamflows (1945–2005)', Journal of Hydrology, 414-415, pp. 463-475.
- Magalhães, M. and Bessa, A. (2012) Qualidade e Sustentabilidade dos Serviços de Abastecimento de Águas e Saneamento.Comissão do Ambiente, Ordenamento do Território e Poder Local.
- Mann, H.B. (1945) 'Nonparametric tests against trend', Econometria, 13(3), pp. 245-259.
- Maraun, D., Wetterhall, F., Ireson, A.M., Chandler, R.E., Kendon, E.J., Widmann, M., Brienen, S., Rust, H.W., Sauter, T., Themel, M., Venema, V.K.C., Chun, K.P., Goodess, C.M., Jones, R.G., Onof, C., Vrac, M. and Thiele-Eich, I. (2010) 'Precipitation downscaling under climate change: Recent developments to bridge the gap between dynamical models and the end user', Reviews of Geophysics, 48(3).
- Masson, D. and Knutti, R. (2011) 'Climate model genealogy', Geophysical Research Letters, 38(8).
- McKee, T.B., Doesken, N.J. and Kleist, J. (1993) 'The relationship of drought frequency and duration to time scales', Eighth Conference on Applied Climatology. Anaheim, California.
- MIMAN (1998) Livro blanco del agua en Espana - White book of water in Spain MIMAN - Ministerio de Medio Ambiente.
- MMA (2000) Libro Blanco del Agua en España - White paper of Water in Spain.
- Moss, R.H., Edmonds, J.A., Hibbard, K.A., Manning, M.R., Rose, S.K., Van Vuuren, D.P., Carter, T.R., Emori, S., Kainuma, M., Kram, T., Meehl, G.A., Mitchell, J.F.B., Nakicenovic, N., Riahi, K., Smith, S.J., Stouffer, R.J., Thomson, A.M., Weyant, J.P. and Wilbanks, T.J. (2010) 'The next generation of scenarios for climate change research and assessment', Nature, 463(7282), pp. 747-756.
- NOAA (2005). Available at: http://www.aoml.noaa.gov/phod/amo_faq.php (Accessed: 24-11-2010).
- NOAA (2008). Available at: http://www.cpc.noaa.gov/data/teledoc/nao.shtml (Accessed: 24-11-2010).
- Osborn, T.J. (2006) 'Recent variations in the winter North Atlantic Oscillation', Weather, 61, pp. 353-355.
- Osborn, T.J., Briffa, K.R., Tett, S.F.B., Jones, P.D. and Trigo, R.M. (1999) 'Evaluation of the North Atlantic Oscillation as simulated by a coupled climate model', Climate Dynamics, 15(9), pp. 685-702.
- Papalexiou, S.M., Koutsoyiannis, D. and Makropoulos, C. (2012) 'How extreme is extreme? An assessment of daily rainfall distribution tails', Hydrol. Earth Syst. Sci. Discuss., 9, pp. 5757–5778.
- Paredes, D., Trigo, R., Garcia-Herrera, R. and Trigo, I. (2006) 'Understanding precipitation changes in Iberia in early spring: weather typing and storm-tracking approaches', Journal of Hydrometeorology, 7, pp. 101-113.
- Paulo, A.A., Rosa, R.D. and Pereira, L.S. (2012) 'Climate trends and behaviour of drought indices based on precipitation and evapotranspiration in Portugal', Natural Hazards and Earth System Sciences, 12, pp. 1481–1491.

- Pechlivanidis, I.G., Jackson, B.M., McIntyre, N.R. and Wheater, H.S. (2011) 'Catchment scale hydrological modelling: A review of model types, calibration approaches and uncertainty analysis methods in the context of recent developments in technology and applications', Global Nest Journal, 13(3), pp. 193-214.
- Pettitt, A.N. (1979) 'A non-parametric approach to the change-point problem', Applied Statistics, 28(2), pp. 126-135.
- Phillips, I.D. and McGregor, G.R. (1998) ' The utility of a drought index for assessing the drought hazard in Devon and Cornwall, South West England', Meteorological Applications, 5, pp. 359-372.
- Portela, M.M. and Quintela, A.C. (2002) 'Evaluation of the water resources in Portuguese watersheds without streamflow data', Conferencia Internacional de organismos de Cuenca (International Conference of Basin Organizations). Madrid, Espanha. p. 6.
- Portela, M.M., Almeida, A.B.d. and Machado, M. (2009) Development in river basin management in Portugal – past and future perspectives in Strategy and methodology for improved IWRM - An integrated interdisciplinary assessment in four twinning river basins (STRIVER).
- Prudhomme, C. and Williamson, J. (2013) 'Derivation of RCM-driven potential evapotranspiration for hydrological climate change impact analysis in Great Britain: a comparison of methods and associated uncertainty in future projections', Hydrol. Earth Syst. Sci., 17, pp. 1365–1377.
- Pulquério, M., Garrett, P., Santos, F.D. and Cruz, M.J. (2014) 'On using a generalized linear model to downscale daily precipitation for the center of Portugal: an analysis of trends and extremes', Theoretical and Applied Climatology.
- Reed, S., Koren, V., Smith, M., Zhang, Z., Moreda, F. and Seo, D. (2004) 'Overall distributed model intercomparison project results', Journal of Hydrology, 298(1–4), pp. 27-60.
- Renard, B., Kavetski, D., Kuczera, G., Thyer, M. and Franks, S.W. (2010) 'Understanding predictive uncertainty in hydrologic modeling: The challenge of identifying input and structural errors', Water Resources Research, 46(5).
- Río, S.d., Herrero, L., Fraile, R. and Penas, A. (2010) 'Spatial distribution of recent rainfall trends in Spain (1961–2006)', International Journal of Climatology, 31(5).
- Rodrigo, F.S. and Trigo, R.M. (2007) 'Trends in daily rainfall in the Iberian Peninsula from 1951 to 2002', International Journal of Climatology, 27, pp. 513-529.
- Rougé, C., Ge, Y. and Cai, X. (2013) 'Detecting Gradual and Abrupt Changes in Hydrological Records', Advances in Water Resources, 53(DOI: http://dx.doi.org/10.1016/j.advwatres.2012.09.008), pp. 33-44.
- Sanderson, B.M., O'Neill, B.C., Kiehl, J.T., Meehl, G.A., Knutti, R. and Washington, W.M. (2011) 'The response of the climate system to very high greenhouse gas emission scenarios', Environmental Research Letters, 6(3).
- Santos, F.D., Forbes, K. and Moita, R. (2002) Climate Change in Portugal. Scenarios, Impacts and Adaptation Measures - SIAM Project. Lisbon, Portugal: Gradiva.
- Santos, J., Corte-Real, J. and Leite, S. (2007) 'Atmospheric large-scale dynamics during the 2004/2005 winter drought in Portugal', International Journal of Climatology, 27, pp. 571-586.
- Santos, J.F., Pulido-Calvo, I. and Portela, M.M. (2010) 'Spatial and temporal variability of droughts in Portugal', Water Resources Research, 46, p. 13pp.

- Sheffield, J., Wood, E.F. and Roderick, M.L. (2012) ' Little change in global drought over the past 60 years', Nature, 491.
- Sienz, F., Bothe, O. and Fraedrich, K. (2012) 'Monitoring and quantifying future climate projections of dryness and wetness extremes: SPI bias', Hydrology and Earth System Sciences, 16(7), pp. 2143-2157.
- Smadi, M.M. and Zghoul, A. (2006) 'A Sudden Change In Rainfall Characteristics In Amman, Jordan During The Mid 1950s', American Journal of Environmental Sciences 2(3), pp. 84-91.
- Soľáková, T., Michele, C.D. and Vezzoli, R. (2013) 'A comparison between parametric and non-parametric approaches for the calculation of two drought indices: SPI and SSI', Journal of Hydrologic Engineering, Preview Manuscript.
- Solomon, S., D. Qin, M. Manning, Z. Chen, M. Marquis, K.B. Averyt, M. Tignor and H.L. Miller (2007) Contribution of Working Group I to the Fourth Assessment Report of the Intergovernmental Panel on Climate Change. Press, C.U.
- Sunyer, M.A., Madsen, H. and Ang, P.H. (2010) 'A comparison of different regional climate models and statistical downscaling methods for extreme rainfall estimation under climate change', Atmospheric Research, 103, pp. 119-128.
- Themeßl, M.J., Gobiet, A. and Leuprecht, A. (2011) 'Empirical-statistical downscaling and error correction of daily precipitation from regional climate models', International Journal of Climatology, 31, pp. 1530-1544.
- Thornthwaite, C.W. (1948) 'An approach toward a rational classification of climate', Geogr. Rev., 38, pp. 55–94.
- Trigo, R.M. and DaCamara, C.C. (2000) 'Circulation weather types and their influence on the precipitation regime in Portugal', International Journal of Climatology, 20, pp. 1559 - 1581.
- Trigo, R.M., Pozo-Vázquez, D., Osborn, T.J., Castro-Díez, Y., Gámiz-Fortiz, S. and Esteban-Parra, M.J. (2004) 'North Atlantic Oscillation influence on precipitation, river flow and water resources in the Iberian Peninsula', International Journal of Climatology, 24, pp. 925-944.
- UN (2013) International decade for action "Water for Life" 2005-2015. Available at: http://www.un.org/waterforlifedecade/water_cooperation_2013/albufeira_convention.shtml (Accessed: 10-10-2003).
- UNEP (2003). Available at: http://www.grid.unep.ch/product/publication/freshwater_europe/douro.php (Accessed: June 2010).
- UNEP (2003b). Available at: http://www.grid.unep.ch/product/publication/freshwater_europe/tagus.php (Accessed: June 2010).
- UNEP (2004). Available at: http://www.grid.unep.ch/product/publication/freshwater_europe/guadiana.php.
- US_Army (1943) ' Ocean Currents and Sea Ice from Atlas of World Maps, United States Army Service Forces', in. Available at: http://commons.wikimedia.org/wiki/File:Ocean_currents_1943_(borderless)3.png
- USGS (2011) Hydro1K Europe. Available at: http://eros.usgs.gov/#/Find_Data/Products_and_Data_Available/gtopo30/hydro/europe (Accessed: 09-02-2011).
- Vicente-Serrano, S.M. (2006a) 'Spatial and temporal analysis of droughts in the Iberian Peninsula (1910–2000) ', Hydrological Sciences - Journal des Sciences Hydrologiques, 51, pp. 83-97.

- Vicente-Serrano, S.M. (2006b) 'Differences in Spatial Patterns of Drought on Different Time Scales: An Analysis of the Iberian Peninsula', Water Resources Management, 20, pp. 37-60.
- Vicente-Serrano, S.M., Beguería, S. and López-Moreno, J.I. (2010) 'A multiscalar drought index sensitive to global warming: The standardized precipitation evapotranspiration index', Journal of Climate, 23(7), pp. 1696-1718.
- Villarini, G., Serinaldi, F., Smith, J. and Krajewski, W. (2009) ' On the stationarity of annual flood peaks in the continental United States during the 20th century', Water Resources Research, 45.
- Villarini, G., Smith, J.A., Baeck, M.L., Vitolo, R., Stephenson, D.B. and Krajewski, W.F. (2011) 'On the frequency of heavy rainfall for the Midwest of the United States', Journal of Hydrology, 400(1-2), pp. 103-120.
- WCRP (2012) CMIP5 - Coupled Model Intercomparison Project Phase 5 - Overview. Available at: http://cmip-pcmdi.llnl.gov/cmip5/ (Accessed: June 2012).
- Weiland, F.C.S., Tisseuil, C., Durr, H.H., Vrac, M. and Beek, L.P.H.v. (2012) 'Selecting the optimal method to calculate daily global reference potential evaporation from CFSR reanalysis data for application in a hydrological model study', Hydrol. Earth Syst. Sci., 16, pp. 983–1000.
- Wilks, D.S. (2006) 'On “Field Significance” and the False Discovery Rate', Journal of Applied Meteorology and Climatology, 45, pp. 1181-1189.
- WMO (2000) Detecting trends and other changes in hydrological data. WMO. [Online]. Available at: water.usgs.gov/osw/wcp-water/detecting-trend.pdf.
- Woollings, T. (2010) 'Dynamical influences on European climate: An uncertain future', Philosophical transactions of Royal Society, 368, pp. 3733-3756.
- Woollings, T., Hannachi, A., Hoskins, B. and Turner, A. (2010) 'A regime view of the North Atlantic oscillation and its response to anthropogenic forcing', Journal of Climate, 23(6), pp. 1291-1307.
- Wu, H., Svoboda, M.D., Hayes, M.J., Wilhite, D.A. and Wen, F. (2007) 'Appropriate application of the Standardized Precipitation Index in arid locations and dry seasons', International Journal of Climatology, 27, pp. 65-79.
- Yue, S., Pilon, P. and Cavadias, G. (2002a) 'Power of the Mann-Kendall and Spearman's rho tests for detecting monotonic trends in hydrological series', Journal of Hydrology, 259, pp. 254-271.
- Yue, S., Pilon, P. and Phinney, B. (2003) 'Canadian streamflow trend detection: impacts of serial and cross-correlation', Hydrological Sciences Journal 48(1), pp. 51-64.
- Yue, S., Pilon, P., Phinney, B. and Cavadias, G. (2002b) 'The influence of autocorrelation on the ability to detect trend in hydrological series', Hydrological Processes, 16(9), pp. 1807-1829.
- Zappa, G., Shaffrey, L.C. and Hodges, K.I. (2013) 'The ability of CMIP5 models to simulate North Atlantic extratropical cyclones', Journal of Climate.